Interference modeling of wireless cooperative systems

Baha Eddine Youcef Belmekki

THÈSE

En vue de l'obtention du

DOCTORAT DE L'UNIVERSITÉ DE TOULOUSE

Délivré par :

Institut National Polytechnique de Toulouse (Toulouse INP)

Discipline ou spécialité :

Informatique et Télécommunication

Présentée et soutenue par :

M. BAHA EDDINE YOUCEF BELMEKKI

le mercredi 24 juin 2020

Titre :

Interference Modeling of Wireless Cooperative Systems

Ecole doctorale :

Mathématiques, Informatique, Télécommunications de Toulouse (MITT)

Unité de recherche :

Institut de Recherche en Informatique de Toulouse (IRIT)

Directeur(s) de Thèse :

M. BENOIT ESCRIG

M. ABDELKRIM HAMZA

Rapporteurs :

M. DANIEL ROVIRAS, CNAM PARIS

M. JEAN-MARIE GORCE, INSA LYON

Membre(s) du jury :

Mme MARIE LAURE BOUCHERET, TOULOUSE INP, Président

M. ABDELKRIM HAMZA, , Membre

M. BENOIT ESCRIG, INSTITUT POLYTECHNIQUE DE BORDEAUX, Membre

M. MARCO DI RENZO, CNRS PARIS, Membre

Remerciements

En premier lieu, je tiens à remercier mes deux encadreurs, M. Benoît Escrig et M. Abdelkrim Hamza qui se sont acquittés de la délicate tâche d'encadrer cette thèse, de l'aide compétente qu'ils m'ont apporté, de leur patience, et de leurs encouragements et qui m'ont laissé une large autonomie dans ce travail.

Mes vifs remerciements vont aux membres de jury qui m'ont fait l'honneur d'accepter d'évaluer ce travail. J'ai été honoré de leur participations à mon jury de soutenance. Je suis reconnaissant à mes deux rapporteurs M. Daniel Roviras professeur à CNAM Paris et M. Jean-Marie Gorce professeur à INSA de Lyon, d'avoir accepté de lire et d'évaluer ma thèse. J'aimerai également remercier Mme Marie-laure Boucheret professeur à INP-ENSEEIT Toulouse pour avoir présidé le jury, ainsi que M. Marco Di Renzo d'avoir accepté d'examiner cette thèse.

Ma gratitude s'adresse aussi à tout le personnel de l'IRIT, enseignants, chercheurs, doctorants et plus spécialement à Annabelle Sansus pour sa gentillesse et sa bonne humeur, et qui m'a beaucoup aidé et qui été toujours disponible durant ces trois années. Je veux aussi remercier Sylvie Armengaud et Isabelle Vasseur qui ont été disponibles à chaque fois que j'ai eu besoin d'une aide et pour leur sympathie et convivialité, sans oublier aussi Fred Peyré.

Ces remerciements ne seraient pas complets sans l'expression de toute ma sympathie envers mes camarades et collègues de l'IRIT, Tatsumi, Maxime, Vinicius, Camille, Asma. Sans oublier bien sûr, Nathalie, Nicolas, Marie, Charly, Marie-laure, Louis, Étienne, Vini-

cius, Yanna, Thomas, Cédric, Alberto, Elene, Serdar, Pierre-Hugo, et Cassio.

Je remercie aussi, Abdelouahab, Abdelaziz et Farouk, pour les moments magnifiques que nous avons passés ensemble. Je passe ensuite une dédicace spéciale à mon ancien et plus proche ami Abdelghafour pour ses encouragements et pour ça bonne humeur communicative, et aussi pour son soutien qu'il m'a apporté.

Mes remerciements s'adressent à mes parents et à mon frère qui ont toujours cru en moi et m'ont soutenu durant ces longues années d'études, pour tous les sacrifices qu'ils ont fait, l'amour et le soutien qu'ils m'ont apportés.

Résumé

L'objectif principal de cette thèse est d'étudier l'impact des interférences dans les communications véhiculaires coopératives via des outils de la géométrie stochastique. Cette thèse propose un cadre formel d'étude d'interférences dans les communications véhiculaires coopératives. Dans un premier temps, nous étudions les effets de la dépendance des interférences sur les probabilités de coupure des transmissions, considérant plusieurs type de transmissions, différents modèles de canaux et deux modèles de mobilité. Dans un second temps, nous évaluons comment la probabilité de coupure et le débit moyen des communications véhiculaires peuvent être améliorés via l'utilisation de techniques d'accès non orthogonales (NOMA). Les résultats montrent que NOMA améliore fortement les performances. Nous établissons également les conditions mathématiques nécessaires pour que les techniques NOMA soient meilleures que les techniques orthogonales classiques (OMA) en termes de probabilité de coupure. Enfin, plusieurs autres études sont menées : 1) un protocole adaptatif et coopératif fondé sur la technique NOMA est proposé, 2) une analyse des réseaux véhiculaires à ondes millimétriques est conduite, 3) plusieurs autres extensions sont étudiées telles que plusieurs relais, plusieurs sauts ou plusieurs voies.

Mots clés : interférence, transmissions coopératives, NOMA, communications véhiculaires, intersections.

Abstract

The main goal of this thesis is to study the impact of interference on cooperative vehicular communications (VCs) with the aid of stochastic geometry tools. This thesis also proposes a framework to model interference in cooperative VCs. First, we study the effects of interference dependence on the received node for several transmission schemes, different channel models, and two mobility models. The performance in terms of outage probability is investigated. Second, we investigate the improvement of using non-orthogonal multiple access (NOMA) in the performance in terms of outage probability and average achievable rate for several transmission schemes. The results show that NOMA improves significantly the performance. We also investigate conditions in which NOMA outperforms OMA. Finally, several studies are conducted: 1) an adaptive cooperative NOMA protocol is proposed, 2) an analysis of millimeter waves (mmWave) vehicular networks is carried out, 3) extension scenarios are investigated such as multiple relays, multiple hops, or multiples lanes.

Keywords: interference, cooperative transmissions, NOMA, vehicular communications, intersections.

Contents

List of Figures

Introduction (in French)

Introduction

Durant les trois dernières décennies, l'usage de terminaux sans fil n'a cessé de croître, que ce soit via le développement des réseaux mobiles ou via celui des réseaux WiFi [Gol05]. Durant cette dernière décennie, les chercheurs se sont penchés sur l'internet des objet (IoT), qui permet de connecter des objets aux réseaux. Selon [Res14], le nombre d'appareils connectés sera ainsi de 8 milliards en 2024. L'IoT constitue, à l'heure actuelle, un nouvel axe de développement dans la mesure où se rajoute au trafic existant, le trafic M2M. Cette augmentation du nombre de terminaux, et donc du trafic de données généré, va engendrer une augmentation du niveau d'interférences sans précèdent sur l'ensemble des communications. Ces interférences dégradent la qualité des transmissions à un tel point qu'il n'est plus possible de négliger ce terme dans le calcul des performances des communications sans fil. La prise en compte de ces interférences constitue l'un des points d'entrée de cette thèse.

Prendre en compte le niveau d'interférences généré par les autres utilisateurs ou les autres terminaux des réseaux sans fil nécessite l'utilisation, voire le développement de nouveaux outils de modélisation. Ainsi, la modélisation de la répartition aléatoire des terminaux sur une surface donnée fera appel à des outils de géométrie stochastique. Dans cette thèse, nous mobiliserons principalement la théorie des processus ponctuels qui est une branche de la géométrie stochastique. Un processus ponctuel peut être vu comme une variable aléatoire, qui, au lieu de générer un nombre réel, génère un ensemble de points. Dans ce domaine, le

processus ponctuel de Poisson (PPP) est le modèle le plus utilisé car il rend bien compte de la position réelles des terminaux et car il permet de résoudre mathématiquement les problèmes posés.

En complément des transmissions directes entre terminaux, nous nous sommes également intéressés aux communications coopératives. Le principe des communications coopératives consiste à faire intervenir un terminal relais entre un terminal source et un terminal destination. Lorsque la source émet une information vers la destination, comme dans le cas de la transmission entre une station de base et un téléphone mobile, le terminal relais retransmet l'information reçue de la source vers la destination. La robustesse de cette communication, dite coopérative, est augmentée car la destination reçoit l'information à deux instants différents, depuis deux endroits différents, ce qui augmente la diversité temporelle et la diversité spatiale. Le prix à payer pour cette augmentation de la robustesse est une dégradation de la capacité du canal dans la mesure où une communication coopérative utilise, non pas une, mais deux tranches de temps pour transmettre la même information.

Concernant à présent le domaine d'application de notre étude, nous avons choisi de travailler dans le domaine des communications véhiculaires. Ces communications facilitent la détection et la prévention des accidents et, plus généralement, elles jouent un rôle dans la régulation du trafic routier. Les communications véhiculaires permettent aux véhicules de communiquer entre eux via des communications véhicule-à-véhicule. Elles permettent également des communications entre véhicules et piétons, et des communications entre véhicules et des infrastructures. Par ailleurs, les communications véhiculaires peuvent avoir accès à une quantité massive de données via le cloud. Par exemple, les données collectées, telles que les données sur les conditions du trafic routier en temps réel, et les données cartographiques peuvent, dans un futur proche, être utilisées par les conducteurs et par les voitures pilotées automatiquement . Enfin, cette thèse nous a amené à étudier deux scénarios dans le contexte des communications véhiculaires : les communications sur autoroutes et les communications

aux intersections.

Selon l'organisation mondiale de la santé (World Health Organization), plus de 1,25 million de personnes meurent chaque année sur les routes, et les accidents de la route constituent la première cause de décès chez les jeunes. Par ailleurs, 50% de tous les accidents se passent aux intersections. C'est une des raisons pour lesquelles nous avons concentré une partie de notre attention sur ce sujet. Dans cette thèse, nous allons étudier les performances des réseaux véhiculaires coopératifs en présence des interférences aux intersections.

En conclusion de cette introduction, nous dirons que cette thèse porte sur le calcul de performance des communications véhiculaires , utilisant des transmissions directes ou coopératives, en présence d'interférences aux intersections en mobilisant des outils de la géométrie stochastique tels que les PPP.

.

.

Introduction

Preliminaries

Wireless communications are the fastest growing segment in the communication industry [Gol05], making them essential parts of several areas, ranging from industry, business, entertainment, and in our daily life. During the last decade, researchers focused their attention on Internet of Things (IoT) which enables the connection of objects to the network and manages their information. According to [Res14], the number of connected devices will reach 8 billion devices in 2024. This will generate a massive traffic load of data and information to manage, to process, and to store. To face the ever-growing number of wireless communications and the advent of IoT, novel and non-incremental advances that use scare resource (wireless spectrum), in terms of reliability data rates and latency, have to be developed.

Consequently, this massive number of devices will generate massive interference due to the broadcasting nature of wireless networks. Hence, communication models and the multiple access schemes have to take into account the characteristics of the wireless medium and interference generated by the users. Additionally, more complex transmission schemes such as inter-device cooperation and relaying transmissions have to be adopted to deal with this interference.

Interference

After Shannon's initial results, several works considered channels with several transmitters and receivers, such as the multiple-access, interference channels [CT06]. For most cases, the expressions of the capacity are known, whereas for other cases, lower and upper bounds of the capacity are known. Even though analysis of networks involving several users is possible, the obtained expressions are involved and sometimes do not give insight on the network behavior. Moreover, wireless networks have several users, hence analysis that takes into consideration several users is needed. Wireless networks signals undergo attenuation due to distance as well as the random structure of the space in which the transmissions occur. In wireless networks, there are several simultaneous communications that occur at the same time, and due to the broadcasting nature of wireless networks and the limited resource in spectrum, interference between the network users will be present [Qui+18; KCG19; Med+09; Med+11]. In most cases, the interference caused by the users are greater and more harmful to the communications than the background noise [Ega+17]. The network users can have one message or several message to transmit to one or several users, whereas some users cooperate and act as relays. At large scale, users cause interference to each other. Realistic wireless models must take into account a large number of randomly deployed users. Thus, an analysis which assumes that a deterministic spatial configuration of the users may not be accurate, and closed form expression may not be possible. Additionally, the interference behavior is affected by the users' decision to transmit (or not) at a given time.

Stochastic Geometry Models for Wireless Networks

Assessing the performance of wireless network can be mathematically intractable [Di +18; DL15]. The theory of point processes, which is a branch of stochastic geometry is a powerful mathematical tool that allows mathematical tractability and helps analysis wireless network

in which the users are randomly distributed [DGC13; DL14b]. A point process can be viewed as a random variable except that the outcome of a realization is not a real number but a set of points. The Poisson point process (PPP) is the most widely used to model the users' locations, and its intensity is the average number of user per unit area of the region studied [DLG16]. We refer the reader to [HG+09; Hae12b; ABG11] for comprehensive presentation about stochastic geometry and Poisson point process.

For the additive white Gaussian noise (AWGN) channel, the capacity is a function of the signal to noise ratio (SNR), where in the presence of interference, the metric is will be the signal-to-inference-noise ratio (SINR). The SINR is defined as the ratio between the power of the signal of interest and the power of the interference generated by other users plus the background noise. We consider a transmission between a source node and a destination node, where the source is denoted by S, and the destination by D. We also consider that there are other transmitting nodes, and they are distributed as a point process $\Phi = \{x_n\}$, where $n \in \mathbb{N}$ as depicted in Fig.0.1. Hence, the SINR can be defined as follows

$$\text{SINR}_{(S,D)} = \frac{P|h_{SD}|^2}{\sum_{x\in\Phi} P|h_{xD}|^2 + \sigma^2}, \tag{0.1}$$

where $|h_{ab}|^2$ is the power fading coefficient between the node a and b, P is the transmitting power, and σ^2 is noise power.

Cooperative Transmissions

Cooperative communications in wireless networks [LTW04] have been shown to improve the system performance by means of relay stations that cover areas suffering harsh channel conditions or by means of mobile users that can act as relays [Ham+16a; Esc+08; Dzi+10; CLR10; Cai+11; Ham+16b; Dzi+11; Apa+10; Gor+09; HAG13; FGG12]. Cooperative transmissions can involve a single relay (as shown in Fig.3.15), or multiple relays (as shown

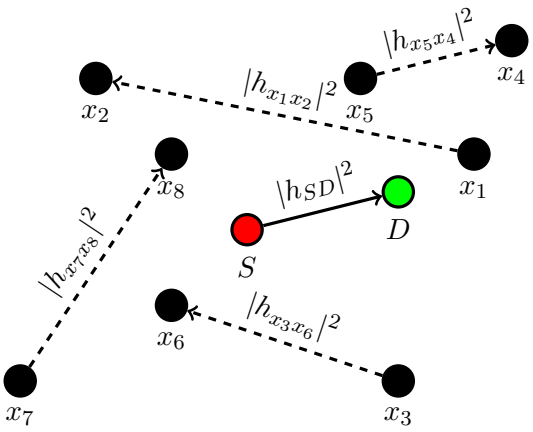

Figure 0.1.: Wireless network composed with a source S and a destination D. The network is also composed with other transmitters nodes (x_n) that try to transmit to their respective destinations and causing interference.

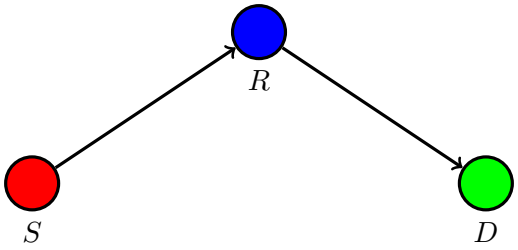

Figure 0.2.: Cooperative transmission between a source S and a destination D with the help of a single relay R.

in Fig.0.3). These relays act as distributed antennas to improve the reliability of the links [DGS10; DIG12]. Since wireless transmissions are not isolated form each other, it is realistic to consider the interference originated from other transmitting users in the network [TJJ13; DL14a].

Our choice of cooperative transmissions was also motivated by the fact that our team worked on cooperative transmissions during the last decade [Esc10; SEB13; Pai+11; SEB13; Esc11].

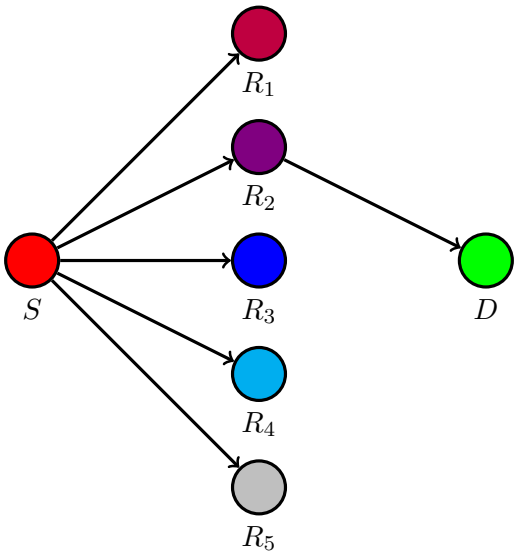

Figure 0.3.: Cooperative transmission between a source S and a destination D with the help of multiple relays $R_i \in \{R_1, R_2, ..., R_5\}$.

Vehicular Communications

The vehicles industry is heading toward fully autonomous and connected vehicles. This enables the deployment of traffic safety applications, and allows a better traffic congestion management. A key enabler of this advance are vehicular communications (VCs). VCs allow vehicles to communicate with each other via vehicle-to-vehicle (V2V) communications, but can also allow vehicles to communicate with pedestrians via vehicle-to-pedestrian (V2P) communications, and with infrastructure via vehicle-to-infrastructure (V2I) communications. VCs enable the exchange of information and data between vehicles, and improve the awareness among them, thus preventing collisions and accidents. Moreover, VCs access a large amount of data via the cloud. For instance, the data collected, such as real time traffic conditions, and mapping data can be used by drivers and by the self-deriving cars in the near future. There are two types of scenarios in which VCs can be used: highways scenarios and intersections scenarios.

Highways Scenarios

Several works have investigated the effect of interference in highway scenarios [BMT09; BMT13; BMA12; FEA16; AlH+18]. The authors in [FEA16] computed the expressions of packet success probability in multi-lane highways with carrier sense multiple access (CSMA) protocols. As far as V2V and V2I communications are concerned, several works have investigated the effect of interference in highway scenarios. In [IUA13], the authors study the performance of Aloha and CSMA multiple access control (MAC) protocols under different attenuation and fading conditions. In [BMT09], the authors derive the success probability, the density progress and the average delay, in the case where the receiver is the nearest neighbor. In [Jeo+13], the authors model the locations of vehicles with stationary Cox processes, and modeling the vehicles density with Fox's H-variate. They derive the average symbol error probability, ergodic capacity, and outage capacity at the nearest neighbor using Fox's H-functions, however the effect of the interference was not considered. In [KS17], the authors derive the expressions for the intensity of concurrent transmitters and packet success probability in multi-lane highways with CSMA MAC protocol. The performance of IEEE 802.11p using tools form queuing theory and stochastic geometry is analyzed in [KS17]. The outage probability is derivated in [Jia+16] for Nakagami-m fading and Rayleigh fading and the authors verify their results with real-world dataset containing locations of Beijing taxis. The authors also propose a road traffic information mechanism based on reputation to ensure a fair and correct share of information between vehicles. The authors in [Tas+17], derivate the outage probability and rate coverage probability of vehicles, when the line of sight path to the base station is obstructed by large vehicles sharing other highway lanes. In [AlH+18], the performance of automotive radar is evaluated in terms of expected SNR, when the location of vehicle follow a Poisson point process and a Bernoulli lattice process. In [CD18], the authors derive the expression for SIR-based coverage probability in vehicular networks, when the roads are modeled by a Poisson line process (PLP) and the

(a) (b)

Figure 0.4.: (a) Highway road [Nav18].(b) intersection road [123a].

nodes on each road by a homogeneous 1D PPP, and when independent Nakagami-m fading is assumed.

Intersections Scenarios

As far as the performance of VCs at intersections is concerned, several works studied the effect of interference in vehicular communications at intersections. Steinmetz *et al.* derivate the success probability when the receiving node and the interferer nodes are aligned on the road [Ste+15a]. Steinmetz *et al.* also investigated the success provability considering both Aloha and CSMA MAC protocols and Erlang fading channels in [Ste+15b]. In [ASW16], the authors analyze the success probability for finite road segments under several channel conditions. The authors in [AW17] evaluate the average and the fine-grained reliability for interference-limited V2V communications with the use of the meta distribution. In [JH17], Jeyara *et al.* analyze the performance of an orthogonal street system which consists of multiple intersections, and show that, in high-reliability regime, the orthogonal street system behaves like a 1-D Poisson network. However, in low-reliability regime, it behaves

like a 2-D Poisson network. Jeyara *et al.* also studied V2V communications at intersections and showed that the performance of the Aloha protocol can be considered as a lower bound of performance of CSMA protocols [JH18]. [KS17] derive the outage probability of V2V communications at the intersection in the presence of interference with a power control strategy.

Recently, researchers started to model the vehicle locations as a Poisson line process (PLP). In [CB18], the authors analyze and derive the coverage probability of V2V, V2I, infrastructure-to-vehicle (I2V), and infrastructure-to-infrastructure (I2I). In [Sia+19], the authors modeled vehicle locations on roads as doubly stochastic Cox process, and the BSs as 2D-PPP. The success probability expressions were derived for V2V links, V2B links, and for V2X links. However, Jeyara *et al.* showed in [JH] that, it is not essential to account for the geometry of every single street as in the PLP, and it suffices to consider the vehicles on the same street as the receiver as a 1D-HPPP and those on the different streets as a 2D-HPPP.

According to World Health organization, over 1.25 million people die each year on the roads, and road traffic crashes are the number one cause of death among young people [Org15]. Moreover, 50 % of all crashes are in junction areas (intersections) including fatal crashes, injury crashes, and property damage crashes [US 17]. The reasons why intersection accidents occur is because of the fact that, there are at least two crossing roads. Typically, roads are composed of at least two lanes, hence, most of intersections involve four lanes. Vehicles at intersections can either turn right, left, or continue on the straight line. Therefore, each driver needs to consider three types of maneuvers. This makes intersections critical areas not only for vehicles, but also for pedestrians and cyclists. Hence, we will focus our study in these critical areas since they are more prone to accidents.

(a) (b)

Figure 0.5.: (a) Traffic jam at the intersection [123b]. (b) accidents at the intersection [Sto].

Thesis overview

All the aforementioned studies that deal with interference at intersections consider only direct transmissions. In addition, they consider that the receiving nodes are on the roads, which is not always the case. The interference dynamic was not considered in these works.

This can be considered as a framework to model the interference with the help of stochastic geometry tools in cooperative VCs at intersections. Several dimensions and scenarios were investigated, as summarized and depicted in Fig.0.6.

We can see, from Fig.0.6, that their several dimensions investigated in thesis: the road geometry considered, the type of transmissions and decoding strategies used, channel characterizations, multiple access schemes and MAC protocols, vehicles mobility, and the number of nodes and hops considered in the transmission.

Road geometry

We consider, in this thesis, two scenarios: the intersection scenario, and highway scenario.

- Intersections: The intersection scenario involves one lane in the horizontal direction,

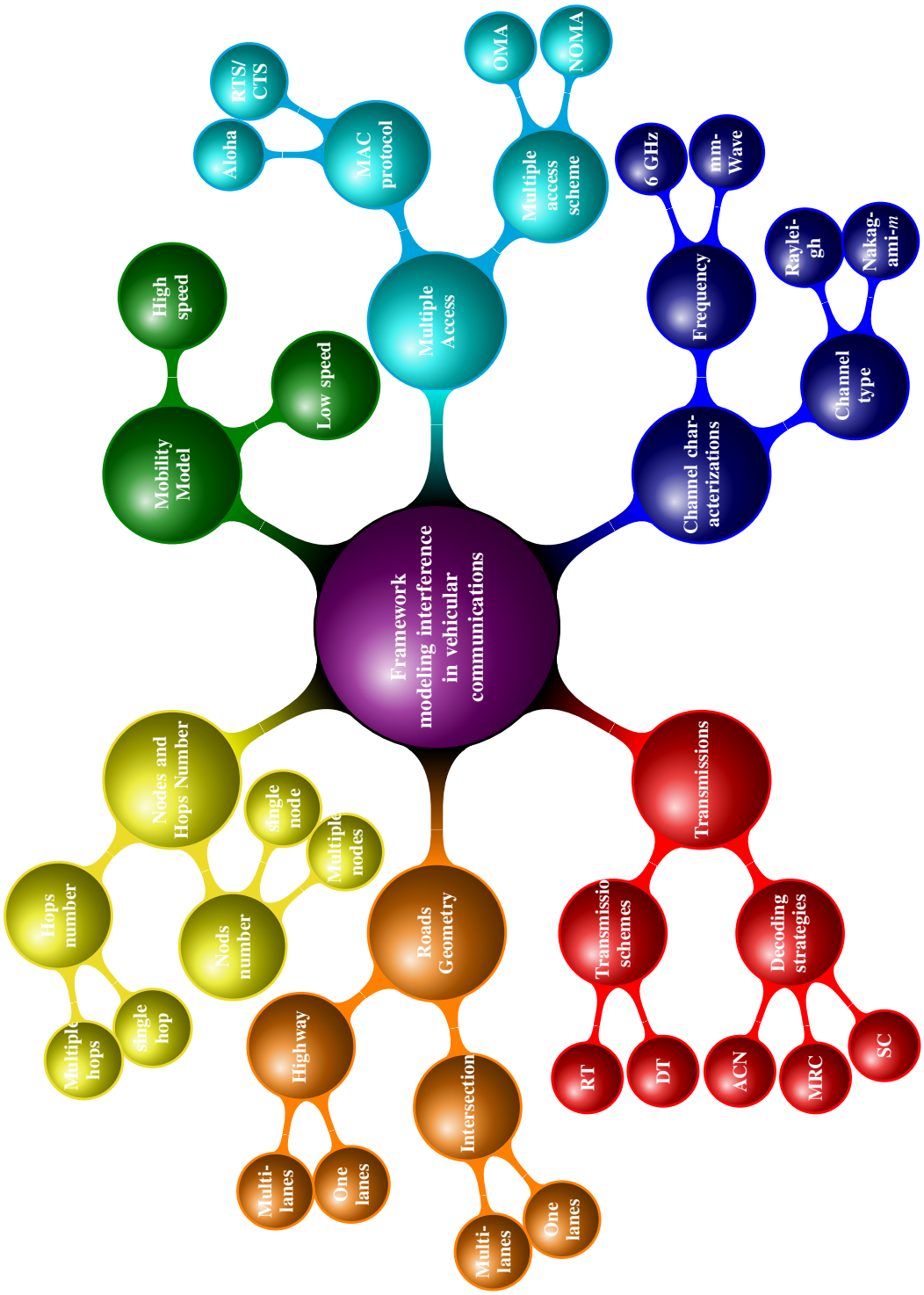

Figure 0.6.: Framework of modeling interference in VCs.

and one lane in the vertical direction. We also consider several lanes and the horizontal direction and the vertical direction.

- Highways: The highway scenario involves one lane only in a given direction (horizontal or vertical), and can also involve several lanes.

Transmissions

We consider several transmission schemes and decoding strategies.

- Transmissions schemes: We consider cooperative transmissions, or relay transmissions (RT) as the main transmission schemes in the thesis. We also consider direct transmissions (DT) for comparison sake.

- Decoding strategies: We also consider several decoding strategies at the receiving node, such as, selection combining (SC) and maximum ratio combining (MRC). We also propose a cooperative protocol based on non-orthogonal multiple access (NOMA), named adaptive cooperative NOMA (ACN) protocol.

Channel characterizations

We take into consideration several characteristics related to the channel. We investigate the type of channels used, and the frequency band.

- Channel types: We consider two types of channels, Rayleigh fading channels and Nakagami-m fading channels.

- Frequency bands: Most of the scenario investigated in this thesis are in a sub 6 GHz frequency band, but we also model the millimeter wave (mmWave) in VCs.

Multiple access

We investigate two dimensions regarding multiple access: MAC protocols and multiple access schemes.

- MAC protocols: Throughout the entire thesis, we consider Aloha MAC protocols.
- Multiple access schemes: We consider the classical orthogonal multiple access (OMA) in the first chapter, but we also consider NOMA in the rest of the thesis.

Mobility

We consider two mobility models: the low speed model, and the high speed model.

- Low speed model: We consider that the interfering vehicle do not move or move slowly during the transmission so that the set of interferers remain unchanged from one slot to another.
- High speed model: We consider that the interfering vehicles move at a high speed during the transmission so that the set of interferers changes from one slot to another.

Nodes and hops

Finally, we consider several nodes involved in the transmissions as well as several hops.

- Nodes: We consider several destination nodes (two and more) when considering NOMA, and we also consider several relays involved in the transmission considering NOMA.
- Hops: Throughout the thesis, we consider one hop transmissions when using DT, and dual hop transmission when using cooperative transmission. We derive the outage probability expressions for several scenarios using multi-hop transmissions.

Structure of the manuscript

Chapter 1 studies the impact of vehicles mobility and interference dependence on the performance of V2V and V2I communications, using two cooperative decoding strategies: SC and MRC, and considering Rayleigh fading channels at intersections. Using tools from stochastic geometry and point process theory, we derive closed form outage probability expressions for different scenarios. Then, we study the effect of interference on different transmission schemes considering Nakagami-m fading channels in line of sigh (LOS) and non line of sigh (NLOS) scenario. Closed form outage probability expressions are derived.

Chapter 2 investigates the improvements of implementing non orthogonal multiple access scheme (NOMA) and the limitations of these improvements. We propose to study the performance of VCs in the presence of interference at intersections considering NOMA direct transmissions, NOMA cooperative transmissions, and NOMA cooperative transmissions using MRC at intersections. The performance of VCs are evaluated in terms of outage probability and average achievable rate. We also investigate the impact of system parameters on performance. Finally, several extensions are considered to generalize the framework.

Chapter 3 considers several scenarios and dimensions. A cooperative NOMA protocol is proposed in the presence of interference at intersections, and its performance is investigated. We also investigated the performance of mmWave VCs at intersections considering cooperative communications. The mathematical derivations of the outage probability are derived in the case of multi-hops scenarios considering several transmission schemes. We also consider the case when multiple relays are involved in the communications. We evaluate the performance of multiple relays in VCs using NOMA in the presence of interference. We also show how to extend the derivation for intersection involving multiple lanes.

Main contributions

Chapter 1 A framework is developed to evaluate the performance of cooperative VCs at intersections in the presence of interference. The analysis takes into account the interference dynamics and vehicles mobility. In addition, the analysis is carried out for several transmission schemes. The second contribution is the derivations of the outage probability considering Nakagami-m fading channels at intersections in the presence of interference. The outage probability is evaluated for several transmissions schemes. The results are evaluated according to two scenarios, LOS scenario and NLOS scenario.

Chapter 2 The main contribution of this chapter lies in the derivation of the outage probability expressions and the average achievable rate for VCs at intersections considering NOMA. The performance are evaluated considering NOMA for direct transmissions, cooperative transmissions, and MRC cooperative transmissions. The limitations of NOMA are discussed and the mathematical conditions for NOMA to outperform OMA are derived. The analysis is performed for extension scenarios involving multiple destinations nodes. Finally, the results are carried out for the aforementioned transmissions schemes and a comparison of the performance is carried out.

Chapter 3 The main contribution of this chapter is the extensions and several scenarios investigated. The results add several dimensions to the analysis. The first contribution is proposing an adaptive cooperative NOMA protocol. The results show how this protocol outperforms the exiting protocol in the literature. The second contribution is modeling a mmWave cooperative vehicular network at intersections in the presence of interference. The third contribution consists in evaluating of the performance in terms of outage probability at intersection in the presence of interference considering: intersections with multiple lanes, multiple relays involved in the transmission, and multi-hops transmissions with different transmission schemes.

List of publications

Accepted Journal Papers

[BHE19b] B. E. Y. Belmekki, A. Hamza, and B. Escrig. "Cooperative vehicular communications at intersections over nakagami-m fading channels". In: *Vehicular Communications* (July 2019), doi:10.1016/j.vehcom.2019.100165 (cit. on p. 23).

[BHE19d] B. E. Y. Belmekki, A. Hamza, and B. Escrig. "On the Performance of 5G Non-Orthogonal Multiple Access for Vehicular Communications at Road Intersections". In: *Vehicular Communications* (2019), doi:10.1016/j.vehcom.2019.100202 (cit. on p. 75).

[BHE19j] B. E. Y. Belmekki, A. Hamza, and B. Escrig. "Performance Analysis of Cooperative NOMA at Intersections for Vehicular Communications in the Presence of Interference". In: *Ad hoc Networks* (2019), doi:10.1016/j.adhoc.2019.102036 (cit. on p. 75).

Accepted Conference Papers

[BHE19c] B. E. Y. Belmekki, A. Hamza, and B. Escrig. "On the Outage Probability of Cooperative 5G NOMA at Intersections". In: *2019 IEEE 89th Vehicular Technology Conference (VTC2019-Spring)*. IEEE. 2019, pp. 1–6 (cit. on p. 75).

[BHE19g] B. E. Y. Belmekki, A. Hamza, and B. Escrig. "Outage analysis of cooperative noma using maximum ratio combining at intersections". In: *2019 International Conference on Wireless and Mobile Computing, Networking and Communications (WiMob)*. IEEE. 2019, pp. 1–6 (cit. on p. 75).

[BHE19h] B. E. Y. Belmekki, A. Hamza, and B. Escrig. "Outage Performance of NOMA at Road Intersections Using Stochastic Geometry". In: *2019 IEEE Wireless Communications and Networking Conference (WCNC) (IEEE WCNC 2019)*. IEEE. 2019, pp. 1–6 (cit. on p. 75).

[BHE20c] B. E. Y. Belmekki, A. Hamza, and B. Escrig. "On the Outage Probability of Vehicular Communications at Intersections Over Nakagami-m Fading Channels". In: *Under review in IEEE 91th Vehicular Technology Conference (VTC2020-Spring)*. IEEE. 2020, pp. 1–6 (cit. on p. 23).

[BHE20d] B. E. Y. Belmekki, A. Hamza, and B. Escrig. "Outage Analysis of Cooperative NOMA for Millimeter Wave Vehicular Networks at Intersections". In: *Under review in IEEE 91th Vehicular Technology Conference (VTC2020-Spring)*. IEEE. 2020, pp. 1–6 (cit. on p. 127).

[BHE20e] B. E. Y. Belmekki, A. Hamza, and B. Escrig. "Performance Evaluation of Adaptive Cooperative NOMA Protocol at Road Junctions". In: *Under review in IEEE 91th Vehicular Technology Conference (VTC2020-Spring)*. IEEE. 2020, pp. 1–6 (cit. on p. 127).

Submitted Journal Papers

[BHE19e] B. E. Y. Belmekki, A. Hamza, and B. Escrig. "On the Performance of Cooperative NOMA Using MRC at Road Intersections". In: *Under review in the*

journal of IEEE Transactions on Cognitive Communications and Networking (2019) (cit. on p. 75).

[BHE19i] B. E. Y. Belmekki, A. Hamza, and B. Escrig. "Performance Analysis of Cooperative Communications at Road Intersections Using Stochastic Geometry Tools". In: *Under review in the journal Ad hoc Networks* (2019) (cit. on p. 23).

Conference Papers to Submit

[BHE20a] B. E. Y. Belmekki, A. Hamza, and B. Escrig. "Interference Dynamic and Vehicles Mobility Analysis in Cooperative Vehicular Communications". In: *2020 IEEE International Symposium on Personal, Indoor and Mobile Radio Communications (PIMRC)*. IEEE. 2020, pp. 1–6 (cit. on p. 23).

[BHE20b] B. E. Y. Belmekki, A. Hamza, and B. Escrig. "Multiple Relays Performance in NOMA Vehicular Networks". In: *2020 IEEE International Symposium on Personal, Indoor and Mobile Radio Communications (PIMRC)*. IEEE. 2020, pp. 1–6 (cit. on p. 127).

Chapter 1.

Cooperative OMA analysis

This chapter has been adapted from the journal papers [BHE19b; BHE19i]. *This work has also been discussed in the conference papers* [BHE20c; BHE20a].

Contents

1.1. Introduction

Several works in the literature focuses on the effect of the interference using tools from stochastic geometry, and nodes placement according to the Poisson point process. However, few researches focus on the interference dynamics, and how temporal and spatial dependence between interferer nodes may affect the performance. Ganti et al [GH09] derivate the conditional outage probability when the interferers are originated form the same set. In [BMT09] Haneggi introduced the concept of “uncertainty cube", which consist of node location, fading, and access scheme. Schilcher et al in [Sch+13] extended Haneggi's work [Hae12a], by introducing a wider range of uncertainties. In [Cri+15] and [FEA16] the authors investigate the performance of MRC considering the effects of interference dynamics. Few researches take the interference into a cooperative transmission. [IUA13] derived the outage probability of a relying scheme using Decode-and-forward protocol [GH09]. The author in [HG+09] derived the outage probability using Decode- and-forward and Compress-and-forward protocol. However the authors assumed that the interferer nodes always transmit. In [Hae09], the authors analyze the performance of a cooperative single-hop scheme with the aid of one relay, and a two-hope cooperative scheme with aid of two relays, considering dependent and independent interference. Tanbourgi et al. derive in [Hae12a] the outage probability of a cooperative scheme with a single relay, where the destination combines the signal obtained from the source and from either a relay transmission or a second source transmission if the relay does not decode the source message. The authors in [Hae12b] extended their work in [Hae09] to a cooperative transmission with multiple relays and multiple packet transmission.

In this chapter we propose to study two cases. In the first case, referred to as study case 1, we study the impact of vehicles mobility and interference dependence on the performance, using two cooperative decoding strategies: SC and MRC, and considering Rayleigh fading

channels. In the second case, termed as study case 2, we study the effect of interference on different transmission schemes considering Nakagami-m fading channels in line of sigh (LOS) and non line of sigh (NLOS) scenario.

1.2. Study cases and Contributions

1.2.1. Study Case 1

In this study case, we focus on direct and cooperative transmissions for intersection scenarios in presence of interference. We develop a framework to model a direct transmission and a relayed transmission between vehicles (V2V) and between vehicles and infrastructure (V2I) at intersections using tools from stochastic geometry and point process theory. We derive the outage probability expression for a direct transmission, when the receiving node can be anywhere on the plan. We then derive the outage probability in a relayed transmission considering different decoding strategies, namely SC and MRC. We also consider two mobility models. The first model is the low speed or static vehicles (LSV) model which assumes that the interferer vehicles move slowly or not at all. The second model is the high speed vehicles (HSV) model which assumes that the interferer vehicles move at high speed. The main contributions are as follows:

- We develop a tractable analysis to model V2V and V2I communications for direct transmissions and for cooperative transmissions in intersection scenarios, and we show that cooperative transmissions always enhance the outage probability performance compared to direct transmissions. We study two mobility models, and compare their outage probability and throughput performance under different traffic densities.

- We evaluate the outage probability when the destination uses SC and MRC, and we show that MRC has a better performance over SC only when the relay is close to the source. We also evaluate the outage probability for several relay positions, and

we find the optimal relay position for different traffic conditions and vehicle mobility models; and we show that the outage probability does not improve after the number of infrastructure relays reached a threshold value.

- We obtain a closed form of the outage probability when the interference are dependent and independent given specific channel conditions. We also obtained closed form of Laplace transform expressions where the relay and/or the destination are located anywhere on the plan, for specific channel conditions.

- We study the outage probability performance of cooperative transmissions in highways and intersection scenarios. We show that, as the vehicles move closer to intersections, the outage probability increases compared to highway scenarios. However, as the vehicles move away from intersections, highway and intersection scenarios exhibit the same performance, which confirms the statement that intersections are critical areas and more prone to incidents. Finally, we show that, depending on the environment, the interference dependence behaves differently. For instance, suburban intersections have a lower interference dependence compared to urban intersections. This is obtained by studying the impact of the path loss exponent on the outage probability performance.

1.2.2. Study Case 2

In this study case, we study the performance VCs which consists of V2V and V2I communications at intersections in presence of interference. We consider Nakagami-m fading channels rather than Rayleigh fading channels. We also investigate the impact of different transmissions schemes on the performance. Finally, we investigate the impact of LOS and NLOS scenario. The main contributions are as follows:

- We investigate three transmission schemes: direct transmission (DT), relay transmission (RT) and hybrid transmission (HT), in the presence of interference at intersec-

tions, and we show that DT outperforms RT, hence RT is useful only when DT is not possible.

- We derive outage probability expressions for three transmission schemes when the receiving nodes are on the roads (V2V), or outside the roads (V2I) considering Nakagami-m fading channels. Closed forms are obtained for specific channel conditions.
- We consider two scenarios: LOS scenario and NLOS scenario. We show that in LOS scenario, DT is better for high densities of vehicles. We show that HT has better performance for low densities of vehicles and low data rates regardless of the scenario. Surprisingly, we find that NLOS scenario outperforms LOS scenario at intersections.
- We investigate the best relay position for RT and HT, and we show that the best relay position in RT is at mid distance between the source and the destination whereas the best relay position in HT is close to the destination.
- We extende our model to a realistic intersection scenario including several lanes, and we show that in LOS scenario, as the number of lane increases, it is better to use DT.
- We validate our analytical results by Mont-Carlo simulations.

1.3. System Model for Case Study 1

1.3.1. Intersection Scenario

We consider a cooperative transmission between a source node S and a destination node D, with the help of a relay node R. For the sake of convenience, we use S, D and R to denote both the nodes and their locations. The intersection scenario involves two perpendicular roads, the horizontal road denoted by X and the vertical road denoted by Y. As we consider both V2V and V2I communications[1], any node of the triplet $\{S, R, D\}$ can be either on

[1]The Doppler shift and time-varying effect of V2V and V2I channels are beyond the scope of this thesis.

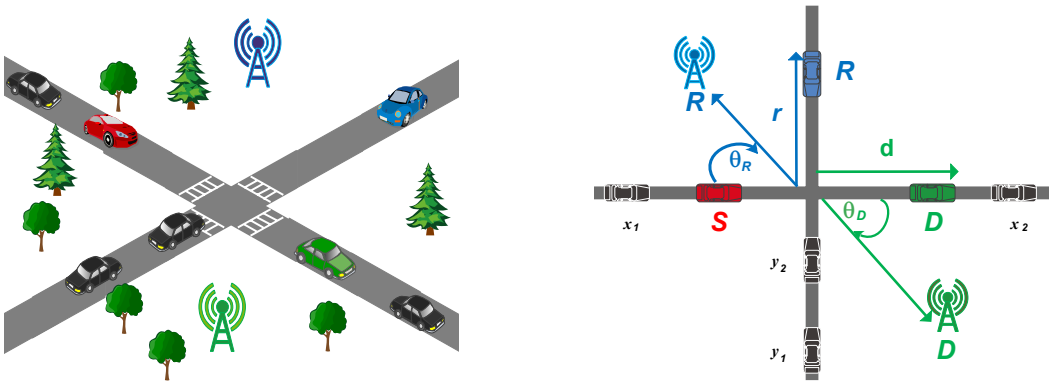

(a) (b)

Figure 1.1.: System model for VCs involving a source S, relay R, and a destination D. The nodes S, R and D can be vehicles or as part of the communication infrastructures.

the road (as a vehicle) or outside the road (as part of the communication infrastructure). We denote by T the receiving node, and by t the distance between the node T and the intersection, where $T \in \{R, D\}$, $t \in \{r, d\}$, and θ_T is the angle between the node T and the X road, as shown in Fig.1.1. Note that the intersection is the point when the road X and Y intersect, i.e., the point $(0, 0)$.

1.3.2. MAC Protocol

Medium access protocols used in VCs are mainly based on CSMA schemes. However, due to mathematical tractability issues, the computation of the outage probability considering these protocols might not be possible in our scenario, and closed form expressions are hard to obtain. We chose to step back to slotted Aloha protocol which can be considered as lower bounds to the performance of the CSMA protocol [JH18]. Moreover, both CSMA and Aloha exhibit the similar performance in the case of dense network [Sub+12; Ngu+13]. Hence, we assume that vehicles use slotted Aloha MAC protocol with parameter p, i.e., every node can access the medium with a probability p.

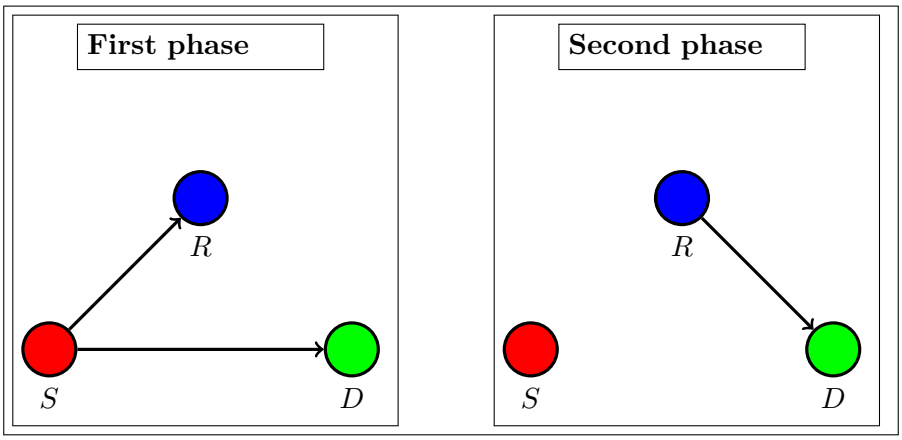

Figure 1.2.: The transmission scheme. The transmission occurs during two phases.

1.3.3. Decoding Strategy Model

We use a DF transmission scheme [Alt+14], i.e., the node R decodes and re-encodes the message then forwards it. We consider a half-duplex transmission during which a transmission occurs during two phases. The duration of each phase is one time–slot as depicted in Fig.1.2. In the first phase, the source broadcasts the message to the relay and destination ($S \longrightarrow R$ and $S \longrightarrow D$).

In the second phase, we consider two decoding schemes. For the first one, named SC, the relay transmits to the destination ($R \longrightarrow D$). For the second one, named MRC, the relay transmits to the destination and the destination adds the power received from the relay and the power received from the source in the first time slot ($R \longrightarrow D$ and $S \longrightarrow D$).

1.3.4. Channel and Interference Model

We also consider a set of interfering vehicles that are located on the roads. We assume that the set of interfering vehicles on the X road, denoted by Φ_X (resp. Y road, denoted by Φ_Y) are distributed according to a one dimensional homogeneous Poisson point process (1D-HPPP) denoted by $\Phi_X \sim$1D-HPPP(λ_X, x) (resp.$\Phi_Y \sim$1D-HPPP(λ_Y, y)) over the space $\mathcal{B}$, where x and λ_X (resp. y and λ_Y) are the position of the interfering vehicles and their

intensity on the X road (resp. Y road). We denote by x and y, both the interfering and their locations. Finally, we consider that the 1D-HPPP can be on infinite road segments, i.e., $\mathcal{B} = \{x \in \mathbb{R}, y \in \mathbb{R}\}$, or on a finite road segments, i.e., $\mathcal{B} = \{x, y \in \mathbb{R} | x < Z, y < Z\}$.

Although assuming that the positions of the interfering vehicles follow a PPP might be unrealistic in some scenarios, in our context, modeling the position of vehicles as PPP can approach real data and still insuring a mathematical tractability with the help of stochastic geometry tools [BMT09; BMT13; BMA12; FEA16; Ton+16; Jia+16; Tas+17; AlH+18; Ste+15a; ASW16; KS17; JH17; JH18]. For instance, in [Jia+16], the authors compared real data set of taxis in Beijing Fig.1.3, with PPP by performing Kolmogorov–Smirnov test. Kolmogorov–Smirnov test is a non parametric test of the equality of probability distributions that can be used to compare a sample with a reference probability distribution, in this case, real data set and PPP. We can see, from Fig.1.4, that the spatial distribution of the real-world vehicles may be deemed reasonably consistent with the PPP distribution characteristics. Also, it has been show in [JH17], that the distribution the vehicles in the intersection scenario cannot be accurately modeled as two dimensional Poisson point processes (2D-PPP). Finally, the authors in [RP16] showed that the single lane model can accurately model the intersection scenario.

The transmission between any pair of two nodes a and b experiences a path loss $l_{ab} = (Ar_{ab})^{-\alpha}$, where A is a constant depending on the antenna characteristics, r_{ab} is the Euclidean distance between the node a and b, i.e., $r_{ab} = \|a - b\|$, and α is the path loss exponent. All nodes transmit with a constant power P, h_{ab} is the fading coefficient between node a and b, and is modeled as $\mathcal{CN}(0, 1)$ (Rayleigh fading)[Che+07]. The power fading coefficient between the node a and b, $|h_{ab}|^2$, follows an exponential distribution with unit mean. We also consider a Gaussian noise (AWGN) with zero mean and variance σ^2. We

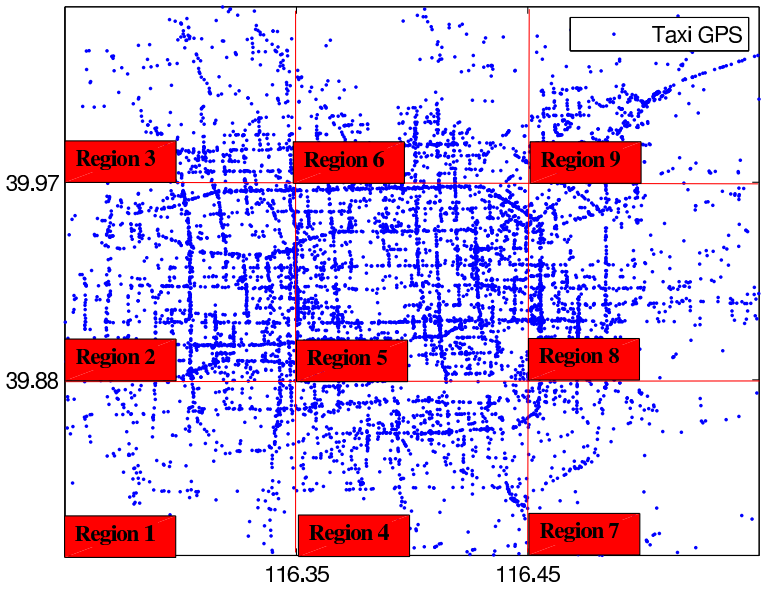

Figure 1.3.: Taxis locations in Beijing [Jia+16].

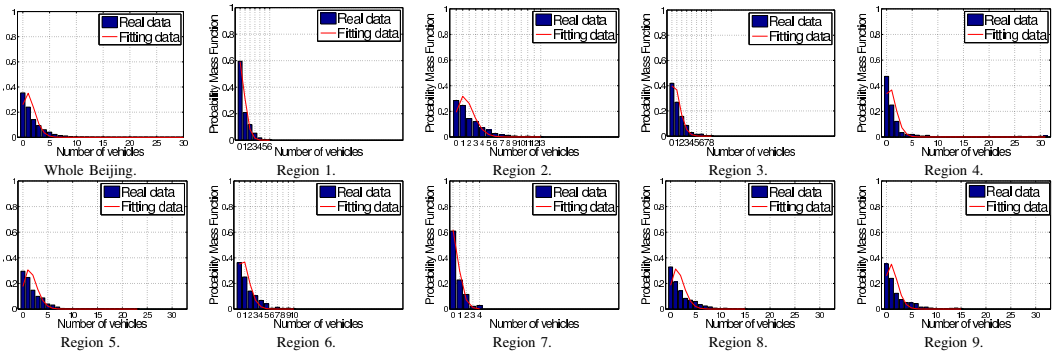

Figure 1.4.: Taxis position distributions of different regions at Beijing [Jia+16].

define the aggregate interference as

$$I_{X_T} = \sum_{x \in \Phi_{X_T}} P|h_{Tx}|^2 l_{Tx}, \tag{1.1}$$

and

$$I_{Y_T} = \sum_{y \in \Phi_{Y_T}} P|h_{Ty}|^2 l_{Ty}, \tag{1.2}$$

where I_{X_T} is the aggregate interference from the X road at T, I_{Y_T} is the aggregate interference from the Y road at T, Φ_{X_T} is the set of the interferers from the road X at T, and Φ_{Y_T} is the set of the interferers from the road Y at T,

1.3.5. Mobility Model

In this work, we consider two mobility models. In the first model, which we referred to as the low speed or static vehicles (LSV), we assume that interfering vehicles do not move or move slowly, that is, their positions remain the same during the two time slots of the transmission as depicted in Fig.1.5(a). Thus the vehicles that interfere at the relay and at the destination are originated from the same set, i.e., $\Phi_{X_R} = \Phi_{X_D} = \Phi_X$ and $\Phi_{Y_R} = \Phi_{Y_D} = \Phi_Y$.

In the second model, which we referred to as the high speed vehicles (HSV), we assume that vehicles move at a high speed, that is, their positions change every time slot. Thus, the vehicles that interfere at the relay during the first time slot are not the same as the one that interfere at the destination during the second time slot as depicted in Fig.1.5(b). This can be modeled by independent realizations of the Poisson point process Φ for each time slot, i.e., $\Phi_{X_R} \cap \Phi_{X_D} = \varnothing$ and $\Phi_{Y_R} \cap \Phi_{Y_D} = \varnothing$.

The HSV model captures the scenario in which the vehicles are highly mobile so that their locations during one time slot do not provide information about their locations during any other time slot.

Clearly, these two models represent two opposite extremes in the mobility of vehicles. How-

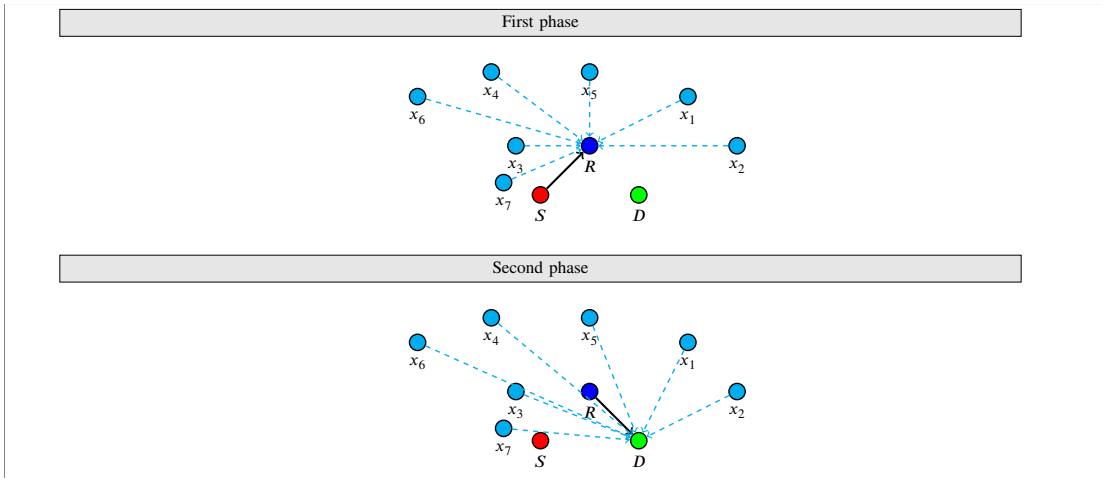

(a) LSV scenario during two time slots.

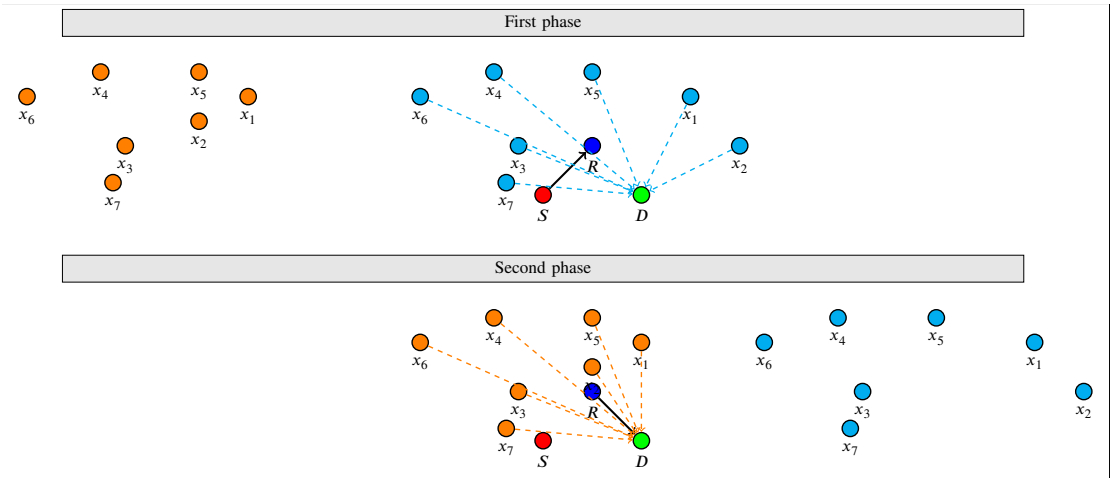

(b) HSV scenario during two time slots.

Figure 1.5.: Two mobility models namely LSV and HSV. (a) In the LSV model, we consider that $\Phi_{X_R} = \Phi_{X_D} = \Phi_X$ and $\Phi_{Y_R} = \Phi_{Y_D} = \Phi_Y$. (b) In the hSV model, we consider that $\Phi_{X_R} \cap \Phi_{X_D} = \varnothing$ and $\Phi_{Y_R} \cap \Phi_{Y_D} = \varnothing$.

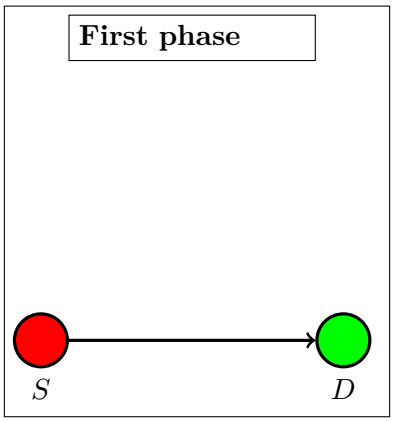

Figure 1.6.: The direct transmission. The transmission occurs in one phases.

ever, this can gives us an insight on the impact of mobility on the performance.

1.4. System Model for Case Study 2

We consider the same intersection scenario and MAC protocol as in section 1.3.1 and section 1.3.2.

1.4.1. Transmission Scheme

In this study, we study three transmission schemes: a direct transmission, a relay transmission, and a combination of a direct transmission and a relay transmission.

Direct Transmission

We consider a direct transmission (DT) between a source S and a destination D. The transmission occurs in one phase as shown in Fig.1.6.

Relay Transmission

When DT link is blocked, we consider a two-hop relay transmission between S and D with help of a relay R. The transmission occurs in two phases. During the first phase, S sends a

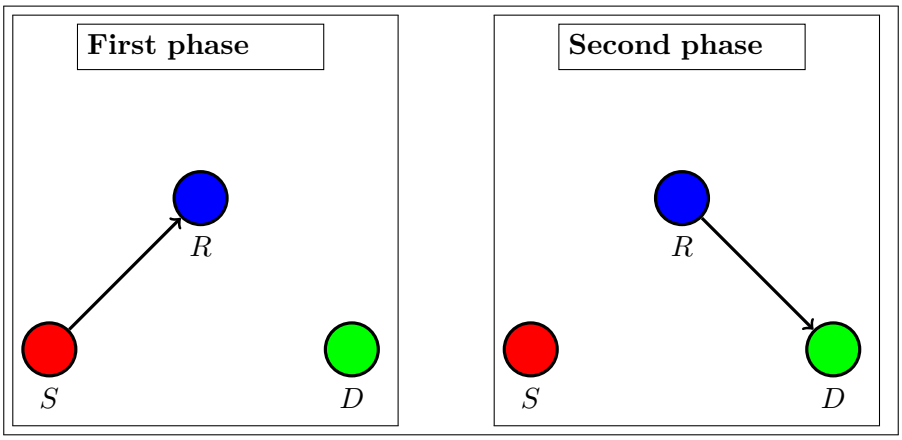

Figure 1.7.: The relay transmission. The transmission occurs during two phases.

message to R ($S \rightarrow R$). During the second phase, R sends the message to D ($R \rightarrow D$). We consider DF protocol, that is, R decodes, re-encodes, then forward the message as shown in Fig.1.7.

Hybrid Transmission

In this transmission, we use both DT and RT, we denoted this transmission by hybrid transmission (HT). This transmission occurs in two phases. During the first phase, S broadcast a message to R and D. Then, if R decodes correctly S message, it sends it to D during the second phase. Otherwise, S will sends the message again to D in the second phase as shown in Fig.1.8. We also consider DF protocol.

1.4.2. Channel and Interference Model

We consider the same interference model and path loss model in section 1.3.4. We consider an interference limited scenario, that is, the power of noise is set to zero ($\sigma^2 = 0$). Without loss of generality, we assume that all nodes transmit with a unit power. The signal received

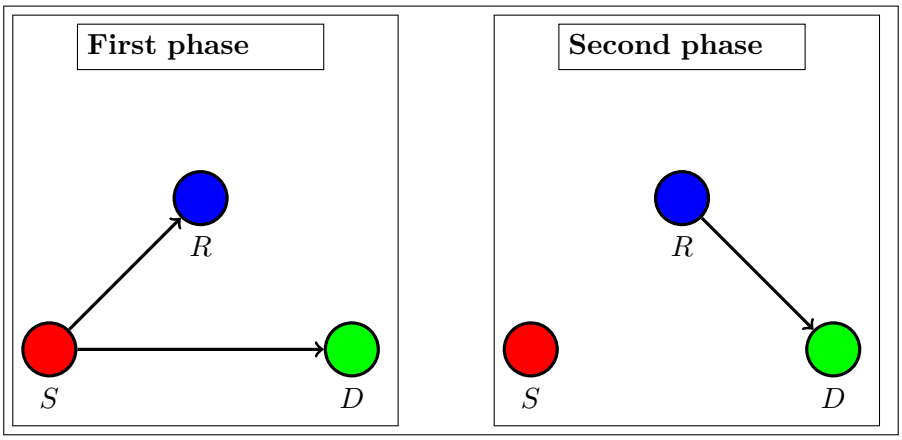

Figure 1.8.: The hybrid transmission. The transmission occurs during two phases.

at R and D in the fist time slot are expressed respectively as

$$\mathcal{Y}_R = h_{SR}\sqrt{l_{SR}}\,\chi_S + \sum_{x\in\Phi_{X_R}} h_{Rx}\sqrt{l_{Rx}}\,\chi_x + \sum_{y\in\Phi_{Y_R}} h_{Ry}\sqrt{l_{Ry}}\,\chi_y,$$

and

$$\mathcal{Y}_D = h_{SD}\sqrt{l_{SD}}\,\chi_S + \sum_{x\in\Phi_{X_D}} h_{Dx}\sqrt{l_{Dx}}\,\chi_x + \sum_{y\in\Phi_{Y_D}} h_{Dy}\sqrt{l_{Dy}}\,\chi_y.$$

The signal received at D in the second time slot if R decodes the message is expressed as

$$\mathcal{Y}_D = h_{RD}\sqrt{l_{RD}}\,\chi_R + \sum_{x\in\Phi_{X_D}} h_{Dx}\sqrt{l_{Dx}}\,\chi_x + \sum_{y\in\Phi_{Y_D}} h_{Dy}\sqrt{l_{Dy}}\,\chi_y,$$

where $\mathcal{Y}_R$ and $\mathcal{Y}_D$ are the signals received by R and by D, χ_S and χ_R are the signals transmitted by S and R. The messages transmitted by the interfere node x and y, are denoted respectively by χ_x and χ_y.

The coefficients h_{SR}, h_{SD}, and h_{RD} denote the fading of the link $S-R$, $S-D$, and $R-D$. The fading coefficients are modeled as Nakagami-m fading with parameter m [HYH13], that is

$$f_{h_u}(x) = 2\frac{m^m}{\Gamma(m)}x^{2m-1}e^{-mx^2}, \tag{1.3}$$

where $u \in \{SR, SD, RD\}$. Hence, the power fading coefficients $|h_{SR}|^2$,$|h_{SD}|^2$, and $|h_{RD}|^2$ follow a gamma distribution distribution, that is,

$$f_{|h_u|^2}(x) = \frac{m^m}{\Gamma(m)} x^{m-1} e^{-mx}. \tag{1.4}$$

The fading coefficients h_{Rx}, h_{Ry}, h_{Dx}, and h_{Dy} denote the fading of the link $R-x$, $R-y$, $D-x$, and $D-y$. The fading coefficients are modeled as Rayleigh fading [Che+07]. Thus, the power fading coefficients $|h_{Rx}|^2$, $|h_{Ry}|^2$, $|h_{Dx}|^2$, and $|h_{Dy}|^2$, follow an exponential distribution with unit mean. The aggregate interference originated from the X road and the Y road are given by (1.1) and (1.2).

1.4.3. Environment Model

We consider two scenarios, LOS scenario, and NLOS scenario. The LOS scenario models the suburban environment due to the absence of buildings. The NLOS scenario models the urban scenario due to buildings that block the transmissions. We denote by α_{LOS} and m_{LOS}, the path exponent, and the fading parameter for LOS scenario. We denote by α_{NLOS} and m_{NLOS}, the path exponent, and the fading parameter for NLOS scenario.

1.5. Outage Computation for Case Study 1

1.5.1. Condition for Outage

We define in this section the outage events related to the DF protocol that uses a half-duplex transmission. We first define the outage event related to the direct link $S-D$. Then, we define the outage events related to the relayed links $S-R$ and $R-D$ when using SC and MRC[2].

[2]We do not consider the bandwidth in computing the achievable rate.

Direct Link

We define the rate related to the direct link $S-D$, denoted $\mathcal{R}_{SD}$, as

$$\mathcal{R}_{SD} = \frac{1}{2}\log_2\left(1+\frac{P|h_{SD}|^2 l_{SD}}{\sigma^2 + I_{X_D} + I_{Y_D}}\right). \tag{1.5}$$

We define the outage event on the direct link $S-D$, denoted O_{SD}, as

$$O_{SD} \triangleq \left[\mathcal{R}_{SD} < \mathcal{R}\right], \tag{1.6}$$

where $\mathcal{R}$ is the target rate.

Relayed link

We define the rates related to the relayed link $S-R$ and $R-D$, denoted respectively $\mathcal{R}_{SR}$ and $\mathcal{R}_{RD}$, as

$$\mathcal{R}_{SR} = \frac{1}{2}\log_2\left(1+\frac{P|h_{SR}|^2 l_{SR}}{\sigma^2 + I_{X_R} + I_{Y_R}}\right), \tag{1.7}$$

and

$$\mathcal{R}_{RD} = \frac{1}{2}\log_2\left(1+\frac{P|h_{RD}|^2 l_{RD}}{\sigma^2 + I_{X_D} + I_{Y_D}}\right). \tag{1.8}$$

We now define the outage events on the relayed link $S-R$ and $R-D$ as

$$O_{SR} \triangleq \left[\mathcal{R}_{SR} < \mathcal{R}\right], \tag{1.9}$$

and

$$O_{RD} \triangleq \left[\mathcal{R}_{RD} < \mathcal{R}\right]. \tag{1.10}$$

Notice that the outage can also be expressed in terms of signal-to-interference-plus-noise ratio (SINR), that is, an outage event occurs when the SINR is lower than a decoding

threshold Θ, which can be expressed by

$$\text{SINR}_{ab} < \Theta,$$

where $\text{SINR}_{ab} = \dfrac{P|h_{ab}|^2 l_{ab}}{\sigma^2 + I_{X_b} + I_{Y_b}}$, $\Theta = 2^{2\mathcal{R}} - 1$, and a and b are the transmitting and the receiving node, respectively.

Since we use SC and MRC, we have two expressions of the outage event as in [Alt+14]. Therefore, we express the outage event using SC, denoted $O_{\mathbf{(SC)}}$, as

$$O_{\mathbf{(SC)}} = [O_{SR} \cap O_{SD}] \cup [O_{SR}^{C} \cap O_{RD}], \tag{1.11}$$

where $O_{SR}^{C} \triangleq [\mathcal{R}_{SR} > \mathcal{R}]$ is the event that the relay successfully decodes the source message. We express the outage event using MRC, denoted $O_{\mathbf{(MRC)}}$, as

$$O_{\mathbf{(MRC)}} = [O_{SR} \cap O_{SD}] \cup [O_{SR}^{C} \cap O_{SRD}], \tag{1.12}$$

where $O_{SRD} \triangleq [\mathcal{R}_{SRD} < \mathcal{R}]$ is the outage event at the destination when the relay and the source transmit simultaneously, and $\mathcal{R}_{SRD}$ is the data rate when using MRC. The rate $\mathcal{R}_{SRD}$ is expressed as

$$\mathcal{R}_{SRD} = \frac{1}{2}\log_2\left(1 + \frac{P|h_{SD}|^2 l_{SD} + P|h_{RD}|^2 l_{RD}}{\sigma^2 + I_{X_D} + I_{Y_D}}\right). \tag{1.13}$$

1.5.2. Outage Behaviour

In this section, we calculate the outage probability for the direct transmission and the relayed transmission.

Direct Transmission

The outage probability for a direct transmission has been derived in [Ste+15a], and is given by

$$\mathbb{P}(O) = 1 - N_{SD}\mathcal{L}_{I_{X_D}}(K_{SD})\mathcal{L}_{I_{Y_D}}(K_{SD}), \tag{1.14}$$

where $K_{ab} = \dfrac{\Theta}{Pl_{ab}}$ and $N_{ab} = \exp(-K_{ab}\sigma^2)$.

Relayed Transmission

The outage probability for the DF protocol using a half-duplex transmission when the destination uses SC is expressed as

$$\mathbb{P}(O_{\mathbf{(SC)}}) = \mathbb{P}(O_{SR} \cap O_{SD}) + \mathbb{P}(O_{SR}^C \cap O_{RD}), \tag{1.15}$$

and the outage probability when the destination uses MRC is expressed as

$$\mathbb{P}(O_{\mathbf{(MRC)}}) = \mathbb{P}(O_{SR} \cap O_{SD}) + \mathbb{P}(O_{SR}^C \cap O_{SRD}). \tag{1.16}$$

Now, we calculate each probability in equations (1.15) and (1.16). First, we calculate the probability $\mathbb{P}(O_{SR} \cap O_{SD})$. This probability is related to the outage during the first phase, its expression does not change whether the destination uses SC or MRC. The expression of $\mathbb{P}(O_{SR} \cap O_{SD})$ is given by

$$\begin{aligned} \mathbb{P}(O_{SR} \cap O_{SD}) &= 1 - \mathbb{P}(O_{SR}^C \cup O_{SD}^C) \\ &= 1 - \mathbb{P}(O_{SR}^C) - \mathbb{P}(O_{SD}^C) + \mathbb{P}(O_{SR}^C \cap O_{SD}^C), \end{aligned} \tag{1.17}$$

where $\mathbb{P}(O_{SD}^C)$ and $\mathbb{P}(O_{SR}^C)$ are given respectively by

$$\mathbb{P}(O_{SD}^C) = N_{SD}\mathcal{L}_{I_{X_D}}(K_{SD})\mathcal{L}_{I_{Y_D}}(K_{SD}), \tag{1.18}$$

and

$$\mathbb{P}(O_{SR}^{C}) = N_{SR}\mathcal{L}_{I_{X_R}}(K_{SR})\mathcal{L}_{I_{Y_R}}(K_{SR}). \tag{1.19}$$

Lemma 1. *The outage probability* $\mathbb{P}(O_{SR}^{C} \cap O_{SD}^{C})$ *is given by*

$$\begin{aligned}\mathbb{P}(O_{SR}^{C} \cap O_{SD}^{C}) &= N_{SR}N_{SD}\mathbb{E}_{I_X}\Big[\exp(-K_{SR}I_{X_R} - K_{SD}I_{X_D})\Big] \\ &\quad \times \mathbb{E}_{I_Y}\Big[\exp(-K_{SR}I_{Y_R} - K_{SD}I_{Y_D})\Big].\end{aligned} \tag{1.20}$$

Proof: See Appendix A.1. ■

Lemma 2. *The outage probability, when using SC, denoted* $\mathbb{P}(O_{SR}^{C} \cap O_{RD})$*, is expressed as*

$$\begin{aligned}\mathbb{P}(O_{SR}^{C} \cap O_{RD}) &= N_{SR}\mathbb{E}_{I_X}\Big[\exp(-K_{SR}I_{X_R})\Big]\mathbb{E}_{I_Y}\Big[\exp(-K_{SR}I_{Y_R})\Big] \\ &\quad - N_{SR}N_{RD}\mathbb{E}_{I_X}\Big[\exp(-K_{SR}I_{X_R} - K_{RD}I_{X_D})\Big] \\ &\quad \times \mathbb{E}_{I_Y}\Big[\exp(-K_{SR}I_{Y_R} - K_{RD}I_{Y_D})\Big].\end{aligned} \tag{1.21}$$

Proof: See Appendix A.2 ■

Lemma 3. *The outage probability, when using MRC, denoted* $\mathbb{P}(O_{SR}^{C} \cap O_{SRD})$ *is given by*

$$\begin{aligned}\mathbb{P}(O_{SR}^{C} \cap O_{SRD}) &= N_{SR}\mathbb{E}_{I_X}\Big[\exp(-K_{SR}I_{X_R})\Big]\mathbb{E}_{I_Y}\Big[\exp(-K_{SR}I_{Y_R})\Big] \\ &\quad - \frac{N_{SR}N_{RD}l_{RD}}{l_{RD} - l_{SD}}\mathbb{E}_{I_X}\Big[\exp(-K_{SR}I_{X_R} - K_{RD}I_{X_D})\Big] \\ &\quad \times \mathbb{E}_{I_Y}\Big[\exp(-K_{SR}I_{Y_R} - K_{RD}I_{Y_D})\Big] \\ &\quad + \frac{N_{SR}N_{SD}l_{SD}}{l_{RD} - l_{SD}}\mathbb{E}_{I_X}\Big[\exp(-K_{SR}I_{X_R} - K_{SD}I_{X_D})\Big] \\ &\quad \times \mathbb{E}_{I_Y}\Big[\exp(-K_{SR}I_{Y_R} - K_{SD}I_{Y_D})\Big].\end{aligned} \tag{1.22}$$

Proof: See Appendix A.3. ■

Note that the outage probability expressions derived before are expressed as a function

of the expectation with respect to I_X and I_Y. The expression of the expectation changes depending on the vehicles mobility models, i.e., the HSV and the LSV models.

Theorem 1. *The outage probability for the HSV model using SC and MRC is given by (1.15) and (1.16), where $\mathbb{P}(O_{SR} \cap O_{SD})$ is given by*

$$\begin{aligned}\mathbb{P}(O_{SR} \cap O_{SD}) &= 1 - N_{SD}\mathcal{L}_{I_{X_D}}(K_{SD})\mathcal{L}_{I_{Y_D}}(K_{SD}) - N_{SR}\mathcal{L}_{I_{X_R}}(K_{SR})\mathcal{L}_{I_{Y_R}}(K_{SR}) \\ &\quad + N_{SR}N_{SD}\mathcal{L}_{I_{X_R}}(K_{SR})\mathcal{L}_{I_{Y_R}}(K_{SR})\mathcal{L}_{I_{X_D}}(K_{SD})\mathcal{L}_{I_{Y_D}}(K_{SD}), \quad (1.23)\end{aligned}$$

and the probability $\mathbb{P}(O_{SR}^C \cap O_{RD})$ and $\mathbb{P}(O_{SR}^C \cap O_{SRD})$ in (1.15) and (1.16) are respectively expressed by

$$\begin{aligned}\mathbb{P}(O_{SR}^C \cap O_{RD}) &= N_{SR}\mathcal{L}_{I_{X_R}}(K_{SR})\mathcal{L}_{I_{Y_R}}(K_{SR}) \\ &\quad - N_{SR}N_{RD}\mathcal{L}_{I_{X_R}}(K_{SR})\mathcal{L}_{I_{Y_R}}(K_{SR})\mathcal{L}_{I_{X_D}}(K_{RD})\mathcal{L}_{I_{Y_D}}(K_{RD}), \quad (1.24)\end{aligned}$$

and

$$\begin{aligned}\mathbb{P}(O_{SR}^C \cap O_{SRD}) &= N_{SR}\mathcal{L}_{I_{X_R}}(K_{SR})\mathcal{L}_{I_{Y_R}}(K_{SR}) \\ &\quad - \frac{N_{SR}N_{RD}l_{RD}}{l_{RD} - l_{SD}}\mathcal{L}_{I_{X_R}}(K_{SR})\mathcal{L}_{I_{Y_R}}(K_{SR})\mathcal{L}_{I_{X_D}}(K_{RD})\mathcal{L}_{I_{Y_D}}(K_{RD}) \\ &\quad + \frac{N_{SR}N_{SD}l_{SD}}{l_{RD} - l_{SD}}\mathcal{L}_{I_{X_R}}(K_{SR})\mathcal{L}_{I_{Y_R}}(K_{SR})\mathcal{L}_{I_{X_D}}(K_{SD})\mathcal{L}_{I_{Y_D}}(K_{SD}). \\ &\quad (1.25)\end{aligned}$$

Proof: See Appendix A.4. ■

Theorem 2. *The outage probability for the LSV model using SC and MRC is given by*

(1.15) and (1.16), $\mathbb{P}(O_{SR} \cap O_{SD})$ *is given by*

$$\begin{aligned}\mathbb{P}(O_{SR} \cap O_{SD}) &= 1 - N_{SD}\mathcal{L}_{I_{X_D}}(K_{SD})\mathcal{L}_{I_{Y_D}}(K_{SD}) - N_{SR}\mathcal{L}_{I_{X_R}}(K_{SR})\mathcal{L}_{I_{Y_R}}(K_{SR}) \\ &\quad + N_{SR}N_{SD}\mathcal{L}_{I_{X_R}}(K_{SR})\mathcal{L}_{I_{X_D}}(K_{SD})\mathcal{L}_{I_{X_R},I_{X_D}}(K_{SR},K_{SD}) \\ &\quad \times \mathcal{L}_{I_{Y_R},I_{Y_D}}(K_{SR},K_{SD}), \end{aligned} \tag{1.26}$$

and the probability $\mathbb{P}(O_{SR}^C \cap O_{RD})$ *and* $\mathbb{P}(O_{SR}^C \cap O_{SRD})$ *in (1.15) and (1.16) are respectively given by*

$$\begin{aligned}\mathbb{P}(O_{SR}^C \cap O_{RD}) &= N_{SR}\mathcal{L}_{I_{X_R}}(K_{SR})\mathcal{L}_{I_{Y_R}}(K_{SR}) \\ &\quad - N_{SR}N_{RD}\mathcal{L}_{I_{X_R},I_{X_D}}(K_{SR},K_{RD})\mathcal{L}_{I_{Y_R},I_{Y_D}}(K_{SR},K_{RD}), \end{aligned} \tag{1.27}$$

and

$$\begin{aligned}\mathbb{P}(O_{SR}^C \cap O_{SRD}) &= N_{SR}\mathcal{L}_{I_{X_R}}(K_{SR})\mathcal{L}_{I_{Y_R}}(K_{SR}) \\ &\quad - \frac{N_{SR}N_{RD}l_{RD}}{l_{RD}-l_{SD}}\mathcal{L}_{I_{X_R},I_{X_D}}(K_{SR},K_{RD})\mathcal{L}_{I_{Y_R},I_{Y_D}}(K_{SR},K_{RD}) \\ &\quad + \frac{N_{SR}N_{SD}l_{SD}}{l_{RD}-l_{SD}}\mathcal{L}_{I_{X_R},I_{X_D}}(K_{SR},K_{SD})\mathcal{L}_{I_{Y_R},I_{Y_D}}(K_{SR},K_{SD}), \end{aligned} \tag{1.28}$$

where

$$\mathcal{L}_{I_{X_R},I_{X_D}}(s,b) = \mathcal{L}_{I_{X_R}}(s)\mathcal{L}_{I_{X_D}}(b)\rho_X(s,b) \tag{1.29}$$

$$\mathcal{L}_{I_{Y_R},I_{Y_D}}(s,b) = \mathcal{L}_{I_{Y_R}}(s)\mathcal{L}_{I_{Y_D}}(b)\rho_Y(s,b) \tag{1.30}$$

$$\rho_X(s,b) = \exp\left(p\lambda_X \int_{\mathcal{B}} \frac{sbP^2 l_{Rx} l_{Dx}}{(1+sPl_{Rx})(1+bPl_{Dx})}dx\right) \tag{1.31}$$

$$\rho_Y(s,b) = \exp\left(p\lambda_Y \int_{\mathcal{B}} \frac{sbP^2 l_{Ry} l_{Dy}}{(1+sPl_{Ry})(1+bPl_{Dy})} dy\right). \tag{1.32}$$

Proof: See Appendix A.5. ■

The cross terms $\rho_X(s,b)$ and $\rho_Y(s,b)$ arise from the dependence between the interference at two locations (the relay and the destination). The integrals inside (1.31) and (1.32) can easily be calculated numerically with MATLAB software or Wolfram Mathematica. Closed form can be obtained for $\alpha = 2$ and $\alpha = 4$.

1.6. Outage Computation for Case Study 2

1.6.1. DT Outage Expression

We calculate the outage probability of DT between S and D. An outage event occurs when the signal-to-interference ratio (SIR) at D is below a given threshold. The SIR at D considering DT, denoted $\mathrm{SIR}_{\mathrm{DT}}$, is defined as

$$\mathrm{SIR}_{SD} \triangleq \frac{|h_{SD}|^2 l_{SD}}{I_{X_D} + I_{Y_D}}. \tag{1.33}$$

The outage event of DT is defined as

$$O_{(\mathbf{DT})} \triangleq [\mathrm{SIR}_{SD} < \Theta_1], \tag{1.34}$$

where $\Theta_1 = 2^{\rho} - 1$, and ρ is the target data rate.

The outage probability expression of DT, denoted $\mathbb{P}(O_{\mathrm{DT}})$, is given by

$$\mathbb{P}(O_{(\mathbf{DT})}) = 1 - \sum_{k=0}^{m-1} \frac{1}{k!} \left(-\frac{m\,\Theta_1}{\mu\, l_{SD}}\right)^k \sum_{n=0}^{k} \binom{k}{n} \frac{\mathrm{d}^{k-n}\mathcal{L}_{I_{X_D}}(\frac{m\,\Theta_1}{\mu\, l_{SD}})}{\mathrm{d}^{k-n}(\frac{m\,\Theta_1}{\mu\, l_{SD}})} \frac{\mathrm{d}^{n}\mathcal{L}_{I_{Y_D}}(\frac{m\,\Theta_1}{\mu\, l_{SD}})}{\mathrm{d}^{n}(\frac{m\,\Theta_1}{\mu\, l_{SD}})}. \tag{1.35}$$

Proof: See Appendix A.6. ■

1.6.2. RT Outage Expression

We calculate the outage probability of RT between S and D, with the help of R. The SIR at R, denoted SIR_{SR}, is defined as

$$\mathrm{SIR}_{SR} \triangleq \frac{|h_{SR}|^2 l_{SR}}{I_{X_R} + I_{Y_R}}. \tag{1.36}$$

Similarly, the SIR at D, denoted SIR_{RD}, is defined as

$$\mathrm{SIR}_{RD} \triangleq \frac{|h_{RD}|^2 l_{RD}}{I_{X_D} + I_{Y_D}}. \tag{1.37}$$

The outage event related to the first phase, and related to the second phase are defined respectively as

$$O_{SR} \triangleq \Big[\mathrm{SIR}_{SR} < \Theta_2\Big], \tag{1.38}$$

and

$$O_{RD} \triangleq \Big[\mathrm{SIR}_{RD} < \Theta_2\Big], \tag{1.39}$$

where $\Theta_2 = 2^{2\rho} - 1$.

Remark. *The target data rate ρ is multiplied by the term 2, because RT requires two phases to transmit the message.*

The outage event related to RT is defined as

$$O_{\mathbf{(RT)}} \triangleq \Big[O_{SR} \cup O_{RD}\Big]. \tag{1.40}$$

The outage probability expression of RT, denoted $\mathbb{P}(O_{\mathbf{(RT)}})$, is given by

$$\begin{aligned}\mathbb{P}(O_{\mathbf{(RT)}}) \;=\; & 1-\sum_{k=0}^{m-1}\sum_{l=0}^{m-1}\frac{1}{k!}\frac{1}{l!}\,(-\frac{m\,\Theta_2}{\mu\,l_{SR}})^k(-\frac{m\,\Theta_2}{\mu\,l_{RD}})^l \\ & \times\sum_{n=0}^{k}\sum_{f=0}^{l}\binom{k}{n}\binom{l}{f}\frac{\mathrm{d}^{k-n}\mathcal{L}_{I_{X_R}}(\frac{m\,\Theta_2}{\mu\,l_{SR}})}{\mathrm{d}^{k-n}(\frac{m\,\Theta_2}{\mu\,l_{SR}})}\frac{\mathrm{d}^{n}\mathcal{L}_{I_{Y_R}}(\frac{m\,\Theta_2}{\mu\,l_{SR}})}{\mathrm{d}^{n}(\frac{m\,\Theta_2}{\mu\,l_{SR}})} \\ & \times\frac{\mathrm{d}^{l-f}\mathcal{L}_{I_{X_D}}(\frac{m\,\Theta_2}{\mu\,l_{RD}})}{\mathrm{d}^{l-f}(\frac{m\,\Theta_2}{\mu\,l_{RD}})}\frac{\mathrm{d}^{f}\mathcal{L}_{I_{Y_D}}(\frac{m\,\Theta_2}{\mu\,l_{RD}})}{\mathrm{d}^{f}(\frac{m\,\Theta_2}{\mu\,l_{RD}})}. \end{aligned} \tag{1.41}$$

Proof: See Appendix A.7. ■

1.6.3. HT Outage Expression

We calculate the outage probability of HT between S and D, with the help of R. The outage event of HT is defined as [TJJ13; Alt+14; LTW04]

$$O_{\mathbf{(HT)}} \triangleq [O_{SD}\cap O_{SR}]\cup[O_{SR}^{C}\cap O_{RD}], \tag{1.42}$$

where $O_{SD}\triangleq[\mathrm{SIR}_{SD}<\frac{\Theta_2}{2}]$. The outage probability expression is then given by

$$\mathbb{P}(O_{\mathbf{(HT)}}) = \mathbb{P}(O_{SD}\cap O_{SR}) + \mathbb{P}(O_{SR}^{C}\cap O_{RD}), \tag{1.43}$$

where $\mathbb{P}(O_{SD} \cap O_{SR})$ and $\mathbb{P}(O_{SR}^{C} \cap O_{RD})$ are respectively given by

$$\begin{aligned}
\mathbb{P}(O_{SD} \cap O_{SR}) &= 1 - \sum_{k=0}^{m-1} \frac{1}{k!} \left(- \frac{m\,\Theta_2}{2\mu\, l_{SD}} \right)^k \\
&\quad \times \sum_{n=0}^{k} \binom{k}{n} \frac{\mathrm{d}^{k-n} \mathcal{L}_{I_{X_D}} \left(\frac{m\,\Theta_2}{2\mu\, l_{SD}} \right)}{\mathrm{d}^{k-n} \left(\frac{m\,\Theta_2}{2\mu\, l_{SD}} \right)} \frac{\mathrm{d}^{n} \mathcal{L}_{I_{Y_D}} \left(\frac{m\,\Theta_2}{2\mu\, l_{SD}} \right)}{\mathrm{d}^{n} \left(\frac{m\,\Theta_2}{2\mu\, l_{SD}} \right)} \\
&\quad - \sum_{k=0}^{m-1} \frac{1}{k!} \left(- \frac{m\,\Theta_2}{\mu\, l_{SR}} \right)^k \sum_{n=0}^{k} \binom{k}{n} \frac{\mathrm{d}^{k-n} \mathcal{L}_{I_{X_R}} \left(\frac{m\,\Theta_2}{\mu\, l_{SR}} \right)}{\mathrm{d}^{k-n} \left(\frac{m\,\Theta_2}{\mu\, l_{SR}} \right)} \frac{\mathrm{d}^{n} \mathcal{L}_{I_{Y_R}} \left(\frac{m\,\Theta_2}{\mu\, l_{SR}} \right)}{\mathrm{d}^{n} \left(\frac{m\,\Theta_2}{\mu\, l_{SR}} \right)} \\
&\quad + \sum_{k=0}^{m-1} \sum_{l=0}^{m-1} \frac{1}{k!} \frac{1}{l!} \left(- \frac{m\,\Theta_2}{2\mu\, l_{SD}} \right)^k \left(- \frac{m\,\Theta_2}{\mu\, l_{SR}} \right)^l \\
&\quad \sum_{n=0}^{k} \sum_{f=0}^{l} \binom{k}{n} \binom{l}{f} \frac{\mathrm{d}^{k-n} \mathcal{L}_{I_{X_D}} \left(\frac{m\,\Theta_2}{2\mu\, l_{SD}} \right)}{\mathrm{d}^{k-n} \left(\frac{m\,\Theta_2}{2\mu\, l_{SD}} \right)} \frac{\mathrm{d}^{n} \mathcal{L}_{I_{Y_D}} \left(\frac{m\,\Theta_2}{2\mu\, l_{SD}} \right)}{\mathrm{d}^{n} \left(\frac{m\,\Theta_2}{2\mu\, l_{SD}} \right)} \\
&\quad \times \frac{\mathrm{d}^{l-f} \mathcal{L}_{I_{X_R}} \left(\frac{m\,\Theta_2}{\mu\, l_{SR}} \right)}{\mathrm{d}^{l-f} \left(\frac{m\,\Theta_2}{\mu\, l_{SR}} \right)} \frac{\mathrm{d}^{f} \mathcal{L}_{I_{Y_R}} \left(\frac{m\,\Theta_2}{\mu\, l_{SR}} \right)}{\mathrm{d}^{f} \left(\frac{m\,\Theta_2}{\mu\, l_{SR}} \right)}, \qquad (1.44)
\end{aligned}$$

and

$$\begin{aligned}
\mathbb{P}(O_{SR}^{C} \cap O_{RD}) &= \sum_{k=0}^{m-1} \frac{1}{k!} \left(- \frac{m\,\Theta_2}{\mu\, l_{SR}} \right)^k \sum_{n=0}^{k} \binom{k}{n} \frac{\mathrm{d}^{k-n} \mathcal{L}_{I_{X_R}} \left(\frac{m\,\Theta_2}{\mu\, l_{SR}} \right)}{\mathrm{d}^{k-n} \left(\frac{m\,\Theta_2}{\mu\, l_{SR}} \right)} \frac{\mathrm{d}^{n} \mathcal{L}_{I_{Y_R}} \left(\frac{m\,\Theta_2}{\mu\, l_{SR}} \right)}{\mathrm{d}^{n} \left(\frac{m\,\Theta_2}{\mu\, l_{SR}} \right)} \\
&\quad \times \sum_{k=0}^{m-1} \sum_{l=0}^{m-1} \frac{1}{k!} \frac{1}{l!} \left(- \frac{m\,\Theta_2}{\mu\, l_{SR}} \right)^k \left(- \frac{m\,\Theta_2}{\mu\, l_{RD}} \right)^l \\
&\quad \times \sum_{n=0}^{k} \sum_{f=0}^{l} \binom{k}{n} \binom{l}{f} \frac{\mathrm{d}^{k-n} \mathcal{L}_{I_{X_R}} \left(\frac{m\,\Theta_2}{\mu\, l_{SR}} \right)}{\mathrm{d}^{k-n} \left(\frac{m\,\Theta_2}{\mu\, l_{SR}} \right)} \frac{\mathrm{d}^{n} \mathcal{L}_{I_{Y_R}} \left(\frac{m\,\Theta_2}{\mu\, l_{SR}} \right)}{\mathrm{d}^{n} \left(\frac{m\,\Theta_2}{\mu\, l_{SR}} \right)} \\
&\quad \times \frac{\mathrm{d}^{l-f} \mathcal{L}_{I_{X_D}} \left(\frac{m\,\Theta_2}{\mu\, l_{RD}} \right)}{\mathrm{d}^{l-f} \left(\frac{m\,\Theta_2}{\mu\, l_{RD}} \right)} \frac{\mathrm{d}^{f} \mathcal{L}_{I_{Y_D}} \left(\frac{m\,\Theta_2}{\mu\, l_{RD}} \right)}{\mathrm{d}^{f} \left(\frac{m\,\Theta_2}{\mu\, l_{RD}} \right)}. \qquad (1.45)
\end{aligned}$$

Proof: See Appendix A.8. ■

1.7. Laplace Transform Expressions

1.7.1. The Receiving Node is Anywhere on the Plan (Infrastructure)

After we obtained the expressions of the outage probability, we derive, in this section, the Laplace transform expressions of the interference originated from the X road and from the Y road. We compute the Laplace transform expression when the interference are originated from vehicles in finite road segments ($\mathcal{B} = [-Z, Z]$), and in infinite road segments ($\mathcal{B} = \mathbb{R}$). As mentioned in the previous section, joint Laplace transforms can be expressed as the product of two Laplace transforms and a cross term.

The Laplace transform of the interference originated from the X road at the received node denoted T, is expressed as

$$\mathcal{L}_{I_{X_T}}(s) = \exp\left(- p\lambda_X \int_{\mathcal{B}} \frac{1}{1 + (A\|x - T\|^{\alpha})/sP} dx \right), \tag{1.46}$$

where

$$\|x - T\| = \sqrt{\left(t\sin(\theta_T)\right)^2 + \left(x - t\cos(\theta_T)\right)^2}. \tag{1.47}$$

The Laplace transform of the interference originated from the Y road is given by

$$\mathcal{L}_{I_{Y_T}}(s) = \exp\left(- p\lambda_Y \int_{\mathcal{B}} \frac{1}{1 + (A\|y - T\|^{\alpha})/sP} dy \right), \tag{1.48}$$

where

$$\|y - T\| = \sqrt{\left(t\cos(\theta_T)\right)^2 + \left(y - t\sin(\theta_T)\right)^2}. \tag{1.49}$$

The notations t and θ_T denote the distance between the node T and the intersection, and the angle between the node T and the X road, respectively.

The expressions (1.46) and (1.48) can easily be calculated numerically with mathematical software such as MATLAB or Mathematica. Closed form can be obtained for $\alpha = 2$ and $\alpha = 4$ when $\mathcal{B} = \mathbb{R}$, and $\mathcal{B} = [-Z, Z]$.

Proposition 1. *The Laplace transform expressions of the interference at the node N for an intersection scenario, when* $\mathcal{B} = \mathbb{R}$, *and when* $\alpha = 2$ *are given by*

$$\mathcal{L}_{I_{X_T}}(s) = \exp\left(- p\lambda_X \frac{sP}{A^2} \frac{\pi}{\sqrt{\left(t\sin(\theta_T)\right)^2 + sP/A^2}}\right), \tag{1.50}$$

and

$$\mathcal{L}_{I_{Y_T}}(s) = \exp\left(- p\lambda_Y \frac{sP}{A^2} \frac{\pi}{\sqrt{\left(t\cos(\theta_T)\right)^2 + sP/A^2}}\right). \tag{1.51}$$

Proof: See Appendix A.9. ■

Proposition 2. *The Laplace transform expressions of the interference at the node T for an intersection scenario, when* $\mathcal{B} = [-Z, Z]$ *and when* $\alpha = 2$ *are given by*

$$\mathcal{L}_{I_{X_T}}(s) = \exp\big(- p\lambda_X \Gamma_X(s)\big), \tag{1.52}$$

and

$$\mathcal{L}_{I_{Y_T}}(s) = \exp\big(- p\lambda_Y \Gamma_Y(s)\big), \tag{1.53}$$

where

$$\Gamma_X(s) = \frac{\arctan\left(\dfrac{Z + t_x}{\sqrt{t_y^2 + sP/A^2}}\right) + \arctan\left(\dfrac{Z - t_x}{\sqrt{t_y^2 + sP/A^2}}\right)}{\dfrac{A^2}{sP}\sqrt{t_y^2 + \dfrac{sP}{A^2}}}, \tag{1.54}$$

and

$$\Gamma_Y(s) = \frac{\arctan\left(\dfrac{Z + t_y}{\sqrt{t_x^2 + sPA^2}}\right) + \arctan\left(\dfrac{Z - t_y}{\sqrt{t_x^2 + sPA^2}}\right)}{\dfrac{A^2}{sP}\sqrt{t_x^2 + \dfrac{sP}{A^2}}}. \tag{1.55}$$

Proof: See Appendix A.10. ■

It is worth noting that the expression of (1.50) does not depend on $t\cos(\theta_T)$, that is t_x. Similarly, (1.51) does not depend on $t\sin(\theta_T)$, that is t_y. However, one can notice that (1.54) and (1.55) both depend on t_x and on t_y. This can be explained by the fact that, as interferers tend to infinity, the term $(x - t_x)$ tends to x and $(y - t_y)$ tends to y, that is $\lim_{x\to\infty}(x - t_x) \longrightarrow x$, and $\lim_{x\to\infty}(y - t_y) \longrightarrow y$. This is no longer the case when the interferers are on finite road segments. In this case, the result depends on t_x and on t_y.

When $\sigma^2 = 0$, the expressions of $\mathcal{L}_{I_{X_T}}(s)$ and $\mathcal{L}_{I_{Y_T}}(s)$ at the node T, when $\alpha = 2$ are given respectively by

$$\mathcal{L}_{I_{X_T}}(s) = \exp\left(- p\lambda_X \frac{s\pi}{\sqrt{\left[d\sin(\theta_T)\right]^2 + s}}\right), \tag{1.56}$$

and

$$\mathcal{L}_{I_{Y_T}}(s) = \exp\left(- p\lambda_Y \frac{s\pi}{\sqrt{\left[d\cos(\theta_T)\right]^2 + s}}\right). \tag{1.57}$$

The expressions of $\mathcal{L}_{I_{X_T}}(s)$ at the node D, when $\alpha = 4$ is given by

$$\mathcal{L}_{I_{X_T}}(s) = \exp\Big(- p\lambda_X \pi \mathcal{V}_x(s)\Big), \tag{1.58}$$

where

$$\mathcal{V}_x(s) = \frac{\sqrt{2\sqrt{(t\sin(\theta_T)^4 + s} + 2(t\sin(\theta_T)^2}}{2\sqrt{(t\sin(\theta_T)^4 + s}} \times \sqrt{(t\sin(\theta_T))^4 + s} - (t\sin(\theta_T))^2. \tag{1.59}$$

The expressions of $\mathcal{L}_{I_{Y_T}}(s)$ at the node D, when $\alpha = 4$ is given by

$$\mathcal{L}_{I_{Y_T}}(s) = \exp\Big(- p\lambda_Y \pi \mathcal{V}_y(s)\Big), \tag{1.60}$$

where

$$\mathcal{V}_y(s) = \frac{\sqrt{2\sqrt{(t\cos(\theta_T)^4 + s} + 2(t\cos(\theta_T)^2}}{2\sqrt{(t\cos(\theta_T)^4 + s}} \times \sqrt{(t\cos(\theta_T)^4 + s} - (t\cos(\theta_T))^2. \quad (1.61)$$

Proof: See Appendix A.9. ■

The expression of $\mathrm{d}^{k-n}\mathcal{L}_{I_{X_T}}(s)/\mathrm{d}^{k-n}(s)$ and $\mathrm{d}^{n}\mathcal{L}_{I_{Y_T}}(s)/\mathrm{d}^{n}(s)$, when $\alpha = 2$, are given respectively by

$$\begin{aligned}\frac{\mathrm{d}^{k-n}\mathcal{L}_{I_{X_T}}(s)}{\mathrm{d}^{k-n}s} &= \left[-\frac{p\lambda_X\pi}{\sqrt{t^2\sin(\theta_T)^2+s}} + \frac{1}{2}\frac{p\lambda_X\pi s}{(t^2\sin(\theta_T)^2+s)^{3/2}}\right]^{k-n} \\ &\quad \times \exp\left(-\frac{p\lambda_X\pi s}{\sqrt{t^2\sin(\theta_T)^2+s}}\right), \end{aligned} \quad (1.62)$$

and

$$\begin{aligned}\frac{\mathrm{d}^{n}\mathcal{L}_{I_{Y_T}}(s)}{\mathrm{d}^{n}s} &= \left[-\frac{p\lambda_Y\pi}{\sqrt{t^2\cos(\theta_T)^2+s}} + \frac{1}{2}\frac{p\lambda_Y\pi s}{(t^2\cos(\theta_T)^2+s)^{3/2}}\right]^{n} \\ &\quad \times \exp\left(-\frac{p\lambda_Y\pi s}{\sqrt{t^2\cos(\theta_T)^2+s}}\right). \end{aligned} \quad (1.63)$$

The expression of $\mathrm{d}^{k-n}\mathcal{L}_{I_{X_T}}(s)/\mathrm{d}^{k-n}(s)$ and $\mathrm{d}^{n}\mathcal{L}_{I_{Y_T}}(s)/\mathrm{d}^{n}(s)$ when $\alpha = 4$ are given re-

spectively by

$$\frac{\mathrm{d}^{k-n}\mathcal{L}_{I_{X_T}}(s)}{\mathrm{d}^{k-n}s} =$$
$$\Bigg[-\frac{1}{4}\frac{p\lambda_X\pi(\sqrt{t^4\sin(\theta_T)^4+s}-t^2\sin(\theta_T)^2)}{\sqrt{2\sqrt{t^4\sin(\theta_T)^4+s}+2t^2\sin(\theta_T)^2}(t^4\sin(\theta_T)^4+s)}$$
$$-\frac{1}{4}\frac{p\lambda_X\pi\sqrt{2\sqrt{t^4\sin(\theta_T)^4+s}+2t^2\sin(\theta_T)^2}}{t^4\sin(\theta_T)^4+s}$$
$$+\frac{1}{4}\frac{p\lambda_X\pi\sqrt{2\sqrt{t^4\sin(\theta_T)^4+s}+2t^2\sin(\theta_T)^2}(\sqrt{t^4\sin(\theta_T)^4+s}-t^2\sin(\theta_T)^2)}{(t^4\sin(\theta_T)^4+s)^{3/2}}\Bigg]^{k-n}$$
$$\times\exp\left(-\frac{1}{2}\frac{p\lambda_X\pi\sqrt{2\sqrt{t^4\sin(\theta_T)^4+s}+2t^2\sin(\theta_T)^2}}{\sqrt{t^4\sin(\theta_T)^4+s}}\times\sqrt{t^4\sin(\theta_T)^4+s}-t^2\sin(\theta_T)^2\right),\tag{1.64}$$

and

$$\frac{\mathrm{d}^{n}\mathcal{L}_{I_{Y_T}}(s)}{\mathrm{d}^{n}s} =$$
$$\Bigg[-\frac{1}{4}\frac{p\lambda_Y\pi(\sqrt{t^4\cos(\theta_T)^4+s}-t^2\cos(\theta_T)^2)}{\sqrt{2\sqrt{t^4\cos(\theta_T)^4+s}+2t^2\cos(\theta_T)^2}(t^4\cos(\theta_T)^4+s)}$$
$$-\frac{1}{4}\frac{p\lambda_Y\pi\sqrt{2\sqrt{t^4\cos(\theta_T)^4+s}+2t^2\cos(\theta_T)^2}}{t^4\cos(\theta_T)^4+s}$$
$$+\frac{1}{4}\frac{p\lambda_Y\pi\sqrt{2\sqrt{t^4\cos(\theta_T)^4+s}+2t^2\cos(\theta_T)^2}(\sqrt{t^4\cos(\theta_T)^4+s}-t^2\cos(\theta_T)^2)}{(t^4\cos(\theta_T)^4+s)^{3/2}}\Bigg]^{n}$$
$$\times\exp\left(-\frac{1}{2}\frac{p\lambda_Y\pi\sqrt{2\sqrt{t^4\cos(\theta_T)^4+s}+2t^2\cos(\theta_T)^2}}{\sqrt{t^4\cos(\theta_T)^4+s}}\times\sqrt{t^4\cos(\theta_T)^4+s}-t^2\cos(\theta_T)^2\right).\tag{1.65}$$

1.7.2. The Receiving Node is on the Road (Vehicle)

When the receiving node is on the road, the Laplace transform expression can be obtained by substituting $\theta_T = 0$ or $\theta_T = \pi$ in (1.56), (1.57), (1.58) and (1.60), when the receiving

node is on the X road. The Laplace transform expression can be obtained by substituting $\theta_T = \pi/2$ or $\theta_T = 3\pi/2$ (1.56), (1.57), (1.58) and (1.60), when the receiving node is on the Y road.

The expression of $\mathcal{L}_{I_{X_T}}(s)$ and $\mathcal{L}_{I_{Y_T}}(s)$, when $\alpha = 2$, are given respectively by

$$\mathcal{L}_{I_{X_T}}(s) = \exp\left(-p\lambda_X \pi\sqrt{s}\right)\Big\{T \in \mathrm{X}\Big\} + \exp\left(-\frac{p\lambda_X \pi s}{\sqrt{d^2+s}}\right)\Big\{T \in \mathrm{Y}\Big\}, \tag{1.66}$$

and

$$\mathcal{L}_{I_{Y_T}}(s) = \exp\left(-p\lambda_Y \pi\sqrt{s}\right)\Big\{T \in \mathrm{Y}\Big\} + \exp\left(-\frac{p\lambda_Y \pi s}{\sqrt{d^2+s}}\right)\Big\{T \in \mathrm{X}\Big\}. \tag{1.67}$$

The expression of $\mathcal{L}_{I_{X_T}}(s)$ and $\mathcal{L}_{I_{Y_T}}(s)$, when $\alpha = 4$, are given respectively by

$$\begin{aligned}\mathcal{L}_{I_{X_T}}(s) &= \exp\left(-\frac{p\lambda_X \pi\, s^{1/4}}{\sqrt{2}}\right)\mathbb{1}\Big\{T \in \mathrm{X}\Big\} \\ &\quad + \exp\left(-\frac{p\lambda_X \pi\sqrt{2\sqrt{t^4+s}+2t^2}\,(\sqrt{t^4+s}-t^2)}{2\sqrt{t^4+s}}\right)\mathbb{1}\Big\{T \in \mathrm{Y}\Big\},\end{aligned} \tag{1.68}$$

and

$$\begin{aligned}\mathcal{L}_{I_{Y_T}}(s) &= \exp\left(-\frac{p\lambda_Y \pi\, s^{1/4}}{\sqrt{2}}\right)\mathbb{1}\Big\{T \in \mathrm{Y}\Big\} \\ &\quad + \exp\left(-\frac{p\lambda_Y \pi\sqrt{2\sqrt{t^4+s}+2t^2}\,(\sqrt{t^4+s}-t^2)}{2\sqrt{t^4+s}}\right)\mathbb{1}\Big\{T \in \mathrm{X}\Big\}.\end{aligned} \tag{1.69}$$

1.8. Simulations and Discussions

1.8.1. Results of Case Study 1

In this section, we evaluate the performance of our model. In order to verify the accuracy of the theoretical results, Monte-Carlo simulations are obtained by averaging over 50,000

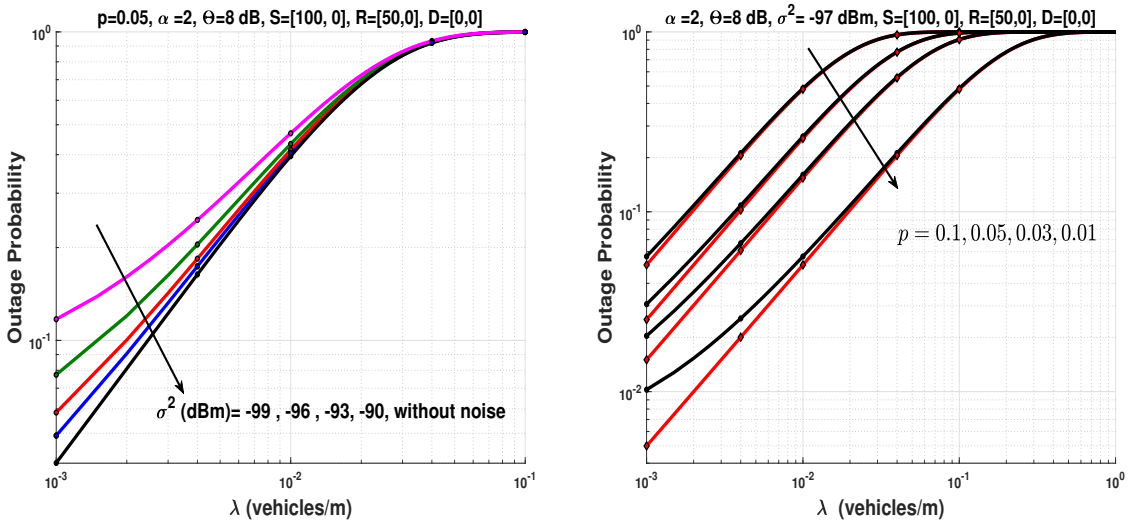

(a) (b)

Figure 1.9.: Outage probability when the vehicles intensity λ considering SC and the HSV model. (a) represents the outage probability for several values of noise power level. (b) represents the outage probability for several values of p with noise (circle), and without noise (diamond).

realizations of the PPPs and fading parameters. Unless stated otherwise, all the figures are plot for intersection scenarios. We also set $A = 650$ (we recall that A is a constant that depends on antenna characteristics), and the transmit power to $P = 120$ mW. Without loss of generality, we set $\lambda_X = \lambda_Y = \lambda$. The vehicles intensity λ can also be interpreted as the average distance between vehicles.

Fig.1.9(a) plots the outage probability for several values of noise power level when $p = 0.05$. For low interference level (low vehicle intensity), the noise becomes predominant, and thus degrades the performance. However, as the number of interfering vehicles increases, the noise becomes negligible. Fig.1.9(b) depicts the outage probability for several values of p when the noise power level is set to $\sigma^2 = -97$ dBm. We can notice that, as p increases, the performance of the outage with noise and without noise converge to the same values. This is because, as p increases, the power of interference increases accordingly, thus making the power of noise negligible compared the interference power, which corresponds to the

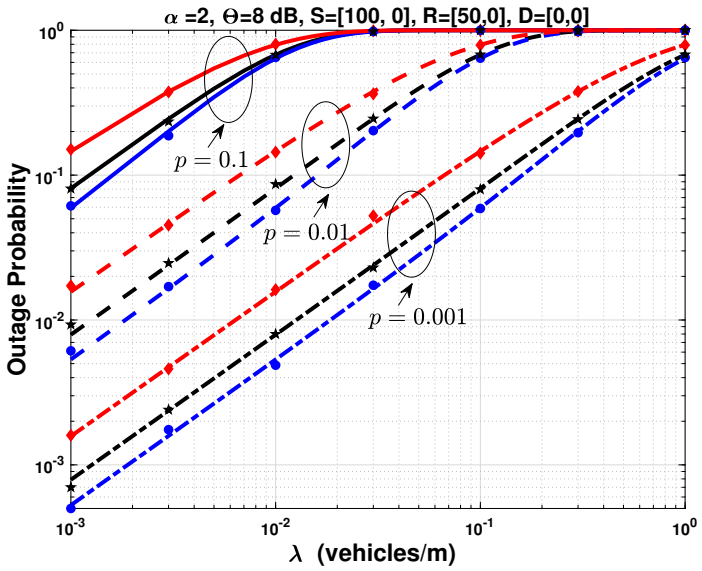

Figure 1.10.: Outage probability when varying λ for different values of p using the direct transmission scenario (diamond), and cooperative transmissions considering SC (star) and MRC (circle), for the HSV model.

interference limited scenario.

In the next figures, since we are mainly interested in the effect of the interference, we will consider only the interference limited scenario, that is, $\sigma^2 = 0$.

From Fig.1.10, we can make the following observations. First, we retrieve that MRC outperforms SC. Second, cooperative transmissions outperform the direct transmission, that is, the outage probability for a cooperative transmission is lower than the one for a direct transmission. The explanation of the second observation is that, when the direct transmission fails, i.e., the link S-D is in outage, it is unlikely that S-R and R-D are in outage too. Thus, the direct transmission is aided by the relaying paths S-R and R-D, and therefore the cooperative transmission always enhance the performance compared to the direct transmission. We notice that, for lower values of p, the outage probability decreases. This is because lower values of p mean lower probability for the vehicles to access the medium, leading to less interferers, and thus reducing the SINR and the outage probability. We can conclude

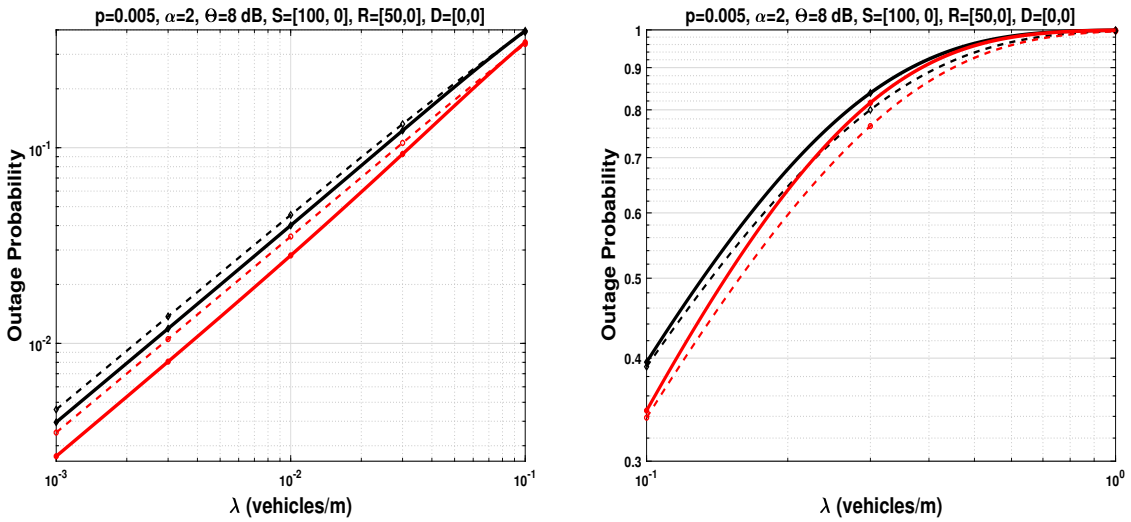

(a) Low traffic scenario

(b) High traffic scenario

Figure 1.11.: Outage probability as a function of λ considering SC (diamond), and MRC (circle), for the HSV model (simple line) and the LSV model (dashed line).

that vehicles should always cooperate in order to minimize the outage probability, and we confirm the superiority of MRC over SC. We study the effect of MRC in Fig.1.13.

We notice from Fig.1.11(a) that, for lower values of λ (low traffic conditions), the HSV model outperforms the LSV model. But we can notice from Fig.1.11(b), as the intensity of vehicles increases (high traffic conditions), the LSV model exhibits better performance. This is explained by the fact that the interference dependence (LSV) in high traffic is beneficial due to highly dependent hops of the relaying path. So, if the S-R link succeeded, it is likely to be the case of the R-D link. Thus, the interference dependence (LSV) leads to higher performance than in the presence of independent interference (HSV) in high traffic conditions, that is, when the number of transmitting vehicles increases [GH09]. In other words, in low traffic conditions, increasing the vehicle speed increases the outage performance, whereas in high traffic conditions, decreasing the vehicle speed increases the performance.

In Fig.1.12, we plot the throughput as a function of Θ, where the throughput $\mathcal{T}$ is defined

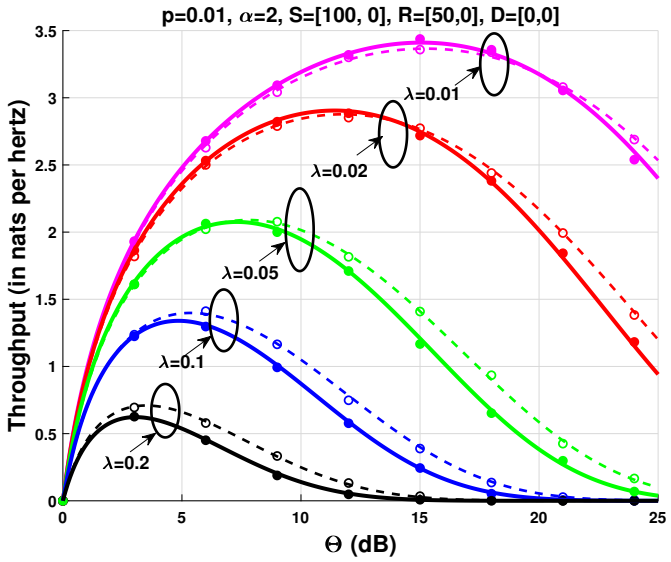

Figure 1.12.: Throughput as a function of Θ for different values of λ considering MRC, for the HSV model (simple line) and the LSV model (dashed line). Simulation results are represented with dots.

as follows

$$\mathcal{T} = \mathbb{P}(O^C)\log_2(1+\Theta),$$

where $\log_2(1+\Theta)$ is the Shannon bound (in nats pers hertz) and $\mathbb{P}(O^C)$ is the success probability [Hae09]. We can notice that in a high traffic scenario ($\lambda = 0.1,\ \lambda = 0.2$), the LSV model allows the highest throughput than the HSV model. This confirms what we concluded in Fig.1.11. We also notice that, in a low traffic scenario ($\lambda = 0.01,\ \lambda = 0.02$), the HSV model allows a slightly higher throughput than the LSV model. However, even for lower values of λ (low traffic), as Θ increases, the LSV model achieves a higher throughput that the HSV model. This is because, for larger values of Θ, in order to have an outage, a large number of vehicles have to transmit at the same time, hence, increases the traffic density.

Note that $\mathcal{T}$ is a function of $\log_2(1+\Theta)$ and $\mathbb{P}(O^C)$. When Θ increases, $\log_2(1+\Theta)$ increases whereas the success probability $\mathbb{P}(O^C)$ decreases. In one hand, we are tempted to

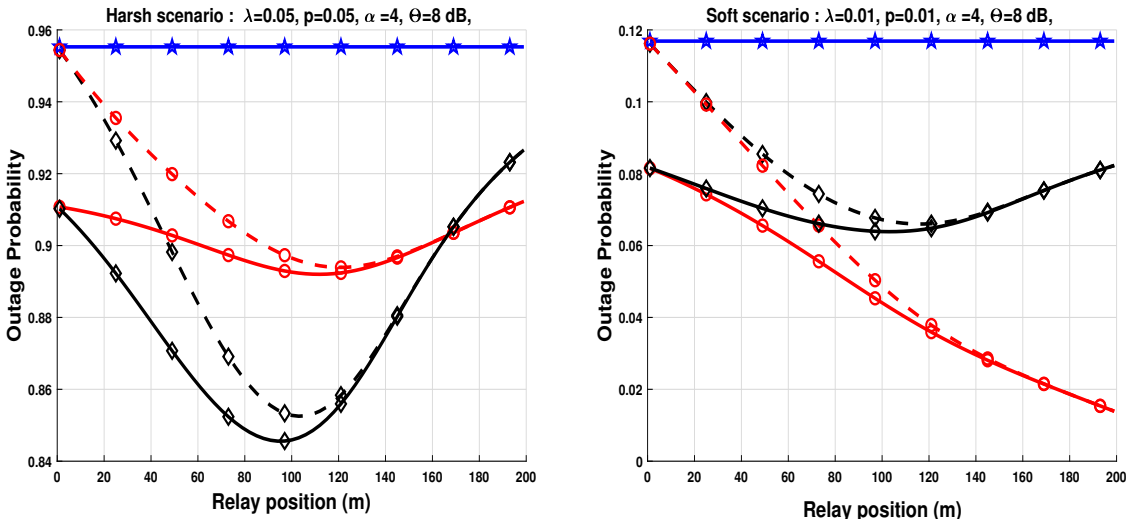

(a) High traffic scenario: $\lambda = 0.25$

(b) Low traffic scenario: $\lambda = 0.01$

Figure 1.13.: Outage probability as a function of the relay position, considering SC (dashed line), MRC (line) and the direct transmission (star), for the HSV model (circle) and the LSV model (diamond).

increase Θ to increase the rate; but, on the other hand, increasing Θ increases the outage probability. An optimal value of Θ must be carefully set in order to maximize the throughput under given traffic conditions and vehicles mobility.

In Fig.1.13, we plot the outage probability as a function of the relay position for a setting where $S = (0, 0)$ and $D = (200, 0)$. We can see from Fig.1.13(a) that the best relay position for the LSV model is in the middle of S and D, whereas the best relay position for the HSV model is slightly shifted from the middle toward D. We also can see from Fig.1.13(a) that, in high traffic scenarios, the LSV model achieves a better performance (as stated in Fig.1.11). However, when the relay is close to the destination, the HSV model has a better performance than the LSV model. This is because, in a high traffic scenario (harsh environment), the direct link S-D is more likely to be in outage, therefore when the relay is close to the destination, that is, $\|S - R\| \approx \|S - D\|$, the S-R link is more likely to be in outage due to highly dependent interference. Furthermore, as stated for Fig.1.11,

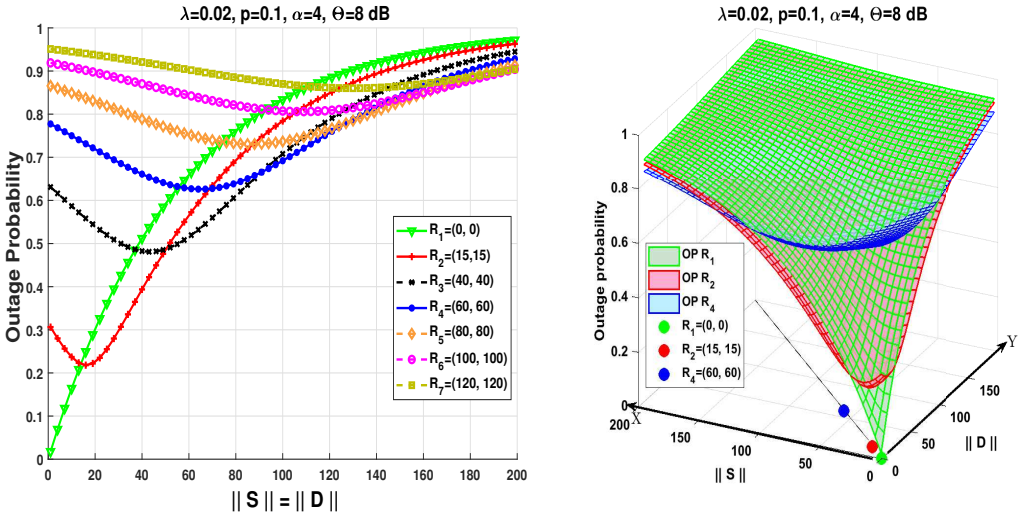

(a) 2D plot

(b) 3D plot

Figure 1.14.: Outage probability when varying the distance of the destination and the source from the intersection, denoted respectively $\|S\|$ and $\|D\|$ for several locations of the relay at the first bisector, in the LSV model. (a) represents the 2 dimensions plot, and (b) represents the 3 dimensions plot.

in low traffic scenario, the HSV model has a better performance than the LSV model. We can notice from Fig.1.13(b) that the best relay position for the HSV model is close to the destination whereas the best relay position for the LSV model is when the relay is equidistant from S and D. The explanation is as follow: in low traffic scenarios, the direct link has a high success probability in the presence of low interference level. However, in the HSV model, even if the direct link fails, it is less likely that the relay path fails too, since there is no dependence between interference. Hence, when the relay moves toward the destination, it increases the diversity gain and enhances the performance. This makes the best relay position in the HSV model close to the destination. However, in the LSV model, when the direct link fails, it is more likely that the relay path fails due to (low but still present) interference dependence. Hence, the best relay position is when the relay is equidistant from S and D.

Finally, we can notice, regardless of traffic conditions or vehicle speeds that, as the relay

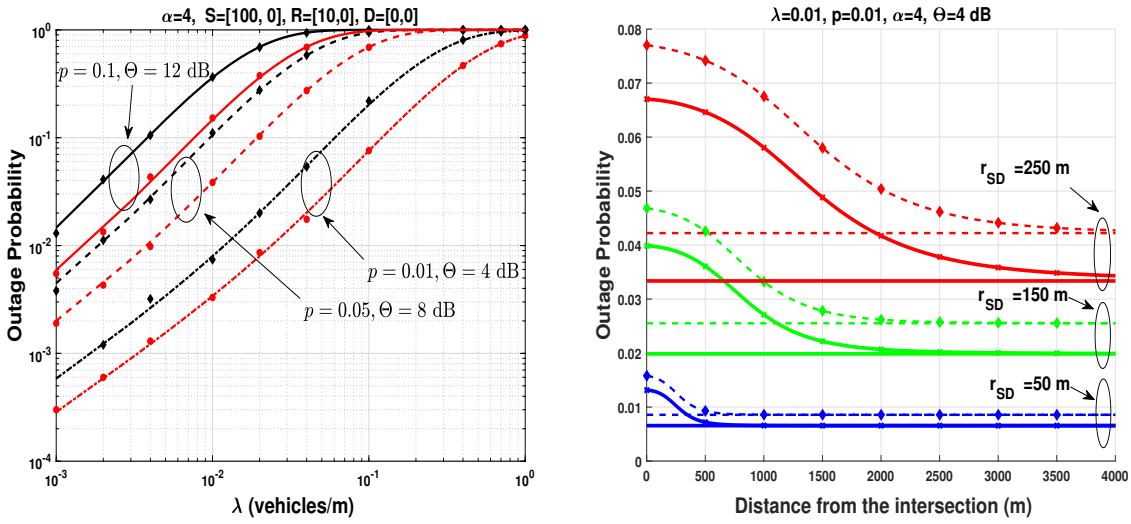

(a) (b)

Figure 1.15.: (a) Outage probability as function of λ for different values of p and Θ in a highway scenario (circle) and intersection scenario (diamond) considering MRC for the HSV model. Analytical results are plot with lines, and simulation results with marks.(b) Outage probability when varying the distance of the triplet $\{S, R, D\}$ from the intersection for different values of r_{SD}. The highway scenario (line without marks) and the intersection scenario (line with marks) are considered, for the HSV model (simple line) and the LSV model (dashed line).

moves closer to the destination, MRC and SC offer the same performance. This is because, when the relay is close to the destination, the power received at the destination from the source is much smaller than the power received from the relays ($l_{RD} \gg l_{SD}$). Thus, adding the power of *S-D* link does not add much power to the *R-D* link, which makes MRC and SC at the same level of performance. When the relay is closer to the source, the level of power received at the destination from source and from the relay is almost the same ($l_{RD} \approx l_{SD}$), which increases the diversity gain, leading to greater performance of MRC over SC.

The relay location plays an important role in the performance. This can be used in the relay-selection based algorithms, where vehicles have to take into account both the relays location and speeds (HSV or LSV). Regarding the decoding strategies, there is also a trade-off between performance and complexity to consider, because MRC is difficult to implement,

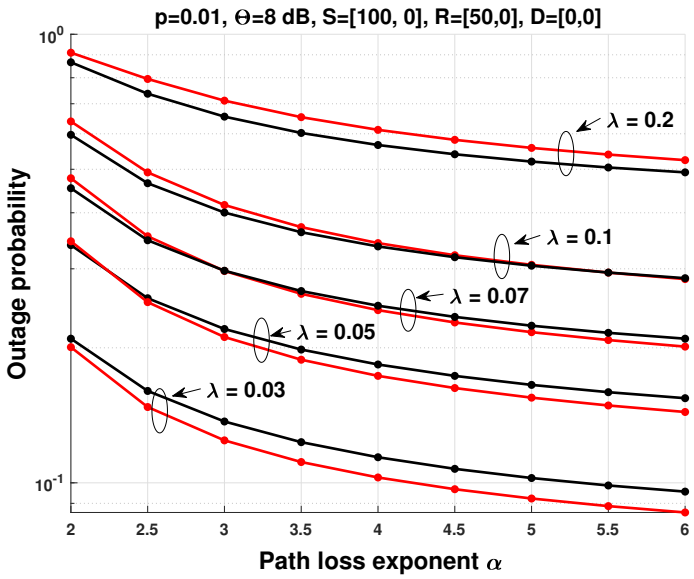

Figure 1.16.: Outage probability as a function of the path loss exponent α for $\lambda \in \{0.03, 0.05, 0.07, 0.1, 0.2\}$, for the HSV model (line) and the LSV model (dashed line) considering MRC.

and it is only beneficial when the relay is close to the source.

In Fig.1.14, we present analytical results when the relay is located on the first bisector. We plot the outage probability as a function of the distance of the source from the intersection, and the distance of the destination from the intersection, denoted respectively $\|S\|$ and $\|D\|$, in 2D in Fig.1.14(a), and in 3D in Fig.1.14(b). Without loss of generality, we set the source on the X road, and the destination on the Y road.

Since the relay is outside the roads, we can consider that it belongs to the roadside infrastructure. A roadside infrastructure with the coordinate $(0, 0)$ can be placed in the center of a roundabout, or mounted on a traffic light pole. We can notice that the outage probability reaches it minimum when the relay is the middle of S and D. We also notice that there is no need to use a relay that would be farther than the coordinate (60, 60) in terms of outage performance. Although there is a little bit of (but still negligible) gain when using R_3, we can state that using only 3 relays in 200 meters or above, offer the same performance than

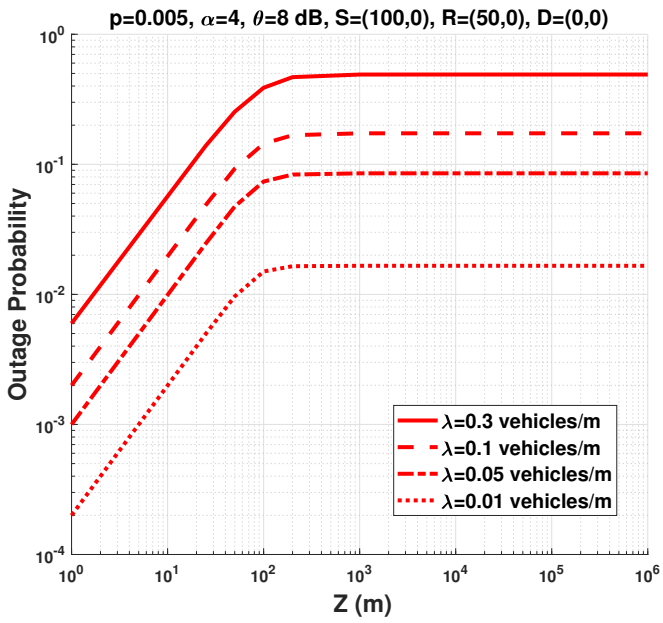

Figure 1.17.: Outage probability as a function of Z for several values of λ.

using 7 relays or more. In Fig.1.14(b), we only plot the outage probability when using the relay R_1, R_2 and R_4. We can notice that the relay R_1 covers the first [0,17 m] x [0,17 m], that is, 289 m^2 (300 m^2). The relay R_2 cover approximately 4600 m^2 (4611 m^2), and then the relay R_4 cover the rest, that is, more than 35000 m^2 (35389 m^2).

Fig.1.15(a) compares the outage probability of a cooperative highway scenario with a single lane [FEA16] and a cooperative intersection scenario with two orthogonal lanes. We can see from Fig.1.15 that the outage probability increases as λ, p and Θ increase (see Fig.1.10). One can notice that the highway scenario outperforms the intersection scenario in terms of outage probability. We infer that the intersection scenario has an additional lane that contributes to the aggregate of interference, therefore increasing the outage probability.

In Fig.1.15(b), we present the results for several values of r_{SD}, the relay is equidistant from the source and the destination. Without loss of generality, we set the triplet $\{S, R, D\}$ on the same road. We plot the outage probability as a function of the distance from the

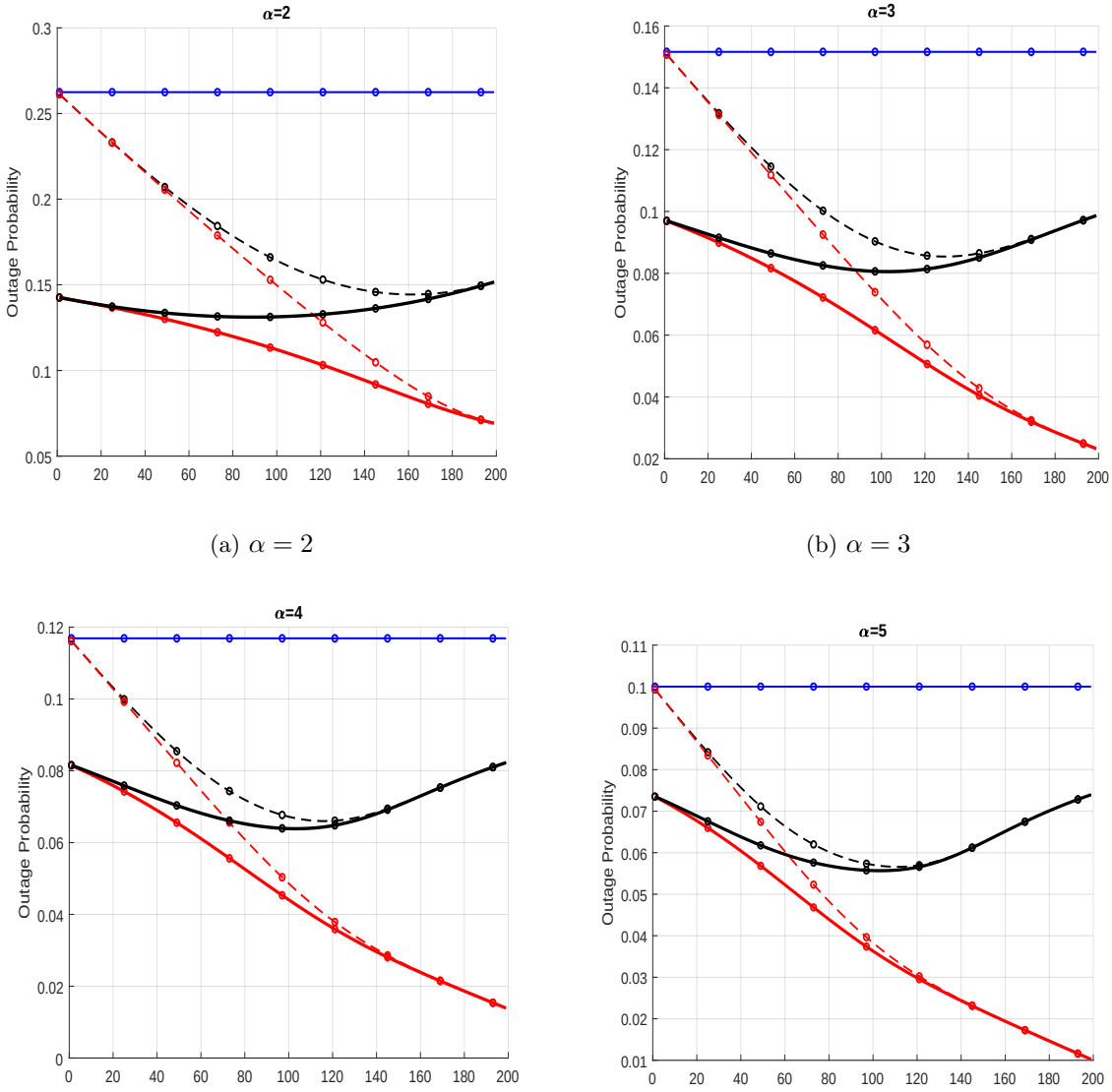

(a) $\alpha = 2$

(b) $\alpha = 3$

(c) $\alpha = 4$

(d) $\alpha = 5$

Figure 1.18.: Outage probability as a function of the relay position, considering SC (dashed line), MRC (line) and the direct transmission (star), for the HSV model (circle) and the LSV model (diamond) for several values of α.

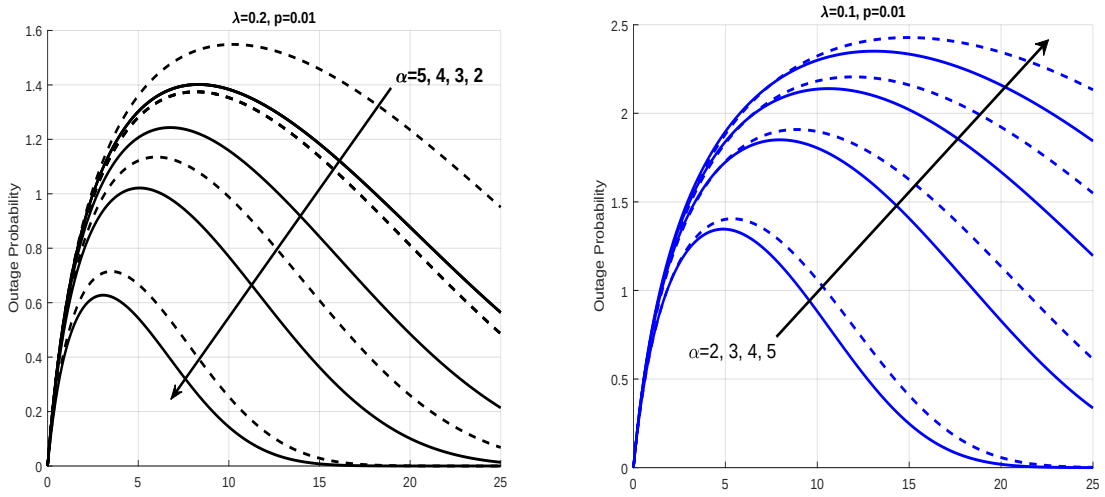

(a) (b)

Figure 1.19.: Throughput as a function of Θ for different values of α considering MRC, for the HSV model (simple line) and the LSV model (dashed line).

intersection for $r_{SD} \in \{50 \text{ m}, 150 \text{ m}, 250 \text{ m}\}$. As for the results in Fig.1.15(a), the highway scenario offers a better performance in terms of outage probability than the intersection scenario. But, as we increase the distance between the triplet and the intersection, the highway scenario and the intersection scenario converge toward the same value. This can be explained by the fact that, as vehicles move away from the intersection, the power of the interference originated from the other road becomes negligible, thus leading to the same performance as in a highway scenario.

This further confirms the statement that the intersection scenario has a higher outage probability compared to the highway scenario, thus making intersections more critical areas because they are more prone to outage.

From Fig.1.16, we see that, as α increases, the outage probability decreases, this is intuitive, since the path loss function decreases faster for larger value of α, thus leading to the rapid decrease of the interference power. We also see that, in a high traffic load ($\lambda = 0.2$), the LSV model exhibits better performance. Inversely, in low traffic load, the HSV model

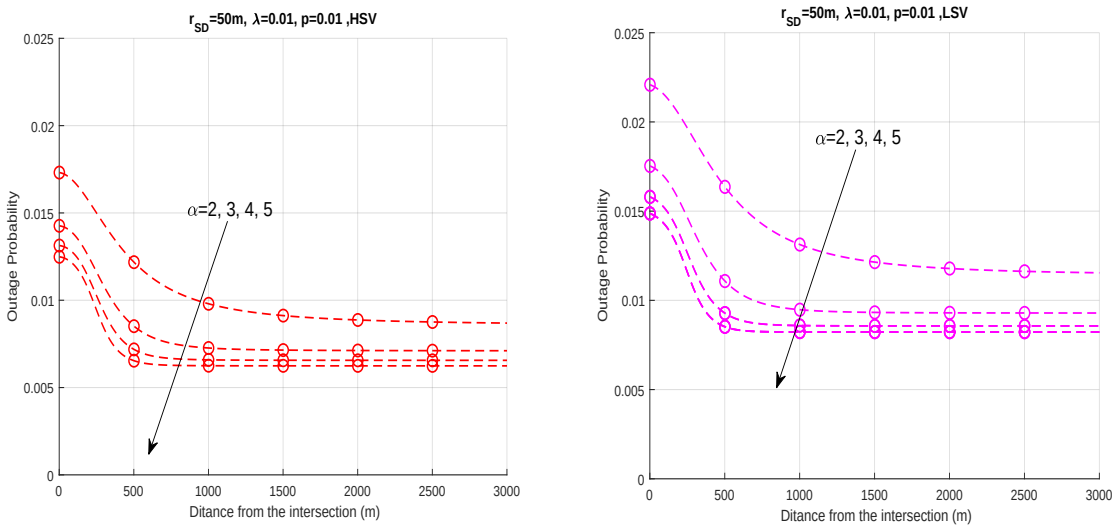

(a) (b)

Figure 1.20.: Outage probability when varying the distance of the triplet $\{S, R, D\}$ from the intersection for different values of α.

exhibits a better performance. This confirms the results in Fig.1.9, Fig.1.10 and Fig.1.13. We note that, for a low traffic scenario ($\lambda = 0.03$, $\lambda = 0.05$), the gap in terms of outage probability between the LSV model and the HSV model, for $\alpha = 2$, is very small, but, as α increases, the gap becomes larger. Also, for $\lambda = 0.07$, the HSV model has a slightly higher value of outage probability than the LSV model when $\alpha = 2$, but, as the value of α increases, the LSV model has a slightly high value of outage probability over the HSV model.

We conclude that larger values of α lead to higher interference dependence, because the interference is dominated by vehicles that are close to the receiving nodes. On the opposite, lower values of α lead to lower interference dependence, because the interference is a summation of several far vehicle signals which, to some extent, decreases the dependence of the interference [Hae12a]. Note that the path loss exponent α depends on the environment. For instance, $\alpha = 2$ corresponds to the free space, $\alpha \in \{2.7, 3.5\}$ to an urban area, and $\alpha \in \{3, 5\}$ to a shadowed urban area [Rap02]. We can state that the environment plays an

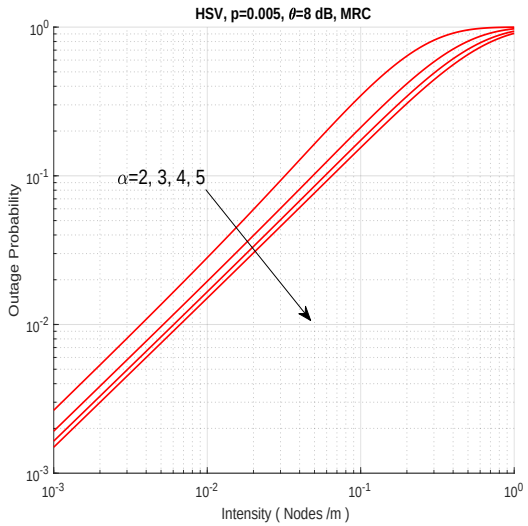

(a) HSV scenario considering MRC

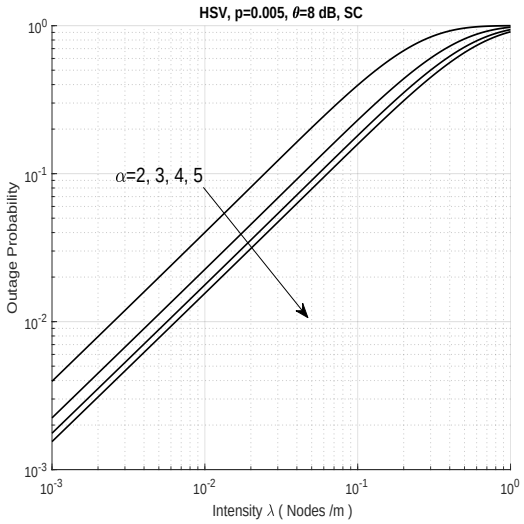

(b) HSV scenario considering SC

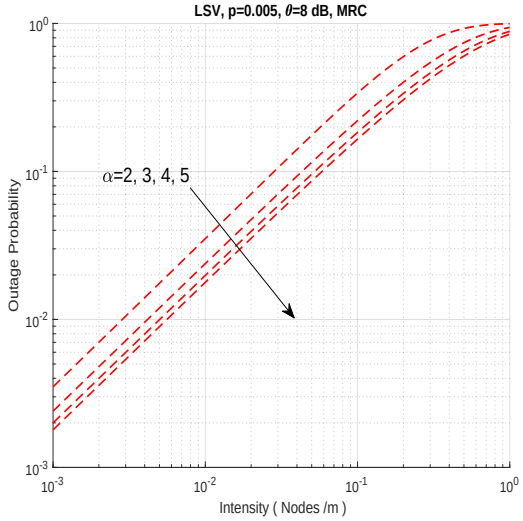

(c) LSV scenario considering MRC

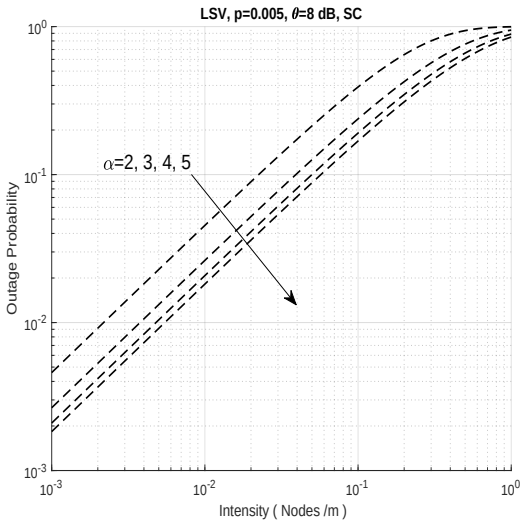

(d) LSV scenario considering SC

Figure 1.21.: Outage probability as a function of λ for several values of α.

important role in the interference dependence. Indeed, an intersection in a suburban area has a lower dependence of interference, whereas an intersection in an urban has a higher interference dependence.

To show the impact of Z on the performance, we plot the outage probability as a function of Z for several values of λ in Fig.1.17. We can see from Fig.1.17 that, as the road segment Z increases, the outage probability increases until Z reaches the value of $Z = 500$ m. However the outage probability is constant for all the values of $Z \in [500 \text{ m}, \infty[$. Hence, we can see that the results obtained when $Z = 10^3$ m are the same as the results obtained when Z tends to infinity ($Z \to \infty$).

Although most of the results were investigated for some values of α, we can see from Fig.1.18, Fig.1.19, Fig.1.20, and Fig.1.21 that the same behavior is observed for different values of α.

1.8.2. Results of Case Study 2

We evaluate the performance of the transmission schemes at intersections considering LOS scenario and NLOS scenario. In order to verify the accuracy of the theoretical results, Monte Carlo simulations are carried out by averaging over 50,000 realizations of the PPPs and fading parameters. In all figures, Monte Carlo simulations are presented by marks, and they match perfectly the theoretical results, which validates our analysis. We set $\alpha_{\text{LOS}} = 2$, $\alpha_{\text{NLOS}} = 4$, $m_{\text{LOS}} = 2$, $m_{\text{NLOS}} = 1$, and $\mu = 1$. Without loss of generality, we set $\lambda_X = \lambda_Y = \lambda$.

From Fig.1.22(a) and Fig.1.22(b), we see that DT outperforms RT. This is because the transmission in DT occurs in one phase whereas the transmission in RT occurs in two phases. This leads to an increases in the decoding threshold, i.e., $\Theta_1 < \Theta_2$, which increases the outage probability of RT. We can also see form Fig.1.22(a) that for low λ, HT outperforms DT, whereas for high λ DT outperforms HT in LOs scenario. This is because for low λ, even

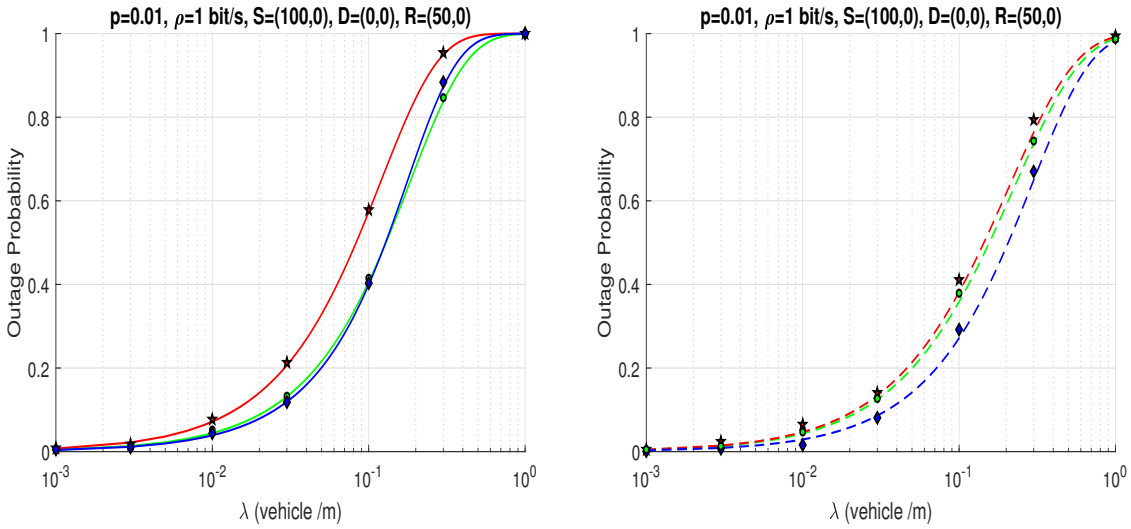

(a) (b)

Figure 1.22.: Outage probability as a function of λ for DT (circle), RT (star) and HT (diamond) (a) LOS scenario (solid line) (b) NLOS scenario (dashed line).

thought $\Theta_1 < \Theta_2$, the aggregate interference are small, hence it converges to an interference free scenario. Thus the HT offers better performance than DT [LTW04]. However for high λ, the interference decreases the performance of HT which makes DT better that HT. Hence, if the intensity of vehicles is high, it is better to use DT over HT in a LOS scenario. However, we can see that Fig.1.22(b), HT always outperforms DT, regardless of the vehicles intensity λ in NLOS scenario.

From Fig.1.23(a) we can see that as the triplet move toward the intersection, the outage probability increases. This is because at the intersection, the X road and the Y road contribute equally to the interference aggregate. However when the triplet move away from the intersection, only one road will contribute to the interference aggregate. The representation of the outage probability behavior can be better seen in the 3D representation in Fig.1.23(b).

We notice from Fig.1.23(a) that the increase in outage probability for LOS scenario begins at 1000 m from the intersection, whereas the increase in outage probability for NLOS

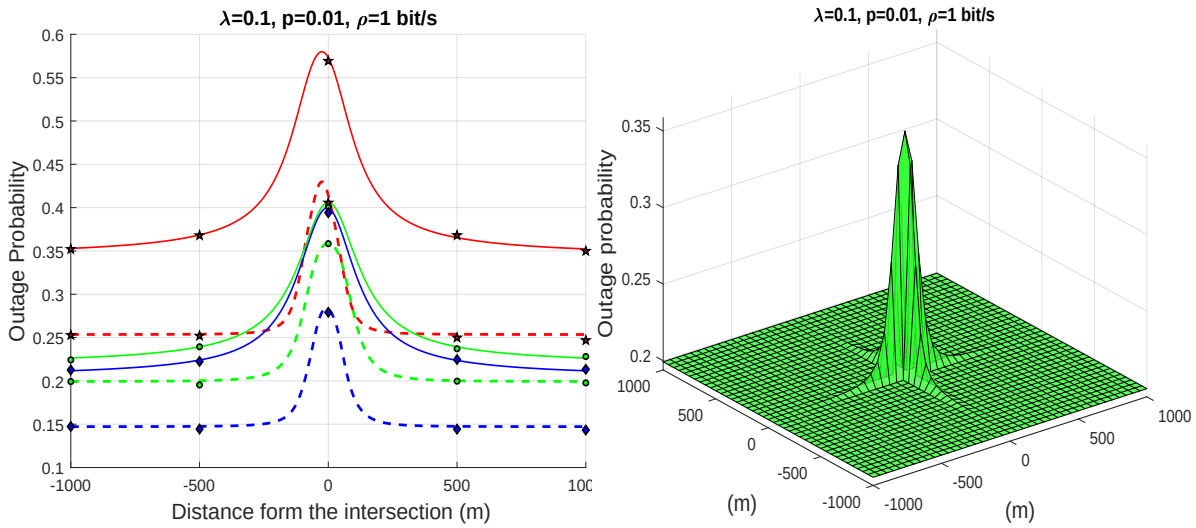

(a) (b)

Figure 1.23.: Outage probability as a function of the distance from the intersection. (a) Outage probability in two dimensions (2D) for DT (circle), RT (star) and HT (diamond), considering LOS (solid line) and NLOS (dashed line)(b) Outage probability in three dimensions (3D) for DT.

scenario begins at 200 m from the intersection. We also notice that at the intersection, the outage probability for LOS scenario is higher than NLOS scenario. This result is counter-intuitive since the transmission in NLOS scenario suffers a blockage of building at the intersection. This can be explained as follows: in LOS scenario, the interference are in LOS with the receiving node, hence it increases the power of interference at the receiver which increases the outage probability. However, in the NLOS scenario the interference are in NLOS with the receiving node, hence it decreases the power of interference at the receiving node which decreases the outage probability. Note that, in an interference free scenario, the LOS scenario outperforms the NLOS scenario. However, in an interference-limited scenario, the power of the interference outweighs the power of the transmitting signal.

We can see from Fig.1.24(a) that in LOS scenario, both DT and HT outperforms RT. We can also see that as the number of lanes increases, the DT and HT have the same performance. This is because when the number of lanes increases, the intensity of the

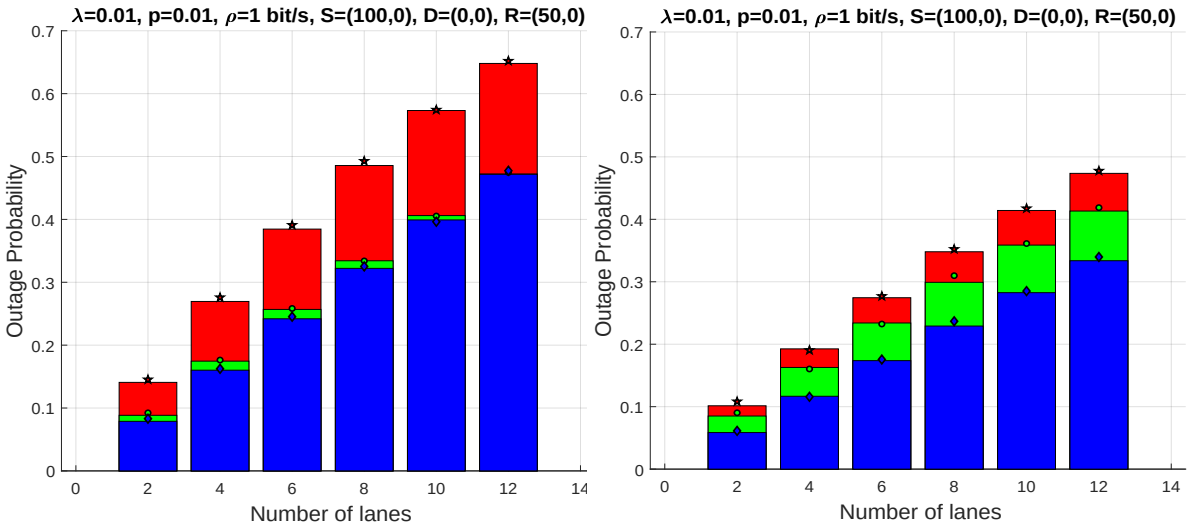

(a) (b)

Figure 1.24.: Outage probability as a function of the number of lanes for DT (circle), RT (star) and HT (diamond)(a) LOS scenario (solid line) (b) NLOS scenario (dashed line).

interferers increases as well. Hence, as explained in Fig.1.22, as the intensity of interferers increases the DT outperforms HT. However, we can see from Fig.1.24(b) in NLOS scenario, that the outage probability increases linearly when the number of lanes increases. We also see that HT always outperforms DT in NLOS scenario even when the intensity of vehicles is high. When comparing Fig.1.24(a) and Fig.1.24(b), we see that the outage probability for LOS scenario of the three transmissions is higher than NLOS scenario. This is due to the fact that, when the interfere vehicles are in LOS with the receiving nodes, the aggregate interference increases and thus,increasing the outage probability.

From Fig.1.25, we can make several observations. For LOS scenario, we can see that for low values of ρ, HT outperforms DT. This is because for low values of ρ, $\Theta_1 \approx \Theta_2$, which makes HT outperforms DT since it benefits from the diversity gain. We also can see that for high values of ρ DT outperforms HT. This because, as ρ increases, the value of Θ_2 increases rapidly compared to Θ_1 ($\Theta_1 >> \Theta_2$). Hence, it increases the outage probability of HT compared to DT. As for NLOS scenario, we can see that HT outperforms DT when

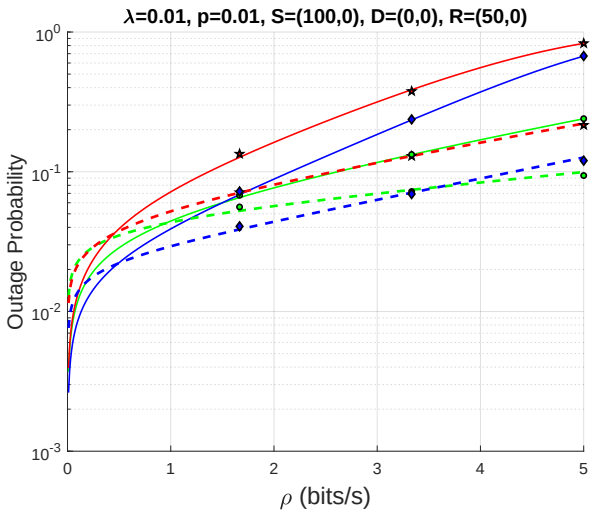

Figure 1.25.: Outage probability as a function the data rate ρ for DT (circle), RT (star) and HT (diamond), for LOS scenario (solid line) and NLOS scenario (dashed line).

$\rho \in [0; 3, 2]$. This is interval is higher than LOS scenario, because the high value of the path loss (i.e, $\alpha = 4$) compensates for the effect of high value of ρ. We can conclude that, for low values of ρ, it is better to use HT, whereas for high values of ρ, it is better to use DT. For instance, when a vehicle need to send emergency message, HT is more suitable since the transmission does not need high data rate.

From Fig.1.26(a) and Fig.1.26(b), we can see that the best relay position for RT is at mid distance between S and D, and that the best relay position for HT is near the destination. We can also notice from Fig.1.26(a) that HT outperforms DT when the relay is closer to the destination. However, we can see from Fig.1.26(b) that HT never outperforms DT in LOS scenario. This confirms what we stated in Fig.1.22, since for high λ, DT outperforms HT. We can conclude that, in LOS scenario and for low values of λ, it is better to use HT when the relay is close to the destination. For for high values of λ, it is better to use DT. In NLOS scenario, if the relay is near the destination, it is better to use HT regardless of λ.

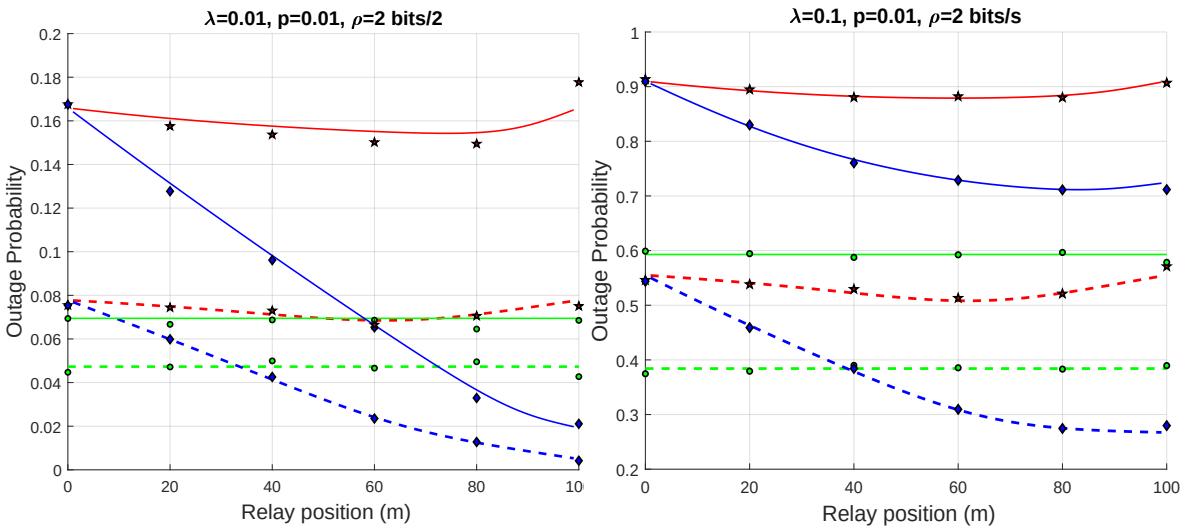

(a) (b)

Figure 1.26.: Outage probability as a function of the relay position for DT (circle), RT (star) and HT (diamond), considering LOS scenario (solid line) and NLOS scenario (dashed line) (a) Low intensity vehicles ($\lambda = 0,01$) (b) High intensity vehicles ($\lambda = 0,1$).

1.9. Conclusion

In this chapter, we investigated two study cases. In the first study case, we studied the performance of direct transmissions and cooperative transmissions for VCs at road intersections in the presence of interference. We presented analytical results for HSV and LSV. Closed-from expressions were obtained for specific channel conditions. We also considered two decoding strategies: SC and MRC. We calculate Laplace transform expressions when the receiving node can be anywhere on the plan, given finite and infinite road segments. We showed that cooperative transmissions always enhance the performance compared to direct transmissions, and the use of MRC is only useful when the relay is closer to the source. We also showed that mobility increases the outage probability performance in good traffic conditions, whereas static or low mobility increases the outage probability performance in harsh traffic conditions. We also showed that the best relay position for the HSV model in low traffic conditions is when relay is closer to the destination. The best relay position for

the HSV model in high traffic conditions is when relay is slightly shifted from the middle toward the destination. However, the best relay position in the LSV model is when the relay is equidistant from the source and the destination regardless of the traffic conditions. We showed that the outage probability does not improve after using three infrastructure relays. We also showed that lower values of the path loss exponent leads to higher interference dependence. Finally, we showed that cooperative transmissions at intersections have higher outage probability than cooperative transmissions on highways.

In the second study case, we investigated three transmission schemes: DT, RT, and HT in the presence of interference at intersections. We derivated the outage probability for the three transmission schemes considering Nakagami-m fading channels. We considered two scenarios: LOS scenario and NLOS scenario. We derive the outage probability when the receiving nodes are on the roads, or outside the roads. Closed forms were obtained for some channel conditions. We showed that DT outperforms RT, hence RT is useful only when DT is not possible. We also showed that in LOS scenario, DT outperforms HT for high densities of vehicles, whereas HT outperforms DT for low densities of vehicles. We also showed that HT has better performance for low densities of vehicles, and for low data rates regardless of the scenario. Counter-intuitively, we found that NLOS scenario offers a better performance that LOS scenario at intersections. Finally, we showed that the best relay position in RT is at mid distance between the source and the destination, whereas the best relay position in HT is close to the destination.

Chapter 2.

Cooperative NOMA analysis

This chapter has been adapted from the journal papers [BHE19d; BHE19j; BHE19e]. *This work has also been discussed in the conference papers* [BHE19h; BHE19c; BHE19g].

Contents

2.1. Introduction

VCs offer several applications for accident prevention, or alerting vehicles when accidents happen in their vicinity. Thus, high reliability and low latency communications are required in safety-based VCs. To increase the data rate and spectral efficiency [Din+17b] in the fifth generation (5G) of communication systems, NOMA is an appropriate candidate as a multiple access scheme. Unlike OMA, NOMA allows multiple users to share the same resource with different power allocation levels

2.1.1. Related Works

The performance of NOMA has been well studied in the literature (see [Dai+15; Isl+17; Din+14] and the references therein). We refer the reader to [Din+17a] for a comprehensive survey on NOMA. As far as the impact of interference on NOMA is concerned, several papers have studied its effect [Zha+16]. The authors in [ZH17] analysed the impact of interference on a NOMA uplink transmission. The authors also analyzed the performance of a NOMA downlink transmission with a selection based pairing in [ZSH17]. e improvement of using cooperative transmissions in NOMA have been also well investigated [DGG18; DGG19]. A scenario involving M number of randomly deployed users was investigated in [Din+14]. The authors also evaluated the ergodic rate and outage performance in [TK15]. In [DDP16a], the authors studied the impact of relay selection on cooperative NOMA, and showed that the two-stage scheme can achieve the optimal diversity gain and the minimal outage probability. However, the impact of implementing NOMA into VCs has been lacking in the literature.

We showed in the previous chapter that the intersections are critical areas since the outage probability increases at these areas. We investigate, in this chapter, the improvements of implementing NOMA and limitation of these improvements. In this chapter we propose

to study three transmission schemes. We will study the direct transmission and cooperative transmission using NOMA in the first part of this chapter. Then, we will study the performance of MRC and compare it with the cooperative transmission.

2.1.2. Contributions

The main contributions of this chapter are summarized as follows:

- We develop a tractable analysis to model VCs at intersections using NOMA in terms of outage probability and average achievable rate considering direct transmission and cooperative transmission. Closed form outage probability expressions are obtained for specific values of the path loss exponent. Quasi-closed form expressions are obtained for the average achievable rate.

- We develop an analysis in terms of outage probability and average achievable rate when a source vehicle sends a message to two destination vehicles, and then extend the results for K destination vehicles when:

    1. Perfect SIC is considered at the receiving nodes, that is, all the extra interference are removed during the SIC.

    2. Imperfect SIC is considered at the receiving nodes, that is, a fraction of interference is not removed during the SIC.

- We show how the system parameters impact the performance of NOMA. We also show how the imperfect SIC process can impact the performance of NOMA and how to ensure that NOMA outperforms OMA. For the sake of completeness, we show that, as the number of destination nodes increases, NOMA performance become greater over OMA.

- We study and investigate how the system parameters impact the performance of cooperative NOMA. For instance, the average achievable rate for D_2 is better for low

density vehicles, and the average achievable rate for D_1 is better for high density vehicles.

- Regarding relay positions, we show that the optimal relay position for D_1 is at mid distance between S and D_1, whereas the optimal relay position for D_2 is close to D_2.

- We show that as we increases the data rate of D_2, cooperative NOMA offers a better performance than cooperative OMA. Whereas for D_1, low data rates are suitable, since there is a condition imposed to its data rate. We also show how the imperfect SIC process can degrade the performance of cooperative NOMA.

- We analyze the performance and the improvement of using MRC in cooperative VCs transmission schemes considering NOMA at intersections in terms of outage probability. Closed form outage probability expressions are obtained.

- We compare the performance of MRC cooperative NOMA with a classical cooperative NOMA, and show that implementing MRC in cooperative NOMA transmission offers a significant improvement over the classical cooperative NOMA in terms of outage probability.

- We also compare the performance of MRC cooperative NOMA with MRC cooperative OMA, and we show that NOMA has a better performance than OMA.

- We show that as we increases the data rate of D_2, MRC transmission using NOMA offers a better performance than MRC transmission using OMA. Whereas for D_1, low data rates are suitable, since there is a condition imposed to its data rate. We also show how the imperfect SIC process can degrade the performance of NOMA. We also show that MRC transmission using NOMA outperforms cooperative NOMA.

- We investigate the best relay position when using MRC, and we show that the optimal relay position for D_1 and D_2 is near the destination nodes.

2.2. System Model

2.2.1. Intersection Scenario

We study the performance of NOMA considering direct transmission and cooperative transmission. The direct transmission involves a source node S and two destination nodes denoted D_1 and D_2 as depicted in Fig.2.1(a). The cooperative transmission occurs between S, and two destinations, denoted D_1 and D_2, with the help of a relay, as denoted by R as depicted in Fig.2.1(b). The use of cooperative transmissions is motivated by the fact that direct transmissions are often unavailable between the source and the destinations due to building and blockages at intersections. The set $\{S, R, D_1, D_2\}$ denotes the nodes and their locations.

We denote by M the receiving node, and by m the distance between the node M and the intersection, where $M \in \{R, D_1, D_2\}$, $m \in \{r, d_1, d_2\}$, and θ_M is the angle between the node M and the X road, as shown in Fig.2.1. Note that the intersection is the point where the X road and the Y road intersect. The intersection scenario that we consider in this study is the same as the one presented in section 1.3.1.

2.2.2. Medium Access Control (MAC) Protocol

We consider the same MAC protocol as in section 1.3.2.

2.2.3. Decoding Strategy Model

We use a Decode and Forward (DF) decoding strategy, i.e., R decodes the message, re-encodes it, then forwards it to D_1 and D_2. We also use a half-duplex transmission in which a transmission occurs during two phases. Each phase lasts one time slot. During the first phase, S broadcasts the message to R ($S \rightarrow R$). During the second phase, R broadcasts the message to D_1 and D_2 ($R \rightarrow D_1$ and $R \rightarrow D_2$).

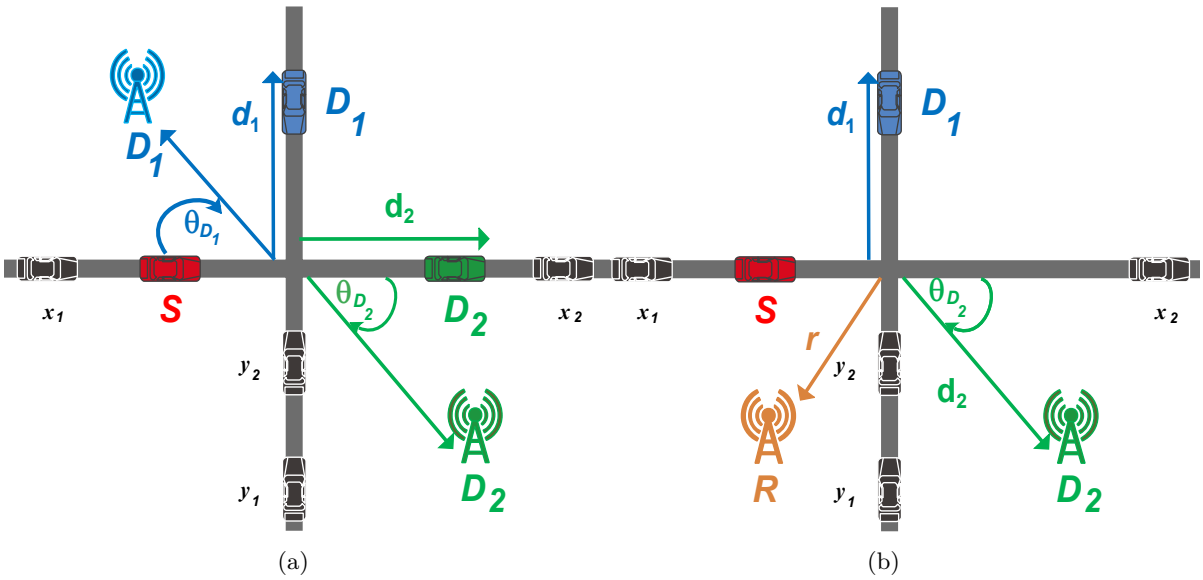

Figure 2.1.: NOMA system model. (a) Direct transmission NOMA system model for VCs involving two receiving node D_1 and D_2. The receiving nodes can be vehicles or as part of the communication infrastructure. (b) Cooperative NOMA system model for VCs involving one relay and two receiving nodes. The receiving nodes can be vehicles or as part of the communication infrastructure. For instance, S and D_1 are vehicles, and R and D_2 are infrastructures.

2.2.4. NOMA destinations order

Several works in NOMA order the receiving nodes by their channel states (see [Din+14; DPP15] and references therein). However, it has been shown in [DDP16a; DDP16b], that it is a more realistic assumption to order the receiving nodes according to their quality of service (QoS) priorities. We study the case when, node D_1 needs a low data rate but has to be served immediately, whereas node D_2 require a higher data rate but can be served later. For instance D_1 can be a vehicle that needs to receive safety data information about an accident happening in its surrounding, whereas D_2 can be a user that accesses the internet connection.

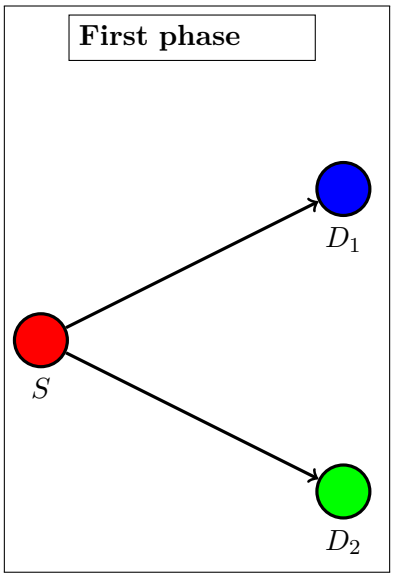

Figure 2.2.: Direct transmission scheme using NOMA.

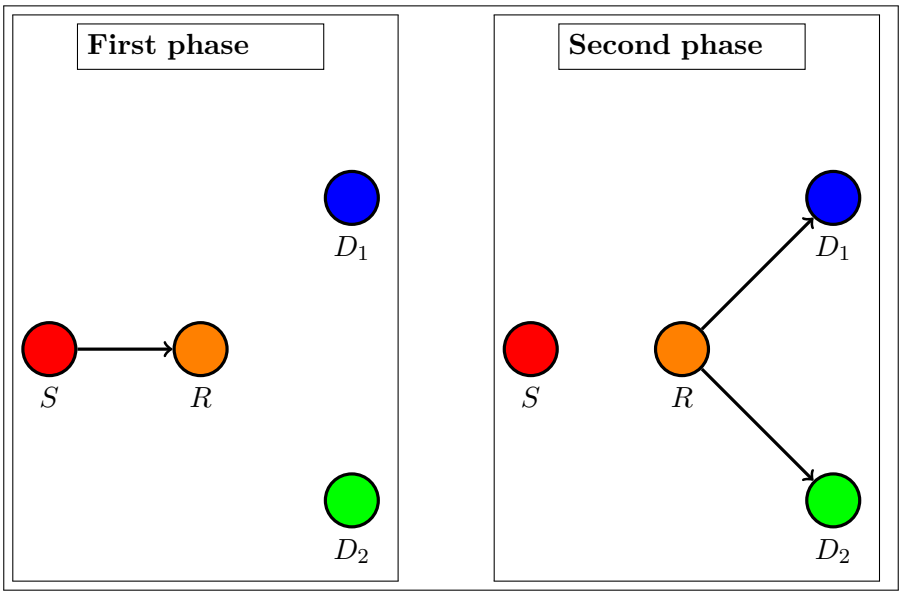

Figure 2.3.: Cooperative transmission scheme using NOMA.

2.2.5. Channel and Interference Model

We consider an interference limited scenario, and thus, we set the power of the additive noise to zero[1]. We assume, without loss of generality, that all nodes transmit with a unit power.

The signal transmitted by S, denoted χ_S is a mixture of the signal intended to D_1 and D_2, and can be expressed as

$$\chi_S = \sqrt{a_1}\chi_{D_1} + \sqrt{a_2}\chi_{D_2},$$

where a_i is the power coefficients of D_i, and χ_{Di} is the message intended to D_i. Since D_1 has higher power than D_2, then it comes first in the decoding order, with $a_1 \geq a_2$. Note that, $a_1 + a_2 = 1$.

The received signal at D_i considering direct tranmission can be expressed as

$$\mathcal{Y}_{D_i} = h_{SD_i}\sqrt{l_{SDi}}\,\chi_S + \sum_{x\in\Phi_X} h_{D_{ix}}\sqrt{l_{D_{ix}}}\,\chi_x + \sum_{y\in\Phi_Y} h_{D_{iy}}\sqrt{l_{D_{iy}}}\,\chi_y,$$

where $\mathcal{Y}_{D_i}$ is the message received by D_i. The messages transmitted by the interfere node x and y from the X road and Y road, are denoted χ_x and χ_y respectively, h_{ab} is the fading coefficient between node a and b, and is modeled as $\mathcal{CN}(0,1)$ (Rayleigh fading) [Che+07]. The power fading coefficient between the node a and b, $|h_{ab}|^2$, follows an exponential distribution with unit mean.

As for the cooperative transmission, the signal received at R during the first time slot is expressed as

$$\mathcal{Y}_R = h_{SR}\sqrt{l_{SR}}\,\chi_S + \sum_{x\in\Phi_{X_R}} h_{Rx}\sqrt{l_{Rx}}\,\chi_x + \sum_{y\in\Phi_{Y_R}} h_{Ry}\sqrt{l_{Ry}}\,\chi_y.$$

[1]We show in the next section how noise can be easily incorporated to the analysis.

The signal received at D_i during the second time slot is expressed as

$$\mathcal{Y}_{D_i} = h_{RD_i}\sqrt{l_{RD_i}}\,\chi_R + \sum_{x\in\Phi_{X_{D_i}}} h_{D_ix}\sqrt{l_{D_ix}}\,\chi_x + \sum_{y\in\Phi_{Y_{D_i}}} h_{D_iy}\sqrt{l_{D_iy}}\,\chi_y,$$

where $\mathcal{Y}_{D_i}$ and χ_R, are respectively the signal received by D_i, and the signal transmitted by R.

The aggregate interference is defined as

$$I_{X_M} = \sum_{x\in\Phi_{X_M}} |h_{Mx}|^2 l_{Mx}, \tag{2.1}$$

and

$$I_{Y_M} = \sum_{y\in\Phi_{Y_M}} |h_{My}|^2 l_{My}, \tag{2.2}$$

where I_{X_M} represents the aggregate interference from the X road at M, I_{Y_M} represents the aggregate interference from the Y road at M, Φ_{X_M} represents the set of the interferers from the X road at M, and Φ_{Y_M} represents the set of the interferers from the Y road at M.

2.3. Outage Computation

2.3.1. NOMA Outage Expressions

The outage probability can be defined as the probability that the SIR at the receiving node is below a certain threshold. We first define the SIR at the receiving node, then we define the outage events and the outage probability related to them, considering direct transmission and cooperative transmission.

Direct Transmission

Since D_1 is assumed to be received with higher power, hence, it will be decoded first according to SIC. Consequently, D_2 message will be considered as interference, and the SIR at D_1, denoted $\mathrm{SIR}_{D_{1-1}}^{\mathrm{DT}}$, is expressed as

$$\mathrm{SIR}_{D_{1\to 1}}^{\mathrm{DT}} = \frac{|h_{SD_1}|^2 l_{SD_1}\, a_1}{|h_{SD_1}|^2 l_{SD_1} a_2 + I_{X_{D_1}} + I_{Y_{D_1}}}. \tag{2.3}$$

However, since D_2 comes second in the decoding order, it has to decode D_1 message first, then decodes its own message. The SIR at D_2 to decode D_1 message, denoted $\mathrm{SIR}_{D_{2-1}}^{\mathrm{DT}}$, is expressed as

$$\mathrm{SIR}_{D_{2\to 1}}^{\mathrm{DT}} = \frac{|h_{SD_2}|^2 l_{SD_2}\, a_1}{|h_{SD_2}|^2 l_{SD_2} a_2 + I_{X_{D_2}} + I_{Y_{D_2}}}. \tag{2.4}$$

The SIR at D_2 to decode its own message, denoted $\mathrm{SIR}_{D_2}^{\mathrm{DT}}$, is expressed as

$$\mathrm{SIR}_{D_{2\to 2}}^{\mathrm{DT}} = \frac{|h_{SD_2}|^2 l_{SD_2}\, a_2}{\beta |h_{SD_2}|^2 l_{SD_2}\, a_1 + I_{X_{D_2}} + I_{Y_{D_2}}}, \tag{2.5}$$

where β is fraction of interference that remains due to SIC error propagation, and $\beta \in [0, 1]$ [Has+03]. When we consider a perfect SIC is carried out at D_2, that is, there is no interference left from the SIC process, then $\beta = 0$.

Now we express the outage event related to D_1 and D_2. The outage event related to D_1, denoted O_{D_1}, is expressed as

$$O_{D_1} \triangleq \left[\mathrm{SIR}_{D_{1-1}}^{\mathrm{DT}} < \Theta_1^{(\mathrm{DT})}\right], \tag{2.6}$$

where $\Theta_1^{(\mathrm{DT})} = 2^{\mathcal{R}_1} - 1$ and $\mathcal{R}_1$ is the target data rate of D_1.

The outage event when D_2 cannot decode D_1 message denoted $O_{D_{2-1}}$, is expressed as

$$O_{D_{2-1}} \triangleq \left[\mathrm{SIR}_{D_{2-1}}^{\mathrm{DT}} < \Theta_1^{(\mathrm{DT})}\right]. \tag{2.7}$$

Finally, the outage event when D_2 cannot decode its own message denoted by $O_{D_{2-2}}$ is expressed as

$$O_{D_{2-2}} \triangleq \left[\mathrm{SIR}^{\mathrm{DT}}_{D_{2-2}} < \Theta_2^{(\mathrm{DT})}\right], \tag{2.8}$$

where $\Theta_2^{(\mathrm{DT})} = 2^{\mathcal{R}_2} - 1$ and $\mathcal{R}_2$ is the target data rate of D_2.

An outage event occurs at D_2 when D_2 cannot decode D_1 message, or when D_2 cannot decode its own message. Then, the outage at D_2 is given by

$$O_{D_2} = [O_{D_{2-1}} \cup O_{D_{2-2}}]. \tag{2.9}$$

Now we express the outage probability related to D_1 and D_2, that is O_{D_1} and O_{D_2}. The outage probability related to D_1, denoted $\mathbb{P}(O_{D_1})$, is expressed as

$$\mathbb{P}(O_{D_1}) = \begin{cases} 1, & \Theta_1^{(\mathrm{DT})} \geq \frac{a_1}{a_2}; \\ 1 - \mathcal{H}_{(D_1)}(\frac{G_1}{l_{SD_1}}), & \text{otherwise.} \end{cases} \tag{2.10}$$

where $G_1 = \Theta_1^{(\mathrm{DT})}/(a_1 - \Theta_1^{(\mathrm{DT})}a_2)$. The function $\mathcal{H}_{(D_i)}\left(\frac{A}{B}\right)$ is expressed as

$$\mathcal{H}_{(D_i)}\left(\frac{A}{B}\right) = \mathcal{L}_{I_{X_{D_i}}}\left(\frac{A}{B}\right)\mathcal{L}_{I_{Y_{D_i}}}\left(\frac{A}{B}\right). \tag{2.11}$$

The outage probability related to D_2, denoted $\mathbb{P}(O_{D_2})$, is expressed as

$$\mathbb{P}(O_{D_2}) = \begin{cases} 1, & \Theta_1^{(\mathrm{DT})} \geq \frac{a_1}{a_2} \text{ or } \Theta_2^{(\mathrm{DT})} \geq \frac{a_2}{\beta a_1}; \\ 1 - \mathcal{H}_{(D_2)}(\frac{G_{(2)\max}}{l_{SD_2}}), & \text{otherwise.} \end{cases} \tag{2.12}$$

where $G_{(2)\max} = \max(G_1, G_2)$ and $G_2 = \Theta_2^{(\mathrm{DT})}/(a_2 - \Theta_2^{(\mathrm{DT})}\beta a_1)$.

When perfect SIC is considered, we set β to zero in (3.67).

Proof: See Appendix B.1. ■

When noise is taken into account, the function $\mathcal{H}_{(D_i)}\left(\frac{A}{B}\right)$ will be a product of two Laplace transform and a noise related term, denoted N_i, where $N_i = \exp(-G_i\,\sigma^2/l_{SD_i})$, and σ^2 is the noise variance.

Cooperative transmission

Now we define the SIR for cooperative transmission. The SIR at R to decode D_1, denoted SIR_{R_1}, is expressed as

$$\mathrm{SIR}_{R_1} = \frac{|h_{SR}|^2 l_{SR}\, a_1}{|h_{SR}|^2 l_{SR}\, a_2 + I_{X_R} + I_{Y_R}}. \tag{2.13}$$

Since D_2 has a lower power allocation, R has to decode D_1 message first, then decode D_2 message. The SIR at R to decode D_2 message, denoted SIR_{R_2}, is expressed as

$$\mathrm{SIR}_{R_2} = \frac{|h_{SR}|^2 l_{SR}\, a_2}{\beta|h_{SR}|^2 l_{SR}\, a_1 + I_{X_R} + I_{Y_R}}, \tag{2.14}$$

where β is fraction of interference that remain due to SIC error propagation.
The SIR at D_1 to decode its intended message, denoted $\mathrm{SIR}_{D_{1\to1}}$, is given by

$$\mathrm{SIR}_{D_{1\to1}} = \frac{|h_{RD_1}|^2 l_{RD_1}\, a_1}{|h_{RD_1}|^2 l_{RD_1} a_2 + I_{X_{D_1}} + I_{Y_{D_1}}}. \tag{2.15}$$

Similarly, in order for D_2 to decode its intended message, it has to decode D_1 message first. The SIR at D_2 to decode D_1 message, denoted $\mathrm{SIR}_{D_{2-1}}$, is expressed as

$$\mathrm{SIR}_{D_{2\to1}} = \frac{|h_{RD_2}|^2 l_{RD_2}\, a_1}{|h_{RD_2}|^2 l_{RD_2} a_2 + I_{X_{D_2}} + I_{Y_{D_2}}}. \tag{2.16}$$

The SIR at D_2 to decode its intended message, denoted $\mathrm{SIR}_{D_{2\to2}}$, is expressed as

$$\mathrm{SIR}_{D_{2\to2}} = \frac{|h_{RD_2}|^2 l_{RD_2}\, a_2}{\beta|h_{RD_2}|^2 l_{RD_2}\, a_1 + I_{X_{D_2}} + I_{Y_{D_2}}}. \tag{2.17}$$

The overall outage event related to D_1, denoted $O_{(1)}$, is given by

$$O_{(1)} \triangleq \left[\mathrm{SIR}_{R_1} < \Theta_1 \cup \mathrm{SIR}_{D_{1\to 1}} < \Theta_1\right]. \tag{2.18}$$

The overall outage event related to D_1, denoted $O_{(1)}$, is given by

$$O_{(1)} \triangleq \left[\mathrm{SIR}_{R_1} < \Theta_1 \cup \mathrm{SIR}_{D_{1\to 1}} < \Theta_1\right], \tag{2.19}$$

where $\Theta_1 = 2^{2\mathcal{R}_1} - 1$, and $\mathcal{R}_1$ is the target data rate of D_1. The target data rate is multiplied by the factor 2 because it requires two time slots to transmit the message.
The outage event that R does not decode D_2 message, denoted O_{R_2}, is given by

$$O_{R_2} \triangleq \left[\mathrm{SIR}_{R_1} < \Theta_1 \cup \mathrm{SIR}_{R_2} < \Theta_2\right], \tag{2.20}$$

where $\Theta_2 = 2^{2\mathcal{R}_2} - 1$, and $\mathcal{R}_2$ is the target data rate of D_2.
Also, the outage event that D_2 does not decode its intended message, denoted O_{D_2}, is given by

$$O_{D_2} \triangleq \left[\mathrm{SIR}_{D_{2\to 1}} < \Theta_1 \cup \mathrm{SIR}_{D_{2\to 2}} < \Theta_2\right]. \tag{2.21}$$

Finally, the overall outage event related to D_2, denoted $O_{(2)}$, is given by

$$O_{(2)} \triangleq \left[O_{R_2} \cup O_{D_2}\right]. \tag{2.22}$$

In the following, we will express the outage probability expressions related to $O_{(1)}$ and $O_{(2)}$. The probability $\mathbb{P}(O_{(1)})$ is given by

$$\mathbb{P}(O_{(1)}) = \begin{cases} 1, & \Theta_1 \geq \frac{a_1}{a_2}; \\ 1 - \mathcal{H}_{(R)}(\frac{G_1}{l_{SR}})\mathcal{H}_{(D_1)}(\frac{G_1}{l_{RD_1}}), & \text{otherwise.} \end{cases} \tag{2.23}$$

where $G_1 = \Theta_1/(a_1 - \Theta_1 a_2)$, and $\mathcal{H}_{(M)}\left(\frac{A}{B}\right)$is expressed as

$$\mathcal{H}_{(M)}\Big(\frac{A}{B}\Big) = \mathcal{L}_{I_{X_M}}\Big(\frac{A}{B}\Big)\mathcal{L}_{I_{Y_M}}\Big(\frac{A}{B}\Big). \tag{2.24}$$

The probability $\mathbb{P}(O_{(2)})$ is given by

$$\mathbb{P}(O_{(2)}) = \begin{cases} 1, & \Theta_1 \geq \frac{a_1}{a_2} \text{ or } \Theta_2 \geq \frac{a_2}{\beta a_1}; \\ 1 - \mathcal{H}_{(R)}(\frac{G_{\max}}{l_{SR}})\mathcal{H}_{(D_1)}(\frac{G_{\max}}{l_{RD_2}}), & \text{otherwise.} \end{cases} \tag{2.25}$$

where $G_{\max} = \max(G_1, G_2)$, and $G_2 = \Theta_2/(a_2 - \Theta_2\beta a_1)$.

Proof: See Appendix B.2. ■

If noise was taken into the analysis, the function $\mathcal{H}_{(M)}\left(\frac{A}{B}\right)$ will be expressed as

$$\mathcal{H}_{(M)}\Big(\frac{A}{B}\Big) = \mathcal{L}_{I_{X_M}}\Big(\frac{A}{B}\Big)\mathcal{L}_{I_{Y_M}}\Big(\frac{A}{B}\Big)\exp\Big(-\frac{A\,\sigma^2}{B}\Big), \tag{2.26}$$

where σ^2 is the noise power.

2.3.2. OMA Outage Expressions

Direct transmission

Now we express the SIR and the outage probability related to OMA considering direct transmission. The SIR at the receiving node D_i, denoted $\text{SIR}_{D_i}^{(\text{OMA})}$, is expressed by

$$\text{SIR}_{D_i}^{(\text{OMA})} = \frac{|h_{SD_i}|^2 l_{SD_i}}{I_{X_{D_i}} + I_{Y_{D_i}}}. \tag{2.27}$$

The outage probability for OMA user D_i is expressed as

$$\mathbb{P}(O_{D_i}^{(\text{OMA})}) = 1 - \mathcal{K}_{(D_i)}\Big(\frac{\Theta^{(\text{DT})}}{l_{SD_i}}\Big), \tag{2.28}$$

where $\Theta^{(\mathrm{DT})} = 2^{2\mathcal{R}_i} - 1$, and $\mathcal{R}_i$ is the target data rate of D_i. Notice that the achievable rate of OMA is multiplied by 1/2. This is because OMA uses twice NOMA resources.

Cooperative transmission

Now we express the SIR and the outage probability related to OMA considering cooperative transmission. The SIR at the receiving node R during the first time slot, and at D_i during the second time slot, are expressed respectively by

$$\mathrm{SIR}_{SR}^{(\mathrm{OMA})} = \frac{|h_{SR}|^2 l_{SR}}{I_{X_R} + I_{Y_R}}, \tag{2.29}$$

and

$$\mathrm{SIR}_{RD_i}^{(\mathrm{OMA})} = \frac{|h_{RD_i}|^2 l_{RD_i}}{I_{X_{D_i}} + I_{Y_{D_i}}}. \tag{2.30}$$

The outage probability for OMA user D_i is expressed as

$$\mathbb{P}(O_{D_i}^{(\mathrm{OMA})}) = 1 - \mathcal{H}_{(R)}\left(\frac{\Theta}{l_{SR}}\right) \times \mathcal{H}_{(D_i)}\left(\frac{\Theta}{l_{RD_i}}\right), \tag{2.31}$$

where $\Theta = 2^{4\mathcal{R}_i} - 1$, and $\mathcal{R}_i$ is the target data rate of D_i. Notice that the achievable rate of OMA is multiplied by 1/4. This is because OMA uses twice NOMA resources.

2.3.3. NOMA Extension to K-destinations

Direct transmission

In this section, we extend the results of NOMA to K-destinations. We define the expression of the SIR at D_i to decode D_t message as follows

$$\mathrm{SIR}_{D_{i\to t}}^{\mathrm{DT}} = \frac{|h_{SD_i}|^2 l_{SD_i}\, a_t}{|h_{SD_i}|^2 l_{SD_i}\left[\beta \sum_{h=1}^{t-1} a_h + \sum_{n=t+1}^{K} a_n\right] + I_{X_{D_i}} + I_{Y_{D_i}}}. \tag{2.32}$$

Note that, when $h > t-1$, then $\sum_{h=1}^{t-1} a_h = 0$, and when $n > K$, then $\sum_{n=t+1}^{K} a_n = 0$. A successful transmission at the user D_i is expressed as

$$O_{D_i}^{C} \triangleq \bigcap_{m=K-i+1}^{K} \{\mathrm{SIR}_{D_{i\to i-(K-m)}}^{\mathrm{DT}} > \mathcal{R}_{i-(K-m)}\}. \tag{2.33}$$

Finally, the outage probability is expressed by

$$\mathbb{P}(O_{D_i}) = \begin{cases} 1, & \bigcup_{t=1}^{K} \frac{a_t}{\beta \sum_{h=1}^{t-1} a_h + \sum_{n=t+1}^{K} a_n} \leq \Theta_t^{(\mathrm{DT})}; \\ 1 - \mathcal{H}_{(D_i)}(\frac{G_{(i)\max}}{l_{SD_i}}), & \text{otherwise.} \end{cases} \tag{2.34}$$

The function $G_{(i)\max}$ is given by

$$G_{(i)\max} = \max\Bigg\{ \frac{\Theta_{i-(K-1)}^{(\mathrm{DT})}}{a_{i-(K-1)} - \Theta_{i-(K-1)}^{(\mathrm{DT})}[\beta \sum_{h=1}^{i-(K-1)-1} a_h + \sum_{n=i-(K-1)+1}^{K} a_n]}, \\ \frac{\Theta_{i-(K-2)}^{(\mathrm{DT})}}{a_{i-(K-2)} - \Theta_{i-(K-2)}^{(\mathrm{DT})}[\beta \sum_{h=1}^{i-(K-2)-1} a_h + \sum_{n=i-(K-2)+1}^{K} a_n]}, ..., \\ \frac{\Theta_{i-(K-l)}^{(\mathrm{DT})}}{a_{i-(K-l)} - \Theta_{i-(K-l)}^{(\mathrm{DT})}[\beta \sum_{h=1}^{i-(K-l)-1} a_h + \sum_{n=i-(K-l)+1}^{K} a_n]} \Bigg\}, \tag{2.35}$$

where $l \in \{1, 2, ..., K\}$. We impose the condition that $l > K - i$. When perfect SIC is considered, we set β to zero in (2.35).

Cooperative transmission

We extend the results of NOMA to K-destinations. We define the expression of the SIRs as follows

$$\mathrm{SIR}_{R_i} = \frac{|h_{SR}|^2 l_{SR}\, a_i}{|h_{SR}|^2 l_{SR}\left[\beta \sum_{h=1}^{i-1} a_h + \sum_{n=i+1}^{K} a_n\right] + I_{X_R} + I_{Y_R}}, \tag{2.36}$$

and

$$\mathrm{SIR}_{D_{i\to t}} = \frac{|h_{RD_i}|^2 l_{RD_i}\, a_t}{|h_{RD_i}|^2 l_{RD_i}\left[\beta \sum_{h=1}^{t-1} a_h + \sum_{n=t+1}^{K} a_n\right] + I_{X_{D_i}} + I_{Y_{D_i}}}. \tag{2.37}$$

Note that, when $h > t-1$, then $\sum_{h=1}^{t-1} a_h = 0$, and when $n > K$, then $\sum_{n=t+1}^{K} a_n = 0$. A successful transmission at D_i is expressed as

$$O_{(\mathrm{i})}^{C} = O_{R_i}^{C} \cap O_{D_i}^{C}, \tag{2.38}$$

where

$$O_{R_i}^{C} \triangleq \bigcap_{m=K-i+1}^{K} \{\mathrm{SIR}_{R_{i-(K-m)}} > \mathcal{R}_{i-(K-m)}\}, \tag{2.39}$$

and

$$O_{D_i}^{C} \triangleq \bigcap_{m=K-i+1}^{K} \{\mathrm{SIR}_{D_{i\to i-(K-m)}} > \mathcal{R}_{i-(K-m)}\}. \tag{2.40}$$

Finally, the outage probability of the user D_i, denoted $O_{(\mathrm{i})}^{C}$, is expressed by

$$\mathbb{P}(O_{(\mathrm{i})}) = \begin{cases} 1, & \bigcup_{t=1}^{i} \frac{a_t}{\beta \sum_{h=1}^{t-1} a_h + \sum_{n=t+1}^{K} a_n} \leq \Theta_t; \\ 1 - \mathcal{H}_{(R)}(\frac{G_{(i)\max}}{l_{SR}})\mathcal{H}_{(D_i)}(\frac{G_{(i)\max}}{l_{RD_i}}), & \text{otherwise.} \end{cases} \tag{2.41}$$

and $G_{(i)\max}$ is given by

$$G_{(i)\max} = \max\Bigg\{ \frac{\Theta_{i-(K-1)}}{a_{i-(K-1)} - \Theta_{i-(K-1)}[\beta \sum_{h=1}^{i-(K-1)-1} a_h + \sum_{n=i-(K-1)+1}^{K} a_n]}, \\ \frac{\Theta_{i-(K-2)}}{a_{i-(K-2)} - \Theta_{i-(K-2)}[\beta \sum_{h=1}^{i-(K-2)-1} a_h + \sum_{n=i-(K-2)+1}^{K} a_n]}, \ldots, \\ \frac{\Theta_{i-(K-l)}}{a_{i-(K-l)} - \Theta_{i-(K-l)}[\beta \sum_{h=1}^{i-(K-l)-1} a_h + \sum_{n=i-(K-l)+1}^{K} a_n]} \Bigg\}, \tag{2.42}$$

where $l \in \{1, 2, ..., K\}$, $\Theta_t = 2^{2\mathcal{R}_t} - 1$, and $\mathcal{R}_t$ is target data rate of D_t. We impose the condition that $l > K - i$. When perfect SIC is considered, we set β to zero in (2.41) and (2.42).

2.4. Average Achievable Rate

2.4.1. Direct transmission

Two destinations

In this section, we derive the average achievable rate related to D_1 and D_2. We assume throughout this section that D_1 and D_2 can use adaptive modulation and coding in order to achieve Shannon bound, that is $\log_2(1+\mathrm{SIR}_{D_i}^{\mathrm{DT}})$.

First, we compute the average achievable rate related to D_1, denoted $\mathcal{T}_{D_1}$, where $\mathcal{T}_{D_1}$ is defined as

$$\mathcal{T}_{D_1} \triangleq \mathbb{E}\big[\log_2(1+\mathrm{SIR}_{D_{1-1}}^{\mathrm{DT}})\big]. \tag{2.43}$$

The expression of $\mathcal{T}_{D_{1-1}}$ is given by

$$\mathcal{T}_{D_1} = \int_{v=0}^{\log_2(1+\frac{a_1}{a_2})} \mathcal{H}_{(D_1)}\Big(\frac{2^v-1}{(a_1+a_2-a_2\,2^v)\,l_{SD_1}}\Big)\mathrm{d}v. \tag{2.44}$$

Proof: See Appendix B.3. ■

The average achievable rate related to D_2, denoted $\mathcal{T}_{D_2}$, is defined as

$$\mathcal{T}_{D_2} \triangleq \mathbb{E}\big[\log_2(1+\mathrm{SIR}_{D_{2-2}}^{\mathrm{DT}})\big]. \tag{2.45}$$

Then, the expression of $\mathcal{T}_{D_2}$ is given by

$$\mathcal{T}_{D_2} = \int_{v=0}^{\log_2(1+\frac{a_2}{\beta a_1})} \mathcal{H}_{(D_1)}\Big(\frac{2^v-1}{a_2+\beta a_1-\beta a_1\,2^v\,l_{SD_1}}\Big)\mathrm{d}v. \tag{2.46}$$

Proof: Same steps as in Appendix B.3. ■

When $\beta = 0$, (2.46) becomes

$$\mathcal{T}_{D_2} = \int_{v=0}^{\infty} \mathcal{H}_{(D_2)}\left(\frac{2^v - 1}{a_2\ l_{SD_2}}\right)\mathrm{d}v. \tag{2.47}$$

The average achievable rate at the receiving node D_i in OMA, denoted $\mathcal{T}_{D_i}^{(\mathrm{OMA})}$, can be expressed as

$$\mathcal{T}_{D_i}^{(\mathrm{OMA})} \triangleq \mathbb{E}\big[\log_2\left(1 + \mathrm{SIR}_{D_i}^{(\mathrm{OMA})}\right)\big]. \tag{2.48}$$

Following the same steps as in NOMA, the average achievable rate in OMA, denoted $\mathcal{T}_{D_i}^{(\mathrm{OMA})}$, is expressed as

$$\mathcal{T}_{D_i}^{(\mathrm{OMA})} = \int_{v=0}^{\infty} \mathcal{H}_{(D_i)}\left(\frac{2^{2v} - 1}{l_{SD_i}}\right)\mathrm{d}v. \tag{2.49}$$

Extension to K-destinations

The expression of the average achievable rate at the user D_i when NOMA is considered is given by

$$\mathcal{T}_{D_i} = \int_{v=0}^{v_{\sup}} \mathcal{H}_{(D_i)}\left(\frac{2^v - 1}{\left\{a_i - (2^v - 1)[\beta \sum_{h=1}^{i-1} a_h + \sum_{n=i+1}^{K} a_n]\right\} l_{SD_i}}\right)\mathrm{d}v, \tag{2.50}$$

where $v_{\sup} = \log_2\left(1 + \frac{a_i}{\beta \sum_{h=1}^{i-1} a_h + \sum_{n=i+1}^{K} a_n}\right)$. Note that, when $\beta = 0$, then $v_{\sup} \to \infty$. The expression of the average achievable rate at the user D_i when OMA is considered is given by

$$\mathcal{T}_{D_i}^{(\mathrm{OMA})} = \int_{v=0}^{\infty} \mathcal{H}_{(D_i)}\left(\frac{2^{Kv} - 1}{l_{SD_i}}\right)\mathrm{d}v. \tag{2.51}$$

2.4.2. Cooperative transmission

In this section, we compute the average achievable rate related to D_1 and D_2. We assume throughout this section that R, D_1 and D_2 can use adaptive modulation and coding in order to achieve Shannon bound for cooperative transmissions, that is $\frac{1}{2}\log_2(1 + \mathrm{SIR})$.

The average achievable rate related to D_1, denoted $\mathcal{T}_{D_1}$, is expressed as

$$\mathcal{T}_{D_1} = \mathbb{E}\left[\min\left\{\frac{1}{2}\log_2(1+\mathrm{SIR}_{R_1}), \frac{1}{2}\log_2(1+\mathrm{SIR}_{D_{1\to 1}})\right\}\right].$$

The final expression of $\mathcal{T}_{D_1}$ is then expressed as

$$\mathcal{T}_{D_1} = \int_{v=0}^{\frac{1}{2}\log_2(1+\frac{a_1}{a_2})} \mathcal{H}_{(R)}\left(\frac{2^{2v}-1}{(a_1+a_2-a_2\,2^{2v})\,l_{SR}}\right) \times \mathcal{H}_{(D_1)}\left(\frac{2^{2v}-1}{(a_1+a_2-a_2\,2^{2v})\,l_{SR}}\right)\mathrm{d}v. \tag{2.52}$$

Proof: See Appendix B.4. ■

The average achievable rate related to D_2, denoted $\mathcal{T}_{D_2}$, is expressed as

$$\mathcal{T}_{D_2} = \mathbb{E}\left[\min\left\{\frac{1}{2}\log_2(1+\mathrm{SIR}_{R_2}), \frac{1}{2}\log_2(1+\mathrm{SIR}_{D_{2\to 2}})\right\}\right].$$

Then, following the same steps as in Appendix B.4, we get

$$\mathcal{T}_{D_2} = \int_{v=0}^{\frac{1}{2}\log_2(1+\frac{a_2}{\beta a_1})} \mathcal{H}_{(R)}\left(\frac{2^{2v}-1}{(a_2+\beta a_1-\beta a_1\,2^{2v})\,l_{SR}}\right) \times \mathcal{H}_{(D_2)}\left(\frac{2^{2v}-1}{(a_2+\beta a_1-\beta a_1\,2^{2v})\,l_{SR}}\right)\mathrm{d}v. \tag{2.53}$$

When perfect SIC is considered, that is $\beta = 0$, then (2.53) becomes

$$\mathcal{T}_{D_2} = \int_{v=0}^{\infty} \mathcal{H}_{(R)}\left(\frac{2^{2v}-1}{a_2\,l_{SR}}\right) \times \mathcal{H}_{(D_2)}\left(\frac{2^{2v}-1}{a_2\,l_{SR}}\right)\mathrm{d}v. \tag{2.54}$$

The expression of the average achievable rate at the user D_i considering NOMA, is given

by

$$\mathcal{T}_{D_i} = \int_{v=0}^{v_{\sup}} \mathcal{H}_{(R)}\left(\frac{2^{2v}-1}{\left\{a_i - (2^{2v}-1)[\beta \sum_{h=1}^{i-1} a_h + \sum_{n=i+1}^{K} a_n]\right\} l_{SR}}\right) \times \mathcal{H}_{(D_i)}\left(\frac{2^{2v}-1}{\left\{a_i - (2^{2v}-1)[\beta \sum_{h=1}^{i-1} a_h + \sum_{n=i+1}^{K} a_n]\right\} l_{RDi}}\right) \mathrm{d}v, \tag{2.55}$$

where $v_{\sup} = \frac{1}{2}\log_2\left(1 + \frac{a_i}{\beta \sum_{h=1}^{i-1} a_h + \sum_{n=i+1}^{K} a_n}\right)$. When $\beta = 0$ and $i = K$, then $v_{\sup} \to \infty$.

2.5. Power Allocation Coefficient and β Setting

In this section, We show how the system parameters impact the performance of NOMA, and how to set the system parameters to ensure that NOMA outperforms OMA in terms of outage probability when destination nods are at the intersection ($d_i = 0$). Without loss of generality, we consider $\lambda_x = \lambda_y = \lambda$, and we consider direct transmission.

2.5.1. The Target Data Rate

For D_1, the following condition regarding $\mathcal{R}_1$ has to be respected

$$\mathcal{R}_1 < \log_2\left(1 + \frac{a_1}{1-a_1}\right). \tag{2.56}$$

Otherwise, $\mathbb{P}(O_{D_1})$ equals 1. For D_2, the following condition regarding $\mathcal{R}_1$ and $\mathcal{R}_2$ has to be respected

$$\left\{\mathcal{R}_1 < \log_2\left(1 + \frac{a_1}{1-a_1}\right)\right\} \cap \left\{\mathcal{R}_2 < \log_2\left(1 + \frac{1-a_1}{\beta a_1}\right)\right\}. \tag{2.57}$$

Otherwise, $\mathbb{P}(O_{D_2})$ equals 1.

2.5.2. The Power Allocation Coefficient a_1

Regarding D_1, the outage probability using NOMA has to be less than the outage probability using OMA. This can be expressed as

$$\mathbb{P}(O_{D_1}) < \mathbb{P}(O_{D_1}^{(\mathrm{OMA})}). \tag{2.58}$$

Then when the condition (2.56) is satisfied, the inequality in (2.58) will be expressed as

$$\mathcal{H}_{(D_1)}\Big(\frac{G_1}{l_{SD_1}}\Big) > \mathcal{H}_{(D_1)}\Big(\frac{\Theta^{(\mathrm{DT})}}{l_{SD_1}}\Big). \tag{2.59}$$

For $\alpha = 2$, the expression further (2.59) simplifies to

$$\exp\Big(-2p\lambda\pi\frac{G_1}{l_{SD_1}}\Big) > \exp\Big(-2p\lambda\pi\frac{\Theta^{(\mathrm{DT})}}{l_{SD_1}}\Big). \tag{2.60}$$

Then after some algebraic manipulations, we obtain

$$a_1 > \frac{\Theta_1^{(\mathrm{DT})}(1+\Theta^{(\mathrm{DT})})}{\Theta^{(\mathrm{DT})}(1+\Theta_1^{(\mathrm{DT})})}. \tag{2.61}$$

So if a_1 respects the condition in (2.61), NOMA will always outperforms OMA.

Regarding D_2, the outage probability using NOMA has to be less than the outage probability using OMA. This can be expressed as

$$\mathbb{P}(O_{D_2}) < \mathbb{P}(O_{D_2}^{(\mathrm{OMA})}). \tag{2.62}$$

Following the same steps as for D_1, (2.62) it can be expressed as

$$\mathbb{P}(O_{D_2}) < \mathbb{P}(O_{D_2}^{(\mathrm{OMA})}). \tag{2.63}$$

Then when the condition (2.57) is satisfied, we get

$$\mathcal{H}_{(D_2)}\Big(\frac{G_{(2)\max}}{l_{SD_2}}) > \mathcal{H}_{(D_2)}\Big(\frac{\Theta^{(\mathrm{DT})}}{l_{SD_2}}\Big). \tag{2.64}$$

which further simplify to

$$\max(\mathrm{G}_1, \mathrm{G}_2) < \Theta^{(\mathrm{DT})}. \tag{2.65}$$

Then after some algebraic manipulations we obtain

$$\begin{cases} a_1 > \frac{\Theta_1^{(\mathrm{DT})}(1+\Theta^{(\mathrm{DT})})}{\Theta^{(\mathrm{DT})}(1+\Theta_1^{(\mathrm{DT})})}, & \text{if} \quad a_1 \in [0, \frac{\Theta_1^{(\mathrm{DT})}(1+\Theta_2^{(\mathrm{DT})})}{\Theta_1^{(\mathrm{DT})}+\Theta_2^{(\mathrm{DT})}+\Theta_1^{(\mathrm{DT})}\Theta_2^{(\mathrm{DT})}+\Theta_1^{(\mathrm{DT})}\Theta_2^{(\mathrm{DT})}\beta}]; \\ a_1 < \frac{\Theta^{(\mathrm{DT})}-\Theta_2^{(\mathrm{DT})}}{\Theta^{(\mathrm{DT})}(1+\Theta_2^{(\mathrm{DT})}\beta)}, & \text{otherwise.} \end{cases} \tag{2.66}$$

2.5.3. The Fraction of Interference After SIC Process β

For the β, the following condition has to be respected

$$\frac{\Theta^{(\mathrm{DT})} - \Theta_2^{(\mathrm{DT})} - a_1\Theta^{(\mathrm{DT})}}{\Theta^{(\mathrm{DT})}\Theta_2^{(\mathrm{DT})}a_1} > \beta. \tag{2.67}$$

2.6. Simulations and Discussions

In this section, we evaluate the performance of NOMA using cooperative transmission and direct transmission at intersections. Monte-Carlo simulations are obtained by averaging over 50,000 realizations of the PPPs and fading parameters. The Monte-Carlo simulations match the theoretical analysis, which confirm the accuracy of our results. Unless stated otherwise, $\beta = 0$, $S = [100, 0]$, $R = [50, 0]$, $D_1 = [0, 0]$ and $D_2 = [0, -10]$. We set, without loss of generality, $\lambda_X = \lambda_Y = \lambda$.

We can see from Fig.2.4 that, as the intensity of vehicles increases, the outage probability increases. This is because, when the number of interfering vehicles increases, the aggregate interference at the receiving node increases, hence increasing the outage probability. We

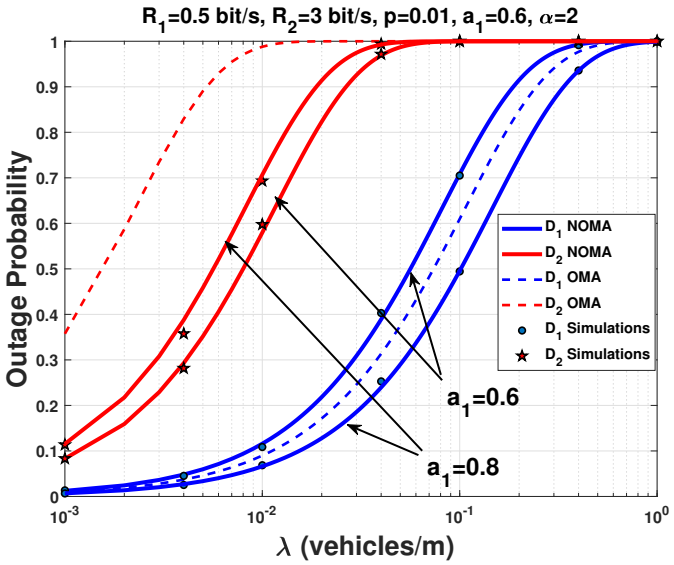

Figure 2.4.: Outage probability as a function of λ using cooperative NOMA and cooperative OMA.

can also see that the performance of cooperative NOMA depends of the value of a_1. For instance, for $a_1 = 0.8$, NOMA outperforms OMA for D_1 and D_2. However, for $a_1 = 0.6$, NOMA outperforms OMA for D_2, but not for D_1. This is because, when a_1 decreases (less power is allocated to D_1), a_2 increases (more power is allocated to D_2). Consequently, the numerators in the equation SIR_{R_1} and $\text{SIR}_{D_{1\to1}}$ become smaller than the denominators. Hence, the values of SIR_{R_1} and $\text{SIR}_{D_{1\to1}}$ decrease. When the values of SIR_{R_1} and $\text{SIR}_{D_{1\to1}}$ decrease, the probability that the SIR values becomes greater than the decoding threshold Θ_1 deceases, which increases the outage probability.

Fig.2.5 plots the average achievable rate of cooperative NOMA and cooperative OMA as a function of λ. Note that, for cooperative OMA, we have only one performance for D_1 and D_2. This is because $\|S - D_1\| = \|S - D_2\|$, which leads to the same performance in the case of cooperative OMA. We notice from Fig.2.5 that D_2 achieves a higher average achievable rate than D_1 in the presence of low density vehicles. This is because, for D_1, there is an extra interference term related to D_2, which decreases the average achievable

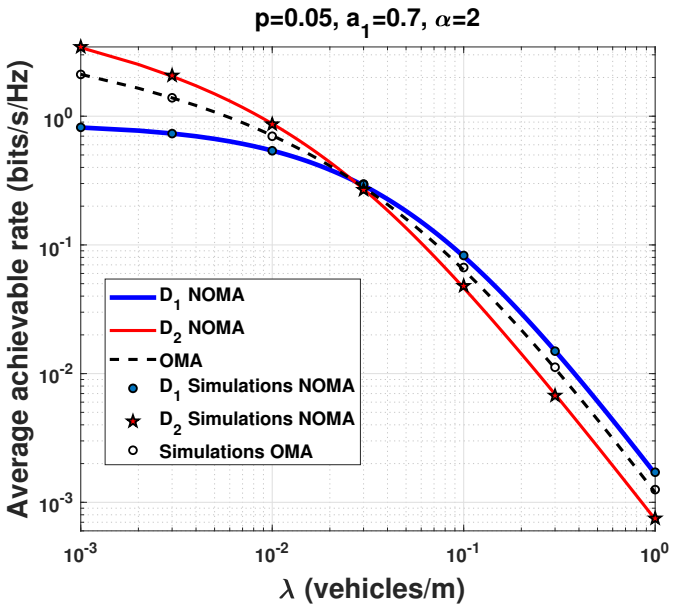

Figure 2.5.: Average achievable rate as a function of λ using cooperative NOMA and cooperative OMA.

rate. However, as the density of vehicles increases, D_1 has better performance. This is because, on one hand, the power allocated to D_1 is higher than the power allocated to D_2, and on the other hand, the extra interference from D_2 at D_1 becomes negligible compared to the interference generated by the interfering vehicles.

Fig.2.6 plots the outage probability for cooperative NOMA as a function of the distance from the intersection. For the performance comparison, we plot the outage probability for cooperative NOMA for a highway scenario which involves one road segment. For a fair comparison between the intersection and highway scenario, we locate the set $\{S, R, D_1, D_2\}$ on the same road segment. We see from Fig.2.6 that, when the vehicles are at 200 m away from the intersection, the performance of D_1 for the intersection and the highway scenarios is the same. However, as the vehicles move toward the intersection, the performance of the intersection decreases, and reaches its maximum at the intersection. The same observations can be made regarding the performance of D_2. This is because, when vehicles are far

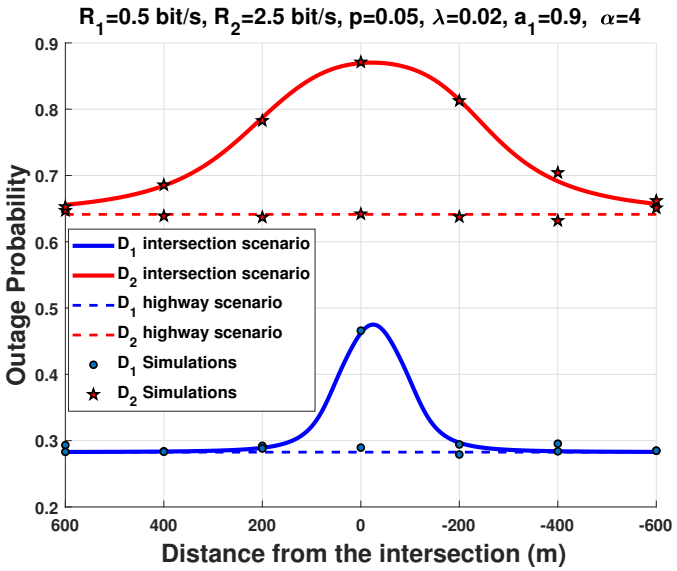

Figure 2.6.: Outage probability as a function of the distance from the intersection using cooperative NOMA for intersection scenario, and highway scenario.

from the intersection, the interference from the other road are negligible, due to the long distance between the interfering vehicles and the receiving nodes. However, as the vehicles get closer to the intersection, the interference from the other road increases until it reaches its maximum at the intersection. The increase of the outage probability confirms the fact that communications at intersections are critical and more prone to outage.

Fig.2.7 depicts the outage probability for cooperative NOMA and cooperative OMA as a function of the distance from the intersection. We can clearly see that the performance of NOMA outperforms OMA for both D_1 and D_2. We can see a gain of 10% in terms of outage probability. Which confirms the superiority of cooperative NOMA over cooperative OMA.

Fig.2.8 plots the average achievable rate for cooperative NOMA and cooperative OMA as a function of the distance from the intersection. We can see that the average achievable rate decreases as the vehicles of set $\{S, R, D_1, D_2\}$ move toward the intersection. We can also see from Fig.2.8(a) the performance of cooperative NOMA for D_1 is worst than cooperative

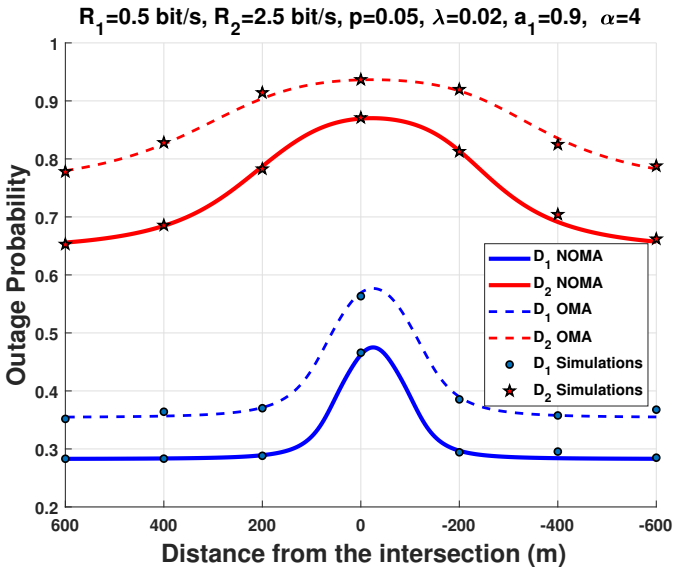

Figure 2.7.: Outage probability as a function of the distance from the intersection using cooperative NOMA and cooperative OMA.

OMA, and the performance of cooperative NOMA for D_2 is better than cooperative OMA. This is because, when less power is allocated to D_1, more power is allocated or D_2. However, in Fig.2.8(b), when more power is allocated to D_1, the average achievable rate of D_1 using cooperative NOMA outperforms cooperative OMA, and cooperative OMA outperforms cooperative NOMA for D_2.

Fig.2.9 depicts the impact of the power allocations a_1 on the outage probability, considering cooperative NOMA and cooperative OMA. We notice from Fig.2.9 that, when using cooperative NOMA, as a_1 increases, $\mathbb{P}(O_{(1)})$ decreases whereas $\mathbb{P}(O_{(2)})$ increases.

This is because, when a_1 increases (more power is allocated to D_1), a_2 decreases (less power is allocated to D_2). Consequently, the numerators in the equation SIR_{R_1} and $\mathrm{SIR}_{D_{1\to1}}$ become greater than the denominators. Hence, the values of SIR_{R_1} and $\mathrm{SIR}_{D_{1\to1}}$ increase. When the values of SIR_{R_1} and $\mathrm{SIR}_{D_{1\to1}}$ increase, the probability that the SIR values becomes greater than the decoding threshold Θ_1 increase, which decreases $\mathbb{P}(O_{(1)})$. Similarly, when a_1 decreases (less power is allocated to D_1), a_2 increases (more power is allocated to D_2).

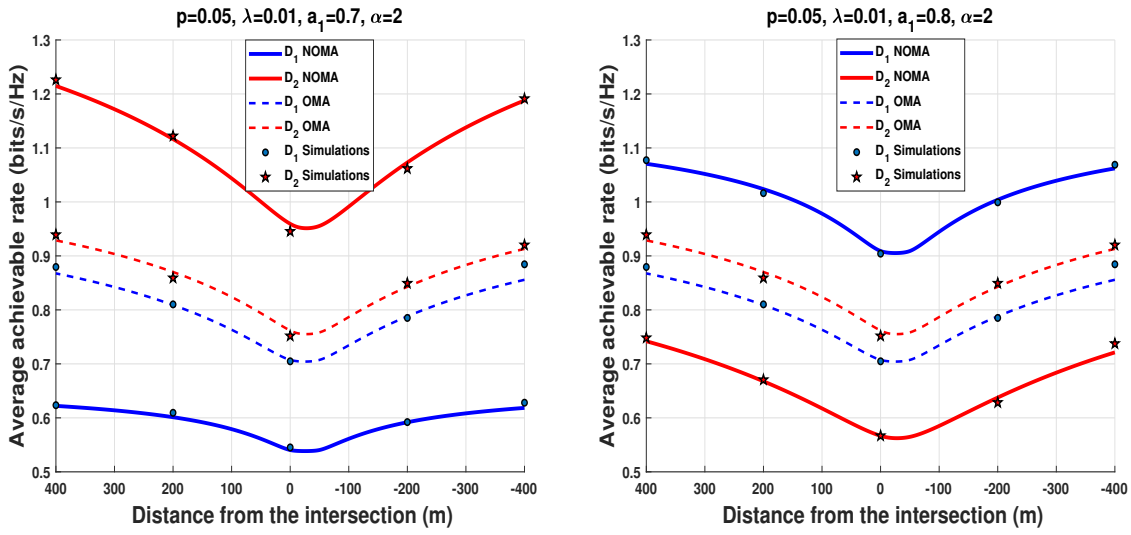

(a) (b)

Figure 2.8.: Average achievable rate as a function of the distance from the intersection (a) $a_1 = 0.7$ (b) $a_1 = 0.9$.

Consequently, the numerators in the equation SIR_{R_2} and $\text{SIR}_{D_{1\to 2}}$ become greater than the denominators. Hence, the values of SIR_{R_2} and $\text{SIR}_{D_{2\to 2}}$ increase. When the values of SIR_{R_2} and $\text{SIR}_{D_{2\to 2}}$ increase, the probability that the SIR values becomes greater than the decoding threshold Θ_2 increases, which decrease $\mathbb{P}(O_{(2)})$.

Now, we compare the outage probability of cooperative NOMA and cooperative OMA. We can see that, for D_1, OMA outperforms NOMA for lower value of a_1. There are two reasons for that, the first one is, smaller values of a_1 leads to a low SIR at D_1, which increases $\mathbb{P}(O_{(1)})$. Second, smaller values of a_1, leads to higher power allocated to D_2, thus increasing the interference, therefore increasing $\mathbb{P}(O_{(1)})$.

We can notice from Fig.2.9(c) and Fig.2.9(d) that, when $\Theta_1 \geq a_1/a_2$, $\mathbb{P}(O_{(1)}) = 1$ and $\mathbb{P}(O_{(2)}) = 1$. This is because, when we increase $\mathcal{R}_1$, it becomes harder to satisfy the condition $\Theta_1 < a_1/a_2$. This will reduce the interval when cooperative NOMA outperforms cooperative OMA for both D_1 and D_2. Note that, there is not restriction for D_2 regarding $\mathcal{R}_2$ when $\beta = 0$.

For D_2, we can notice that, as $\mathcal{R}_2$ increases (Fig.2.9(a) and Fig.2.9(b)), cooperative NOMA outperforms OMA for any value of a_1 (given that a_1<1). This is because, when D_2 has a higher data rate, it means that the threshold of cooperative OMA increases dramatically ($\Theta = 2^{4\mathcal{R}_2} - 1$). Thus, increases the gap in terms of outage probability between NOMA and OMA for D_2.

Finally, it is worth noticing that $\mathbb{P}(O_{(1)})$ is always smaller than $\mathbb{P}(O_{(2)})$. The reasons are as follows. First, D_2 has to decode D_1 message, then decoding its intended message, which increases the probability of outage. Second, $\mathcal{R}_2$ is larger that $\mathcal{R}_1$, therefore increasing the decoding threshold and increasing $\mathbb{P}(O_{(2)})$.

Fig.2.10 plots the average achievable rate as a function of a_1 considering cooperative NOMA and cooperative OMA. We can notice from Fig.2.10 that the average achievable rate using NOMA for D_1 outperforms OMA only for high value of a_1 ($a_1 \in [0.82, 1]$). We also notice that the average achievable rate using NOMA for D_2 outperforms OMA for low value of a_1 ($a_1 \in [0.6, 0.81]$). This means that as a_1 increases, the average achievable rate of D_1 increases whereas the average achievable rate of D_2 decreases. This is because, as we stated before, as a_1 increases, more power is allocated to D_1 and less power is allocated to D_2, therefore the average achievable rate of D_1 increases whereas the average achievable rate of D_2 decreases.

Fig.2.11 plots the outage probability as a function of the relay position for D_1 considering cooperative NOMA for several values of a_1. Without loss of generality, we set $S = [0, 0]$ and $D_1 = [100, 0]$. We can see from Fig.2.11 that the optimal position of R for D_1 lies in the interval $R \in [58, 73]$. We can also notice that as we increases a_1, the optimal position moves toward the mid distance between S and D_1. For instance, when $a_1 = 0.6$, the optimal position is $R = [73, 0]$, as we increases the value of a_1, for instance $a_1 = 0.9$, the optimal position becomes $R = [58, 0]$.

Fig.2.12 depicts the outage probability as a function of the relay position for D_2 consider-

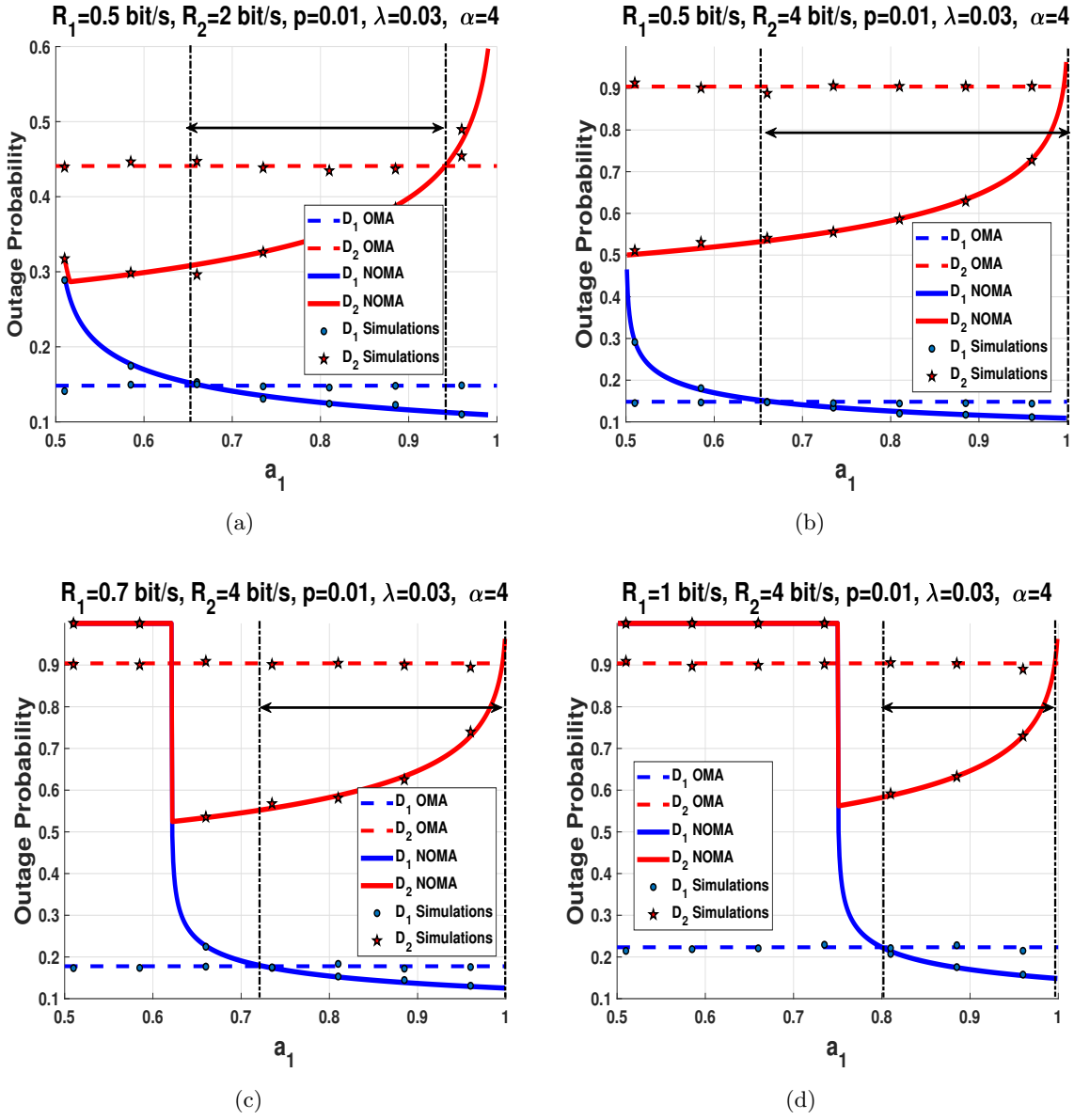

Figure 2.9.: Outage probability as a function of a_1 using cooperative NOMA and cooperative OMA for several value of data rates. (a) $\mathcal{R}_1 = 0.5$ bits/s and $\mathcal{R}_2 = 2$ bits/s. (b) $\mathcal{R}_1 = 0.5$ bits/s and $\mathcal{R}_2 = 4$ bits/s. (c) $\mathcal{R}_1 = 0.7$ bits/s and $\mathcal{R}_2 = 4$ bits/s. (d) $\mathcal{R}_1 = 1$ bits/s and $\mathcal{R}_2 = 4$ bits/s.

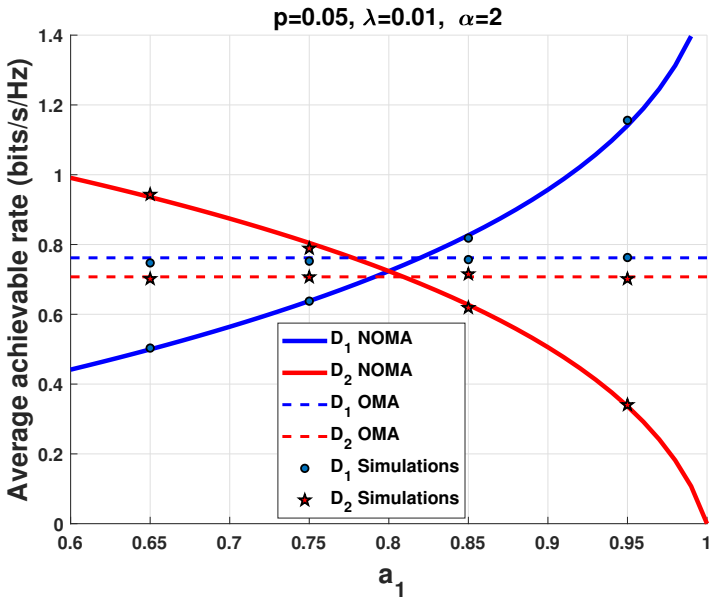

Figure 2.10.: Average achievable rate as a function of a_1 considering cooperative NOMA and cooperative OMA.

ing cooperative NOMA for several values of a_1. Without loss of generality, we set $S = [0, 0]$ and $D_2 = [100, 0]$. We see from Fig.2.12 that the optimal position of R for D_2 lies in the interval $R \in [87, 94]$. We can also notice that as we increases a_1, the optimal position moves toward D_2. Hence, when we allocate less power to D_2, the optimal position of R is close to D_2.

In Fig2.13(a), we can see that, for a large value of a_1 (e.g, $a_1 = 0.9$), cooperative NOMA outperforms OMA in terms of outage probability. This is because more power is allocated to D_1. We can also see that, for small value of a_1 ($a_1 = 0.7$), the NOMA outage probability of NOMA is slightly smaller than the OMA outage probability for smaller value of $\mathcal{R}_1$. However, the gap increases as $\mathcal{R}_1$ increases. This is because, as $\mathcal{R}_1$ increases, $\Theta_1$increases as well, which results in an outage at D_1 due to the smaller value of a_1.

We can see from Fig.2.13(b) that from small values of $\mathcal{R}_2$, that is, $\mathcal{R}_2 < 0.6$ bit/s, OMA offers better performance than NOMA in terms of outage probability, even when more power

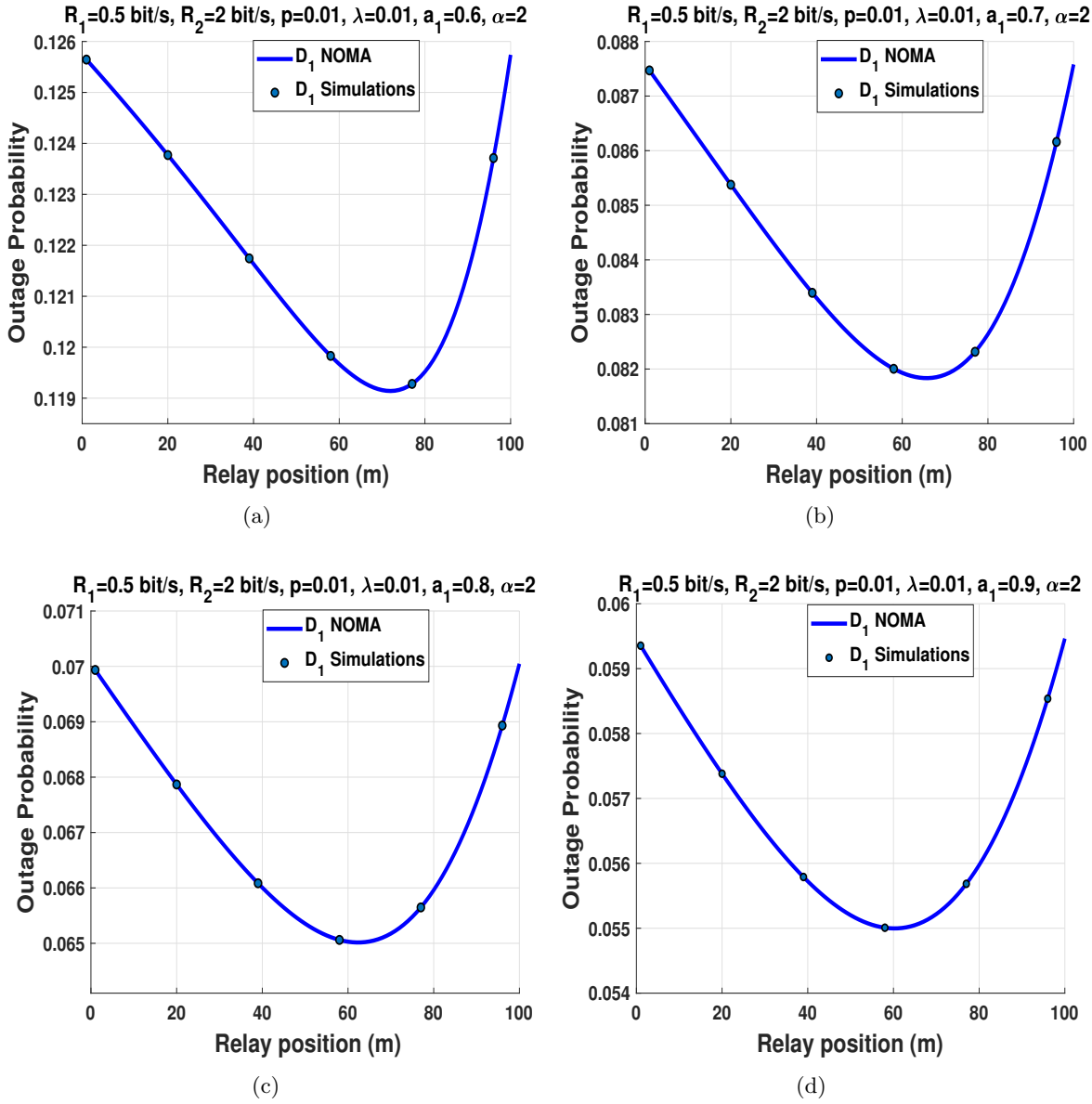

Figure 2.11.: Outage probability as a function of the relay position for D_1 considering cooperative NOMA (a) $a_1 = 0.6$. (b) $a_1 = 0.7$. (c) $a_1 = 0.8$. (d) $a_1 = 0.9$.

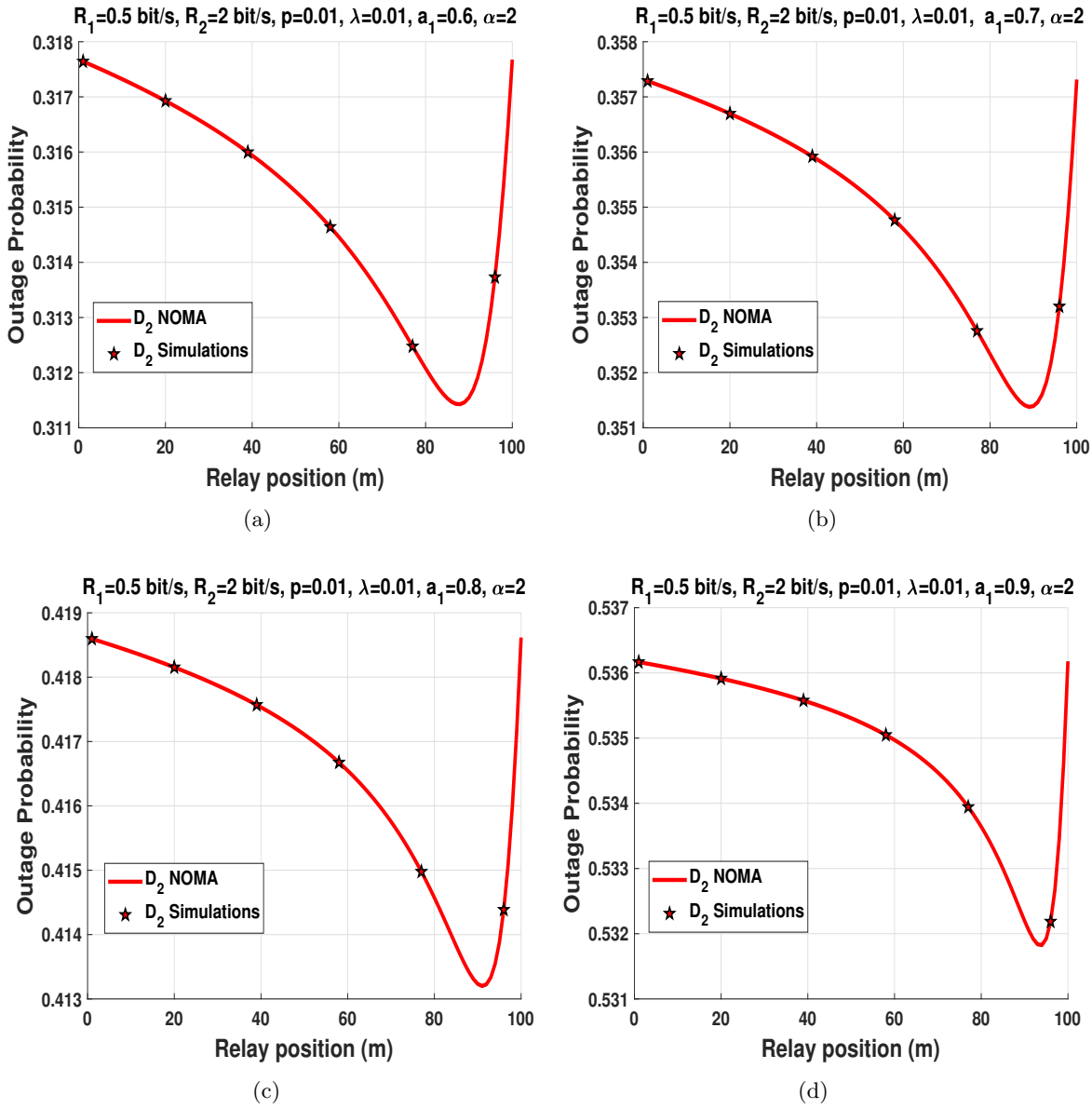

Figure 2.12.: Outage probability as a function of the relay position for D_2 considering cooperative NOMA (a) $a_1 = 0.6$. (b) $a_1 = 0.7$. (c) $a_1 = 0.8$. (d) $a_1 = 0.9$.

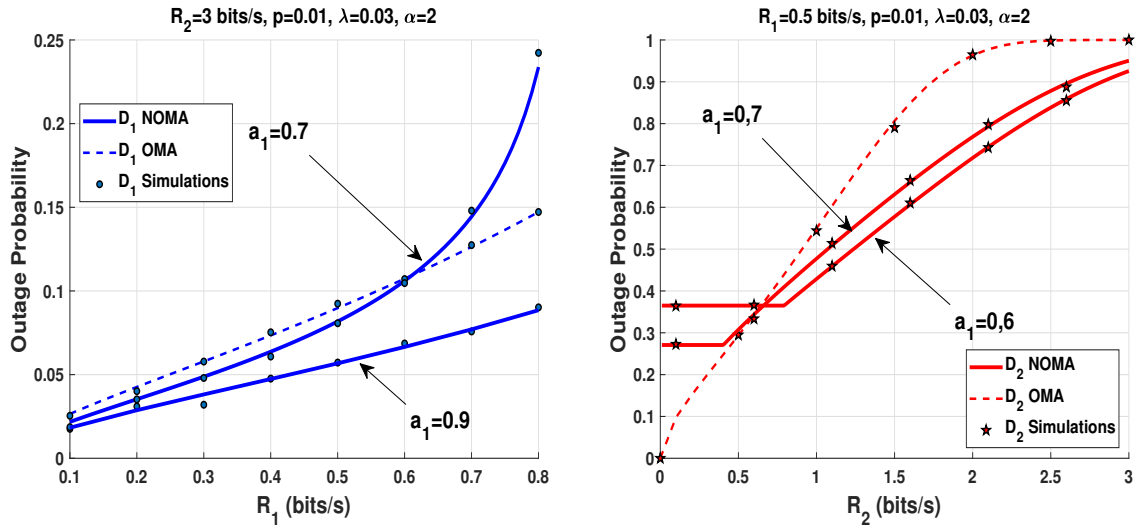

(a) (b)

Figure 2.13.: Outage probability as a function of the data rates considering cooperative NOMA and cooperative OMA. (a) outage probability of D_1 as a function of $\mathcal{R}_1$. (b) outage probability of D_2 as a function of $\mathcal{R}_2$.

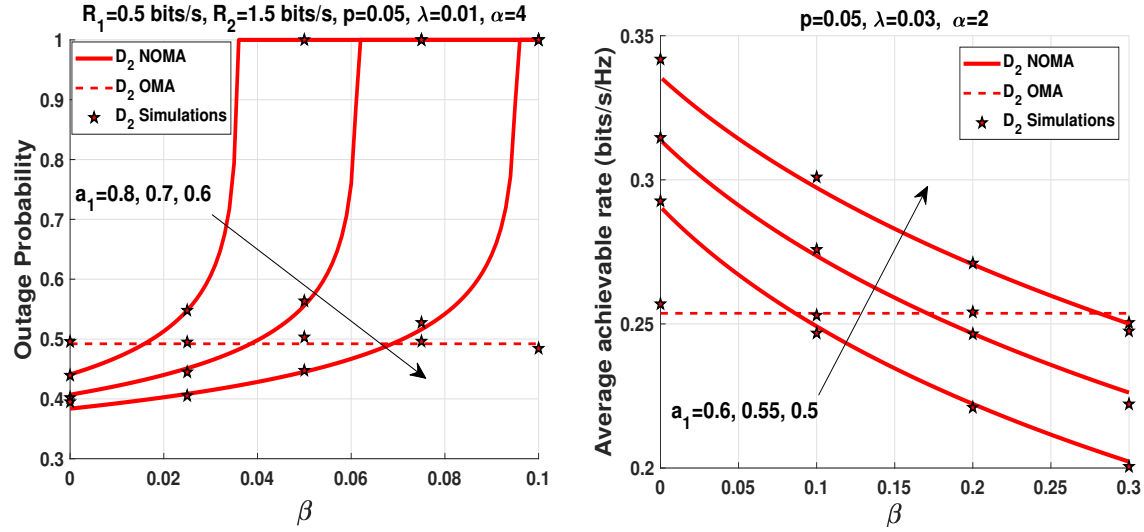

(a) (b)

Figure 2.14.: The performance of D_2 as a function β considering cooperative NOMA and cooperative OMA. (a) outage probability for several values of a_1. (b) average achievable rate for several values of a_1.

is allocated to D_2 (small value of a_1). This is because, unlike the vehicle D_1, the vehicle D_2 has to decode D_1 message first, and then decode its own message. Hence, $\mathbb{P}(O_{(2)})$ depends solely on $\mathcal{R}_1$ for small values of $\mathcal{R}_2$.

Counter-intuitively, we notice that, for low values of $\mathcal{R}_2$, NOMA outage probability when more power is allocated to D_2 (e.g, $a_1 = 0.6$) is greater than the NOMA outage probability when less power is allocated to D_2 (e.g, $a_1 = 0.7$). This can be explained as follows: when more power is allocated to D_2, less power is allocated to D_1, hence D_2 cannot decode D_1 message. We also notice that, for large values of $\mathcal{R}_2$ ($\mathcal{R}_2 > 2$bit/s), NOMA has better performance in terms of outage probability than OMA. This is because for large values of $\mathcal{R}_2$, the decoding threshold of cooperative OMA increases linearly since it is multiplied by a factor of 4. This proves that cooperative NOMA has a better outage performance for high data rates.

We can see from Fig.2.14(a) that, as β increases, the outage probability of cooperative NOMA increases. We can also see that the for $a_1 = 0.8$, when $1,5\%$ of interference is not removed, cooperative OMA outperforms NOMA. This percentage increases when we decreases a_1. This makes the SIC a critical part in the design of cooperative NOMA vehicular systems.

As shown in Fig.2.14(b), the average achievable rate decreases as β increases. This is because increasing β increases in the interference at D_2 as stated in Fig2.14(a). We notice that, as a_1 increases, the average achievable rate at D_2 decreases because less power is allocated to D_2.

From Fig.2.15(a), we can see that the outage probability of D_1 increases as $\mathcal{R}_1$, which is intuitive since the decoding threshold increases accordingly. We can also see that, the outage probability of D_2 is constant when $\mathcal{R}_1 < 1.1$ bit/s. This due to the fact that the outage at D_2 for relatively small values of $\mathcal{R}_1$, does not depend on $\mathcal{R}_1$, since the outage occurs because D_2 cannot decode its own message. In other words, when $\mathcal{R}_1$ is small, the outage

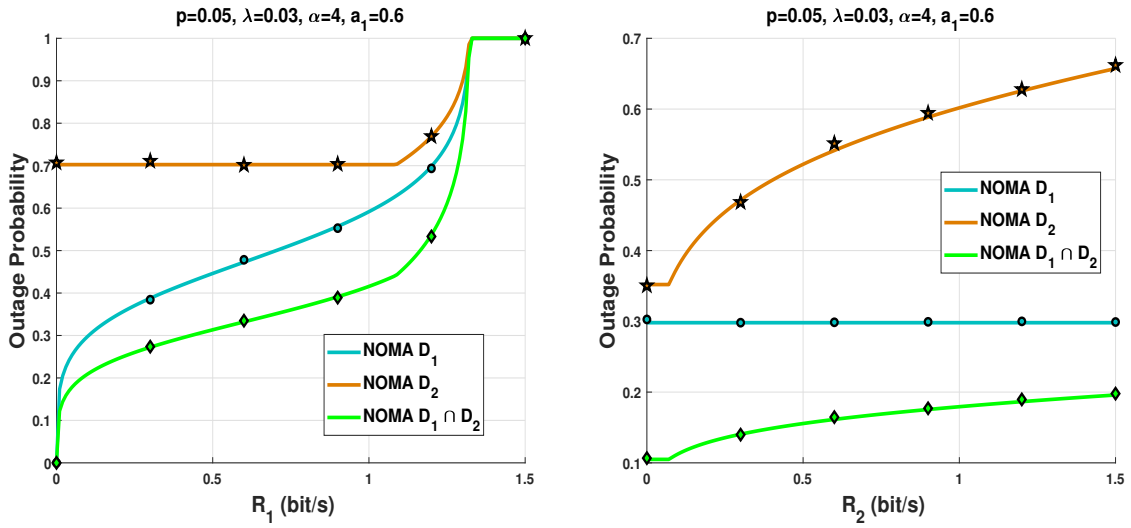

(a) (b)

Figure 2.15.: NOMA outage probability considering direct transmission. as a function of the data rates, for D_1, D_2, and the overall system outage. (a) Outage probability as a function of $\mathcal{R}_1$ (when $\mathcal{R}_2$ is set to 2 bits/s).(b) Outage probability as a function of $\mathcal{R}_2$ (when $\mathcal{R}_1$ is set to 0.1 bits/s).

probability depends only on the values of $\mathcal{R}_2$, but as R_1 increases, the outage probability at D_2 will depends on $\mathcal{R}_1$ and $\mathcal{R}_2$. However, when $\Theta_1 \geq a_1/a_2$, the outage occurs on both D_1, D_2. This is because, the outage probability at D_1 is set to 1, hence the outage probability at D_2 is also set to 1, since D_2 can no longer decode D_1 message due to the aforementioned condition. Therefore, D_1, D_2 and the overall system, has an outage probability of 1.

From Fig.2.15(b), we can see that the outage probability of D_1 remains constant regardless of $\mathcal{R}_2$ value. This is because the outage at D_1 does not depend on $\mathcal{R}_2$. We can also see that the outage probability of D_2 is constant for small values of $\mathcal{R}_2$ ($\mathcal{R}_2 < 0.07$ bit/s). This due to the same reason as we mentioned for Fig.2.15(a). The outage at D_2 for small values of $\mathcal{R}_2$ does not depend on $\mathcal{R}_2$, since the outage occurs because D_2 cannot decode D_1 message. The shape of the curve for the overall system is the same as for as D_2, since the outage of D_1 is constant.

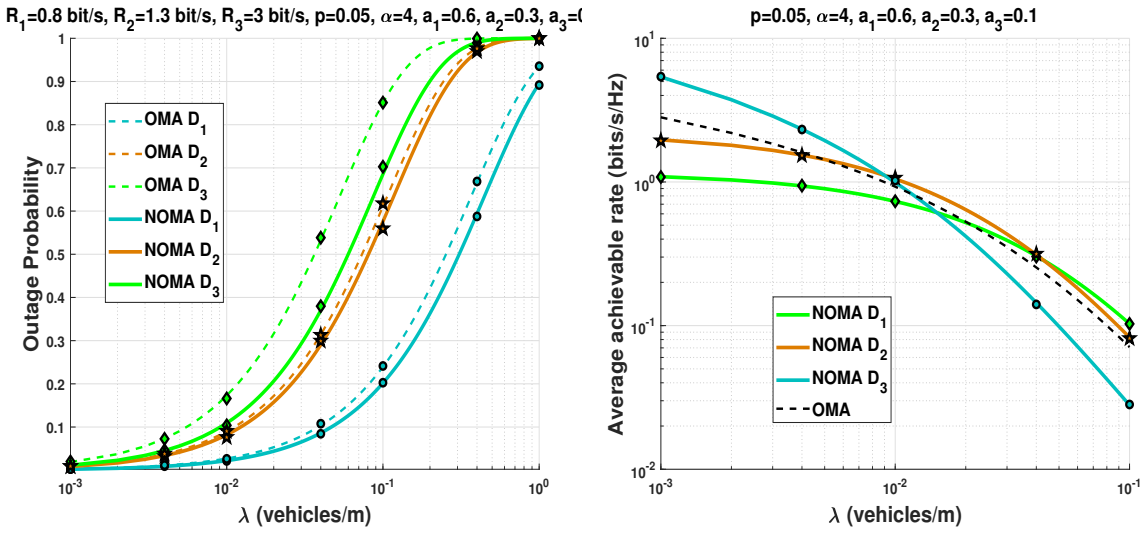

(a) (b)

Figure 2.16.: Performance of a transmission as a function of vehicles density λ, considering NOMA and OMA, when $K = 3$. (a) Outage probability as a function of λ considering NOMA and OMA for D_1, D_2, and D_3. (b) Average achievable rate as a function of λ considering NOMA and OMA for D_1, D_2, and D_3.

For the sake of completeness, we carried out performance analysis when three receiving vehicles are involved considering direct transmission. We can see from Fig.2.16(a) that NOMA outperforms OMA for all the vehicles, that is, D_1, D_2 and D_3. Surprisingly, even though the vehicle D_3 has a small power allocation ($a_3 = 0.1$) in NOMA, the gap between performance of NOMA and OMA is significant. This is because, as explained for Fig.**??**, as the target data rates increase, OMA performances decreases. For instance, when three vehicles are involved, the target data rate of OMA is multiplied by a factor of 3, which increases significantly the decoding threshold. We can see, from Fig.2.16(b) that the vehicles D_3 has a larger average achievable rate than D_1 and D_2. This is because D_3 does not have extra interference. However, this holds true only when density of vehicles is low. In the presence of high density vehicles, the performance of D_3 in terms of average achievable rate decreases drastically. We can also see that D_1 and D_2 are more robust to the interference for high values of λ. For highly dense environments ($\lambda > 0.4$ vehicles/m), D_1 has a better

than D_2 and D_3.

2.7. System Model

We consider the same intersection scenario and MAC protocol as in section 1.3.1 and section 1.3.2. Also, we consider the same NOMA assumption and channel and interference model as in section 2.2.4 and section 2.2.5.

2.8. MRC cooperative NOMA Outage Expressions

We use a DF decoding strategy, i.e., R decodes the message, re-encodes it, then forwards it to D_1 and D_2. We also use a half-duplex transmission in which a transmission occurs during two phases. Each phase lasts one timeslot. During the first phase, S broadcasts the message, and the receiving nodes R, D_1 and D_2 try to decode it, that is, ($S \to R$, $S \to D_1$, and $S \to D_2$). During the second phase, R broadcasts the message to D_1 and D_2 ($R \to D_1$ and $R \to D_2$). Then D_1 and D_2 add the power received in the first phase from S and the power received from R during the second phase to decode the message as shown in Fig.2.17.

2.8.1. Outage Events

We define an outage event at the receiving node when the SIR at the receiver is below a given threshold. According to SIC [Has+03], D_1 is decoded first since it has the higher power allocation, and D_2 message is considered as interference. The outage event at R to not decode D_1, denoted $\mathcal{A}_{R_1}(\Theta_1)$, is defined as

$$\mathcal{A}_{R_1}(\Theta_1) \triangleq \frac{P|h_{SR}|^2 l_{SR}\, a_1}{P|h_{SR}|^2 l_{SR} a_2 + I_{X_R} + I_{Y_R} + \sigma^2} < \Theta_1, \tag{2.68}$$

where $\Theta_1 = 2^{2\mathcal{R}_1} - 1$, and $\mathcal{R}_1$ is the target data rate of D_1.

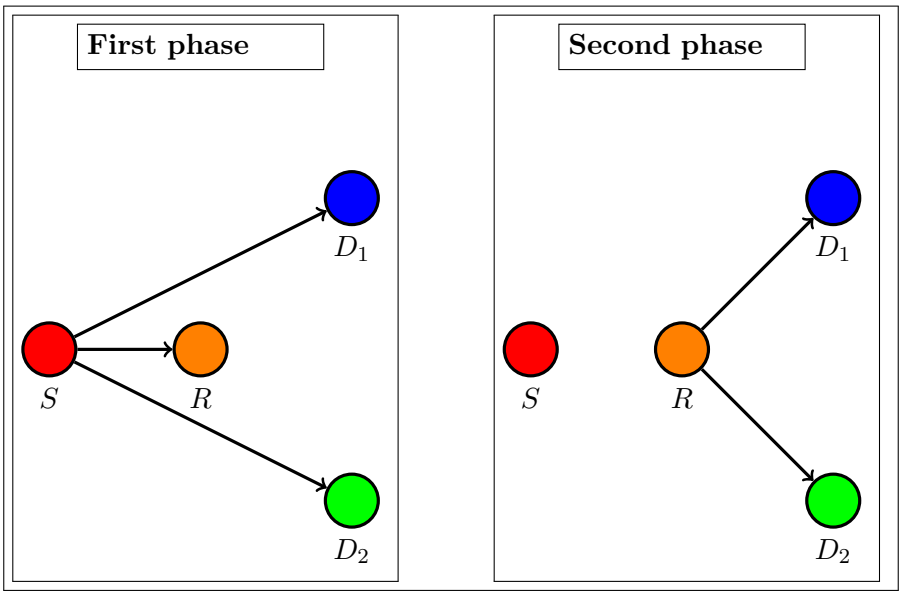

Figure 2.17.: Transmission scheme using MRC and NOMA.

Since D_2 has a lower power allocation, R has to decode D_1 message, then decode D_2 message. The outage event at R to not decode D_2 message, denoted $\mathcal{A}_{R_2}(\Theta_2)$, is defined as

$$\mathcal{A}_{R_2}(\Theta_2) \triangleq \frac{P|h_{SR}|^2 l_{SR}\, a_2}{\beta P|h_{SR}|^2 l_{SR}\, a_1 + I_{X_R} + I_{Y_R} + \sigma^2} < \Theta_2, \tag{2.69}$$

where $\Theta_2 = 2^{2\mathcal{R}_2} - 1$, and $\mathcal{R}_2$ is the target data rate of D_2.

Similarly, the outage event at D_1 to not decode its intended message in the first phase ($S \to D_1$), denoted $\mathcal{B}_{D_1}(\Theta_1)$, is given by

$$\mathcal{B}_{D_1}(\Theta_1) \triangleq \frac{P|h_{SD_1}|^2 l_{SD_1}\, a_1}{P|h_{SD_1}|^2 l_{SD_1} a_2 + I_{X_{D_1}} + I_{Y_{D_1}} + \sigma^2} < \Theta_1. \tag{2.70}$$

Finally, in order for D_2 to decode its intended message, it has to decode D_1 message. The outage event at D_2 to not decode D_1 message in the first phase ($S \to D_2$), denoted $\mathcal{B}_{D_{2-1}}(\Theta_1)$, and the outage event at D_2 to not decode its intended message, denoted

$\mathcal{B}_{D_{2-2}}(\Theta_2)$, are respectively given by

$$\mathcal{B}_{D_{2-1}}(\Theta_1) \triangleq \frac{P|h_{SD_2}|^2 l_{SD_2}\, a_1}{P|h_{SD_2}|^2 l_{SD_2} a_2 + I_{X_{D_2}} + I_{Y_{D_2}} + \sigma^2} < \Theta_1, \tag{2.71}$$

and

$$\mathcal{B}_{D_{2-2}}(\Theta_2) \triangleq \frac{P|h_{SD_2}|^2 l_{SD_2}\, a_2}{\beta P|h_{SD_2}|^2 l_{SD_2}\, a_1 + I_{X_{D_2}} + I_{Y_{D_2}} + \sigma^2} < \Theta_2. \tag{2.72}$$

During the second phase, D_1 adds the power received from S and from R. Hence, the outage event at D_1 to not decode its message in the second phase, denoted $\mathcal{C}_{D_{1\to1}}(\Theta_1)$, is expressed as

$$\mathcal{C}_{D_{1\to1}}(\Theta_1) \triangleq \frac{P\sum_{[SD_1,RD_1]}(|h|^2, l)\, a_1}{P\sum_{[SD_1,RD_1]}(|h|^2, l)\, a_2 + I_{X_{D_1}} + I_{Y_{D_1}} + \sigma^2} < \Theta_1, \tag{2.73}$$

where

$$\sum_{[SD_i,RD_i]}(|h|^2, l) = |h_{SD_i}|^2 l_{SD_i} + |h_{RD_i}|^2 l_{RD_2}.$$

In the same way, in the second phase, D_2 adds the power received from S and from R. Hence, the outage event at D_2 to not decode D_1 message, denoted $\mathcal{C}_{D_{2\to1}}(\Theta_1)$, and the outage event at D_2 to not decode its message, denoted $\mathcal{C}_{D_{2\to2}}(\Theta_2)$, are respectively expressed as

$$\mathcal{C}_{D_{2\to1}}(\Theta_1) \triangleq \frac{P\sum_{[SD_2,RD_2]}(|h|^2, l)\, a_1}{P\sum_{[SD_2,RD_2]}(|h|^2, l)\, a_2 + I_{X_{D_2}} + I_{Y_{D_2}} + \sigma^2} < \Theta_1, \tag{2.74}$$

and

$$\mathcal{C}_{D_{2\to2}}(\Theta_2) \triangleq \frac{P\sum_{[SD_2,RD_2]}(|h|^2, l)\, a_2}{\beta P\sum_{[SD_2,RD_2]}(|h|^2, l)\, a_1 + I_{X_{D_2}} + I_{Y_{D_2}} + \sigma^2} < \Theta_2. \tag{2.75}$$

The overall outage event related to D_1, denoted $O_{(1)}$, is given by

$$O_{(1)} \triangleq \Big[\mathcal{B}_{D_{1\to1}}(\Theta_1) \cap \mathcal{A}_{R_1}(\Theta_1)\Big] \cup \Big[\mathcal{A}^C_{R_1}(\Theta_1) \cap \mathcal{C}_{D_{1\to1}}(\Theta_1)\Big]. \tag{2.76}$$

Finally, the overall outage event related to D_2, denoted $O_{(2)}$, is given by

$$O_{(2)} \triangleq \left[\left\{\bigcup_{i=1}^{2}\mathcal{B}_{D_{2-i}}(\Theta_i)\right\}\cap\left\{\bigcup_{i=1}^{2}\mathcal{A}_{R_i}(\Theta_i)\right\}\right]\bigcup\left[\left\{\bigcap_{i=1}^{2}\mathcal{A}^{C}_{R_i}(\Theta_i)\right\}\cap\left\{\bigcup_{i=1}^{2}\mathcal{C}_{D_{2-i}}(\Theta_i)\right\}\right]. \tag{2.77}$$

2.8.2. Outage Probability Expressions

In the following, we will express the outage probability $O_{(1)}$ and $O_{(2)}$. The probability $\mathbb{P}(O_{(1)})$, when $\Theta_1 < a_1/a_2$, is given by

$$\begin{aligned}\mathbb{P}(O_{(1)}) &= 1-\mathcal{H}_{(D_1)}(\frac{G_1}{l_{SD_1}})-\mathcal{H}_{(R)}(\frac{G_1}{l_{SR}})+\mathcal{H}_{(D_1)}(\frac{G_1}{l_{SD_1}})\mathcal{H}_{(R)}(\frac{G_1}{l_{SR}})\\ &\quad+\mathcal{H}_{(R)}(\frac{G_1}{l_{SR}})-\frac{l_{RD_1}\mathcal{H}_{(R)}(\frac{G_1}{l_{SR}})\mathcal{H}_{(D_1)}(\frac{G_1}{l_{RD_1}})-l_{SD_1}\mathcal{H}_{(R)}(\frac{G_1}{l_{SR}})\mathcal{H}_{(D_1)}(\frac{G_1}{l_{SD_1}})}{l_{RD_1}-l_{SD_1}},\end{aligned} \tag{2.78}$$

where $G_1 = \Theta_1/(a_1-\Theta_1 a_2)$, and $\mathcal{J}_{(M)}\left(\frac{A}{B}\right)$ is expressed as

$$\mathcal{H}_{(M)}\left(\frac{A}{B}\right) = \mathcal{L}_{I_{X_M}}\left(\frac{A}{B}\right)\mathcal{L}_{I_{Y_M}}\left(\frac{A}{B}\right)\exp\left(-\frac{\sigma^2 A}{PB}\right). \tag{2.79}$$

The probability $\mathbb{P}(O_{(2)})$, when $\Theta_1 < a_1/a_2$ and $\Theta_2 < a_2/\beta a_1$, is given by

$$\begin{aligned}\mathbb{P}(O_{(2)}) &= 1-\mathcal{H}_{(D_2)}(\frac{G_{\max}}{l_{SD_2}})-\mathcal{H}_{(R)}(\frac{G_{\max}}{l_{SR}})+\mathcal{H}_{(D_2)}(\frac{G_{\max}}{l_{SD_2}})\mathcal{H}_{(R)}(\frac{G_{\max}}{l_{SR}})\\ &\quad+\mathcal{H}_{(R)}(\frac{G_{\max}}{l_{SR}})-\frac{l_{RD_2}\mathcal{H}_{(R)}(\frac{G_{\max}}{l_{SR}})\mathcal{H}_{(D_2)}(\frac{G_{\max}}{l_{RD_2}})-l_{SD_2}\mathcal{H}_{(R)}(\frac{G_{\max}}{l_{SR}})\mathcal{H}_{(D_2)}(\frac{G_{\max}}{l_{SD_2}})}{l_{RD_2}-l_{SD_2}},\end{aligned} \tag{2.80}$$

where $G_{\max} = \max(G_1, G_2)$, and $G_2 = \Theta_2/(a_2-\Theta_2\beta a_1)$.

Proof: See Appendix B.5. ■

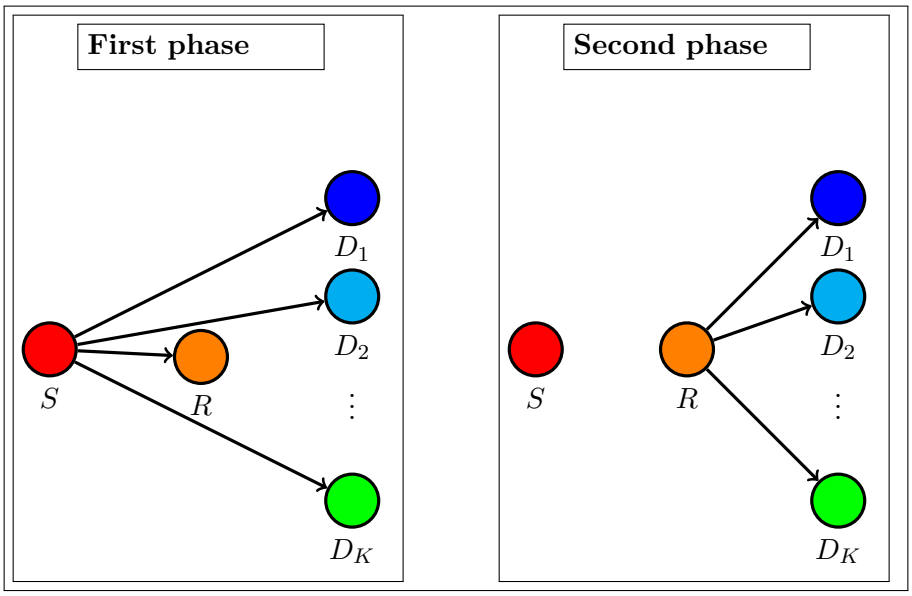

Figure 2.18.: Transmission scheme using MRC and NOMA considering multiple destinations.

2.8.3. NOMA With K-Destinations

We extend the results of NOMA to K-destinations as depicted in Fig.2.18. We generalize the following events to K destination nodes D_K as

$$\mathcal{A}_{R_i}(\Theta_i) \triangleq \frac{P|h_{SR}|^2 l_{SR}\, a_i}{P|h_{SR}|^2 l_{SR}\left[\beta \sum_{h=1}^{i-1} a_h + \sum_{n=i+1}^{K} a_n\right] + I_{X_R} + I_{Y_R} + \sigma^2} < \Theta_i, \tag{2.81}$$

$$\mathcal{B}_{D_{i\to t}}(\Theta_t) \triangleq \frac{P|h_{SD_i}|^2 l_{SD_i}\, a_t}{P|h_{SD_i}|^2 l_{SD_i}\left[\beta \sum_{h=1}^{t-1} a_h + \sum_{n=t+1}^{K} a_n\right] + I_{X_{D_i}} + I_{Y_{D_i}} + \sigma^2} < \Theta_t, \tag{2.82}$$

and

$$\mathcal{C}_{D_{i\to t}}(\Theta_1) \triangleq \frac{P\sum_{[SD_i,RD_i]}(|h|^2,l)\,a_t}{[\beta\sum_{h=1}^{t-1}a_h+\sum_{n=t+1}^{K}a_n]P\sum_{[SD_i,RD_i]}(|h|^2,l)+I_{X_{D_1}}+I_{Y_{D_1}}+\sigma^2} < \Theta_t. \tag{2.83}$$

Note that, when $h > t-1$, then $\sum_{h=1}^{t-1} a_h = 0$, and when $n > K$, then $\sum_{n=t+1}^{K} a_n = 0$.

The outage event at the ith destination node, denoted $O_{(i)}$, is given by

$$O_{(i)} \triangleq \left[\left\{\bigcup_{m=K-i+1}^{K}\mathcal{B}_{D_{i\to i-(K-m)}}(\Theta_{i-(K-m)})\right\}\cap\left\{\bigcup_{m=K-i+1}^{K}\mathcal{A}_{R_{i-(K-m)}}(\Theta_{i-(K-m)})\right\}\right] \bigcup \left[\left\{\bigcap_{m=K-i+1}^{K}\mathcal{A}^{C}_{R_{i-(K-m)}}(\Theta_{i-(K-m)})\right\}\cap\left\{\bigcup_{m=K-i+1}^{K}\mathcal{C}_{D_{i\to i-(K-m)}}(\Theta_{i-(K-m)})\right\}\right].$$

Finally, the outage probability of D_i when $\bigcup_{t=1}^{i}\frac{a_t}{\beta\sum_{h=1}^{t-1}a_h+\sum_{n=t+1}^{K}a_n} \leq \Theta_t$, is expressed by

$$\mathbb{P}(O_{(i)}) = 1-\mathcal{J}_{(D_i)}(\frac{G_{(i)\max}}{l_{SD_i}})-\mathcal{J}_{(R)}(\frac{G_{(i)\max}}{l_{SR}})+\mathcal{J}_{(D_i)}(\frac{G_{(i)\max}}{l_{SD_i}})\mathcal{J}_{(R)}(\frac{G_{\max}}{l_{SR}})+\mathcal{J}_{(R)}(\frac{G_{(i)\max}}{l_{SR}}) - \frac{l_{RD_i}\mathcal{J}_{(R)}(\frac{G_{(i)\max}}{l_{SR}})\mathcal{J}_{(D_i)}(\frac{G_{(i)\max}}{l_{RD_i}})-l_{SD_i}\mathcal{J}_{(R)}(\frac{G_{(i)\max}}{l_{SR}})\mathcal{J}_{(D_i)}(\frac{G_{(i)\max}}{l_{SD_i}})}{l_{RD_i}-l_{SD_i}},$$

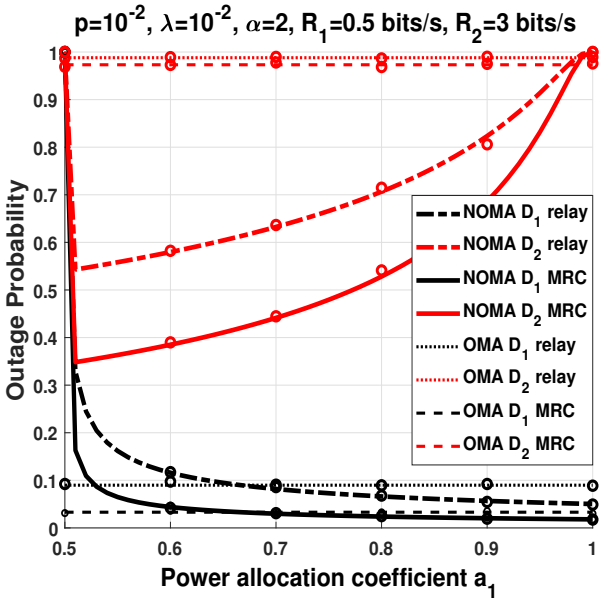

Figure 2.19.: Outage probability as a function of a_1 considering NOMA and OMA.

and $G_{(i)\max}$ is given by

$$G_{(i)\max} = \max\left\{ \frac{\Theta_{i-(K-1)}}{a_{i-(K-1)} - \Theta_{i-(K-1)}[\beta \sum_{h=1}^{i-(K-1)-1} a_h + \sum_{n=i-(K-1)+1}^{K} a_n]}, \right.$$
$$\frac{\Theta_{i-(K-2)}}{a_{i-(K-2)} - \Theta_{i-(K-2)}[\beta \sum_{h=1}^{i-(K-2)-1} a_h + \sum_{n=i-(K-2)+1}^{K} a_n]}, \ldots,$$
$$\left. \frac{\Theta_{i-(K-l)}}{a_{i-(K-l)} - \Theta_{i-(K-l)}[\beta \sum_{h=1}^{i-(K-l)-1} a_h + \sum_{n=i-(K-l)+1}^{K} a_n]} \right\},$$

where $l \in \{1, 2, ..., K\}$, $\Theta_t = 2^{2\mathcal{R}_t} - 1$, and $\mathcal{R}_t$ is target data rate of D_t. We impose the condition that $l > K - i$.

2.9. Simulations and Discussions

In this section, we evaluate the performance of MRC using NOMA at intersections. Monte-Carlo simulation are carried out by generating samples (which correspond to the interfering

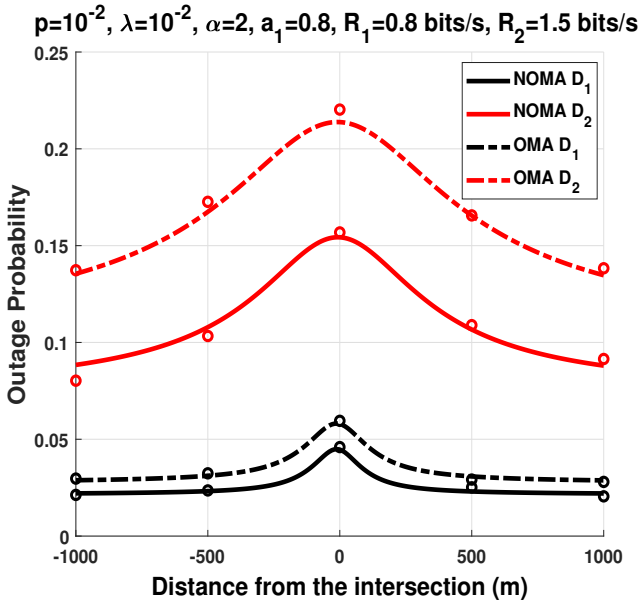

Figure 2.20.: Outage probability as a function of the distance from the intersection considering NOMA and OMA.

vehicles) according to a PPP, and we average over 50.000 iterations of Rayleigh fading channel. The Monte-Carlo simulations match the theoretical analysis, which confirm the accuracy of our results. Unless stated otherwise, $\beta = 0$, $S = [100, 0]$, $R = [50, 0]$, $D_1 = [0, 0]$ and $D_2 = [0, -10]$. We set, without loss of generality, $\lambda_X = \lambda_Y = \lambda$.

Fig.2.19 shows the outage probability as a function of a_1, using a relay transmission (cooperative transmission in section 2.3.3) and MRC transmission, considering NOMA and OMA. We can see from Fig.2.19, that using MRC offers a significant improvement over the relay transmission. We can also see that the improvement that MRC offers compared to the the relay transmission is greater for D_2 using NOMA. We can also see that MRC using NOMA has a decreases in outage of 34% compared to relay using NOMA. Whereas the improvement of MRC using OMA compared to relay OMA is 2%. On the other hand, we can notice an improvement of 60% when using MRC in NOMA compared to MRC in OMA.

Fig.2.20 shows the outage probability as a function of the distance between the nodes

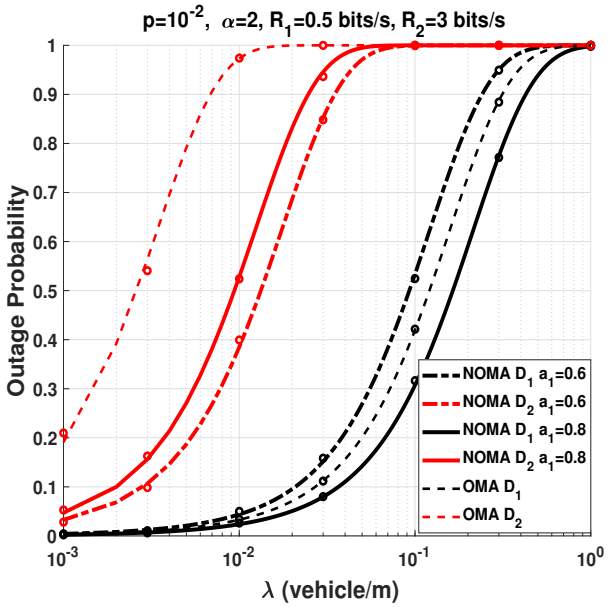

Figure 2.21.: Outage probability as a function of λ considering NOMA and OMA.

and the intersection, considering NOMA and OMA. We can see that the outage probability reaches its maximum value at the intersection, that is, when the distance between the nodes and the intersection equals zero. This is because when the nodes are far from the intersection, the aggregate interference of the vehicles that are located on the same road is greater than the aggregate interference of the vehicles that are on the other road. However, when the nodes are at the intersection, the interfering vehicles of both roads interfere equally on the receiving nodes. We can also see from Fig.2.20 that NOMA outperforms OMA for both D_1 and D_2. The gap in performance between NOMA and OMA is greater for D_2.

Fig.2.21 investigates the impact of the vehicles density λ on the outage probability, considering NOMA and OMA. We can see from Fig.2.21 that, as the intensity of the vehicles increases, the outage probability increases. We can also see that, when $a_1 = 0.6$, NOMA outperforms OMA for both D_1 and D_2. However, we can see that, when when $a_1 = 0.8$, NOMA outperforms OMA only for D_1, whereas OMA outperforms NOMA for D_2. This is because, when we allocate more power to D_1, less power is allocated to D_2, which decreases

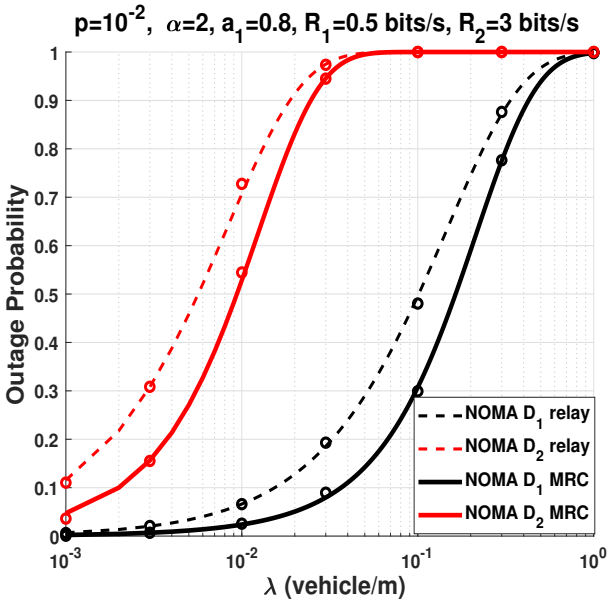

Figure 2.22.: Outage probability as a function of λ considering NOMA using different transmission schemes.

the performance of NOMA compared to OMA.

Fig.2.22 shows the outage probability as a function of λ considering NOMA using different transmission schemes. We can clearly see that the MRC using NOMA outperforms the classical relay transmission using NOMA. This holds true for both D_1 and D_2. This result is intuitive since in the relay transmission using NOMA, D_1 and D_2 decode the message transmitted by the relay. However, in the MRC transmission scheme using NOMA, D_1 and D_2 combine the signal from the source, and from the relay, which increases the power at the D_1 and D_2, and consequently increases the SIR.

Fig.2.23 depicts the outage probability as a function of the relay position, using a relay transmission and MRC transmission considering NOMA. Without loss of generality, we set $\|S - D_1\| = \|S - D_2\| = 100$ m. We can notice, from Fig.2.23(a), that when $\alpha = 2$, the optimal position for the relay, using a relay transmission, is near the destinations, D_1 and D_2, whereas for MRC, the optimal relay position is when the relay is close to the destination

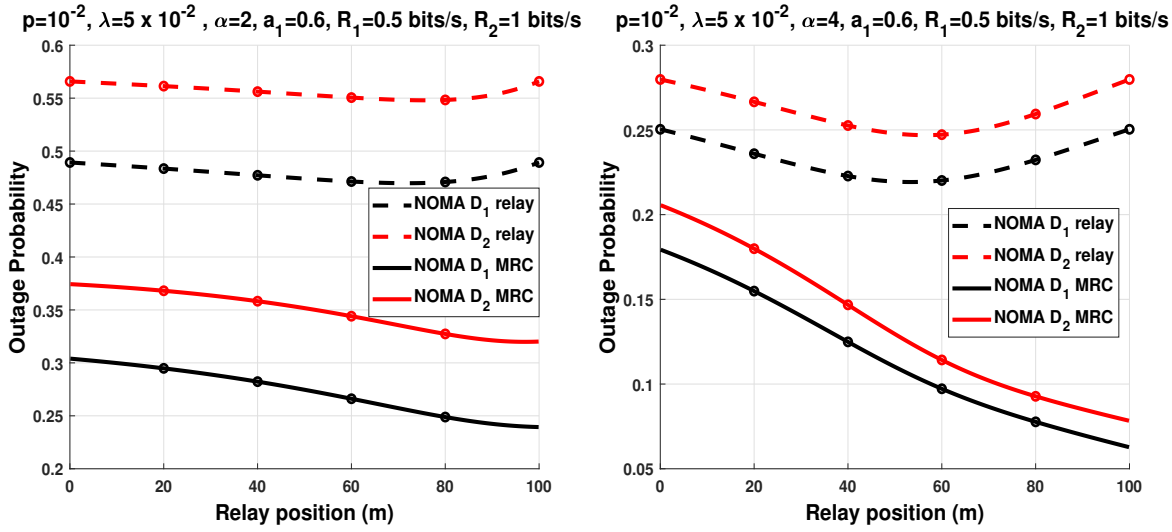

(a) (b)

Figure 2.23.: Outage probability as a function of the relay position.

nodes. We also can notice, from Fig.2.23(b), that when $\alpha = 4$, the optimal position for the relay using a relay transmission is at the mid distance between the source S, and the destinations, D_1 and D_2. However, we can see that for MRC, the optimal relay position is when the relay is close to the destination nodes. This can be explained as follows: when the relay is close to the destination (D_1 or D_2), the channel between S and D_1 ($S \rightarrow D_1$) and the channel between R and D_1 ($R \rightarrow D_1$) will be decorrelated, thus, increasing the diversity gain.

We can see form the Fig.2.24 that the noise power greatly impact the performance only for low values of λ. However, as the value of λ increases, the performance when considering noise power and without noise power tends the same values. This is because, for high value of λ, the power of noise becomes negligible compared to the power of interference.

Finally, we investigate the impact of the data rates $\mathcal{R}_1$ and $\mathcal{R}_2$ on the performance considering NOMA and OMA using MRC and the relay transmission. We can see from Fig.2.26(a) that as $\mathcal{R}_1$ increases, the outage probability of D_1 increases. This is intuitive

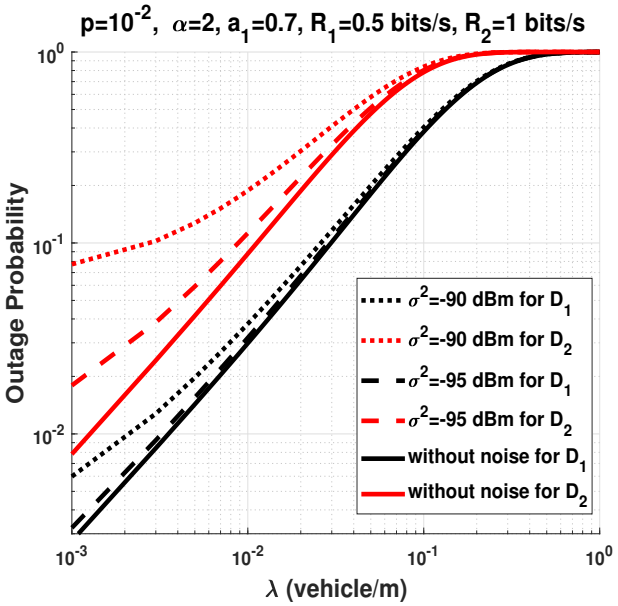

Figure 2.24.: Outage probability as a function of λ for several noise power values.

since increasing the data rate increases the decoding threshold which increases the outage probability. We can also see that NOMA offers better performance than OMA. However, as $\mathcal{R}_1$ increases, OMA outperforms NOMA for both MRC transmission and relay transmission.

Also, we can see from Fig.2.26(b) that, from small values of $\mathcal{R}_2$, that is, $\mathcal{R}_2 < 0.5$ bit/s, OMA offers better performance than NOMA in terms of outage probability. This is because, unlike the vehicle D_1, the vehicle D_2 has to decode D_1 message first, and then decodes its own message. Hence, $\mathbb{P}(D_2)$ depends solely on $\mathcal{R}_1$ for small values of $\mathcal{R}_2$. We also notice that, for large values of $\mathcal{R}_2$ ($\mathcal{R}_2 > 2$bit/s), NOMA has better performance in terms of outage probability than OMA. This is because, for large values of $\mathcal{R}_2$, the decoding threshold of OMA increases linearly since it is multiplied by a factor of 4. This proves that cooperative NOMA has a better outage performance for high data rates. Finally, we can see that MRC transmission outperforms cooperative transmission for both NOMA and OMA.

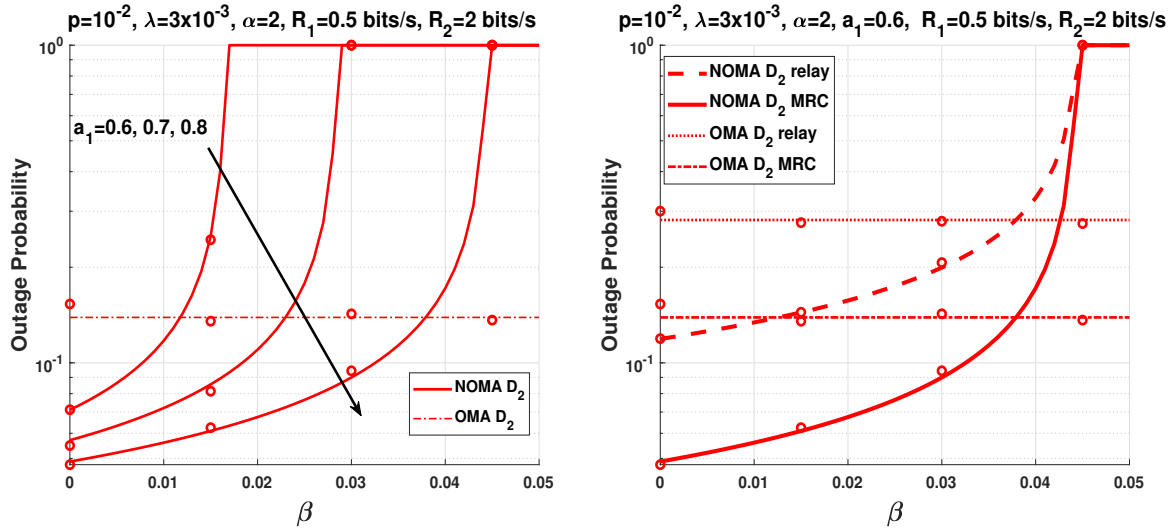

(a) (b)

Figure 2.25.: Outage probability of D_2 as a function of β considering NOMA and OMA.

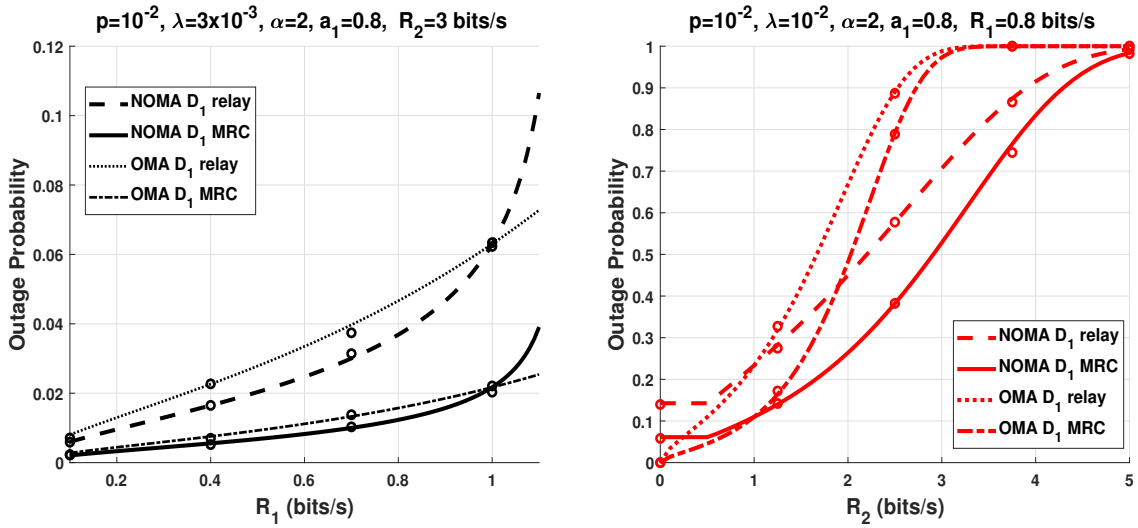

(a) (b)

Figure 2.26.: Outage probability as a function of $\mathcal{R}_1$ and $\mathcal{R}_2$ considering NOMA and OMA.

2.10. Conclusion

In this chapter, we studied the performance of VCs with NOMA at intersections in presence of interference. Using stochastic geometry tools, we derived the outage probability and the average achievable rate expressions. We studied the case when the source sends a message to two destination nodes, and then generalized the study to K destination nodes. We took into account both perfect and imperfect SIC. We also made the following observations:

- As the vehicles move toward to the intersection (400m), the outage probability increases. We notice that the outage probability increased by 62% for D_1, and by 43% for D_2 at the intersection. The average achievable rate decreased by 50% at the intersection. We compared the performance of VCs at intersections and the performance of VCs at highways, and showed that the performance of VCs at intersections is worse that at highways.

- NOMA outperforms OMA in terms of outage probability and average achievable rate. The benefit of NOMA over OMA become greater as the target data rates increase. However, when the system parameters (e.g,. power allocation coefficient, data rates) do not respect certain conditions, NOMA performance decreases drastically.

- The SIC process degrades the performance of NOMA. However, we noticed that the effect of imperfect SIC can be alleviated by allocating more power to the second destination node.

To improve the performance, we investigated the impact of the relay position. We found that, the best relay position forD_1 was at mid-distance between S and D_1, whereas the best relay position for D_2 was near D_2.

We found that the outage probability increased whereas and average achievable rate decreased at the intersection. We also found that using cooperative NOMA improved the performance in terms of outage probability and average achievable rate compared to OMA at intersections. We showed that the performance of cooperative NOMA increased compared to cooperative OMA for larger data rates. However, when the system parameters (e.g,. power

allocation coefficient, data rates) were not chosen carefully, the performance of cooperative NOMA decreased drastically.

We also studied the improvement of using MRC in cooperative VCs transmission schemes considering NOMA at intersections. We compared the performance of MRC cooperative NOMA with a classical cooperative NOMA, and showed that MRC in cooperative NOMA transmission offers a significant improvement over the classical cooperative NOMA in terms of outage probability. We also compared the performance of MRC cooperative NOMA with MRC cooperative orthogonal multiple access (OMA), and we showed that NOMA has a better performance than OMA. Finally, we showed that the outage probability increases when the nodes come closer to the intersection, and that using MRC considering NOMA improves the performance in this context.

Chapter 3.

Extension scenarios

Parts of this chapter have been adapted from the conference papers [BHE20e; BHE20d; BHE20b].

Contents

3.1. Introduction

In this last chapter, we will investigate some extensions related to vehicular networks at intersections. We will investigate the performance of a proposed cooperative NOMA protocol. We will also investigate the performance and behavior of mmWave cooperative vehicular networks at intersections.

Regarding cooperative NOMA protocols, the authors in [DPP15] propose a cooperative NOMA protocol in a half duplex mode with a help of a relay. This conventional cooperative NOMA (CCN) protocol [DPP15] improves the performance of the transmission by adding a diversity gain. However, the spectral efficiency of this protocol is reduced due to the use of the half duplex mode. To cope with this limitation, the authors in [HGS17] propose a cooperative protocol, named relaying with NOMA back-haul. In this protocol, the source adjusts the time duration of the transmission based on the global instantaneous channel state information (CSI). However, global instantaneous CSI at the source can be hard to obtain in practice, especially for real time scenarios such as road safety scenarios. Hence, we propose an adaptive cooperative NOMA (ACN) protocol.

Regarding mm wave networks, several works have studied their modeling in the literature [Di 15; DL15; Zho+17; Wan+15; Mes+16; LDS16; Per+16; LD17; LDS17]. Few works studied cooperative communications using tools from stochastic geometry [Bis+16; Wu+17; BTJ18; Bel+18]. However, in [Bis+16; Wu+17; BTJ18], the effect of small-scale fading is not taken into consideration. In [Bel+18], the authors investigate the performance of mmWave relaying networks in terms of coverage probability with best relay selection. However, there are no prior works that consider both an intersection scenario with cooperative transmissions using NOMA and considering mmWave networks. Our analysis includes the effects of blockage from the building in intersections, and Nakagami-m fading channels

between the transmitting nodes with difference values of m for LOS and NLOS are considered. Unlike other works that uses approximations, closed form expressions are obtained for Nakagami-m fading channel.

Finally, we will as some extension scenarios, such as multiple lanes scenarios, multiple relays, and multi-hops scenarios.

3.1.1. Contributions

The contributions of this chapter are as follows:

- We propose and evaluate the performance of VCs protocol at at road intersections in the presence of interference. We calculate the outage probability related to ACN protocol, and closed form expressions are obtained considering a scenario involving a source, and two destinations. We compare the performance of ACN protocol with other existing protocols in the literature. We show that ACN protocol offers a significant improvement in terms of outage probability, especially at intersections. We show that the performance of ACN protocol increase compared to other existing protocols for high data rates.

- We study cooperative NOMA for mmWave vehicular networks at intersection roads. We derive closed form outage probability expressions for cooperative NOMA, and compare them with cooperative OMA. We show that cooperative NOMA exhibits a significant improvement compared to cooperative OMA, especially for high data rates. However, data rates have to respect a given condition, if not, the performance of cooperative NOMA will decreases drastically. We also show that as the nodes reach the intersection, the outage probability increased. Counter-intuitively, we show that NLOS scenario has a better performance than LOS scenario.

- We studied the impact of adding several relays on the performance and several lanes scenarios. We show that adding relays significantly increases the performance in terms

of outage probability. We also show that the single lane model can perfectly emulate the multiple lanes model. Finally, we derive the outage probability expression for several cases of multi-hops scenarios.

3.2. ACN Protocol

We consider a NOMA transmission between a source S, and two destinations, denoted D_1 and D_2. The triplet $\{S, D_1, D_2\}$ denotes the nodes and their locations as depicted in Fig.3.1.

We consider the same intersection scenario and MAC protocol as in section 2.2.1 and section 1.3.2. Also, we consider the same NOMA assumption and channel and interference model as in section 2.2.4 and section 2.2.5.

First, we consider the scenario in which D_1 acts as a relay to transmit the message to D_2. At the beginning of each transmission, S sends the superimposed signals to D_1 and D_2 using a direct transmission [BHE19a]. If D_2 decodes its desired message, it sends a 1-bit positive acknowledgement (ACK) to S and D_1, and thus, the transmission occurs in one phase. However, if D_2 is unable to decode its desired message, it sends a 1-bit negative acknowledge (NACK) to S and D_1. Hence, if D_1 decodes its desired message and D_2 message, it sends D_2 message using cooperative transmission [BHE19f] using OMA. Thus, the transmission occurs in two phases.

Then, we consider the scenario in which D_2 acts as relay to transmit the message to D_1. In this same way, S sends the superimposed message to D_1 and D_2 using a direct transmission. If D_1 decodes its desired message, it sends a 1-bit ACK to S and D_2, and thus, the transmission occurs in one phase. However, if D_1 is unable to decode its desired message, it sends a 1-bit NACK to S and D_1. Hence, if D_2 decodes D_1 message, it sends D_1 message using cooperative transmission, and without using NOMA. Thus, the transmission occurs in two phases[1]. The flow charts of ACN protocol at D_1 and D_2 are respectively given

[1]Note that ACN protocol does no need to perform channel estimation to switch between direct transmission

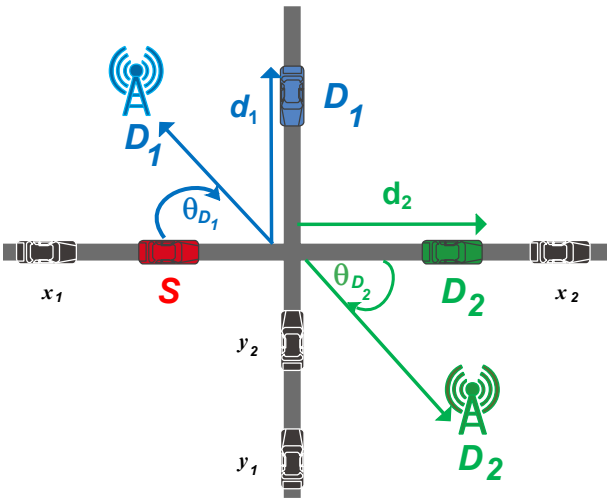

Figure 3.1.: NOMA system model for VCs. The nodes D_1 and D_2 can be vehicles or as part of the communication infrastructure.

by Fig.3.2 and Fig.3.3.

3.3. ACN Protocol Outage Expressions

3.3.1. SIR Expressions

The outage probability is defined as the probability that the SIR at the receiver node is below a given threshold. According to SIC [Has+03], D_1 will be decoded first since it has the higher power allocation, and D_2 message will be considered as interference. The SIR at D_1 to decode its desired message, denoted $\mathrm{SIR}_{D_{1-1}}$, is expressed as

$$\mathrm{SIR}_{D_{1-1}} = \frac{|h_{SD_1}|^2 l_{SD_1}\, a_1}{|h_{SD_1}|^2 l_{SD_1} a_2 + I_{X_{D_1}} + I_{Y_{D_1}}}. \tag{3.1}$$

Similarly, the SIR at D_1 to decode D_2 message, denoted $\mathrm{SIR}_{D_{1-2}}$, is expressed as

$$\mathrm{SIR}_{D_{1-2}} = \frac{|h_{SD_1}|^2 l_{SD_1}\, a_2}{I_{X_{D_1}} + I_{Y_{D_1}}}. \tag{3.2}$$

and cooperative transmission.

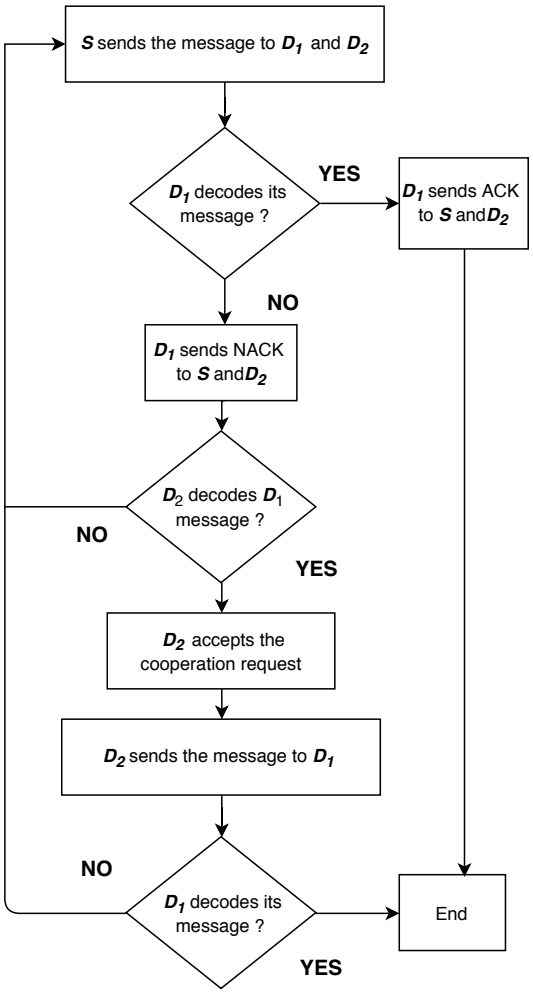

Figure 3.2.: Flow chart of ACN protocol at D_1.

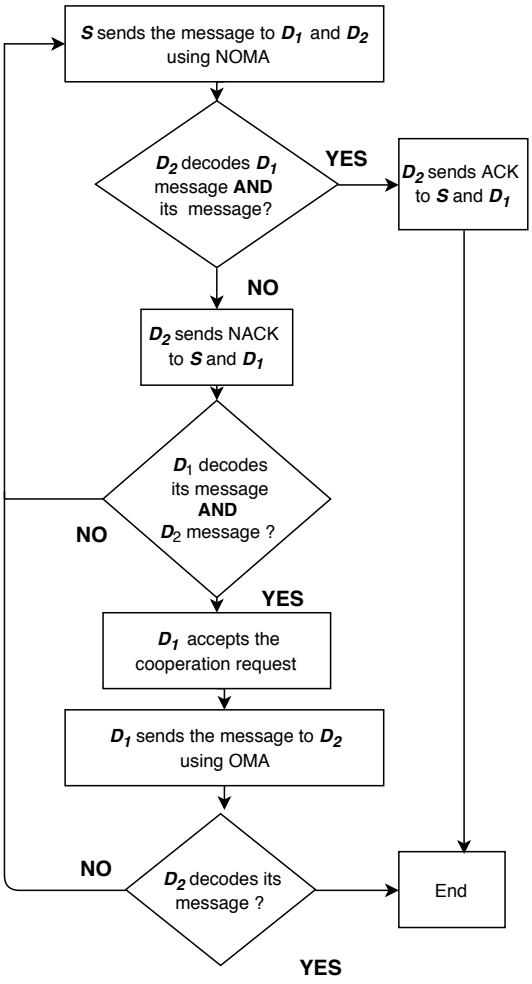

Figure 3.3.: Flow chart of ACN protocol at D_2.

Since D_2 has the lower power allocation, it decodes D_1 message first, then decodes its intended message. The SIR at D_2 to decode D_1 message, denoted $\mathrm{SIR}_{D_{2-1}}$, is expressed as

$$\mathrm{SIR}_{D_{2-1}} = \frac{|h_{SD_2}|^2 l_{SD_2}\, a_1}{|h_{SD_2}|^2 l_{SD_2} a_2 + I_{X_{D_2}} + I_{Y_{D_2}}}. \tag{3.3}$$

The SIR at D_2 to decode its desired message, denoted $\mathrm{SIR}_{D_{2-2}}$, is expressed as

$$\mathrm{SIR}_{D_{2-2}} = \frac{|h_{SD_2}|^2 l_{SD_2}\, a_2}{I_{X_{D_2}} + I_{Y_{D_2}}}. \tag{3.4}$$

When using the cooperative transmission, the node that acts as a relay uses OMA instead of NOMA, since the transmission involves only one receiving node. Hence, the SIR at the receiver is then expressed as

$$\mathrm{SIR}_{D_k D_l}^{(\mathrm{OMA})} = \frac{|h_{D_k D_l}|^2 l_{D_k D_l}}{I_{X_{D_l}} + I_{Y_{D_l}}}, \tag{3.5}$$

where $\{k, l\} \in \{1, 2\}$.

3.3.2. ACN Outage Event Expressions

Now, we will express the outage events related to the ACN protocol for D_1 and D_2. The outage events related to D_1 and D_2 using ACN protocol, denoted respectively by $\mathcal{O}_{\mathrm{ACN}}(D_1)$ and $\mathcal{O}_{\mathrm{ACN}}(D_2)$, can be expressed as

$$\mathcal{O}_{\mathrm{ACN}}(D_1) = 1 - \mathcal{O}_{\mathrm{ACN}}^{C}(D_1), \tag{3.6}$$

and

$$\mathcal{O}_{\mathrm{ACN}}(D_2) = 1 - \mathcal{O}_{\mathrm{ACN}}^{C}(D_2), \tag{3.7}$$

where $\mathcal{O}_{\mathrm{ACN}}(D_1)$ and $\mathcal{O}_{\mathrm{ACN}}(D_2)$ denote respectively the success events related to D_1 and D_2. The expression of $\mathcal{O}^C_{\mathrm{ACN}}(D_1)$ and $\mathcal{O}^C_{\mathrm{ACN}}(D_2)$ are respectively given by

$$\mathcal{O}^C_{\mathrm{ACN}}(D_1) = \{\mathrm{DT}^C_{SD_1}\} \cup \{\mathrm{DT}_{SD_1} \cap \mathrm{RT}^C_{S,D_2,D_1}\}, \tag{3.8}$$

and

$$\mathcal{O}^C_{\mathrm{ACN}}(D_2) = \{\mathrm{DT}^C_{SD_2}\} \cup \{\mathrm{DT}_{SD_2} \cap \mathrm{RT}^C_{S,D_1,D_2}\}, \tag{3.9}$$

where $\mathrm{DT}^C_{SD_n}$, $\mathrm{RT}^C_{S,D_2,D_1}$, and $\mathrm{RT}^C_{S,D_1,D_2}$, are expressed as

$$\mathrm{DT}^C_{SD_n} = \bigcap_{i=1}^{n} \mathrm{SIR}_{SD_{n-i}} < \Theta_i^{(1)}, \tag{3.10}$$

and

$$\mathrm{RT}^C_{S,D_2,D_1} = \left\{\mathrm{SIR}_{SD_{2-1}} \geq \Theta_1^{(2)} \cap \mathrm{SIR}^{(\mathrm{OMA})}_{D_2D_1} \geq \Theta_1^{(2)}\right\}, \tag{3.11}$$

and

$$\mathrm{RT}^C_{S,D_1,D_2} = \left\{ \bigcap_{i=1}^{2} \mathrm{SIR}_{SD_{1-i}} \geq \Theta_i^{(2)} \cap \mathrm{SIR}^{(\mathrm{OMA})}_{D_1D_2} \geq \Theta_2^{(2)}\right\}. \tag{3.12}$$

The decoding threshold $\Theta_i^{(n)}$ is defined as

$$\Theta_i^{(n)} \triangleq 2^{n\mathcal{R}_i} - 1, \tag{3.13}$$

where $\mathcal{R}_i$ is the target data rate of D_i. Note that, $n = 1$ when direct transmission is used, and $n = 2$ when cooperative transmission is used.

3.3.3. ACN Outage Probability Expressions

In the following, we will express the probabilities related to $\mathcal{O}_{\mathrm{ACN}}(D_1)$ and $\mathcal{O}_{\mathrm{ACN}}(D_2)$. The outage probability expressions related to D_1 and D_2, denoted $\mathbb{P}[\mathcal{O}_{\mathrm{ACN}}(D_1)]$ and $\mathbb{P}[\mathcal{O}_{\mathrm{ACN}}(D_2)]$,

are respectively given by

$$\begin{aligned}\mathbb{P}[\mathcal{O}_{\mathrm{ACN}}(D_1)] &= 1-\Bigg[\mathcal{H}_{(D_1)}\Big(\frac{\mathcal{G}_1^{(1)}}{l_{SD_1}}\Big) \\ &\quad +\Bigg\{\Bigg(1-\mathcal{H}_{(D_1)}\Big(\frac{\mathcal{G}_1^{(1)}}{l_{SD_1}}\Big)\Bigg)\times\mathcal{H}_{(D_2)}\Big(\frac{\mathcal{G}_1^{(2)}}{l_{SD_2}}\Big)\times\mathcal{H}_{(D_1)}\Big(\frac{\Theta_1^{(2)}}{l_{D_2D_1}}\Big)\Bigg\},\end{aligned} \tag{3.15}$$

and

$$\begin{aligned}\mathbb{P}[\mathcal{O}_{\mathrm{ACN}}(D_2)] &= 1-\Bigg[\mathcal{H}_{(D_2)}\Big(\frac{\mathcal{G}_{\max}^{(1)}}{l_{SD_2}}\Big) \\ &\quad +\Bigg\{\Bigg(1-\mathcal{H}_{(D_2)}\Big(\frac{\mathcal{G}_{\max}^{(1)}}{l_{SD_2}}\Big)\Bigg)\times\mathcal{H}_{(D_1)}\Big(\frac{\mathcal{G}_{\max}^{(2)}}{l_{SD_1}}\Big)\times\mathcal{H}_{(D_2)}\Big(\frac{\Theta_2^{(2)}}{l_{D_1D_2}}\Big)\Bigg\},\end{aligned} \tag{3.17}$$

where the function $\mathcal{H}_{(D_i)}\Big(\frac{A}{B}\Big)$ is given by (2.11), and $\mathcal{G}_1^{(n)}$ and $\mathcal{G}_{\max}^{(n)}$, are respectively given by

$$\mathcal{G}_1^{(n)} = \frac{\Theta_1^{(n)}}{a_1-\Theta_1^{(n)}a_2}, \tag{3.18}$$

and

$$\mathcal{G}_{\max}^{(n)} = \max(\mathcal{G}_1^{(n)},\mathcal{G}_2^{(n)}), \tag{3.19}$$

where $\mathcal{G}_2^{(n)} = \Theta_2^{(n)}/a_2$.

Proof: See Appendix C.1. ■

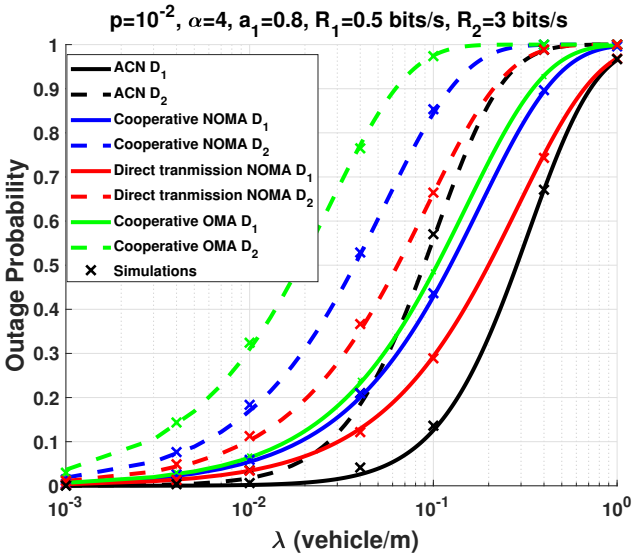

Figure 3.4.: Outage probability as a function of λ considering ACN, cooperative NOMA, direct transmission NOMA, and cooperative OMA.

3.4. Simulations and Discussions

In this section, we evaluate the performance of NOMA at road intersections. To verify the accuracy of our theoretical analysis, Monte Carlo simulations are performed by averaging over 50.000 realizations of PPPs and fading channel parameters. In all figures, the marks represent the Monte Carlo simulations. We set, without loss of generality, $\lambda_X = \lambda_Y = \lambda$.

Fig.3.4 shows the outage probability as a function of λ considering ACN, cooperative transmission using NOMA [BHE19f], direct transmission using NOMA [BHE19a], and the classical cooperative OMA. We can see from Fig.3.4, that as the intensity of vehicles λ increases, the outage probability increases. This is because as the intensity increases, the number of interfering vehicles increases, which decreases the SIR at the receiving node. We can also see from Fig.3.4, that the ACN protocol outperforms the cooperative transmission

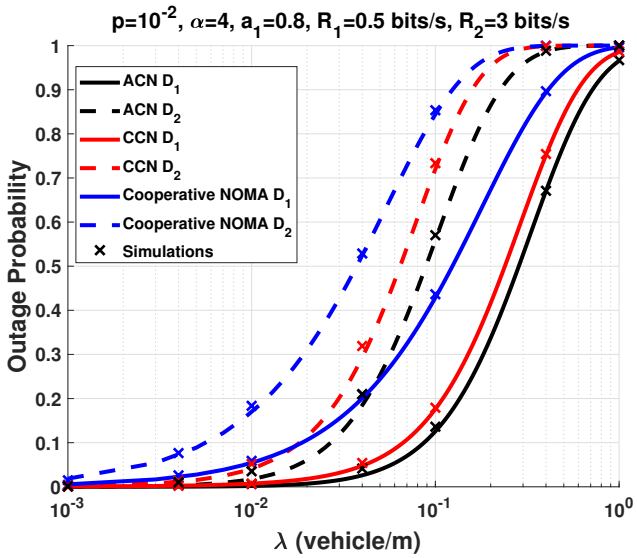

Figure 3.5.: Outage probability as a function of λ considering ACN, CCN, and cooperative NOMA.

using NOMA, direct transmission using NOMA, and the classical cooperative OMA. This is because, the ACN protocol is adaptive. Hence, it uses the direct transmission in the first phase, and when it fails, it switches to the cooperative transmission in the second phase.

Fig.3.5 shows the outage probability as a function of λ considering ACN, CCN [DPP15], and cooperative NOMA. We can see from Fig.3.5, that both ACN and CCN outperforms the cooperative transmission using NOMA. We can also see that ACN outperforms CCN for both D_1 and D_2. This is because the transmission in CCN occurs in two phases, hence it reduces its spectral efficiency. On the other hand, the ACN protocol occurs in one phase if the direct transmission succeeds, which increases the spectral efficiency compared to CCN. Also, during the second phase of the cooperative transmission, the ACN uses OMA to transmit the message since there is only one signal to transmit in the second hop ($D_1 \rightarrow D_2$ or $D_2 \rightarrow D_1$). Hence, it increases the SIR at the receiver node.

Fig.3.6 plots the outage probability as a function of the nodes distance from the intersection, considering ACN, CCN, and cooperative NOMA. We can see from Fig.3.6, that

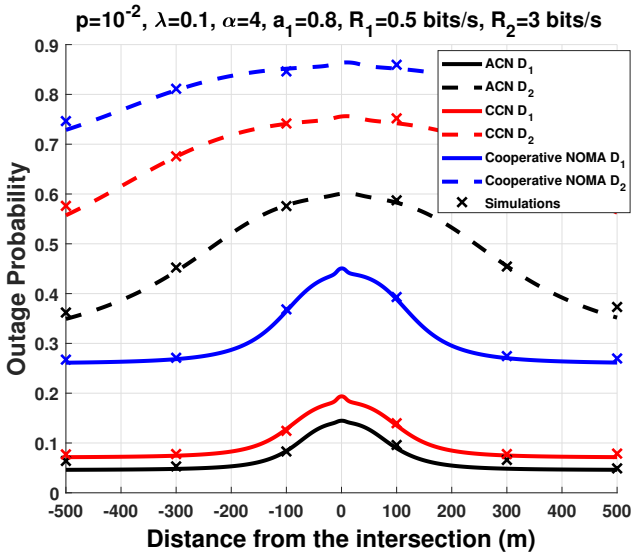

Figure 3.6.: Outage probability as a function of the distance from the intersection, considering ACN, CCN, and cooperative NOMA.

as the nodes come closer to the intersection (200 m for D_1 and 500m for D_2), the outage probability increases. This is because, when the nodes are at the intersection, the interfering vehicles from the X road and the Y road both contribute to the aggregate interference, which decreases the SIR at the receiving nodes. We can also see that, ACN outperforms both CCN and cooperative NOMA at the intersection. However, we can see that there is a big gap in performance between ACN and CCN regarding D_2. This is because, the spectral efficiency of CCN decreases drastically for high data rates. This is why, ACN protocol offers a better performance for high data rates compared to CCN. Finally, we can see in CCN and cooperative NOMA, that the outage probability increases more in the last ten meters. However, there is no increases in the outage probability when using ACN.

Fig.3.7 plots the outage probability as a function of a_1, considering ACN, CCN, cooperative NOMA, and cooperative OMA. We can see from Fig.3.7, that ACN outperforms CCN and cooperative NOMA and cooperative OMA regardless of a_1 value. We can also see that when a_1 increases, the outage probability of D_1 decreases, whereas the outage probability

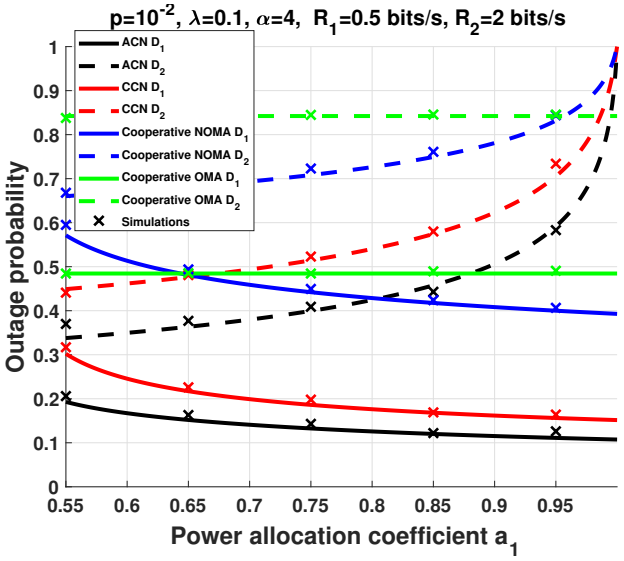

Figure 3.7.: Outage probability as a function of the power allocation coefficient a_1, considering ACN, CCN, cooperative NOMA, and cooperative OMA.

of D_2 decreases. Finally, we can see that the performance of ACN are higher for D_2, since D_2 has a high data rate.

3.5. mm-Wave System Model

3.5.1. Scenario Model

In this paper, we consider a mm-Wave vehicular network using a cooperative NOMA transmission between a source, denoted S, and two destinations denoted D_1 and D_2 with the help of a relay denoted R. The set $\{S, R, D_1, D_2\}$ denotes the nodes and their locations as depicted in Fig.3.8.

We consider, an intersection scenario involving two perpendicular roads, an horizontal road denoted by X, and a vertical road denoted by Y. In this paper, we consider both V2V and V2I communications[2], hence, any node of the set $\{S, R, D_1, D_2\}$ can be on the road or outside the roads. We denote by M the receiving node, and by m the distance

[2]The Doppler shift and time-varying effect of V2V and V2I channels is beyond the scope of this paper.

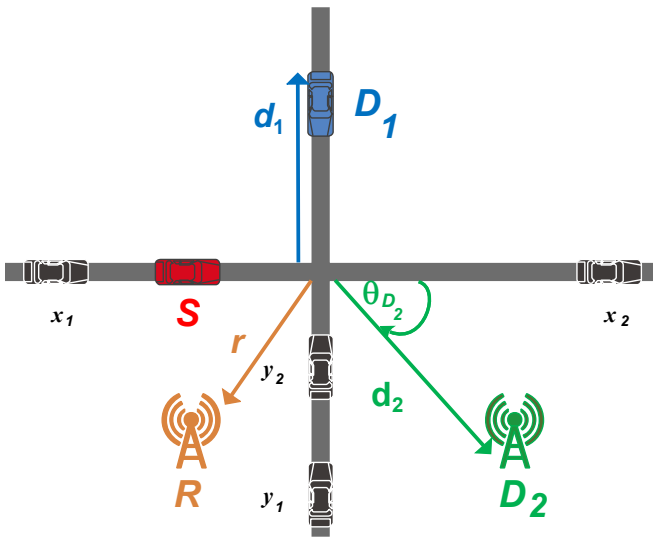

Figure 3.8.: Cooperative NOMA system model for vehicular communications involving one relay two receiving node. The receiving nodes can be vehicles or as part of the communication infrastructure. For instance, S and D_1 are vehicles, and R and D_2 are infrastructures.

between the node M and the intersection, where $M \in \{R, D_1, D_2\}$ and $m \in \{r, d_1, d_2\}$, as shown in Fig.1. The angle θ_M is the angle between the node M and the X road (see Fig.1). Note that the intersection is the point where the X road and the Y road intersect. The set $\{S, R, D_1, D_2\}$ is subject to interference that are originated from vehicles located on the roads.

The set of interfering vehicles located on the X road that are in a LOS with $\{S, R, D_1, D_2\}$, denoted by Φ_X^{LOS} (resp. on axis Y, denoted by Φ_Y^{LOS}) are modeled as a One-Dimensional Homogeneous Poisson Point Process (1D-HPPP), that is, $\Phi_X^{\text{LOS}} \sim$ 1D-HPPP$(\lambda_X^{\text{LOS}}, x)$ (resp.Φ_Y^{LOS} $\sim$ 1D-HPPP$(\lambda_Y^{\text{LOS}}, y)$, where x and λ_X^{LOS} (resp. y and λ_Y^{LOS}) are the position of the LOS interferer vehicles and their intensity on the X road (resp. Y road).

Similarly, the set of interfering vehicles located on the X road that are in a NLOS with $\{S, R, D_1, D_2\}$, denoted by Φ_X^{NLOS} (resp. on axis Y, denoted by Φ_Y^{NLOS}) are modeled as a One-Dimensional Homogeneous Poisson Point Process (1D-HPPP), that is, $\Phi_X^{\text{NLOS}} \sim$ 1D-HPPP$(\lambda_X^{\text{NLOS}}, x)$ (resp.$\Phi_Y^{\text{NLOS}} \sim$ 1D-HPPP$(\lambda_Y^{\text{NLOS}}, y)$, where x and λ_X^{NLOS} (resp. y and

λ_Y^{NLOS}) are the position of the NLOS interferer vehicles and their intensity on the X road (resp. Y road). The notation x and y denotes both the interferer vehicles and their locations.

3.5.2. Blockage Model

At the intersection, the mmWave signals cannot penetrate the buildings and other obstacles, which causes the link to be in LOS, or in NLOS. The event of a link between a node a and b is in a LOS and NLOS, are respectively defined as LOS_{ab}, and NLOS_{ab}. The LOS probability function $\mathbb{P}(\text{LOS}_{ab})$ is used, where the link between a and b has a LOS probability $\mathbb{P}(\text{LOS}_{ab}) = \exp(-\beta r_{ab})$ and NLOS probability $\mathbb{P}(\text{NLOS}_{ab}) = 1 - \mathbb{P}(\text{LOS}_{ab})$, where the constant rate β depends on the building size, shape and density [BVH14].

3.5.3. Transmission and Decoding Model

The transmission is subject to a path loss, denoted by $r_{ab}^{-\alpha}$ between the nodes a and b, where $r_{ab} = \|a - b\|$, and α is the path loss exponent. The path exponent $\alpha \in \{\alpha_{\text{LOS}}, \alpha_{\text{NLOS}}\}$, where $\alpha = \alpha_{\text{LOS}}$, when the transmission is in LOS, whereas $\alpha = \alpha_{\text{NLOS}}$, when transmission is in NLOS.

We consider slotted ALOHA protocol with parameter p, i.e., every node accesses the medium with a probability p.

We use a Decode and Forward (DF) decoding strategy, i.e., R decodes the message, re-encodes it, then forwards it to D_1 and D_2. We also use a half-duplex transmission in which a transmission occurs during two phases. Each phase lasts one time slot. During the first phase, S broadcasts the message to R ($S \to R$). During the second phase, R broadcasts the message to D_1 and D_2 ($R \to D_1$ and $R \to D_2$).

3.5.4. NOMA Model

We consider, in this paper, that the receiving nodes, D_1 and D_2, are ordered according to their quality of service (QoS) priorities [DDP16a; DDP16b]. We consider the case when node D_1 needs a low data rate but has to be served immediately, whereas node D_2 requires a higher data rate but can be served later. For instance, D_1 can be a vehicle that needs to receive safety data information about an accident in its surrounding, whereas D_2 can be a user that accesses the internet connection.

3.5.5. Directional Beamforming Model

We model the directivity similar to in [Sin+15], where the directional gain, denoted $G(\omega)$, within the half power beamwidth $(\phi/2)$ is G_{max} and is G_{min} in all other directions. The gain is then expressed as

$$G(\omega) = \begin{cases} G_{max}, & \text{if } |\omega| \leq \frac{\phi}{2}; \\ G_{min}, & \text{otherwise.} \end{cases} \tag{3.20}$$

In this paper, we consider a perfect beam alignment between the nodes, hence $G_{eq} = G_{max}^2$. The impact of beam misalignment is beyond the scope of this paper.

3.5.6. Channel and Interference Model

We consider an interference limited scenario, that is, the power of noise is set to zero $(\sigma^2 = 0)$. Without loss of generality, we assume that all nodes transmit with a unit power. The signal transmitted by S, denoted χ_S is a mixture of the message intended to D_1 and D_2. This can be expressed as

$$\chi_S = \sqrt{a_1}\chi_{D1} + \sqrt{a_2}\chi_{D2},$$

where a_i is the power coefficients allocated to D_i, and χ_{Di} is the message intended to D_i, where $i \in \{1, 2\}$. Since D_1 has higher power than D_2, that is $a_1 \geq a_2$, then D_1 comes first in the decoding order. Note that, $a_1 + a_2 = 1$.

The signal received at R during the first time slot is expressed as

$$\begin{aligned}\mathcal{Y}_R &= h_{SR}\sqrt{r_{SR}^{-\alpha_{\text{LOS}}}\Upsilon}\,\chi_S\mathbb{1}(\text{LOS}_{SR}) + h_{SR}\sqrt{r_{SR}^{-\alpha_{\text{NLOS}}}\Upsilon}\,\chi_S\mathbb{1}(\text{NLOS}_{SR}) \\ &+ \sum_{x\in\Phi_{X_R}^{\text{LOS}}} h_{Rx}\sqrt{r_{Rx}^{-\alpha_{\text{LOS}}}\Upsilon}\,\chi_x + \sum_{y\in\Phi_{Y_R}^{\text{LOS}}} h_{Ry}\sqrt{r_{Ry}^{-\alpha_{\text{LOS}}}\Upsilon}\,\chi_y \\ &+ \sum_{x\in\Phi_{X_R}^{\text{NLOS}}} h_{Rx}\sqrt{r_{Rx}^{-\alpha_{\text{NLOS}}}\Upsilon}\,\chi_x + \sum_{y\in\Phi_{Y_R}^{\text{NLOS}}} h_{Ry}\sqrt{r_{Ry}^{-\alpha_{\text{NLOS}}}\Upsilon}\,\chi_y.\end{aligned}$$

The signal received at D_i during the second time slot is expressed as

$$\begin{aligned}\mathcal{Y}_{D_i} &= h_{RD_i}\sqrt{r_{RD_i}^{-\alpha}\Upsilon}\,\chi_R\mathbb{1}(\text{LOS}_{RD_i}) + h_{RD_i}\sqrt{r_{RD_i}^{-\alpha}\Upsilon}\,\chi_R\mathbb{1}(\text{NLOS}_{RD_i}) \\ &+ \sum_{x\in\Phi_{X_{D_i}}^{\text{LOS}}} h_{Dix}\sqrt{r_{D_ix}^{-\alpha_{\text{LOS}}}\Upsilon}\,\chi_x + \sum_{y\in\Phi_{Y_{D_i}}^{\text{LOS}}} h_{Diy}\sqrt{r_{D_iy}^{-\alpha_{\text{LOS}}}\Upsilon}\,\chi_y \\ &+ \sum_{x\in\Phi_{X_{D_i}}^{\text{NLOS}}} h_{Dix}\sqrt{r_{D_ix}^{-\alpha_{\text{NLOS}}}\Upsilon}\,\chi_x + \sum_{y\in\Phi_{Y_{D_i}}^{\text{NLOS}}} h_{Diy}\sqrt{r_{D_iy}^{-\alpha_{\text{NLOS}}}\Upsilon}\,\chi_y,\end{aligned}$$

where $\mathcal{Y}_M$ is the signal received by M, and χ_R is the message transmitted by R. The messages transmitted by the interfere node x and y, are denoted respectively by χ_x and χ_y. The term $\Upsilon = G_{eq}\eta^2/(4\pi)^2$ models the directional gain, the reference path loss at one meter, and η is the wavelength of the operating frequency.

The coefficients h_{SR}, and h_{RD_i} denote the fading of the link $S - R$, and $R - D_i$. The fading coefficients are distributed according to a Nakagami-m distribution with parameter m [Bel+18], that is

$$f_{h_u}(x) = 2\Big(\frac{m}{\mu}\Big)^m \frac{x^{2m-1}}{\Gamma(m)} e^{-\frac{m}{\mu}x^2}, \tag{3.21}$$

where $u \in \{SR, RD_i\}$. The parameter $m \in \{m_{\text{LOS}}, m_{\text{NLOS}}\}$, where $m = m_{\text{LOS}}$ when u is in a LOS, whereas $m = m_{\text{NLOS}}$, when u is in a NLOS. The parameter μ is the average received power.

Hence, the power fading coefficients $|h_{SR}|^2$, and $|h_{RD_i}|^2$ are distributed according to a gamma distribution, that is,

$$f_{|h_u|^2}(x) = \left(\frac{m}{\mu}\right)^m \frac{x^{m-1}}{\Gamma(m)} e^{-\frac{m}{\mu}x}. \tag{3.22}$$

The fading coefficients h_{Rx},h_{Ry},h_{D_ix} and h_{D_iy} denote the fading of the link $R-x$, $R-y$, D_i-x, and D_i-y. The fading coefficients are modeled as Rayleigh fading [DH17]. Thus, the power fading coefficients $|h_{Rx}|^2$, $|h_{Ry}|^2$ $|h_{D_ix}|^2$ and $|h_{D_iy}|^2$, are distributed according to an exponential distribution with unit mean.

The aggregate interference is defined as from the X road at M, denoted I_{X_M}, is expressed as

$$\begin{aligned} I_{X_M} &= I_{X_M}^{\text{LOS}} + I_{X_M}^{\text{NLOS}} \\ &= \sum_{x \in \Phi_{X_M}^{\text{LOS}}} |h_{Mx}|^2 r_{Mx}^{-\alpha_{\text{LOS}}} \Upsilon + \sum_{y \in \Phi_{X_M}^{\text{NLOS}}} |h_{Mx}|^2 r_{Mx}^{-\alpha_{\text{NLOS}}} \Upsilon, \end{aligned} \tag{3.23}$$

where $I_{X_M}^{\text{LOS}}$ denotes the aggregate interference from the X road that are in a LOS with M, and $I_{X_M}^{\text{NLOS}}$ denotes the aggregate interference from the X road that are in a NLOS with M. Similarly, $\Phi_{X_M}^{\text{LOS}}$ and $\Phi_{X_M}^{\text{NLOS}}$, denote respectively, the set of the interferers from the X road at M in a LOS, and in NLOS.

In the same way, the aggregate interference is defined as from the Y road at M, denoted

I_{Y_M}, is expressed as

$$\begin{aligned} I_{Y_M} &= I_{Y_M}^{\text{LOS}} + I_{Y_M}^{\text{NLOS}} \\ &= \sum_{y \in \Phi_{Y_M}^{\text{LOS}}} |h_{My}|^2 r_{My}^{-\alpha_{\text{LOS}}} \Upsilon + \sum_{y \in \Phi_{Y_M}^{\text{NLOS}}} |h_{My}|^2 r_{My}^{-\alpha_{\text{NLOS}}} \Upsilon, \end{aligned} \tag{3.24}$$

where $I_{Y_M}^{\text{LOS}}$ denotes the aggregate interference from the X road that are in a LOS with M, and $I_{Y_M}^{\text{NLOS}}$ denotes the aggregate interference from the Y road that are in a NLOS with M. Similarly, $\Phi_{Y_M}^{\text{LOS}}$ and $\Phi_{Y_M}^{\text{NLOS}}$, denote respectively, the set of the interferers from the Y road at M in a LOS, and in NLOS.

3.6. Cooperative mm-Wave NOMA Outage Expressions

3.6.1. SIR Expressions

We define the outage probability as the probability that the signal-to-interference ratio (SIR) at the receiver is below a given threshold. According to successive interference cancellation (SIC) [Has+03], D_1 will be decoded first at the receiver since it has the higher power allocation, and D_2 message will be considered as interference. The SIR at R to decode D_1, denoted $\text{SIR}_{R_1}^{(\alpha)}$, is expressed as

$$\text{SIR}_{R_1}^{(\alpha)} = \frac{|h_{SR}|^2 r_{SR}^{-\alpha} \Upsilon \, a_1}{|h_{SR}|^2 r_{SR}^{-\alpha} \Upsilon a_2 + I_{X_R} + I_{Y_R}}. \tag{3.25}$$

Since D_2 has a lower power allocation, R has to decode D_1 message, then decode D_2 message. The SIR at R to decode D_2 message, denoted $\text{SIR}_{R_2}^{(\alpha)}$, is expressed as

$$\text{SIR}_{R_2}^{(\alpha)} = \frac{|h_{SR}|^2 r_{SR}^{-\alpha} \Upsilon \, a_2}{I_{X_R} + I_{Y_R}}. \tag{3.26}$$

The SIR at D_1 to decode its intended message, denoted $\text{SIR}_{D_1}^{(\alpha)}$, is given by

$$\mathrm{SIR}_{D_1}^{(\alpha)} = \frac{|h_{RD1}|^2 r_{RD1}^{-\alpha} \Upsilon \, a_1}{|h_{RD1}|^2 r_{RD1}^{-\alpha} \Upsilon a_2 + I_{X_{D1}} + I_{Y_{D1}}}. \tag{3.27}$$

In order for D_2 to decode its intended message, it has to decode D_1 message. The SIR at D_2 to decode D_1 message, denoted $\mathrm{SIR}_{D_{2-1}}^{(\alpha)}$, is expressed as

$$\mathrm{SIR}_{D_{2-1}}^{(\alpha)} = \frac{|h_{RD2}|^2 r_{RD2}^{-\alpha} \Upsilon \, a_1}{|h_{RD2}|^2 r_{RD2}^{-\alpha} \Upsilon a_2 + I_{X_{D2}} + I_{Y_{D2}}}. \tag{3.28}$$

The SIR at D_2 to decode its intended message, denoted $\mathrm{SIR}_{D_2}^{(\alpha)}$, is expressed as

$$\mathrm{SIR}_{D_2}^{(\alpha)} = \frac{|h_{RD2}|^2 r_{RD2}^{-\alpha} \Upsilon \, a_2}{I_{X_{D2}} + I_{Y_{D2}}}. \tag{3.29}$$

3.6.2. Outage Event Expressions

The outage event that R does not decode D_1 message, denoted O_{R_1}, is given by

$$O_{R_1} \triangleq \bigcup_{\mathrm{Z} \in \{\mathrm{LOS,NLOS}\}} \{\mathrm{Z}_{SR} \cap (\mathrm{SIR}_{R_1}^{(\alpha_\mathrm{Z})} < \Theta_1)\}, \tag{3.30}$$

where $\Theta_1 = 2^{2\mathcal{R}_1} - 1$, and $\mathcal{R}_1$ is the target data rate of D_1.

Also, the outage event that D_1 does not decode its intended message, denoted O_{D_1}, is given by

$$O_{D_1} \triangleq \bigcup_{\mathrm{Z} \in \{\mathrm{LOS,NLOS}\}} \{\mathrm{Z}_{RD_1} \cap (\mathrm{SIR}_{D_1}^{(\alpha_\mathrm{Z})} < \Theta_1)\}. \tag{3.31}$$

Then, the overall outage event related to D_1, denoted $O_{(1)}$, is given by

$$O_{(1)} \triangleq [O_{R_1} \cup O_{D_1}], \tag{3.32}$$

The outage event that R does not decode D_2 message, denoted O_{R_2}, is given by

$$O_{R_2} \triangleq \bigcup_{\mathrm{Z}\in\{\mathrm{LOS,NLOS}\}} \bigcup_{i=1}^{2} \{\mathrm{Z}_{SR} \cap (\mathrm{SIR}_{R_i}^{(\alpha_\mathrm{Z})} < \Theta_i)\}, \tag{3.33}$$

where $\Theta_2 = 2^{2\mathcal{R}_2} - 1$ $(i = 2)$, and $\mathcal{R}_2$ is the target data rate of D_2. Also, the outage event that D_2 does not decode its intended message, denoted O_{D_2}, is given by

$$O_{D_2} \triangleq \bigcup_{\mathrm{Z}\in\{\mathrm{LOS,NLOS}\}} \bigcup_{i=1}^{2} \{\mathrm{Z}_{RD_2} \cap (\mathrm{SIR}_{D_{2-i}}^{(\alpha_\mathrm{Z})} < \Theta_i)\}. \tag{3.34}$$

Finally, the overall outage event related to D_2, denoted $O_{(2)}$, is given by

$$O_{(2)} \triangleq [O_{R_2} \cup O_{D_2}]. \tag{3.35}$$

3.6.3. Outage Probability Expressions

In the following, we will express the outage probability related to $O_{(1)}$ and $O_{(2)}$. The probability $\mathbb{P}(O_{(1)})$ is given, when $\Theta_1 < \frac{a_1}{a_2}$, by

$$\mathbb{P}(O_{(1)}) = 1 - \Bigg\{ \sum_{\mathrm{Z}\in\{\mathrm{LOS,NLOS}\}} \mathbb{P}(\mathrm{Z}_{SR}) \Lambda\Big(\frac{m_\mathrm{Z}\,\Psi_1}{\mu\, r_{SR}^{-\alpha_\mathrm{Z}} \Upsilon}\Big) \times \sum_{\mathrm{Z}\in\{\mathrm{LOS,NLOS}\}} \mathbb{P}(\mathrm{Z}_{RD_1}) \Lambda\Big(\frac{m_\mathrm{Z}\,\Psi_1}{\mu\, r_{RD_1}^{-\alpha_\mathrm{Z}} \Upsilon}\Big) \Bigg\}, \tag{3.36}$$

where $\Psi_1 = \Theta_1/(a_1 - \Theta_1 a_2)$. The expression of $\Lambda\Big(\frac{m\,\Psi}{\mu\, r_{ab}^{-\alpha} \Upsilon}\Big)$ is given by

$$\begin{aligned} \Lambda\Big(\frac{m\,\Psi}{\mu\, r_{ab}^{-\alpha} \Upsilon}\Big) \;=\; & \prod_{\mathrm{K}\in\{\mathrm{LOS,NLOS}\}} \sum_{k=0}^{m-1} \frac{1}{k!} \big(-\frac{m\,\Psi}{\mu\, r_{ab}^{-\alpha} \Upsilon}\big)^k \\ & \sum_{n=0}^{k} \binom{k}{n} \frac{\mathrm{d}^{k-n} \mathcal{L}_{I_{X_b}^\mathrm{K}}(\frac{m\,\Psi}{\mu\, r_{ab}^{-\alpha} \Upsilon})}{\mathrm{d}^{k-n}(\frac{m\,\Psi}{\mu\, r_{ab}^{-\alpha_L} \Upsilon})} \frac{\mathrm{d}^{n} \mathcal{L}_{I_{Y_b}^\mathrm{K}}(\frac{m\,\Psi}{\mu\, r_{ab}^{-\alpha} \Upsilon})}{\mathrm{d}^{n}(\frac{m\,\Psi}{\mu\, r_{ab}^{-\alpha} \Upsilon})}. \end{aligned} \tag{3.37}$$

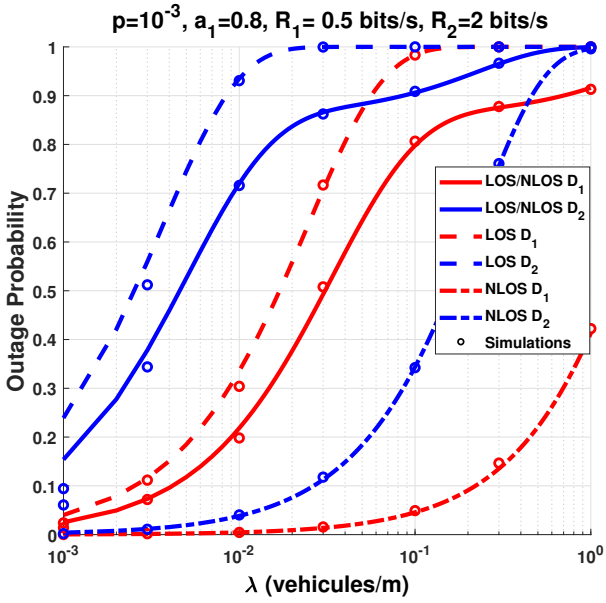

Figure 3.9.: Outage probability as function of λ considering cooperative NOMA, for LOS transmission, NLOS, and LOS/NLOS (the equation (3.36) and (3.38)).

The probability $\mathbb{P}(O_{(2)})$ is given, when $\Theta_1 < \frac{a_1}{a_2}$, by

$$\mathbb{P}(O_{(2)}) = 1 - \left\{ \sum_{\mathrm{Z}\in\{\mathrm{LOS,NLOS}\}} \mathbb{P}(\mathrm{Z}_{SR}) \Lambda\Big(\frac{m_{\mathrm{Z}}\, \Psi_{\max}}{\mu\, r_{SR}^{-\alpha_{\mathrm{Z}}} \Upsilon}\Big) \times \sum_{\mathrm{Z}\in\{\mathrm{LOS,NLOS}\}} \mathbb{P}(\mathrm{Z}_{RD_2}) \Lambda\Big(\frac{m_{\mathrm{Z}}\, \Psi_{\max}}{\mu\, r_{RD_2}^{-\alpha_{\mathrm{Z}}} \Upsilon}\Big) \right\}, \tag{3.38}$$

where $\Psi_{\max} = \max(\Psi_1, \Psi_2)$, and $\Psi_2 = \Theta_2/a_2$.

Proof: See Appendix C.2. ■

3.7. Simulations and Discussions

In this section, we evaluate the performance of cooperative NOMA at road intersections. In order to verify the accuracy of the theoretical results, Monte Carlo simulations are carried out by averaging over 10000 realizations of the PPPs and fading parameters. In all figures, Monte Carlo simulations are presented by marks, and they match perfectly the theoretical

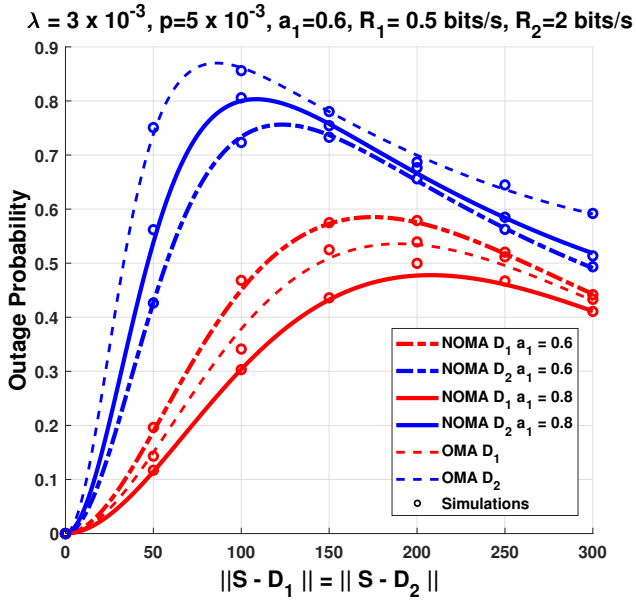

Figure 3.10.: Outage probability as a function of $\|S - D_1\| = \|S - D_2\|$. The relay R is always at mid distance between the source and the destination.

results, which validates the correctness of our analysis. We set, without loss of generality, $\lambda_X^{\text{LOS}} = \lambda_Y^{\text{LOS}} = \lambda_X^{\text{NLOS}} = \lambda_Y^{\text{NLOS}} = \lambda$. $S = (0,0), R = (50,0), D_1 = (100,10), D_2 = (100,-10)$, $\beta = 9.5 \times 10^3$ [BVH14], $\mu = 1$. We set $\alpha_{\text{LOS}} = 2$, $\alpha_{\text{NLOS}} = 4$, $m_{\text{LOS}} = 2$, and $m_{\text{NLOS}} = 1$. Finally, we set $G_{max} = 18$ dBi, $\eta = 30$ GHz.

Fig. 3.9 plots the outage probability as function of λ considering cooperative NOMA, for LOS transmission, NLOS, and LOS/NLOS. We can see that LOS scenario has the highest outage probability. This is because, when the interference are in direct line of sight with the set $\{S, R, D_1, D_2\}$, the power of aggregate interference increases, hence reducing the SIR and increasing the outage. on the other hand, the NLOS scenario has the smallest outage, since the interference are in non line of sight with the transmitting nodes. The model for this paper include a blockage model that includes both LOS and NLOS. Therefore, we wan see that the performance are between the LOS scenario and NLOS scenario, which are two extreme cases.

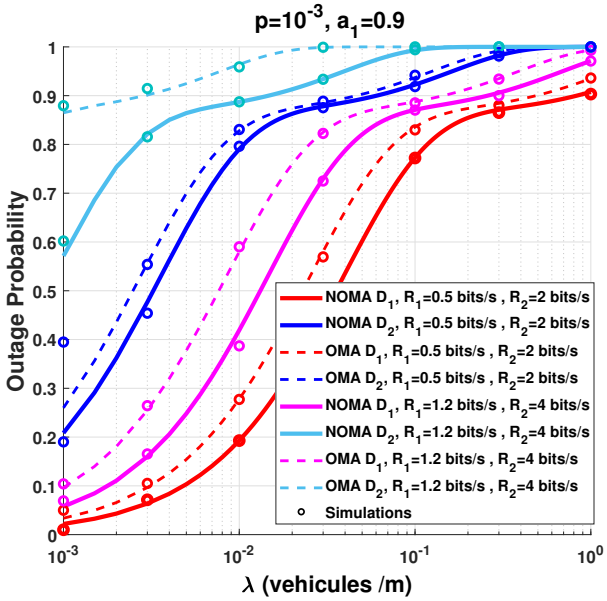

Figure 3.11.: Outage probability as a function of λ considering cooperative NOMA and cooperative OMA.

Fig.3.10 plots the outage probability as a function of the distance between the source and the destinations. Without loss of generality, we set R at mid distance between S and the two destinations D_1 and D_2. We can see that cooperative NOMA outperforms cooperative OMA when $a_1 = 0.8$ for both D_1 and D_2. However, this is not the case for $a_1 = 0.6$, when NOMA outperforms OMA only for D_2. This is because when a_1 decreases, less power is allocated to D_1, hence it increases the outage probability. We can also see from Fig.3.10 that the outage probability increases until 200 m for D_1 (100 m for D_2). This is because, as the distance between the transmitting and the receiving nodes increases, the LOS probability decreases, and the NLOS probability increases, hence decreasing the outage probability.

Fig.3.11 plots the outage probability as a function of λ considering cooperative NOMA and cooperative OMA for several values of data rates. We can see that NOMA outperforms OMA. We can also see that D_1 has a better performance than D_2. This is because D_1 has a smaller target data rate, since D_1 need to be served quickly (e.g., alert message). We

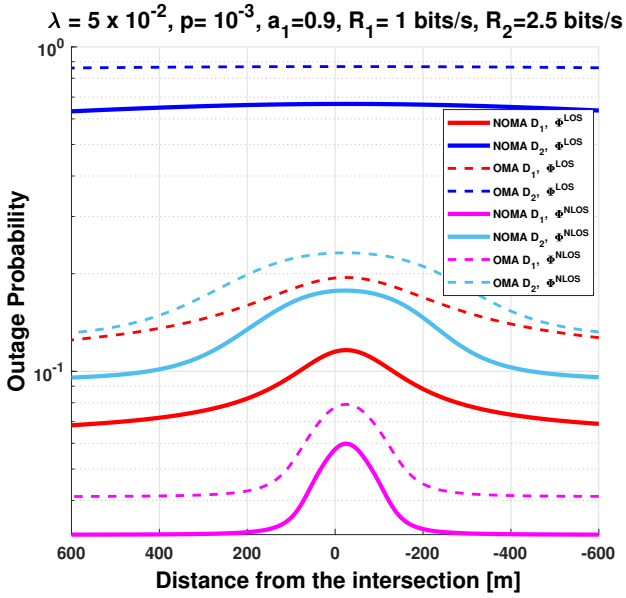

Figure 3.12.: Outage probability as a function of the distance form the intersection considering cooperative NOMA and cooperative OMA, for LOS scenarion and NLOS scenario.

can also see that, as the data rates increases ($R_1 = 1.2$bits/s and $R_2 = 4$bits/s), the gap of performance between NOMA and OMA increases. This is because, as the data rates increases, the decoding threshold of OMA increases dramatically ($\Theta_{\text{OMA}} = 2^{4\mathcal{R}} - 1$). The increase of the threshold becomes larger for D_2, since it has a higher data rate that D_1.

Fig.3.12 plots the outage probability of the distance from the intersection considering cooperative NOMA and cooperative OMA, for LOS scenario and NLOS scenario. Without loss of generality, we set R at mid distance between S and the two destinations D_1 and D_2. We notice from Fig.3.12 that as nodes approach the intersection, the outage probability increases. This is because when the nodes are far from the intersection, only the interferes in the same road segment contribute to the aggregate interference, but as the node approach the intersection, both road segments contribute to the aggregate interference. However, we can see that D_2 has a severe outage in LOS scenario compared to NLOS, and that the increases of the outage for D_2 in LOS, when the nodes move toward the intersection is

negligible. This is because, in a LOS scenario, the interferers from both road segment contributes the aggregate interference, whether the nodes are close or far away from the intersection.

3.8. Multi Hopes Outage Events

Two relays (without direct link)

The success event that the transmission is successful at D_1, with the help of two relays can be formulated as follows

$$O_{(1)}^{C} \triangleq \Big\{ \bigcap_{i=1}^{2} R_{i\to 1}^{C} \Big\} \cap D_{1\to 1}^{C}. \tag{3.39}$$

The event for D_2 is defined as

$$O_{(2)}^{C} \triangleq \Big\{ \bigcap_{i=1}^{2} \bigcap_{j=1}^{2} R_{i\to j}^{C} \Big\} \cap \Big\{ \bigcap_{j=1}^{2} D_{2\to j}^{C} \Big\}. \tag{3.40}$$

N relays (without direct link)

The success event that the transmission is successful at D_1, with help of N relays can be formulated as follows

$$O_{(1)}^{C} \triangleq \Big\{ \bigcap_{i=1}^{N} R_{i\to 1}^{C} \Big\} \cap D_{1\to 1}^{C}. \tag{3.41}$$

The event for D_2 is defined as

$$O_{(2)}^{C} \triangleq \Big\{ \bigcap_{i=1}^{N} \bigcap_{j=1}^{2} R_{i\to j}^{C} \Big\} \cap \Big\{ \bigcap_{j=1}^{2} D_{2\to j}^{C} \Big\}. \tag{3.42}$$

N relays and K destinations (without direct link)

The success event that the transmission is successful at D_K, with the help of N relays can be formulated as follows

$$O_{(K)}^{C} \triangleq \Big\{ \bigcap_{i=1}^{N} \bigcap_{j=1}^{K} R_{i\to j}^{C} \Big\} \cap \Big\{ \bigcap_{j=1}^{K} D_{K\to j}^{C} \Big\}. \tag{3.43}$$

Two relays and two destinations (with direct transmission link)

$$O_{(1)} \triangleq \bigg\{ \Big\{ \bigcup_{i=1}^{2} R_{i\to 1} \Big\} \cap S_{1\to 1} \bigg\} \cup \bigg\{ \Big\{ \bigcap_{i=1}^{2} R_{i\to 1}^{C} \Big\} \cap D_{1\to 1} \bigg\}. \tag{3.44}$$

The event for D_2 is defined as

$$O_{(2)} \triangleq \bigg\{ \Big\{ \bigcup_{i=1}^{2} \bigcup_{j=1}^{2} R_{i\to j} \Big\} \cap \Big\{ \bigcup_{j=1}^{2} S_{2\to j} \Big\} \bigg\} \cup \bigg\{ \Big\{ \bigcap_{i=1}^{2} \bigcap_{j=1}^{2} R_{i\to j}^{C} \Big\} \cap \bigcup_{j=1}^{2} D_{2\to j} \bigg\}. \tag{3.45}$$

Two relays and two destinations (with broadcast every hop)

$$O_{(1)} \triangleq \bigg\{ \Big\{ \bigcup_{i=1}^{2} R_{i\to 1} \Big\} \cap \Big\{ SD_{1\to 1} \cap R_1 D_{1\to 1} \Big\} \bigg\} \cup \bigg\{ \Big\{ \bigcap_{i=1}^{2} R_{i\to 1}^{C} \Big\} \cap D_{1\to 1} \bigg\}. \tag{3.46}$$

The event for D_2 is defined as

$$O_{(2)} \triangleq \bigg\{ \Big\{ \bigcup_{i=1}^{2} \bigcup_{j=1}^{2} R_{i\to j} \Big\} \cap \Big\{ \bigcup_{j=1}^{2} SD_{2\to j} \cap \bigcup_{j=1}^{2} R_1 D_{2\to j} \Big\} \bigg\} \cup \bigg\{ \Big\{ \bigcap_{i=1}^{2} \bigcap_{j=1}^{2} R_{i\to j}^{C} \Big\} \cap \bigcup_{j=1}^{2} D_{2\to j} \bigg\}. \tag{3.47}$$

N relays and two destinations (with broadcast every hop)

$$O_{(1)} \triangleq \bigg\{ \Big\{ \bigcup_{i=1}^{N} R_{i\to 1} \Big\} \cap \Big\{ SD_{1\to 1} \cap \bigcap_{i=1}^{N-1} R_i D_{1\to 1} \Big\} \bigg\} \cup \bigg\{ \Big\{ \bigcap_{i=1}^{N} R_{i\to 1}^{C} \Big\} \cap D_{1\to 1} \bigg\}. \tag{3.48}$$

The event for D_2 is defined as

$$O_{(2)} \triangleq \bigg\{ \Big\{ \bigcup_{i=1}^{N} \bigcup_{j=1}^{2} R_{i\to j} \Big\} \cap \Big\{ \bigcup_{j=1}^{2} SD_{2\to j} \cap \bigcap_{i=1}^{N-1} \bigcup_{j=1}^{2} R_i D_{2\to j} \Big\} \bigg\} \cup \bigg\{ \Big\{ \bigcap_{i=1}^{N} \bigcap_{j=1}^{2} R_{i\to j}^{C} \Big\} \cap \bigcup_{j=1}^{2} D_{2\to j} \bigg\}. \tag{3.49}$$

N relays and K destinations (with broadcast every hop)

$$O_{(K)} \triangleq \Big\{ \Big\{ \bigcup_{i=1}^{N} \bigcup_{j=1}^{K} R_{i\to j} \Big\} \cap \Big\{ \bigcup_{j=1}^{K} SD_{K\to j} \cap \bigcap_{i=1}^{N-1} \bigcup_{j=1}^{K} R_i D_{K\to j} \Big\} \Big\} \cup \Big\{ \Big\{ \bigcap_{i=1}^{N} \bigcap_{j=1}^{K} R^C_{i\to j} \Big\} \cap \bigcup_{j=1}^{K} D_{K\to j} \Big\}. \tag{3.50}$$

3.9. Multi Hopes Outage Probability

The success event that the transmission is successful at D_1, with the help of two relays can be formulated as follows

$$\mathbb{P}(O^C_{(1)}) = \Big\{ \prod_{i=1}^{2} \mathbb{P}(R^C_{i\to 1}) \Big\} \times \mathbb{P}(D^C_{1\to 1}). \tag{3.51}$$

The event for D_2 is defined as

$$\mathbb{P}(O^C_{(2)}) = \Big\{ \prod_{i=1}^{2} \mathbb{P}(\bigcap_{j=1}^{2} R^C_{i\to j}) \Big\} \times \Big\{ \mathbb{P}(\bigcap_{j=1}^{2} D^C_{2\to j}) \Big\}. \tag{3.52}$$

N relays (without direct link)

The success event that the transmission is successful at D_1, with help of N relays can be formulated as follows

$$\mathbb{P}(O^C_{(1)}) = \Big\{ \prod_{i=1}^{N} \mathbb{P}(R^C_{i\to 1}) \Big\} \times \mathbb{P}(D^C_{1\to 1}). \tag{3.53}$$

The event for D_2 is defined as

$$\mathbb{P}(O^C_{(2)}) = \Big\{ \prod_{i=1}^{N} \mathbb{P}(\bigcap_{j=1}^{2} R^C_{i\to j}) \Big\} \times \Big\{ \mathbb{P}(\bigcap_{j=1}^{2} D^C_{2\to j}) \Big\}. \tag{3.54}$$

N relays and K destinations (without direct link)

The success event that the transmission is successful at D_K, with help of N relays can be formulated as follows

$$\mathbb{P}(O_{(K)}^{C}) = \Big\{ \prod_{i=1}^{N} \mathbb{P}(\bigcap_{j=1}^{K} R_{i\to j}^{C}) \Big\} \times \Big\{ \mathbb{P}(\bigcap_{j=1}^{K} D_{K\to j}^{C}) \Big\}. \tag{3.55}$$

Two relays and two destinations (with direct transmission link)

$$\mathbb{P}(O_{(1)}) = \mathbb{P}\Bigg\{ \Big\{ \bigcup_{i=1}^{2} R_{i\to 1} \Big\} \cap S_{1\to 1} \Bigg\} + \Bigg\{ \Big\{ \prod_{i=1}^{2} \mathbb{P}(R_{i\to 1}^{C}) \Big\} \times \Big\{ 1 - \mathbb{P}(D_{1\to 1}^{C}) \Big\} \Bigg\}. \tag{3.56}$$

where the probability $\mathbb{P}\Bigg\{ \Big\{ \bigcup\limits_{i=1}^{2} R_{i\to 1} \Big\} \cap S_{1\to 1} \Bigg\}$ can be calculated as follows

$$\begin{aligned}
\mathbb{P}\Bigg\{ \Big\{ \bigcup_{i=1}^{2} R_{i\to 1} \Big\} \cap S_{1\to 1} \Bigg\} &= 1 - \mathbb{P}\Bigg\{ \Big\{ \bigcup_{i=1}^{2} R_{i\to 1} \Big\}^{C} \cup {S_{1\to 1}}^{C} \Bigg\} \\
&= 1 - \mathbb{P}\Bigg\{ \Big\{ \bigcup_{i=1}^{2} R_{i\to 1} \Big\}^{C} \Bigg\} - \mathbb{P}({S_{1\to 1}}^{C}) \\
&\quad + \mathbb{P}\Bigg\{ \Big\{ \bigcup_{i=1}^{2} R_{i\to 1} \Big\}^{C} \cap {S_{1\to 1}}^{C} \Bigg\} \\
&= 1 - \Bigg\{ \prod_{i=1}^{2} \mathbb{P}(R_{i\to 1}^{C}) \Bigg\} - \mathbb{P}({S_{1\to 1}}^{C}) \\
&\quad + \mathbb{P}\Bigg\{ \Big\{ \prod_{i=1}^{2} \mathbb{P}(R_{i\to 1}^{C}) \times \mathbb{P}({S_{1\to 1}}^{C}) \Bigg\}.
\end{aligned} \tag{3.57}$$

The event for D_2 is defined as

$$\begin{aligned}
\mathbb{P}(O_{(2)}) &= \mathbb{P}\Bigg\{ \Big\{ \bigcup_{i=1}^{2} \bigcup_{j=1}^{2} R_{i\to j} \Big\} \cap \Big\{ \bigcup_{j=1}^{2} S_{2\to j} \Big\} \Bigg\} + \mathbb{P}\Bigg\{ \Big\{ \bigcap_{i=1}^{2} \bigcap_{j=1}^{2} R_{i\to j}^{C} \Big\} \cap \bigcup_{j=1}^{2} D_{2\to j} \Bigg\} \\
&= 1 - \Big\{ \prod_{i=1}^{2} \mathbb{P}(\bigcap_{j=1}^{2} R_{i\to j}^{C}) \Big\} - \Big\{ \mathbb{P}(\bigcap_{j=1}^{2} S_{2\to j}^{C}) \Big\} + \Bigg\{ \Big\{ \prod_{i=1}^{2} \mathbb{P}(\bigcap_{j=1}^{2} R_{i\to j}^{C}) \Big\} \times \mathbb{P}(\bigcap_{j=1}^{2} S_{2\to j}^{C}) \Bigg\} \\
&\quad + \Bigg\{ \Big\{ \prod_{i=1}^{2} \mathbb{P}(\bigcap_{j=1}^{2} R_{i\to j}^{C}) \Big\} \times \Big\{ 1 - \mathbb{P}(\bigcap_{j=1}^{2} D_{2\to j}^{C}) \Big\} \Bigg\}.
\end{aligned} \tag{3.58}$$

Two relays and two destinations (with broadcast every hop)

$$\begin{aligned}
\mathbb{P}(O_{(1)}) &= \mathbb{P}\Big\{\Big\{\bigcup_{i=1}^{2} R_{i\to 1}\Big\}\cap\Big\{SD_{1\to 1}\cap R_1D_{1\to 1}\Big\}\Big\}+\mathbb{P}\Big\{\Big\{\bigcap_{i=1}^{2} R^C_{i\to 1}\Big\}\cap D_{1\to 1}\Big\}\\
&= 1-\Big\{\prod_{i=1}^{2}\mathbb{P}(R^C_{i\to 1})\Big\}-\mathbb{P}(SD^C_{1\to 1})-\mathbb{P}(R_1D^C_{1\to 1})\\
&\quad+\Big\{\Big\{\prod_{i=1}^{2}\mathbb{P}(R^C_{i\to 1})\Big\}\times\Big\{\mathbb{P}(SD^C_{1\to 1})+\mathbb{P}(R_1D^C_{1\to 1})\Big\}\Big\}\\
&\quad+\Big\{\Big\{\prod_{i=1}^{2}\mathbb{P}(R^C_{i\to 1})\Big\}\times\Big\{1-\mathbb{P}(D^C_{1\to 1})\Big\}\Big\}. \qquad (3.59)
\end{aligned}$$

The event for D_2 is defined as

$$\begin{aligned}
\mathbb{P}(O_{(2)}) &= \mathbb{P}\Big\{\Big\{\bigcup_{i=1}^{2}\bigcup_{j=1}^{2} R_{i\to j}\Big\}\cap\Big\{\bigcup_{j=1}^{2} SD_{2\to j}\cap\bigcup_{j=1}^{2} R_1D_{2\to j}\Big\}\Big\}\\
&\quad+\mathbb{P}\Big\{\Big\{\bigcap_{i=1}^{2}\bigcap_{j=1}^{2} R^C_{i\to j}\Big\}\cap\bigcup_{j=1}^{2} D_{2\to j}\Big\}\\
&= 1-\Big\{\prod_{i=1}^{2}\mathbb{P}(\bigcap_{j=1}^{2} R^C_{i\to j})\Big\}-\mathbb{P}(\bigcap_{j=1}^{2} SD^C_{2\to j})-\mathbb{P}(\bigcap_{j=1}^{2} R_1D^C_{2\to j})\\
&\quad+\Big\{\Big\{\prod_{i=1}^{2}\mathbb{P}(\bigcap_{j=1}^{2} R^C_{i\to j})\Big\}\times\Big\{\mathbb{P}(\bigcap_{j=1}^{2} SD^C_{2\to j})+\mathbb{P}(\bigcap_{j=1}^{2} R_1D^C_{2\to j})\Big\}\Big\}\\
&\quad+\Big\{\Big\{\prod_{i=1}^{2}\mathbb{P}(\bigcap_{j=1}^{2} R^C_{i\to j})\Big\}\times\Big\{1-\mathbb{P}(\bigcap_{j=1}^{2} D^C_{2\to j})\Big\}\Big\}. \qquad (3.60)
\end{aligned}$$

N relays and two destinations (with broadcast every hop)

$$\begin{aligned}
\mathbb{P}(O_{(1)}) &= \mathbb{P}\Big\{\Big\{\bigcup_{i=1}^{N} R_{i\to 1}\Big\}\cap\Big\{SD_{1\to 1}\cap\bigcap_{i=1}^{N-1} R_i D_{1\to 1}\Big\}\Big\}+\mathbb{P}\Big\{\Big\{\bigcap_{i=1}^{N} R^C_{i\to 1}\Big\}\cap D_{1\to 1}\Big\}\\
&= 1-\Big\{\prod_{i=1}^{N}\mathbb{P}(R^C_{i\to 1})\Big\}-\mathbb{P}(SD^C_{1\to 1})-\Big\{1-\sum_{i=1}^{N}\mathbb{P}(R_iD^C_{1\to 1})\Big\}\\
&\quad+\Big\{\Big\{\prod_{i=1}^{N}\mathbb{P}(R^C_{i\to 1})\Big\}\times\Big\{1+\mathbb{P}(SD^C_{1\to 1})-\sum_{i=1}^{N}\mathbb{P}(R_iD^C_{1\to 1}\Big\}\Big\}\\
&\quad+\Big\{\Big\{\prod_{i=1}^{N}\mathbb{P}(R^C_{i\to 1})\Big\}\times\Big\{1-\mathbb{P}(D^C_{1\to 1})\Big\}\Big\}. \qquad (3.61)
\end{aligned}$$

The event for D_2 is defined as

$$\begin{aligned}
\mathbb{P}(O_{(2)}) &= \mathbb{P}\Big\{\Big\{\bigcup_{i=1}^{N}\bigcup_{j=1}^{2} R_{i\to j}\Big\}\cap\Big\{\bigcup_{j=1}^{2} SD_{2\to j}\cap\bigcap_{i=1}^{N-1}\bigcup_{j=1}^{2} R_iD_{2\to j}\Big\}\Big\}\\
&\quad+\mathbb{P}\Big\{\Big\{\bigcap_{i=1}^{N}\bigcap_{j=1}^{2} R^C_{i\to j}\Big\}\cap\bigcup_{j=1}^{2} D_{2\to j}\Big\}\\
&= 1-\Big\{\prod_{i=1}^{N}\mathbb{P}(\bigcap_{j=1}^{2} R^C_{i\to j})\Big\}-\Big\{1+\mathbb{P}(\bigcap_{j=1}^{2} SD^C_{2\to j})-\sum_{i=1}^{N-1}\mathbb{P}(\bigcap_{j=1}^{2} R_iD^C_{2\to j})\Big\}\\
&\quad+\Big\{\Big\{\prod_{i=1}^{N}\mathbb{P}(\bigcap_{j=1}^{2} R^C_{i\to j})\Big\}\times\Big\{1+\mathbb{P}(\bigcap_{j=1}^{2} SD^C_{2\to j})-\sum_{i=1}^{N-1}\mathbb{P}(\bigcap_{j=1}^{2} R_iD^C_{2\to j})\Big\}\Big\}\\
&\quad+\Big\{\Big\{\prod_{i=1}^{N}\mathbb{P}(\bigcap_{j=1}^{2} R^C_{i\to j})\Big\}\times\Big\{1-\mathbb{P}(\bigcap_{j=1}^{2} D^C_{2\to j})\Big\}\Big\}. \qquad (3.62)
\end{aligned}$$

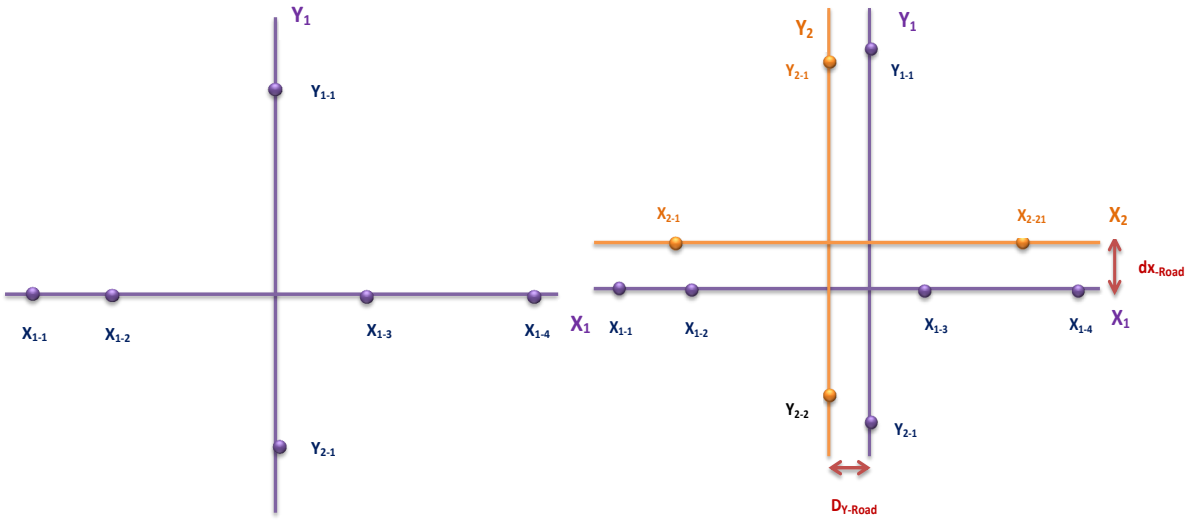

Figure 3.13.: (a) one lane scenario.(b) two lanes scenario.

N relays and K destinations (with broadcast every hop)

$$
\begin{aligned}
\mathbb{P}(O_{(K)}) &= \mathbb{P}\Big\{\Big\{\bigcup_{i=1}^{N}\bigcup_{j=1}^{K} R_{i\to j}\Big\}\cap\Big\{\bigcup_{j=1}^{K} SD_{K\to j}\cap\bigcap_{i=1}^{N-1}\bigcup_{j=1}^{K} R_i D_{K\to j}\Big\}\Big\} \\
&\quad +\mathbb{P}\Big\{\Big\{\bigcap_{i=1}^{N}\bigcap_{j=1}^{K} R^C_{i\to j}\Big\}\cap\bigcup_{j=1}^{K} D_{K\to j}\Big\} \\
&= 1-\Big\{\prod_{i=1}^{N}\mathbb{P}(\bigcap_{j=1}^{K} R^C_{i\to j})\Big\}-\Big\{1+\mathbb{P}(\bigcap_{j=1}^{K} SD^C_{K\to j})-\sum_{i=1}^{N-1}\mathbb{P}(\bigcap_{j=1}^{K} R_i D^C_{K\to j})\Big\} \\
&\quad +\Big\{\Big\{\prod_{i=1}^{N}\mathbb{P}(\bigcap_{j=1}^{K} R^C_{i\to j})\Big\}\times\Big\{1+\mathbb{P}(\bigcap_{j=1}^{K} SD^C_{K\to j})-\sum_{i=1}^{N-1}\mathbb{P}(\bigcap_{j=1}^{K} R_i D^C_{K\to j})\Big\}\Big\} \\
&\quad +\Big\{\Big\{\prod_{i=1}^{N}\mathbb{P}(\bigcap_{j=1}^{K} R^C_{i\to j})\Big\}\times\Big\{1-\mathbb{P}(\bigcap_{j=1}^{K} D^C_{K\to j})\Big\}\Big\}. \qquad (3.63)
\end{aligned}
$$

3.10. Multi Lanes Scenario

Regarding lanes modeling, there are two main approaches to model vehicles on multi-lane roads. The first approach, which the authors used in this paper, is the single lane abstraction model or simply the line abstraction model shown in Fig.3.13(a) in which all the traffic lanes are merged into a single lane with the aggregated traffic intensity (see Appendix.C in [RP16]). The second approach is to consider that the traffic is restricted into individual lanes separated by a fixed inter-lane distance, as illustrated in Fig.3.13(b). We carried out the analysis for both cases. We will derive the outage probability for the two road scenario, then generalize the results for multiple lanes.

3.10.1. Two-lanes case scenario

We address the case where vehicles can drive in two opposite directions, on the horizontal roads and the vertical roads, and further on extend the analysis to Nb_{lanes} number of roads. We refer to the case when we have two roads in the horizontal, and two roads in the vertical as the two-way road case (two lanes on each road). In this case, the horizontal road on which vehicles drive from left to right (resp. right to left) is denoted X_1 (resp. X_2). The same modification holds for the vertical road on which, vehicles drive from bottom up (resp. top down) is denoted Y_1 (resp. Y_2). For $\alpha = 2$, the expressions of the Laplace transform from the X_1 road and the Y_1 road at the receiving node M denoted respectively $\mathcal{L}_{I_{X_1M}}(s)$ and $\mathcal{L}_{I_{Y_1M}}(s)$, are given by (3.64) and (3.65). The expressions of the Laplace transform from the X_2 road and from the Y_2 road at M are given respectively by

$$\mathcal{L}_{I_{X_2M}}(s) = \exp\left(- p\lambda_{X_2} \frac{s\pi}{\sqrt{(m\sin(\theta_M) - d_{Y_{Road}})^2 + s}} \right), \tag{3.64}$$

and

$$\mathcal{L}_{I_{Y_2M}}(s) = \exp\left(- p\lambda_{Y_2} \frac{s\pi}{\sqrt{(m\cos(\theta_M) - d_{X_{Road}})^2 + s}} \right), \tag{3.65}$$

where λ_{X_2} and λ_{Y_2} are the intensities of the interfering vehicles on the X_2 road and Y_2 road respectively, and $d_{X_{Road}}$ and $d_{Y_{Road}}$ are the distance between X_1 and X_2, and between Y_1 and Y_2 respectively. Note that $M \in \{R, D_1, D_2\}$ and $m \in \{r, d_1, d_2\}$.

proof: See Appendix C.3. ■

In the case when there are two roads on the vertical and two roads on the horizontal, the interference are generated from four roads, and then the expressions of the outage probability have to be changed accordingly. For instance, the equations (2.23) and (3.80) become respectively

$$\mathbb{P}(O_{D_{(1)}}) = \begin{cases} 1, & \Theta_1 \geq \frac{a_1}{a_2}; \\ 1 - \mathcal{L}_{I_{X_R}}\left(\frac{G_1}{l_{SR}}\right)\mathcal{L}_{I_{Y_R}}\left(\frac{G_1}{l_{SR}}\right)\mathcal{L}_{I_{X_{2_R}}}\left(\frac{G_1}{l_{SR}}\right)\mathcal{L}_{I_{Y_{2_R}}}\left(\frac{G_1}{l_{SR}}\right) & \\ \times\mathcal{L}_{I_{X_{D_1}}}\left(\frac{G_1}{l_{RD_1}}\right)\mathcal{L}_{I_{Y_{D_1}}}\left(\frac{G_1}{l_{RD_1}}\right)\mathcal{L}_{I_{X_{2_{D_1}}}}\left(\frac{G_1}{l_{RD_1}}\right)\mathcal{L}_{I_{Y_{2_{D_1}}}}\left(\frac{G_1}{l_{RD_1}}\right), & \text{otherwise.} \end{cases} \tag{3.66}$$

$$\mathbb{P}(O_{D_{(2)}}) = \begin{cases} 1, & \Theta_1 \geq \frac{a_1}{a_2} \text{ or } \Theta_2 \geq \frac{a_2}{\beta a_1}; \\ 1 - \mathcal{L}_{I_{X_R}}\left(\frac{G_{(2)\max}}{l_{SR}}\right)\mathcal{L}_{I_{Y_R}}\left(\frac{G_{(2)\max}}{l_{SR}}\right) & \\ \times\mathcal{L}_{I_{X_{2_R}}}\left(\frac{G_{(2)\max}}{l_{SR}}\right)\mathcal{L}_{I_{Y_{2_R}}}\left(\frac{G_{(2)\max}}{l_{SR}}\right) & \\ \times\mathcal{L}_{I_{X_{D_2}}}\left(\frac{G_{(2)\max}}{l_{RD_2}}\right)\mathcal{L}_{I_{Y_{D_2}}}\left(\frac{G_{(2)\max}}{l_{RD_2}}\right) & \\ \times\mathcal{L}_{I_{X_{2_{D_2}}}}\left(\frac{G_{(2)\max}}{l_{RD_2}}\right)\mathcal{L}_{I_{Y_{2_{D_2}}}}\left(\frac{G_{(2)\max}}{l_{RD_2}}\right), & \text{otherwise.} \end{cases} \tag{3.67}$$

3.10.2. Multi-lanes case scenario

To generalize the above expressions form Nb_{lanes} roads, we calculate the Laplace transform for the interference for $i^{th}X$ road, and $i^{th}Y$ road when $\alpha = 2$ is respectively given by:

$$\mathcal{L}_{I_{X_{iM}}}(s) = \exp\left(- p\lambda_{X_i} \frac{s\pi}{\sqrt{(m\sin(\theta_M) - \sum_{i=1}^{Nb_{lanes}-1}(i-1)d_{Y_{Road}})^2 + s}} \right), \tag{3.68}$$

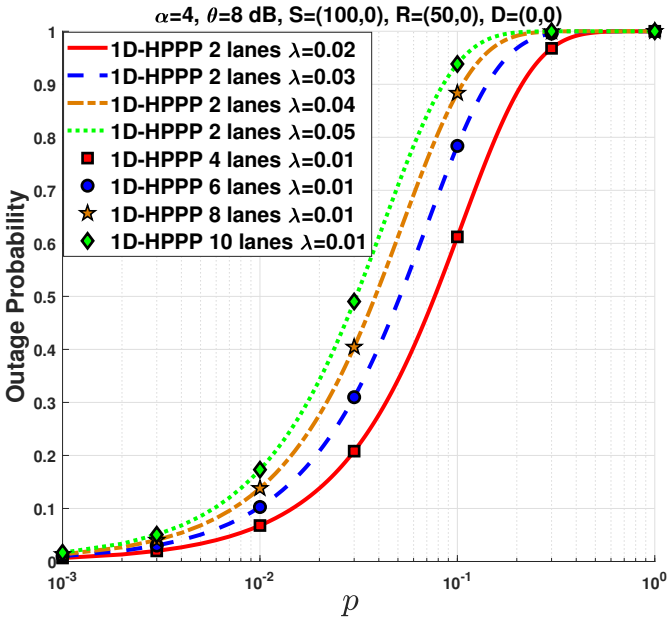

Figure 3.14.: Outage probability as a function of p considering the 1D-HPPP with 2 lanes model (our model), and the 1D-HPPP with multiple lanes.

$$\mathcal{L}_{I_{Y_{i_M}}}(s) = \exp\left(- p\lambda_{Y_i} \frac{s\pi}{\sqrt{(m\cos(\theta_M) - \sum_{i=1}^{Nb_{lanes}-1}(i-1)d_{X_{Road}})^2 + s}} \right), \tag{3.69}$$

where λ_{X_i} and λ_{Y_i} are the intensities of the interferer nodes on the X_i road and Y_i road respectively. The outage probability expressions change accordingly. From instance, the equations (2.23) and (3.80) in the paper become respectively

$$\mathbb{P}(O_{(1)}) = \begin{cases} 1, & \Theta_1 \geq \frac{a_1}{a_2}; \\ 1 - \prod_{i=1}^{Nb_{lanes}} \mathcal{L}_{I_{X_{i_R}}}\left(\frac{G_1}{l_{SR}}\right)\mathcal{L}_{I_{Y_{i_R}}}\left(\frac{G_1}{l_{SR}}\right)\mathcal{L}_{I_{X_{i_{D_1}}}}\left(\frac{G_1}{l_{RD_1}}\right)\mathcal{L}_{I_{Y_{i_{D_1}}}}\left(\frac{G_1}{l_{RD_1}}\right), & \text{otherwise.} \end{cases} \tag{3.70}$$

$$\mathbb{P}(O_{(2)}) = \begin{cases} 1, & \Theta_1 \geq \frac{a_1}{a_2} \text{ or } \Theta_2 \geq \frac{a_2}{\beta a_1}; \\ 1 - \prod_{i=1}^{Nb_{lanes}} \mathcal{L}_{I_{X_{i_R}}}\left(\frac{G_{(2)\max}}{l_{SR}}\right)\mathcal{L}_{I_{Y_{i_R}}}\left(\frac{G_{(2)\max}}{l_{SR}}\right) & \\ \times\mathcal{L}_{I_{X_{i_{D_2}}}}\left(\frac{G_{(2)\max}}{l_{RD_2}}\right)\mathcal{L}_{I_{Y_{i_{D_2}}}}\left(\frac{G_{(2)\max}}{l_{RD_2}}\right), & \text{otherwise.} \end{cases} \tag{3.71}$$

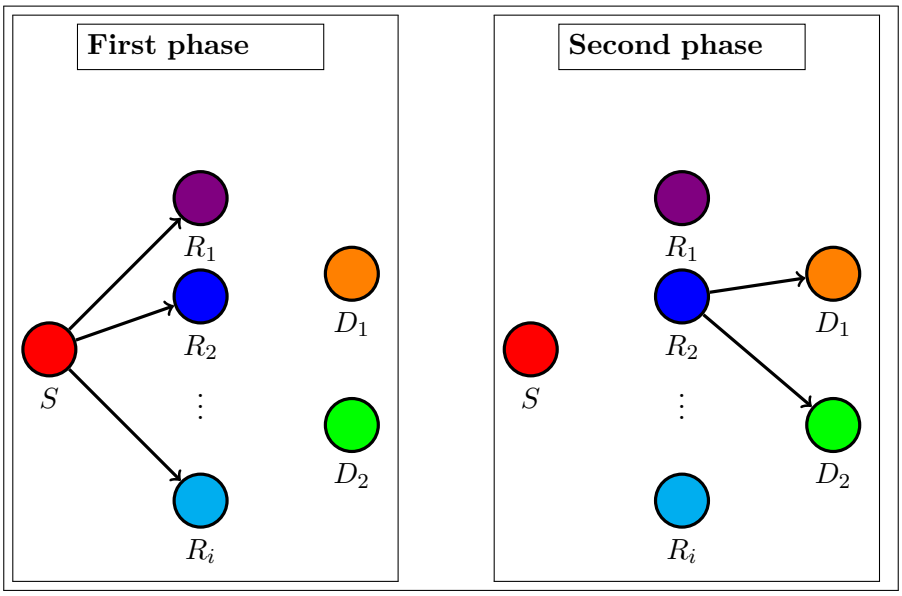

Figure 3.15.: Cooperative transmission using NOMA considering multiple relays.

Fig.3.14 shows the outage probability as a function of p considering the 1D-HPPP with 2 lanes model (our model), and the 1D-HPPP with multiple lanes. We can see from the Fig.3.14 that the our model involving match perfectly the model of multiple lanes given that $\lambda_{Nb\,lanes} = \frac{Nb}{2} \times \lambda_{2\,lanes}$.

3.11. Multiple Relays Scenario

Our work can also be extended to multiple relay scenario. For instance, we can add multiple relays and investigate different selection strategies to investigate their impact on the performance. We will show in the following some results to demonstrate the effect of adding relays on the performance in terms of outage probability.

We consider a NOMA cooperative transmission occurs between S, and two destinations, denoted D_1 and D_2, with the help of nb_{Relay} relays, where the set of the relays, is denoted by $\mathcal{S}_{Relay} = \{R_1, R_2, ..., R_{nb_{Relay}}\}$.

The SIR at the relay R_i to decode D_1 message, denoted $\mathrm{SIR}_{SR_{i\to 1}}$, is expressed as

$$\mathrm{SIR}_{SR_{i\to 1}} = \frac{|h_{SR_i}|^2 l_{SR_i}\, a_1}{|h_{SR_i}|^2 l_{SR_i}\, a_2 + I_{X_{R_i}} + I_{Y_{R_i}}}. \tag{3.72}$$

Since D_2 has a lower power allocation, R_i has to decode D_1 message first, then decodes D_2 message. The SIR at R_i to decode D_2 message, denoted $\mathrm{SIR}_{SR_{i\to 2}}$, is expressed as

$$\mathrm{SIR}_{SR_{i\to 2}} = \frac{|h_{SR_i}|^2 l_{SR_i}\, a_2}{I_{X_{R_i}} + I_{Y_{R_i}}}. \tag{3.73}$$

The SIR at D_1 to decode its intended message received from R_i, denoted $\mathrm{SIR}_{R_i D_{1\to 1}}$, is given by

$$\mathrm{SIR}_{R_i D_{1\to 1}} = \frac{|h_{R_i D_1}|^2 l_{R_i D_1}\, a_1}{|h_{R_i D_1}|^2 l_{R_i D_1}\, a_2 + I_{X_{D_1}} + I_{Y_{D_1}}}. \tag{3.74}$$

Similarly, in order for D_2 to decode its intended message received from R_i, it has to decode D_1 message first. The SIR at D_2 to decode D_1 message, denoted $\mathrm{SIR}_{R_i D_{2\to 1}}$, is expressed as

$$\mathrm{SIR}_{R_i D_{2\to 1}} = \frac{|h_{R_i D_2}|^2 l_{R_i D_2}\, a_1}{|h_{R_i D_2}|^2 l_{R_i D_2}\, a_2 + I_{X_{D_2}} + I_{Y_{D_2}}}. \tag{3.75}$$

The SIR at D_2 to decode its intended message received from R_i, denoted $\mathrm{SIR}_{R_i D_{2\to 2}}$, is expressed as

$$\mathrm{SIR}_{R_i D_{2\to 2}} = \frac{|h_{R_i D_2}|^2 l_{R_i D_2}\, a_2}{I_{X_{D_2}} + I_{Y_{D_2}}}. \tag{3.76}$$

We denote by $\mathcal{V}_f^{(1)}$, the set of the relays that successfully decoded D_1 message, where $\mathcal{V}_f^{(1)}$ is defined as

$$\mathcal{V}_f^{(1)} \triangleq \left\{ k \in \mathcal{S}_{Relay} : \mathrm{SIR}_{SR_{k\to 1}} \geq \Theta_1 \right\}, \tag{3.77}$$

where $f = |\mathcal{V}_f^{(1)}|$.

Similarly, we denote by $\mathcal{V}_g^{(2)}$, the set of the relays that successfully decoded D_2 message, where $\mathcal{V}_g^{(2)}$ is defined as

$$\mathcal{V}_g^{(2)} \triangleq \left\{ l \in \mathcal{S}_{Relay} : \mathrm{SIR}_{SR_{l\to l}} \geq \Theta_1 \bigcap \mathrm{SIR}_{SR_{l\to 2}} \geq \Theta_2 \right\}, \tag{3.78}$$

where $g = |\mathcal{V}_g^{(2)}|$. Note that $\mathcal{V}_g^{(2)} \subseteq \mathcal{V}_f^{(1)}$.

The outage probability at D_1, denoted $\mathbb{P}(O_{(1)})$, is given by

$$\mathbb{P}(O_{(1)}) = \begin{cases} 1, & \Theta_1 \geq \frac{a_1}{a_2}; \\ \prod_{k=1}^{nb_{Relay}} \left(1 - \mathcal{H}_{(R_k)}(\frac{G_1}{l_{SR_k}})\mathcal{H}_{(D_1)}(\frac{G_1}{l_{R_k D_1}})\right), & \text{otherwise.} \end{cases} \tag{3.79}$$

The outage probability at D_2, denoted $\mathbb{P}(O_{(2)})$, is given by

$$\mathbb{P}(O_{(2)}) = \begin{cases} 1, & \Theta_1 \geq \frac{a_1}{a_2} \text{ or } \Theta_2 \geq \frac{a_2}{\beta a_1}; \\ \prod_{l=1}^{nb_{Relay}} \left(1 - \mathcal{H}_{(R_l)}(\frac{G_{\max}}{l_{SR_l}})\mathcal{H}_{(D_2)}(\frac{G_{\max}}{l_{R_l D_2}})\right), & \text{otherwise.} \end{cases} \tag{3.80}$$

proof: See Appendix C.4. ■

Fig.3.16 shows the impact of adding relays to NOMA performance in terms of outage probability. We can see from Fig.3.16 that adding relay decreases significantly the outage probability. For instance we can see that the outage probability when one relay is used is around 0.2 for D_1 and 0.4 for D_2, whereas the outage probability when using eight relays is around 3×10^{-5} for D_1 and 0.1 for D_2.

Fig.3.17 plots the outage probability as a function of λ for several number of relays. We can clearly see the significant improvement in the performance as the number of the relays increases. For instance, we can see that the outage probability of D_1 using one relay is 4×10^{-2} whereas the outage probability using 8 relays is 9×10^{-12}.

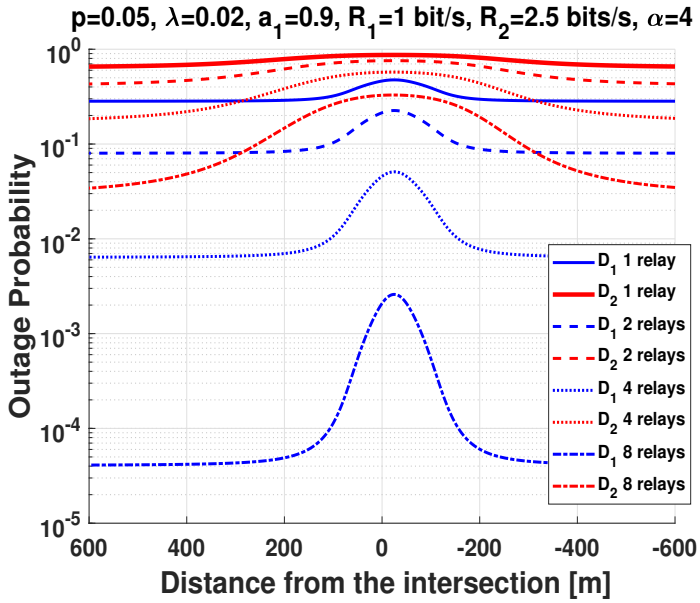

Figure 3.16.: Outage probability as a function of the distance from the intersection considering NOMA using multiple relays.

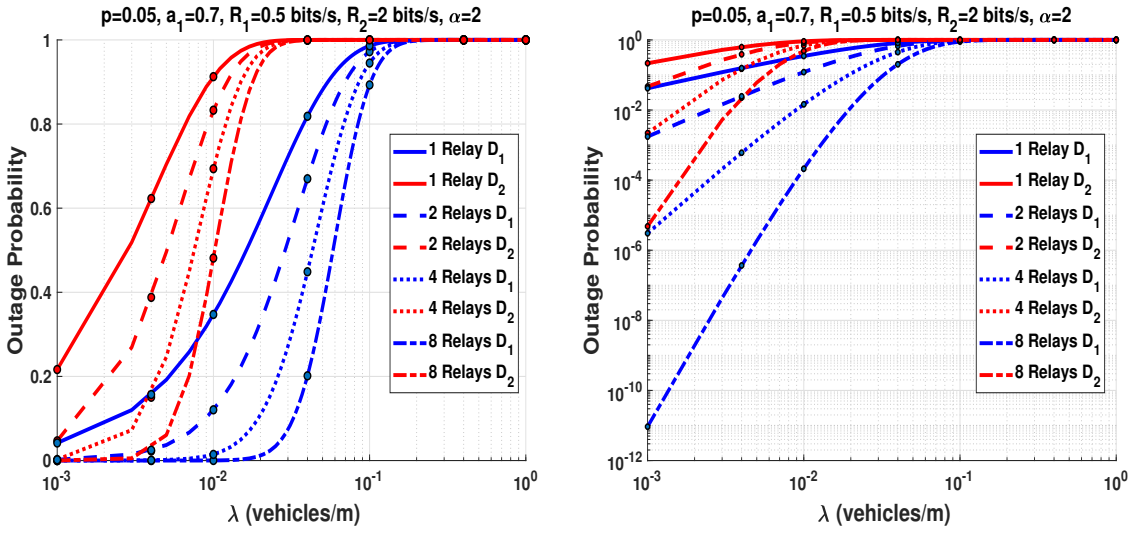

(a) (b)

Figure 3.17.: Outage probability as a function of λ considering NOMA for several number of. (a) linear scale. (b) log scale.

3.12. Conclusion

In this chapter, we proposed several extensions of our work. We proposed an adaptive cooperative protocol using NOMA (ACN) at intersections. We studied the performance and the behavior of mmWave vehicular networks using cooperative NOMA. We also studied the impact of adding several relays on the performance and several lanes scenarios. Finally, there are some extension that have not been simulated such as multi hop transmissions scenarios.

Regarding the ACN protocol, we compared it with cooperative NOMA protocol, direct NOMA protocol, and the classical cooperative OMA protocol, and we showed that ACN protocol outperforms these protocols in terms of outage probability, especially at intersections. We also compared the performance of ACN protocol with the CCN protocol, and we showed that the ACN protocol offers better performance than CCN protocol at road intersections in terms of outage probability. Finally, we showed that the performance of ACN protocol increases compared to other existing protocols for high data rates.

Regarding the performance of cooperative NOMA for mmWave vehicular networks at intersections, we derived closed form outage probability expressions for cooperative NOMA, and compared them with cooperative OMA. We showed that cooperative NOMA exhibited a significant improvement compared to cooperative OMA, especially for high data rates. However, data rates have to respect a given condition, if not, the performance of cooperative NOMA will decreases drastically. We also showed that as the nodes reach the intersection, the outage probability increased. Counter-intuitively, we showed that NLOS scenario has a better performance than LOS scenario.

Conclusions and perspectives

Conclusions

The main goal of this thesis was to offer a framework of cooperative VCs in the presence of interference, through models in which their principal characteristics and parameters could be considered, mainly, a large number of vehicles, their random spatial distribution, and the inherent broadcasting properties of the wireless medium. This was motivated by the fact that VCs have increased in numbers and in quality requirements. Moreover, VCs offer various and diverse applications, such as, traffic safety, traffic management and autonomous driving. Hence, the increasing demands of these applications require new approaches. The goal was also to obtain models in which general conclusions, regarding the network and its performance characteristics, could be drawn. We wanted to derive and obtain simple and closed form expressions that could be evaluated without large scale Monte Carlo simulations. Stochastic geometry models had shown to be a useful and powerful tool, that is why we used this approach.

We started by considering the half duplex cooperative VCs under the effect of the interference generated by vehicles modeled by a 1D-HPPP. We also considered VCs with several transmission schemes and vehicles mobility by mimicking the vehicles speed via the dependence and the independence of the interference. This analysis served as a starting point for studying how vehicles mobility and transmission schemes impact the performance of VCs. We also considered a more generalized fading channels, which is the Nakagami-m

fading channels, and studied the impact of several transmission schemes and under LOS and NLOS scenarios. A comparison was made between the performance of VCs in intersection scenarios and highway scenarios, and it has been shown that the performance of interference scenarios decreases when the vehicles come closer to the intersection. Additionally, one counter intuitive result was that the performance of VCs under NLOS scenarios were greater than LOS scenarios.

After considering the classical OMA schemes in cooperative VCs in the presence of interference, we wanted to study the benefits and the improvements of using NOMA in cooperation VCs. We studied the performance in terms of outage probability and average achievable rate. We considered direct transmissions, cooperative transmissions, cooperative transmissions using MRC. The results showed that NOMA improves the performance compared to OMA. However, there are some conditions that have to be meet in order for NOMA to outperform OMA, otherwise, the performance of NOMA will decrease drastically. We derived mathematical conditions for different system parameters in order for NOMA to outperforms OMA at intersections. The comparison between cooperative NOMA and cooperative NOMA using MRC showed that there is a significant improvement of using MRC. Although using MRC increases the interference at the receiving nodes, the cooperative NOMA using MRC still offers significant improvements compared to the classical OMA using MRC and the classical cooperative transmissions using NOMA.

In the third part of this thesis, we investigated several scenarios and aspects of cooperative VCs. Each of these scenarios can be investigated in great details for future works. First, we proposed an adaptive cooperative protocol using NOMA, named ACN at intersections. We compared the proposed protocol with several protocols existing in the literature, and showed that the ACN offers better performance at road intersections compared to other existing protocols, especially for high data rates. Second, we studied the performance and the behavior of mmWave vehicular networks using cooperative NOMA, and how to model

mmWave systems in VCs at intersections. Although the model uses strong assumptions, it can be used as a starting point for the analysis of more complex mmWave vehicular networks and to study the interactions among vehicles under different scenarios. Finally, we studied the impact of adding several relays, and we studied the performance of intersections scenarios involving several lanes. There are some extensions that have not been simulated such as multi hop transmissions, but we derived the outage probability expressions so they can be used as a starting point for future works.

Perspectives and future works

In the context of cooperative communications in VCs, it would be interesting to investigate and compare the performance of other decoding protocols, such as Amplify and Forward (AF) and Compress and Forward (CF). It will also be interesting to analyze the performance of full duplex transmissions. Regarding vehicles mobility, we could use realistic channels such as double Rayleigh fading channel sand double Nakagami fading channels. Since VCs mainly use CSMA Based protocols, investigating the performance of VCs would be interesting. Also, investigating the impact of the Doppler shift and time-varying effect of VCs could yield some insight on the performance. It would be realistic to consider a in-homogeneous PPP instead of HPPP, which can capture the inherent properties of intersections, and model the gathering vehicles near the intersection. The analysis of mmWave VCs introduces several possible ideas to continue. We used in this thesis a strong assumptions regarding the interfering vehicles and the blockage models. We assumed that the interfering vehicles are composed of a set of interfering vehicles that are in LOS and NLOS. A realistic assumption would be to use the blockage model which results in a dependent thinning of the PPP. On the other hand, in the context of NOMA, we could investigate several NOMA-based relays selection algorithms. Also, we could compare the performance of NOMA when the nodes are ordered according to their channels conditions and when the nodes are ordered

according to their QoS.

Conclusions (in French)

Conclusion

L'objectif principal de cette thèse était de proposer un cadre formel d'étude des communications véhiculaires coopératives en présence d'interférences aux intersections. Nous avons calculé les performances des réseaux véhiculaires principalement en termes de probabilité de coupure avec l'aide d'outil mathématique issus de la géométrie stochastique. Les calculs ont été validés par des simulations Monte-Carlo.

Au début, nous avons considéré des transmissions véhiculaires coopératives en présence de véhicules interférant modélisés par un 1D-PPP en présence d'un canal de Ralyleigh. Nous avons également considéré différents types de transmissions, et différents modèles de mobilité. Cette analyse nous a permis d'étudier comment la mobilité des véhicules et le type de transmissions employées peuvent impacter les performance des communications véhiculaires. Nous avons aussi considéré des types de canaux plus généraux, comme les canaux Nakagami-m, et nous avons étudié l'impact de différents types de transmissions quand les terminaux sont en ligne de mire (LOS), ou bien pas du tout en ligne de mire (NLOS). Nous avons aussi comparé les performances des communications véhiculaires sur les autoroutes et aux intersections, et nous avons constaté que les performances des communications véhiculaires aux intersections se dégradent quand les véhicules s'approchent de l'intersection. De plus, nous avons obtenue un résultat contre-intuitif : les performances des communications véhiculaires dans des scénarios NLOS sont meilleurs que dans les scénarios LOS.

Après avoir considéré les techniques classiques OMA dans les communications véhiculaires coopératives, nous nous sommes intéressés aux bénéfices et aux amélioration des performances en utilisant les techniques NOMA dans les communications véhiculaires. Nous avons étudié les performances en termes de probabilité de coupure et de débit atteignable. Nous avons considéré les transmissions directes, les transmissions coopératives et les transmissions coopératives en utilisant le MRC. Les résultats ont montré que les techniques NOMA appliquées aux communications véhiculaires améliorent les performances comparé aux techniques OMA. Cependant, certaines conditions doivent être respectées pour que les techniques NOMA soient supérieures aux techniques OMA, au risque que les performances des techniques NOMA décroissent de façon drastique. Les comparaisons entre les communications véhiculaires coopératives utilisant les techniques NOMA, et les communications véhiculaires coopératives utilisant les techniques NOMA avec MRC ont montré que le MRC apporte une amélioration significative aux performances.

Dans la dernière partie de cette thèse, nous avons traité plusieurs scénarios de communications véhiculaires coopératives. À noter que chaque scénario pourrait être traité plus en détails dans de futurs travaux. Dans un premier temps, nous avons proposé un protocole adaptatif coopératif utilisant les techniques NOMA nommé ACN. Nous avons comparé ce protocole avec plusieurs protocoles de la littérature, et nous avons montré que l'ACN donne de meilleures performances comparé aux autres protocoles dans le contexte des communications véhiculaires. Dans un second temps, nous avons étudié les performances des réseaux véhiculaires coopératifs à onde millimétrique utilisant les techniques NOMA. Enfin, nous avons étudié l'impact du nombre de relais sur les performances, l'impact de l'ajout de plusieurs routes dans les performances. Certains scénarios n'ont pas été simulés comme les communications véhiculaires coopératives à plusieurs sauts. Cependant, nous avons développé les expressions des probabilités de coupure, pour qu'ils puissent servir comme point de départ pour de futurs travaux.

Appendices

Appendix A.

Appendix to chapter 1

A.1. PROOF OF LEMMA 1

We calculate the probability $\mathbb{P}(O_{SR}^{C} \cap O_{SD}^{C})$ in equation (1.17) as follows

$$\begin{aligned}
\mathbb{P}(O_{SR}^{C} \cap O_{SD}^{C}) &= \mathbb{E}_{I_X,I_Y}\Bigg[\mathbb{P}\Bigg\{\Big(\frac{1}{2}\log_2\Big[1+\frac{P|h_{SR}|^2 l_{SR}}{\sigma^2+I_{X_R}+I_{Y_R}}\Big] \geq \mathcal{R} \\
&\quad \bigcap \frac{1}{2}\log_2\Big[1+\frac{P|h_{SD}|^2 l_{SD}}{\sigma^2+I_{X_D}+I_{Y_D}}\Big] \geq \mathcal{R}\Bigg\}\Bigg] \\
&= \mathbb{E}_{I_X,I_Y}\Bigg[\mathbb{P}\Bigg\{\Big(|h_{SR}|^2 \geq \frac{\Theta}{P l_{SR}}(\sigma^2+I_{X_R}+I_{Y_R}) \\
&\quad \bigcap |h_{SD}|^2 \geq \frac{\Theta}{P l_{SD}}(\sigma^2+I_{X_R}+I_{Y_R})\Bigg\}\Bigg].
\end{aligned}$$

Since $|h_{SR}|^2$ and $|h_{SD}|^2$ both follow an exponential distribution with unit mean, we get

$$\begin{aligned}
\mathbb{P}(O_{SR}^{C} \cap O_{SD}^{C}) &= \mathbb{E}_{I_X,I_Y}\Big[\exp(-K_{SR}I_{X_R})\exp(-K_{SR}I_{Y_R})\exp(-K_{SR}\sigma^2) \\
&\quad \exp(-K_{SD}I_{X_D})\exp(-K_{SD}I_{Y_D})\exp(-K_{SD}\sigma^2)\Big] \\
&= \mathbb{E}_{I_X,I_Y}\Big[N_{SR}\exp(-K_{SR}I_{X_R})\exp(-K_{SR}I_{Y_R}) \\
&\quad N_{SD}\exp(-K_{SD}I_{X_D})\exp(-K_{SD}I_{Y_D})\Big].
\end{aligned}$$

Given that the noise is independent of the interference, and using the independence of the PPP on the road X and Y, we finally get (1.20).

A.2. PROOF OF LEMMA 2

To calculate the probability $\mathbb{P}(O_{SR}^{C} \cap O_{RD})$, we proceed as follows

$$\begin{aligned}
\mathbb{P}(O_{SR}^{C} \cap O_{RD}) &= \mathbb{E}_{I_X,I_Y}\Bigg[\mathbb{P}\Bigg\{|h_{SR}|^2 \geq \frac{\Theta}{Pl_{SR}}(\sigma^2 + I_{X_R} + I_{Y_R}) \\
&\qquad \bigcap |h_{RD}|^2 < \frac{\Theta}{Pl_{RD}}(\sigma^2 + I_{X_D} + I_{Y_D})\Bigg\}\Bigg] \\
&= \mathbb{E}_{I_X,I_Y}\Big[\exp(-K_{SR}I_{X_R})\exp(-K_{SR}I_{Y_R})\exp(-K_{SR}\sigma^2) \\
&\quad \Big(1 - \exp(-K_{RD}I_{X_D})\exp(-K_{RD}I_{Y_D})\exp(-K_{RD}\sigma^2)\Big)\Big] \\
&= N_{SR}\,\mathbb{E}_{I_X,I_Y}\big[\exp(-K_{SR}I_{X_R})\exp(-K_{SR}I_{Y_R})\big] \\
&\quad - N_{SR}N_{RD}\,\mathbb{E}_{I_X,I_Y}\big[\exp(-K_{SR}I_{X_R})\exp(-K_{SR}I_{Y_R}) \\
&\quad \times \exp(-K_{RD}I_{X_D})\exp(-K_{RD}I_{Y_D})\big].
\end{aligned}$$

A.3. PROOF OF LEMMA 3

To calculate the probability $\mathbb{P}(O_{SR}^{C} \cap O_{SRD})$, we follow the same steps as in **??**, then we obtain

$$\begin{aligned}
\mathbb{P}(O_{SR}^{C} \cap O_{SRD}) = \mathbb{E}_{I_X,I_Y}\Bigg[&N_{SR}\exp\Big(-K_{SR}I_{X_R}\Big)\exp\Big(-K_{SR}I_{Y_R}\Big) \\
&\times\left(1 - \mathbb{P}\left\{|h_{RD}|^2 l_{RD} + |h_{SD}|^2 l_{SD} \geq \frac{\Theta}{P}(\sigma^2 + I_{X_D} + I_{Y_D})\right\}\right)\Bigg]. \quad \text{(A.1)}
\end{aligned}$$

We write the probability inside the expectation in (A.1) as

$$\mathbb{P}(\delta \geq \eta[\sigma^2 + I_{X_D} + I_{Y_D}]),$$

where $\delta = |h_{RD}|^2 l_{RD} + |h_{SD}|^2 l_{SD}$ and $\eta = \Theta/P$.
We set $\mathbb{P}\left\{ (|h_{RD}|^2 l_{RD} + |h_{SD}|^2 l_{SD}) \geq \eta(\sigma^2 + I_{X_D} + I_{Y_D}) \right\} = \mathbb{P}(RD, SD)$, then

$$
\begin{aligned}
\mathbb{P} &= \mathbb{E}_{|h_{SD}|^2}\left[\mathbb{P}\Big(|h_{RD}|^2 \geq \frac{\eta[\sigma^2 + I_{X_D} + I_{Y_D}] - |h_{SD}|^2 l_{SD}}{l_{RD}}\Big)\right] \\
&= \mathbb{E}_{|h_{SD}|^2}\left[\exp\Big(-\frac{\eta[\sigma^2 + I_{X_D} + I_{Y_D}] - |h_{SD}|^2 l_{SD}}{l_{RD}}\Big)\right] \\
&= \int_0^{\frac{\eta[\sigma^2+I_{X_D}+I_{Y_D}]}{l_{SD}}} \exp\Big(-\frac{\eta[\sigma^2 + I_{X_D} + I_{Y_D}] - |h_{SD}|^2 l_{SD}}{l_{RD}}\Big)\exp\big(-|h_{SD}|^2\big)\mathrm{d}|h_{SD}|^2 \\
&\quad + \int_{\frac{\eta[\sigma^2+I_{X_D}+I_{Y_D}]}{l_{SD}}}^{\infty} \exp\big(-|h_{SD}|^2\big)\mathrm{d}|h_{SD}|^2 \\
&= e^{-\frac{\eta[\sigma^2+I_{X_D}+I_{Y_D}]}{l_{RD}}} \int_0^{\frac{\eta[\sigma^2+I_{X_D}+I_{Y_D}]}{l_{SD}}} e^{-|h_{SD}|^2(1-\frac{l_{SD}}{l_{RD}})}\mathrm{d}|h_{SD}|^2 + e^{-\frac{\eta[\sigma^2+I_{X_D}+I_{Y_D}]}{l_{SD}}} \\
&= e^{-\frac{\eta[\sigma^2+I_{X_D}+I_{Y_D}]}{l_{RD}}}\left[\frac{1}{1-\frac{l_{SD}}{l_{RD}}} - \frac{e^{-\frac{\eta[\sigma^2+I_{X_D}+I_{Y_D}]}{l_{SD}}\left(1-\frac{l_{SD}}{l_{RD}}\right)}}{1-\frac{l_{SD}}{l_{RD}}}\right] + e^{-\frac{\eta[\sigma^2+I_{X_D}+I_{Y_D}]}{l_{SD}}} \\
&= e^{-\frac{\eta[\sigma^2+I_{X_D}+I_{Y_D}]}{l_{RD}}}\left[\frac{1}{1-\frac{l_{SD}}{l_{RD}}} - \frac{e^{-\frac{\eta[\sigma^2+I_{X_D}+I_{Y_D}]}{l_{SD}}}e^{\frac{\eta[\sigma^2+I_{X_D}+I_{Y_D}]}{l_{RD}}}}{1-\frac{l_{SD}}{l_{RD}}}\right] + e^{-\frac{\eta[\sigma^2+I_{X_D}+I_{Y_D}]}{l_{SD}}} \\
&= \frac{1}{1+\frac{l_{SD}}{l_{RD}}}e^{-\frac{\eta[\sigma^2+I_{X_D}+I_{Y_D}]}{l_{RD}}} - \frac{1}{1+\frac{l_{SD}}{l_{RD}}}e^{-\frac{\eta[\sigma^2+I_{X_D}+I_{Y_D}]}{l_{SD}}} + e^{-\frac{\eta[\sigma^2+I_{X_D}+I_{Y_D}]}{l_{SD}}} \\
&= \left(\frac{1}{1+\frac{l_{SD}}{l_{RD}}}\right)e^{-\frac{\eta[\sigma^2+I_{X_D}+I_{Y_D}]}{l_{RD}}} + \left(1 - \frac{1}{1+\frac{l_{SD}}{l_{RD}}}\right)e^{-\frac{\eta[\sigma^2+I_{X_D}+I_{Y_D}]}{l_{SD}}} \\
&= \left(\frac{l_{RD}}{l_{RD}-l_{SD}}\right)e^{-\frac{\eta[\sigma^2+I_{X_D}+I_{Y_D}]}{l_{RD}}} + \left(1 - \frac{l_{RD}}{l_{RD}-l_{SD}}\right)e^{-\frac{\eta[\sigma^2+I_{X_D}+I_{Y_D}]}{l_{SD}}} \\
&= \left(\frac{l_{RD}}{l_{RD}-l_{SD}}\right)e^{-\frac{\eta[\sigma^2+I_{X_D}+I_{Y_D}]}{l_{RD}}} + \left(-\frac{l_{SD}}{l_{RD}-l_{SD}}\right)e^{-\frac{\eta[\sigma^2+I_{X_D}+I_{Y_D}]}{l_{SD}}} \\
&= \frac{l_{RD}e^{-\frac{\eta[\sigma^2+I_{X_D}+I_{Y_D}]}{l_{RD}}} - l_{SD}e^{-\frac{\eta[\sigma^2+I_{X_D}+I_{Y_D}]}{l_{SD}}}}{l_{RD}-l_{SD}}.
\end{aligned} \tag{A.2}
$$

The complementary cumulative distribution function of the random variable δ, denoted $\bar{F}_\delta(\cdot)$, is given by

$$\bar{F}_\delta(u) = \frac{l_{RD}e^{-u/l_{RD}} - l_{SD}e^{-u/l_{SD}}}{l_{RD}-l_{SD}}.$$

Then

$$\mathbb{P}[\delta \geq \eta(\sigma^2 + I_{X_D} + I_{Y_D})] = \frac{l_{RD}\exp\Big[-\frac{\eta}{l_{RD}}(\sigma^2 + I_{X_D} + I_{Y_D})\Big] - l_{SD}\exp\Big(-\frac{\eta}{l_{SD}}[\sigma^2 + I_{X_D} + I_{Y_D})\Big]}{l_{RD} - l_{SD}}. \quad \text{(A.3)}$$

Plugging (A.3) into (A.1), and with some algebraic manipulations, we get (1.22).

In the case when $\|S - D\| = \|R - D\|$, we set

$$\mathbb{P}\Big\{(|h_{RD}|^2 l_{SD} + |h_{SD}|^2 l_{SD}) \geq \eta(\sigma^2 + I_{X_D} + I_{Y_D})\Big\} = \mathbb{P}(RD, SD).$$

Then

$$\begin{aligned}
\mathbb{P}(RD, SD) &= \mathbb{E}_{|h_{SD}|^2}\left[\mathbb{P}\Big(|h_{RD}|^2 \geq \frac{\eta[\sigma^2 + I_{X_D} + I_{Y_D}]}{l_{SD}} - |h_{SD}|^2\Big)\right] \\
&= \mathbb{E}_{|h_{SD}|^2}\left[e^{-\left(\frac{\eta[\sigma^2 + I_{X_D} + I_{Y_D}]}{l_{SD}} - |h_{SD}|^2\right)}\right] \\
&= \int_0^{\frac{\eta[\sigma^2 + I_{X_D} + I_{Y_D}]}{l_{SD}}} e^{\left(-\frac{\eta[\sigma^2 + I_{X_D} + I_{Y_D}]}{l_{SD}} + |h_{SD}|^2\right)} e^{-|h_{SD}|^2} \mathrm{d}|h_{SD}|^2 \\
&\quad + \int_{\frac{\eta[\sigma^2 + I_{X_D} + I_{Y_D}]}{l_{SD}}}^{\infty} e^{-|h_{SD}|^2} \mathrm{d}|h_{SD}|^2 \\
&= e^{-\frac{\eta[\sigma^2 + I_{X_D} + I_{Y_D}]}{l_{SD}}} \int_0^{\frac{\eta[\sigma^2 + I_{X_D} + I_{Y_D}]}{l_{SD}}} 1 \, \mathrm{d}|h_{SD}|^2 \\
&\quad + \int_{\frac{\eta[\sigma^2 + I_{X_D} + I_{Y_D}]}{l_{SD}}}^{\infty} e^{-|h_{SD}|^2} \mathrm{d}|h_{SD}|^2 \\
&= e^{-\frac{\eta[\sigma^2 + I_{X_D} + I_{Y_D}]}{l_{SD}}} \left[\frac{\eta[\sigma^2 + I_{X_D} + I_{Y_D}]}{l_{SD}}\right] + e^{-\frac{\eta[\sigma^2 + I_{X_D} + I_{Y_D}]}{l_{SD}}} \\
&= \left[1 + \frac{\eta[\sigma^2 + I_{X_D} + I_{Y_D}]}{l_{SD}}\right] e^{-\frac{\eta[\sigma^2 + I_{X_D} + I_{Y_D}]}{l_{SD}}}. \quad \text{(A.4)}
\end{aligned}$$

A.4. PROOF OF THEOREM 1

When the interference at the relay and the destination are generated from two independent sets, the following expectation can be written as

$$\mathbb{E}_{I_X}\left[e^{-(sI_{X_R}+bI_{X_D})}\right] = \mathbb{E}_{I_X}\left[e^{-sI_{X_R}}\right]\mathbb{E}_{I_X}\left[e^{-bI_{X_D}}\right]. \tag{A.5}$$

Given that $\mathbb{E}[e^{sI}] = \mathcal{L}_I(s)$, we then develop the expression of the first expectation in (A.5) as

$$\mathcal{L}_{I_{X_R}}(s) = \mathbb{E}\left[\exp(-sI_{X_R})\right]. \tag{A.6}$$

Plugging (1.1) into (A.6) yields

$$\begin{aligned}
\mathcal{L}_{I_{X_R}}(s) &= \mathbb{E}\left[\exp\left(-\sum_{x\in\Phi_{X_R}} sP|h_{Rx}|^2 l_{Rx}\right)\right] \\
&= \mathbb{E}\left[\prod_{x\in\Phi_{X_R}} \exp\left(-sP|h_{Rx}|^2 l_{Rx}\right)\right] \\
&\overset{(a)}{=} \mathbb{E}\left[\prod_{x\in\Phi_{X_R}} \mathbb{E}_{|h_{Rx}|^2}\left\{\exp\left(-sP|h_{Rx}|^2 l_{Rx}\right)\right\}\right] \\
&\overset{(b)}{=} \mathbb{E}\left[\prod_{x\in\Phi_{X_R}} \frac{p}{1+sPl_{Rx}} + 1 - p\right] \\
&\overset{(c)}{=} \exp\left(-\lambda_X \int_{\mathcal{B}} \left[1 - \left(\frac{p}{1+sPl_{Rx}} + 1 - p\right)\right] dx\right) \\
&= \exp\left(-p\lambda_X \int_{\mathcal{B}} \frac{1}{1+1/sPl_{Rx}} dx\right),
\end{aligned} \tag{A.7}$$

where (a) follows from having independent fading; (b) follows from calculating the expectation over $|h_{Rx}|^2$ which follows an exponential distribution with unit mean, and then calculating the expectation over the indicator function $\mathbb{1}$; (c) follows from the probability

generating functional (PGFL) of a PPP [Hae12b]. Then (A.5) can be expressed as

$$\mathbb{E}_{I_X}\left[e^{-sI_{X_R}}\right]\mathbb{E}_{I_X}\left[e^{-bI_{X_D}}\right] = \mathcal{L}_{I_{X_R}}(s)\mathcal{L}_{I_{X_D}}(b), \tag{A.8}$$

where

$$\mathcal{L}_{I_{X_R}}(s) = \exp\left(- p\lambda_X \int_{\mathcal{B}} \frac{1}{1 + (A\|x - R\|^{\alpha})/sP} dx\right), \tag{A.9}$$

and

$$\mathcal{L}_{I_{X_D}}(s) = \exp\left(- p\lambda_X \int_{\mathcal{B}} \frac{1}{1 + (A\|x - D\|^{\alpha})/sP} dx\right). \tag{A.10}$$

In the same way, when the interference originating from the Y road at the relay and the destination are generated from two independent sets, the following expectation can be written as

$$\mathbb{E}_{I_Y}\left[e^{-sI_{Y_R}}\right]\mathbb{E}_{I_Y}\left[e^{-bI_{Y_D}}\right] = \mathcal{L}_{I_{Y_R}}(s)\mathcal{L}_{I_{Y_D}}(b), \tag{A.11}$$

where

$$\mathcal{L}_{I_{Y_R}}(s) = \exp\left(- p\lambda_Y \int_{\mathcal{B}} \frac{1}{1 + (A\|y - R\|^{\alpha})/sP} dy\right) \tag{A.12}$$

$$\mathcal{L}_{I_{Y_D}}(s) = \exp\left(- p\lambda_Y \int_{\mathcal{B}} \frac{1}{1 + (A\|y - D\|^{\alpha})/sP} dy\right). \tag{A.13}$$

After substituting all the expressions of the expectation in (1.20), (1.21) and (1.22), we obtain (1.23), (1.24) and (1.25).

A.5. PROOF OF THEOREM 2

When the interference at the relay and the destination are generated from the same set, the equality in (A.5) does not hold true. Then, the expectation in left side of (A.5) will be

expressed as

$$\begin{aligned}
\mathbb{E}_{I_X}\left[e^{-\left(sI_{X_R}+bI_{X_D}\right)}\right] &= \mathbb{E}_{I_X}\left[\prod_{x\in\Phi_X}\mathbb{E}_{|h|^2}\left[e^{-sP|h_{Rx}|^2 l_{Rx}+bP|h_{Dx}|^2 l_{Dx}}\right]\right] \\
&= \mathbb{E}_{I_X}\left[\prod_{x\in\Phi_X}\frac{p}{(1+sPl_{Rx})(1+bPl_{Dx})}+1-p\right] \\
&= \exp\left(-\lambda_X\int_{\mathcal{B}}1-\left[\frac{p}{(1+sPl_{Rx})(1+bPl_{Dx})}+1-p\right]dx\right) \\
&= \exp\left(-p\lambda_X\int_{\mathcal{B}}\frac{sPl_{Rx}}{1+sPl_{Rx}}+\frac{bPl_{Dx}}{1+bPl_{Dx}}\right. \\
&\quad \left.-\frac{sbP^2 l_{Rx}l_{Dx}}{(1+sPl_{Rx})(1+bPl_{Dx})}dx\right) \\
&= \exp\left(-p\lambda_X\int_{\mathcal{B}}\frac{dx}{1+1/sPl_{Rx}}\right)\exp\left(-p\lambda_X\int_{\mathcal{B}}\frac{dx}{1+1/bPl_{Dx}}\right) \\
&\quad \times\exp\left(p\lambda_X\int_{\mathcal{B}}\frac{sbP^2 l_{Rx}l_{Dx}}{(1+sPl_{Rx})(1+bPl_{Dx})}dx\right). \qquad \text{(A.14)}
\end{aligned}$$

Then (A.14) can be written as

$$\mathbb{E}_{I_X}\left[e^{-\left(sI_{X_R}+bI_{X_D}\right)}\right]=\mathcal{L}_{I_{X_R}}(s)\mathcal{L}_{I_{X_D}}(b)\rho_X(s,b)=\mathcal{L}_{I_{X_R},I_{X_D}}(s,b). \qquad \text{(A.15)}$$

Following the same steps, we obtain

$$\mathbb{E}_{I_Y}\left[e^{-\left(sI_{Y_R}+bI_{Y_D}\right)}\right]=\mathcal{L}_{I_{Y_R}}(s)\mathcal{L}_{I_{Y_D}}(b)\rho_Y(s,b)=\mathcal{L}_{I_{Y_R},I_{Y_D}}(s,b). \qquad \text{(A.16)}$$

After substituting all the expressions of the expectation in (1.20), (1.21) and (1.22), we obtain (1.26), (1.27), and (1.28).

A.6. Outage probability of DT transmission

The outage probability expression of DT is given by

$$\mathbb{P}(O_{\mathbf{(DT)}}) = 1 - \mathbb{P}(O^{C}_{\mathbf{(DT)}}) = 1 - \mathbb{P}(\mathrm{SIR}_{SD} \geq \Theta_1). \tag{A.17}$$

To calculate $\mathbb{P}(\mathrm{SIR}_{SD} \geq \Theta_1)$, we proceed as follows

$$\begin{aligned} \mathbb{P}(\mathrm{SIR}_{SD} \geq \Theta_1) &= \mathbb{E}_{I_X, I_Y}\left[\mathbb{P}\left\{\frac{|h_{SD}|^2 l_{SD}}{I_X + I_Y} \geq \Theta_1\right\}\right] \\ &= \mathbb{E}_{I_X, I_Y}\left[\mathbb{P}\left\{|h_{SD}|^2 \geq \frac{\Theta_1}{l_{SD}}(I_X + I_Y)\right\}\right]. \end{aligned} \tag{A.18}$$

Since $|h_{SD}|^2$ follows a gamma distribution, its complementary cumulative distribution function (CCDF) is given by

$$\bar{F}_{|h_{SD}|^2}(X) = \mathbb{P}(|h_{SD}|^2 > X) = \frac{\Gamma(m, \frac{m}{\mu}X)}{\Gamma(m)}. \tag{A.19}$$

Hence

$$\mathbb{P}(\mathrm{SIR}_{SD} \geq \Theta_1) = \mathbb{E}_{I_X, I_Y}\left[\frac{\Gamma\Big(m, \dfrac{m\,\Theta_1}{\mu\, l_{SD}}(I_X + I_Y)\Big)}{\Gamma(m)}\right]. \tag{A.20}$$

The exponential sum function when m is an integer is defined as

$$e_{(m)} = \sum_{k=0}^{m-1} \frac{(\frac{m}{\mu}X)^k}{k!} = e^{x}\frac{\Gamma(m, \frac{m}{\mu}X)}{\Gamma(m)}. \tag{A.21}$$

Then

$$\frac{\Gamma(m, \frac{m}{\mu}X)}{\Gamma(m)} = e^{-\frac{m}{\mu}X} \sum_{k=0}^{m-1} \frac{1}{k!}\Big(\frac{m\,X}{\mu}\Big)^{k}. \tag{A.22}$$

The equation (A.20) then becomes

$$\begin{aligned}\mathbb{P}(\mathrm{SIR}_{SD} \geq \Theta_1) &= \mathbb{E}_{I_X,I_Y}\left[\exp\Big(-\frac{m\,\Theta_1}{\mu\, l_{SD}}(I_X+I_Y)\Big)\times\sum_{k=0}^{m-1}\frac{1}{k!}\Big(\frac{m\,\Theta_1}{\mu\, l_{SD}}(I_X+I_Y)\Big)^k\right]\\ &= \sum_{k=0}^{m-1}\frac{1}{k!}\Big(\frac{m\,\Theta_1}{\mu\, l_{SD}}\Big)^k\mathbb{E}_{I_X,I_Y}\left[\exp\Big(-\frac{m\,\Theta_1}{\mu\, l_{SD}}(I_X+I_Y)\Big)(I_X+I_Y)^k\right].\end{aligned} \tag{A.23}$$

Applying the binomial theorem to (A.23), we get

$$\mathbb{P}(\mathrm{SIR}_{SD} \geq \Theta_1) = \sum_{k=0}^{m-1}\frac{1}{k!}\,G^k\mathbb{E}_{I_X,I_Y}\left[\exp\Big(-G[I_X+I_Y]\Big)\sum_{n=0}^{k}\binom{k}{n}{I_X}^{k-n}\,{I_Y}^n\right], \tag{A.24}$$

where $G = \dfrac{m\,\Theta_1}{\mu\, l_{SD}}$.
To calculate the expectation in (A.24), denoted $\mathcal{Z}(I_X, I_Y)$, we process as follows

$$\begin{aligned}\mathcal{Z}(I_X,I_Y) &= \mathbb{E}_{I_X,I_Y}\left[e^{-G\,I_X}\,e^{-G\,I_Y}\sum_{n=0}^{k}\binom{k}{n}{I_X}^{k-n}\,{I_Y}^n\right]\\ &= \sum_{n=0}^{k}\binom{k}{n}\mathbb{E}_{I_X,I_Y}\left[e^{-G\,I_{X_D}}\,e^{-G\,I_Y}{I_X}^{k-n}\,{I_Y}^n\right]\\ &\overset{(a)}{=} \sum_{n=0}^{k}\binom{k}{n}\mathbb{E}_{I_X}\left[e^{-G\,I_X}{I_X}^{k-n}\right]\mathbb{E}_{I_Y}\left[e^{-G\,I_Y}\,{I_Y}^n\right]\\ &\overset{(b)}{=} \sum_{n=0}^{k}\binom{k}{n}(-1)^{k-n}\frac{\mathrm{d}^{k-n}\mathcal{L}_{I_X}(G)}{\mathrm{d}^{k-n}G}(-1)^n\frac{\mathrm{d}^n\mathcal{L}_{I_Y}(G)}{\mathrm{d}^nG}\\ &= (-1)^k\sum_{n=0}^{k}\binom{k}{n}\frac{\mathrm{d}^{k-n}\mathcal{L}_{I_X}(G)}{\mathrm{d}^{k-n}G}\frac{\mathrm{d}^n\mathcal{L}_{I_Y}(G)}{\mathrm{d}^nG},\end{aligned} \tag{A.25}$$

where (a) follows from the independence of the PPP on the X road and the road Y; (b) follows from the following property

$$\begin{aligned}\mathbb{E}_I\left[e^{-gI}I^N\right] &= (-1)^N\frac{\mathrm{d}^N\mathbb{E}_I\left[e^{-gI}I^N\right]}{\mathrm{d}^N g}\\ &= (-1)^N\frac{\mathrm{d}^N\mathcal{L}_I(g)}{\mathrm{d}^N g}.\end{aligned} \tag{A.26}$$

Then

$$\mathbb{P}(\mathrm{SIR}_{SD}\geq\Theta_1)=\sum_{k=0}^{m-1}\frac{1}{k!}\,(-\frac{m\,\Theta_1}{\mu\,l_{SD}})^k\sum_{n=0}^{k}\binom{k}{n}\frac{\mathrm{d}^{k-n}\mathcal{L}_{I_X}(\frac{m\,\Theta_1}{\mu\,l_{SD}})}{\mathrm{d}^{k-n}(\frac{m\,\Theta_1}{\mu\,l_{SD}})}\frac{\mathrm{d}^{n}\mathcal{L}_{I_Y}(\frac{m\,\Theta_1}{\mu\,l_{SD}})}{\mathrm{d}^{n}(\frac{m\,\Theta_1}{\mu\,l_{SD}})}. \tag{A.27}$$

Plugging (A.27) into (A.17), we get (1.35).

A.7. Outage probability of RT transmission

The outage probability of RT is expressed as

$$\mathbb{P}(O_{(\mathbf{RT})})=\mathbb{P}(O_{SR}\cup O_{RD})=1-\mathbb{P}(O_{SR}^C\cap O_{RD}^C). \tag{A.28}$$

To calculate the probability $\mathbb{P}(O_{SR}^C \cap O_{RD}^C)$, we proceed as follows

$$
\begin{aligned}
\mathbb{P}(O_{SR}^C \cap O_{RD}^C) &= \mathbb{E}_{I_X,I_Y}\left[\mathbb{P}\left\{\frac{|h_{SR}|^2 l_{SR}}{I_{X_R}+I_{Y_R}} \geq \Theta_2, \frac{|h_{RD}|^2 l_{RD}}{I_{X_D}+I_{Y_D}} \geq \Theta_2\right\}\right] \\
&= \mathbb{E}_{I_X,I_Y}\left[\mathbb{P}\left\{|h_{SR}|^2 \geq \frac{\Theta_2}{l_{SR}}(I_{X_R}+I_{Y_R}), |h_{RD}|^2 \geq \frac{\Theta_2}{l_{RD}}(I_{X_D}+I_{Y_D})\right\}\right] \\
&= \mathbb{E}_{I_X,I_Y}\left[\frac{\Gamma\Big(m, \frac{m\,\Theta_2}{\mu\, l_{SR}}(I_{X_R}+I_{Y_R})\Big)}{\Gamma(m)} \times \frac{\Gamma\Big(m, \frac{m\,\Theta_2}{\mu\, l_{RD}}(I_{X_D}+I_{Y_D})\Big)}{\Gamma(m)}\right] \\
&= \mathbb{E}_{I_X,I_Y}\Bigg[\exp\Big(-\frac{m\,\Theta_2}{\mu\, l_{SR}}(I_{X_R}+I_{Y_R})\Big)\exp\Big(-\frac{m\,\Theta_2}{\mu\, l_{RD}}(I_{X_D}+I_{Y_D})\Big) \\
&\quad \times \sum_{k=0}^{m-1}\sum_{l=0}^{m-1}\frac{1}{k!}\frac{1}{l!}\Big(\frac{m\,\Theta_2}{\mu\, l_{SR}}(I_{X_R}+I_{Y_R})\Big)^k\Big(\frac{m\,\Theta_2}{\mu\, l_{RD}}(I_{X_D}+I_{Y_D})\Big)^l\Bigg] \\
&= \sum_{k=0}^{m-1}\sum_{l=0}^{m-1}\frac{1}{k!}\frac{1}{l!}\Big(\frac{m\,\Theta_2}{\mu\, l_{SR}}\Big)^k\Big(\frac{m\,\Theta_2}{\mu\, l_{RD}}\Big)^l \\
&\quad \times \mathbb{E}_{I_X,I_Y}\left[\exp\Big(-\frac{m\,\Theta_2}{\mu\, l_{SR}}[I_{X_R}+I_{Y_R}]\Big)[I_{X_R}+I_{Y_R}]^k\right] \\
&\quad \times \mathbb{E}_{I_X,I_Y}\left[\exp\Big(-\frac{m\,\Theta_2}{\mu\, l_{RD}}[I_{X_D}+I_{Y_D}]\Big)[I_{X_D}+I_{Y_D}]^l\right] \\
&= \sum_{k=0}^{m-1}\sum_{l=0}^{m-1}\frac{1}{k!}\frac{1}{l!}\Big(\frac{m\,\Theta_2}{\mu\, l_{SR}}\Big)^k\Big(\frac{m\,\Theta_2}{\mu\, l_{RD}}\Big)^l \\
&\quad \times \mathbb{E}_{I_X,I_Y}\left[\exp\Big(-\frac{m\,\Theta_2}{\mu\, l_{SR}}[I_{X_R}+I_{Y_R}]\Big)\sum_{n=0}^{k}\binom{k}{n}{I_{X_R}}^{k-n}{I_{Y_R}}^n\right] \\
&\quad \times \mathbb{E}_{I_X,I_Y}\left[\exp\Big(-\frac{m\,\Theta_2}{\mu\, l_{RD}}[I_{X_D}+I_{Y_D}]\Big)\sum_{f=0}^{l}\binom{l}{f}{I_{X_D}}^{l-f}{I_{Y_D}}^f\right]. \quad \text{(A.29)}
\end{aligned}
$$

Then, following the same steps as in A.6, we obtain (1.41).

A.8. Outage probability of HT transmission

The outage probability of HT is expressed as

$$\mathbb{P}(O_{\mathbf{(HT)}}) = \mathbb{P}(O_{SD} \cap O_{SR}) + \mathbb{P}(O_{SR}^{C} \cap O_{RD}).$$

The probability $\mathbb{P}(O_{SD} \cap O_{SR})$ can be expressed as follows

$$\begin{aligned} \mathbb{P}(O_{SD} \cap O_{SR}) &= 1 - \mathbb{P}(O_{SD}^{C} \cup O_{SR}^{C}) \\ &= 1 - \mathbb{P}(O_{SD}^{C}) - \mathbb{P}(O_{SR}^{C}) + \mathbb{P}(O_{SD}^{C} \cap O_{SR}^{C}). \end{aligned} \tag{A.30}$$

The expression of $\mathbb{P}(O_{SD}^{C})$ and $\mathbb{P}(O_{SR}^{C})$ can be acquired following the same steps as in A.6. The probability $\mathbb{P}(O_{SD}^{C} \cap O_{SR}^{C})$ is calculated following the same steps as in A.7.

To calculate the probability $\mathbb{P}(O_{SR}^{C} \cap O_{RD})$, we proceed as follows

$$\begin{aligned} \mathbb{P}(O_{SR}^{C} \cap O_{RD}) &= \mathbb{E}_{I_X, I_Y}\left[\mathbb{P}\left\{\frac{|h_{SR}|^2 l_{SR}}{I_{X_R} + I_{Y_R}} \geq \Theta_2 \bigcap \frac{|h_{RD}|^2 l_{RD}}{I_{X_D} + I_{Y_D}} < \Theta_2\right\}\right] \\ &= \mathbb{E}_{I_X, I_Y}\left[\mathbb{P}\left\{|h_{SR}|^2 \geq \frac{\Theta_2}{l_{SR}}(I_{X_R} + I_{Y_R}) \bigcap |h_{RD}|^2 < \frac{\Theta_2}{l_{RD}}(I_{X_D} + I_{Y_D})\right\}\right] \\ &= \mathbb{E}_{I_X, I_Y}\left[\frac{\Gamma\left(m, \frac{m\,\Theta_2}{\mu\, l_{SR}}(I_{X_R} + I_{Y_R})\right)}{\Gamma(m)}\left(1 - \frac{\Gamma\left(m, \frac{m\,\Theta_2}{\mu\, l_{RD}}(I_{X_D} + I_{Y_D})\right)}{\Gamma(m)}\right)\right] \\ &= \mathbb{E}_{I_X, I_Y}\left[\frac{\Gamma\left(m, \frac{m\,\Theta_2}{\mu\, l_{SR}}(I_{X_R} + I_{Y_R})\right)}{\Gamma(m)}\right] \\ &\quad - \mathbb{E}_{I_X, I_Y}\left[\frac{\Gamma\left(m, \frac{m\,\Theta_2}{\mu\, l_{SR}}(I_{X_R} + I_{Y_R})\right)}{\Gamma(m)} \times \frac{\Gamma\left(m, \frac{m\,\Theta_2}{\mu\, l_{RD}}(I_{X_D} + I_{Y_D})\right)}{\Gamma(m)}\right]. \end{aligned} \tag{A.31}$$

The first expectation in (A.31) is calculated following the same steps as in A.6. The second expectation in (A.31) is calculated following the same steps as in A.7 .

A.9. PROOF OF PROPOSITION 1

In order to calculate the Laplace transform of interference originated from the X road at T, we have to calculate the integral in (1.46). We calculate the integral in (1.46) for $\mathcal{B} = \mathbb{R}$ and $\alpha = 2$. Let us take $k = sP/A^2$, $t_x = n\cos(\theta_T)$ and $t_y = t\sin(\theta_T)$, then (1.46) becomes

$$\mathcal{L}_{I_{X_T}}(s) = \exp\left(- p\lambda_X k \int_{\mathbb{R}} \frac{1}{k + t_y^2 + (x - t_x)^2} dx \right), \tag{A.32}$$

and the integral inside the exponential in (A.32) equals

$$\int_{\mathbb{R}} \frac{1}{k + t_y^2 + (x - t_x)^2} dx = \frac{\pi}{\sqrt{t_y^2 + k}}. \tag{A.33}$$

Then, plugging (A.33) into (A.32) we obtain

$$\mathcal{L}_{I_{X_T}}(s) = \exp\left(- p\lambda_X k \frac{\pi}{\sqrt{t_y^2 + k}} \right). \tag{A.34}$$

Finally, substituting k and t_y in (A.34) yields (1.50). Following the same steps above, and without details for the derivation, we obtain (1.51).

To calculate $\mathcal{L}_{I_{X_T}}(s)$ for $\alpha = 4$. we get

$$\mathcal{L}_{I_{X_T}}(s) = \exp\left(- p\lambda_X \int_{\mathbb{R}} \frac{1}{1 + \left(\sqrt{t_y^2 + (x - t_x)^2}\right)^4 / s} \mathrm{d}x \right) \tag{A.35}$$

$$= \exp\left(- p\lambda_X s \int_{\mathbb{R}} \frac{1}{s + \left(\sqrt{t_y^2 + (x - t_x)^2}\right)^4} \mathrm{d}x \right), \tag{A.36}$$

and the integral inside the exponential in (A.35) equals

$$\int_{\mathbb{R}} \frac{1}{s + \left(\sqrt{t_y^2 + (x - t_x)^2}\right)^4} \mathrm{d}x = \frac{\sqrt{2\sqrt{{t_y}^4 + s} + 2{t_y}^2}\left(\sqrt{{t_y}^4 + s} - {t_y}^2\right)}{2\sqrt{{t_y}^4 + s}}. \tag{A.37}$$

Then, plugging (A.37) into (A.35), and substituting t_y by $t\sin(\theta_T)$ yields (1.58). Following the same steps, we obtain (1.59).

A.10. PROOF OF PROPOSITION 2

We calculate the integral in (1.46) for $\mathcal{B} = [-Z, Z]$ and $\alpha = 2$. We use the same change of variables as in **Proposition 1**, then we get

$$\begin{aligned}\int_{-Z}^{+Z} \frac{1}{1+(A\|x-T\|^2)/sP}dx &= \int_{-Z}^{+Z} \frac{1}{1+t_y^2+(x-t_x)^2/k}dx \\ &= \int_{-Z}^{+Z} 1-\frac{t_y^2+(x-t_x)^2/k}{1+t_y^2+(x-t_x)^2/k}dx \\ &= 2Z-\int_{-Z}^{+Z} \frac{t_y^2+(x-t_x)^2}{k+t_y^2+(x-t_x)^2}dx. \end{aligned} \tag{A.38}$$

The integral in the last equality in (A.38) equals

$$\begin{aligned}\int_{-Z}^{+Z} \frac{t_y^2+(x-t_x)^2}{k+t_y^2+(x-t_x)^2}dx &= \frac{2Z\sqrt{t_y^2+k}}{\sqrt{t_y^2+k}} \\ &\quad -\frac{k\arctan\left(\frac{Z+t_x}{\sqrt{t_y^2+k}}\right)-k\arctan\left(\frac{Z-t_x}{\sqrt{t_y^2+k}}\right)}{\sqrt{t_y^2+k}}. \end{aligned} \tag{A.39}$$

Then plugging (A.39) into (A.38) yields (1.52). Following the same steps above, we obtain (1.53).

Appendix B.

Appendix to chapter 2

B.1. NOMA Outage probability of D_1 and D_2 using direct transmission

In order to calculate $\mathbb{P}(O_{D_1})$, it is more convenient to express it as a function of a success probability $\mathbb{P}(O_{D_1}^C)$. Then $\mathbb{P}(O_{D_1})$ is expressed as

$$\mathbb{P}(O_{D_1}) = 1 - \mathbb{P}(O_{D_1}^C). \tag{B.1}$$

We calculate $\mathbb{P}(O_{D_1}^C)$ as follows

$$\begin{aligned}
\mathbb{P}(O_{D_1}^C) &= \mathbb{P}(\mathrm{SIR}_{D_1} \geq \Theta_1) \\
&= \mathbb{E}_{I_X, I_Y}\left[\mathbb{P}\left\{\frac{|h_{SD_1}|^2 l_{SD_1} a_1}{|h_{SD_1}|^2 l_{SD_1} a_2 + I_{X_{D_1}} + I_{Y_{D_1}}} \geq \Theta_1\right\}\right] \qquad \text{(B.2)} \\
&= \mathbb{E}_{I_X, I_Y}\left[\mathbb{P}\left\{|h_{SD_1}|^2 l_{SD_1}(a_1 - \Theta_1 a_2) \geq \Theta_1\left[I_{X_{D_1}} + I_{Y_{D_1}}\right]\right\}\right]. \qquad \text{(B.3)}
\end{aligned}$$

We can see from (B.2) that, when $\Theta_1 \geq a_1/a_2$, the success probability $\mathbb{P}(O_{D_1}^C)$ is always zero, that is, $\mathbb{P}(O_{D_1}) = 1$. Then, when $\Theta_1 < a_1/a_2$, and after setting $G_1 = \Theta_1/(a_1 - \Theta_1 a_2)$,

we obtain

$$\mathbb{P}(O_{D_1}^C) = \mathbb{E}_{I_X,I_Y}\left[\mathbb{P}\left\{|h_{SD_1}|^2 \geq \frac{G_1}{l_{SD_1}}[I_{X_{D_1}} + I_{Y_{D_1}}]\right\}\right].$$

Since $|h_{SD_1}|^2$ follows an exponential distribution with unit mean, and using the independence of the PPP on the X road and Y road, we get

$$\mathbb{P}(O_{D_1}^C) = \mathbb{E}_{I_X}\left[\exp\left(-\frac{G_1}{l_{SD_1}}I_{X_{D_1}}\right)\right]\mathbb{E}_{I_Y}\left[\exp\left(-\frac{G_1}{l_{SD_1}}I_{Y_{D_1}}\right)\right].$$

Given that $\mathbb{E}[e^{sI}] = \mathcal{L}_I(s)$, we finally get

$$\mathbb{P}(O_{D_1}^C) = \mathcal{L}_{I_{X_{D_1}}}\left(\frac{G_1}{l_{SD_1}}\right)\mathcal{L}_{I_{Y_{D_1}}}\left(\frac{G_1}{l_{SD_1}}\right). \tag{B.4}$$

Plugging (B.4) into (B.1) yields (3.66).

In the same way, we express $\mathbb{P}(O_{D_2})$ as a function of a success probability $\mathbb{P}(O_{D_2}^C)$, that is

$$\mathbb{P}(O_{D_2}) = 1 - \mathbb{P}(O_{D_2}^C). \tag{B.5}$$

The probability $\mathbb{P}(O_{D_2}^C)$ is expressed as

$$\mathbb{P}(O_{D_2}^C) = \mathbb{P}(\{O_{D_{2-1}} \cup O_{D_2}\}^C) = \mathbb{P}(O_{D_{2-1}}^C \cap O_{D_2}^C). \tag{B.6}$$

Following the same steps as for $\mathbb{P}(O_{D_1}^C)$, we obtain

$$\mathbb{P}(O_{D_2}^C) = \mathbb{E}_{I_X,I_Y}\left[\mathbb{P}\left\{\frac{|h_{SD_2}|^2 l_{SD_2} a_1}{|h_{SD_2}|^2 l_{SD_2} a_2 + I_{X_{D_2}} + I_{Y_{D_2}}} \geq \Theta_1 \right.\right.$$
$$\left.\left. \bigcap \frac{|h_{SD_2}|^2 l_{SD_2} a_2}{\beta|h_{SD_2}|^2 l_{SD_2} a_1 + I_{X_{D_2}} + I_{Y_{D_2}}} \geq \Theta_2 \right\}\right].$$

When $\Theta_1 > a_1/a_2$, then $\mathbb{P}(O_{D_2}) = 1$, otherwise we continue the derivation. We set $\Theta_2 = 2^{\mathcal{R}_2} - 1$ and $G_2 = \Theta_2/(a_2 - \Theta_2\beta a_1)$, then

$$\mathbb{P}(O_{D_2}^C) = \mathbb{E}_{I_X,I_Y}\left[\mathbb{P}\left\{|h_{SD_2}|^2 \geq \frac{G_1}{l_{SD_2}}[I_{X_{D_2}} + I_{Y_{D_2}}] \bigcap |h_{SD_2}|^2 \geq \frac{G_2}{l_{SD_2}}[I_{X_{D_2}} + I_{Y_{D_2}}]\right\}\right]. \tag{B.7}$$

Finally, $\mathbb{P}(O_{D_2}^C)$ equals

$$\mathbb{P}(O_{D_2}^C) = \mathcal{L}_{I_{X_{D_2}}}\left(\frac{G_{\max}}{l_{SD_2}}\right)\mathcal{L}_{I_{Y_{D_2}}}\left(\frac{G_{\max}}{l_{SD_2}}\right), \tag{B.8}$$

where $G_{\max} = \max(G_1, G_2)$. Plugging (B.8) into (B.5) yields (3.67).

B.2. NOMA Outage probability of D_1 and D_2 using cooperative transmission

To calculate $\mathbb{P}(O_{(1)})$, we proceed as follows

$$\begin{aligned}
\mathbb{P}(O_{(1)}) &= 1 - \mathbb{P}(O_{(1)}^C) \\
&= 1 - \mathbb{P}\left(\{\mathrm{SIR}_{R_1} < \Theta_1 \cup \mathrm{SIR}_{D_{1\to1}} < \Theta_1\}^C\right) \\
&= 1 - \mathbb{P}\left(\mathrm{SIR}_{R_1} \geq \Theta_1 \cap \mathrm{SIR}_{D_{1\to1}} \geq \Theta_1\right) \\
&= 1 - \mathbb{P}\left(\mathrm{SIR}_{R_1} \geq \Theta_1\right) \times \mathbb{P}\left(\mathrm{SIR}_{D_1} \geq \Theta_1\right).
\end{aligned} \tag{B.9}$$

We calculate the probability $\mathbb{P}(\text{SIR}_{R_1} \geq \Theta_1)$ as

$$\begin{aligned}\mathbb{P}(\text{SIR}_{R_1} \geq \Theta_1) &= \mathbb{E}_{I_X,I_Y}\left[\mathbb{P}\left\{ \frac{|h_{SR}|^2 l_{SR} a_1}{|h_{SR}|^2 l_{SR} a_2 + I_{X_R} + I_{Y_R}} \geq \Theta_1 \right\}\right] \\ &= \mathbb{E}_{I_X,I_Y}\left[\mathbb{P}\left\{ |h_{SR}|^2 l_{SR}(a_1 - \Theta_1 a_2) \geq \Theta_1 \left[I_{X_R} + I_{Y_R}\right] \right\}\right].\end{aligned} \tag{B.10}$$

We can notice from (B.10) that, when $\Theta_1 \geq a_1/a_2$, the probability $\mathbb{P}(\text{SIR}_{R_1} > \Theta_1)$ is always zero, that is, $\mathbb{P}(\text{SIR}_{R_1} < \Theta_1) = 1$. Then, when $\Theta_1 < a_1/a_2$, and after setting $G_1 = \Theta_1/(a_1 - \Theta_1 a_2)$, the expression becomes

$$\mathbb{P}(\text{SIR}_{R_1} \geq \Theta_1) = \mathbb{E}_{I_X,I_Y}\left[\mathbb{P}\left\{ |h_{SR}|^2 \geq \frac{G_1}{l_{SR}} \left[I_{X_R} + I_{Y_R}\right] \right\}\right].$$

Since $|h_{SR}|^2$ follows an exponential distribution with unit mean, and using the independence of the PPP on the roads X and Y, we get

$$\mathbb{P}(\text{SIR}_{R_1} \geq \Theta_1) = \mathbb{E}_{I_X}\left[\exp\left(-\frac{G_1}{l_{SR}} I_{X_R}\right)\right] \mathbb{E}_{I_Y}\left[\exp\left(-\frac{G_1}{l_{SR}} I_{Y_R}\right)\right].$$

Given that $\mathbb{E}[e^{sI}] = \mathcal{L}_I(s)$, we finally get

$$\mathbb{P}(\text{SIR}_{R_1} \geq \Theta_1) = \mathcal{L}_{I_{X_R}}\left(\frac{G_1}{l_{SR}}\right) \mathcal{L}_{I_{Y_R}}\left(\frac{G_1}{l_{SR}}\right). \tag{B.11}$$

The probability $\mathbb{P}(\text{SIR}_{D_1} \geq \Theta_1)$ can be calculated following the same as for $\mathbb{P}(\text{SIR}_{R_1} \geq \Theta_1)$. In the same way we express $\mathbb{P}(O_{(2)})$ as

$$\mathbb{P}(O_{(2)}) = 1 - \mathbb{P}(O_{(2)}^C), \tag{B.12}$$

where $\mathbb{P}(O_{(2)}^C)$is given by

$$\begin{aligned}\mathbb{P}(O_{(2)}^C) &= \mathbb{P}(O_{R_2}^C \cap O_{D_2}^C) \\ &= \mathbb{P}(O_{R_2}^C)\mathbb{P}(O_{D_2}^C). \end{aligned} \tag{B.13}$$

The probability $\mathbb{P}(O_{D_2}^C)$ is expressed as

$$\mathbb{P}(O_{D_2}^C) = \mathbb{P}(\mathrm{SIR}_{D_{2-1}} \geq \Theta_1 \cap \mathrm{SIR}_{D_2} \geq \Theta_2). \tag{B.14}$$

Following the same steps as for $\mathbb{P}(O_{D_1}^C)$, we get

$$\mathbb{P}(O_{D_2}^C) = \mathbb{E}_{I_X,I_Y}\left[\mathbb{P}\left\{\frac{|h_{RD_2}|^2 l_{RD_2} a_1}{|h_{RD_2}|^2 l_{RD_2} a_2 + I_{X_{D_2}} + I_{Y_{D_2}}} \geq \Theta_1 \right.\right. \\ \left.\left. \bigcap \frac{|h_{RD_2}|^2 l_{RD_2} a_2}{\beta |h_{RD_2}|^2 l_{RD_2} a_1 + I_{X_{D_2}} + I_{Y_{D_2}}} \geq \Theta_2 \right\}\right].$$

When $\Theta_1 > a_1/a_2$ or $\Theta_2 > a_2/\beta a_1$, then $\mathbb{P}(O_{D_2}) = 1$, otherwise we continue the derivation We set $G_2 = \Theta_2/(a_2 - \Theta_2 \beta a_1)$, then expression becomes

$$\mathbb{P}(O_{D_2}^C) = \mathbb{E}_{I_X,I_Y}\left[\mathbb{P}\left\{|h_{RD_2}|^2 \geq \frac{G_1}{l_{RD_2}}[I_{X_{D_2}} + I_{Y_{D_2}}] \right.\right. \\ \left.\left. \bigcap |h_{RD_2}|^2 \geq \frac{G_2}{l_{RD_2}}[I_{X_{D_2}} + I_{Y_{D_2}}] \right\}\right].$$

Finally, $\mathbb{P}(O_{D_2}^C)$ equals

$$\mathbb{P}(O_{D_2}^C) = \mathcal{L}_{I_{X_{D_2}}}\left(\frac{G_{\max}}{l_{RD_2}}\right)\mathcal{L}_{I_{Y_{D_2}}}\left(\frac{G_{\max}}{l_{RD_2}}\right), \tag{B.15}$$

where $G_{\max} = \max(G_1, G_2)$.

The probability $\mathbb{P}(O_{R_2}^C)$ can be calculated following the same steps above.

B.3. NOMA average achievable rate of D_1 using direct transmission

To compute $\mathcal{T}_{D_1}$, we proceed as follows

$$\begin{aligned}\mathcal{T}_{D_1} &= \mathbb{E}_{I_X,I_Y}\left[\log_2\left(1+\mathrm{SIR}_{D_1}\right)\right]\\ &\overset{(a)}{=} \int_{v>0}\mathbb{E}_{I_X,I_Y}\left[\mathbb{P}\left\{\log_2\left(1+\mathrm{SIR}_{D_1}\right)>v\right\}\right]\mathrm{d}v\\ &\overset{(b)}{=} \int_{v=0}^{\log_2(1+\frac{a_1}{a_2})}\mathbb{E}_{I_X,I_Y}\left[\mathbb{P}\left\{\mathrm{SIR}_{D_1}>2^v-1\right\}\right]\mathrm{d}v,\end{aligned} \tag{B.16}$$

where (a) follows from $\mathbb{E}[\mathcal{X}]=\int_{v>0}\mathbb{P}(\mathcal{X}>v)\mathrm{d}v$ when the random variable $\mathcal{X}$ is positive, and (b) follows from $\lim_{(I_{X_{D_1}},I_{Y_{D_1}})\to(0,0)}\log_2\left(1+\mathrm{SIR}_{D_1}\right)=\log_2(1+\frac{a_1}{a_2})$. Then following the same steps as in B.1, we obtain (2.44).

B.4. NOMA average achievable rate of D_1 using cooperative transmission

The expression of $\mathcal{T}_{D_1}$ is given by

$$\begin{aligned}\mathcal{T}_{D_1} &= \mathbb{E}\left[\min\left\{\frac{1}{2}\log_2(1+\mathrm{SIR}_{R_1}),\frac{1}{2}\log_2(1+\mathrm{SIR}_{D_{1\to1}})\right\}\right]\\ &= \mathbb{E}\left[\frac{1}{2}\log_2\left(1+\min\left\{\mathrm{SIR}_{R_1},\mathrm{SIR}_{D_{1\to1}}\right\}\right)\right].\end{aligned}$$

Then computing the expectation with respect to the interference distribution yields

$$\begin{aligned}
\mathcal{T}_{D_1} &= \int_{z_1>0}\int_{z_2>0} \mathbb{E}\left[\frac{1}{2}\log_2\left(1+\min\left\{\mathrm{SIR}_{R_1},\mathrm{SIR}_{D_{1\to 1}}\right\}\right)\right] f_{I_X}(z_1) f_{I_Y}(z_2)\mathrm{d}z_1\mathrm{d}z_2 \\
&= \mathbb{E}_{I_X,I_Y}\left[\frac{1}{2}\log_2\left(1+\min\left\{\frac{|h_{SR}|^2 l_{SR}\, a_1}{|h_{SR}|^2 l_{SR} a_2 + I_{X_R} + I_{Y_R}},\right.\right.\right. \\
&\qquad\qquad \left.\left.\left.\frac{|h_{RD_1}|^2 l_{RD_1}\, a_1}{|h_{RD_1}|^2 l_{RD_1} a_2 + I_{X_{D_1}} + I_{Y_{D_1}}}\right\}\right)\right] \\
&\overset{(a)}{=} \int_{v>0} \mathbb{P}\left[\frac{1}{2}\log_2\left(1+\min\left\{\frac{|h_{SR}|^2 l_{SR}\, a_1}{|h_{SR}|^2 l_{SR} a_2 + I_{X_R} + I_{Y_R}},\right.\right.\right. \\
&\qquad\qquad \left.\left.\left.\frac{|h_{RD_1}|^2 l_{RD_1}\, a_1}{|h_{RD_1}|^2 l_{RD_1} a_2 + I_{X_{D_1}} + I_{Y_{D_1}}}\right\}\right) > v\right]\mathrm{d}v \\
&\overset{(b)}{=} \int_{v=0}^{\frac{1}{2}\log_2(1+\frac{a_1}{a_2})} \mathbb{P}\left[\min\left\{\frac{|h_{SR}|^2 l_{SR}\, a_1}{|h_{SR}|^2 l_{SR} a_2 + I_{X_R} + I_{Y_R}},\right.\right. \\
&\qquad\qquad \left.\left.\frac{|h_{RD_1}|^2 l_{RD_1}\, a_1}{|h_{RD_1}|^2 l_{RD_1} a_2 + I_{X_{D_1}} + I_{Y_{D_1}}}\right\} > 2^{2v}-1\right]\mathrm{d}v \\
&\overset{(c)}{=} \int_{v=0}^{\frac{1}{2}\log_2(1+\frac{a_1}{a_2})} \mathbb{P}\left[\frac{|h_{SR}|^2 l_{SR}\, a_1}{|h_{SR}|^2 l_{SR} a_2 + I_{X_R} + I_{Y_R}} > 2^{2v}-1\right. \\
&\qquad\qquad \left.\bigcap \frac{|h_{RD_1}|^2 l_{RD_1}\, a_1}{|h_{RD_1}|^2 l_{RD_1} a_2 + I_{X_{D_1}} + I_{Y_{D_1}}} > 2^{2v}-1\right]\mathrm{d}v \\
&= \int_{v=0}^{\frac{1}{2}\log_2(1+\frac{a_1}{a_2})} \mathbb{P}\left[\frac{|h_{SR}|^2 l_{SR}\, a_1}{|h_{SR}|^2 l_{SR} a_2 + I_{X_R} + I_{Y_R}} > 2^{2v}-1\right] \\
&\qquad\qquad \times \mathbb{P}\left[\frac{|h_{RD_1}|^2 l_{RD_1}\, a_1}{|h_{RD_1}|^2 l_{RD_1} a_2 + I_{X_{D_1}} + I_{Y_{D_1}}} > 2^{2v}-1\right]\mathrm{d}v, \qquad \text{(B.17)}
\end{aligned}$$

where (a) follows from $\mathbb{E}[\mathcal{X}] = \int_{v>0}\mathbb{P}(\mathcal{X}>v)\mathrm{d}v$ when the random variable $\mathcal{X}$ is positive, (b) follows from $\lim_{(I_X,I_Y)\to(0,0)} \frac{1}{2}\log_2(1+\min\{\mathrm{SIR}_{R_1},\mathrm{SIR}_{D_{1\to 1}}\}) = \frac{1}{2}\log_2(1+\frac{a_1}{a_2})$, and (c) follows from $\mathbb{P}(\min\{a,b\}>c) = \mathbb{P}(a>c \cap b>c)$. To calculate the probability in (B.17), we proceed as in B.2 and we obtain (2.52). Following the same steps above, we obtain (2.53).

B.5. NOMA outage probability using MRC

The outage probability related to D_1, denoted $\mathbb{P}(O_{(1)})$, is expressed as

$$\mathbb{P}(O_{(1)}) = \mathbb{P}\Big(\mathcal{B}_{D_1} \cap \mathcal{A}_{D_1}\Big) + \mathbb{P}\Big(\mathcal{A}_{D_1}^{C} \cap \mathcal{C}_{D_1}\Big). \tag{B.18}$$

First, we calculate the probability $\mathbb{P}\Big(\mathcal{A}_{R_1}^{C} \cap \mathcal{C}_{D_1}\Big)$ as follows

$$\begin{aligned}
\mathbb{P}\Big(\mathcal{A}_{R_1}^{C} \cap \mathcal{C}_{D_1}\Big) &= \mathbb{E}_{I_X,I_Y}\Bigg[\mathbb{P}\Bigg\{ \frac{P|h_{SR}|^2 l_{SR} a_1}{P|h_{SR}|^2 l_{SR} a_2 + I_{X_R} + I_{Y_R} + \sigma^2} \geq \Theta_1 \bigcap \\
&\qquad \frac{P\left(|h_{SD_1}|^2 l_{SD_1} + |h_{RD_1}|^2 l_{RD_1}\right) a_1}{P\left(|h_{SD_1}|^2 l_{SD_1} + |h_{RD_1}|^2 l_{RD_1}\right) a_2 + I_{X_{D_1}} + I_{Y_{D_1}} + \sigma^2} < \Theta_1 \Bigg\}\Bigg] \\
&= \mathbb{E}_{I_X,I_Y}\Bigg[\mathbb{P}\Bigg\{ P|h_{SR}|^2 l_{SR}(a_1 - \Theta_1 a_2) \geq \Theta_1\left[I_{X_R} + I_{Y_R} + \sigma^2\right] \bigcap \\
&\qquad P\left(|h_{SD_1}|^2 l_{SD_1} + |h_{RD_1}|^2 l_{RD_1}\right)(a_1 - \Theta_1 a_2) < \Theta_1\left[I_{X_{D_1}} + I_{Y_{D_1}} + \sigma^2\right] \Bigg\}\Bigg].
\end{aligned} \tag{B.19}$$

When $\Theta_1 < a_1/a_2$, and after setting $G_1 = \Theta_1/(a_1 - \Theta_1 a_2)$, then

$$\begin{aligned}
\mathbb{P}\Big(\mathcal{A}_{R_1}^{C} \cap \mathcal{C}_{D_1}\Big) &= \mathbb{E}_{I_X,I_Y}\Bigg[\mathbb{P}\Bigg\{ |h_{SR}|^2 \geq \frac{G_1}{l_{SR}}\left[I_{X_R} + I_{Y_R} + \sigma^2/P\right] \bigcap \\
&\qquad \left(|h_{SD_1}|^2 l_{SD_1} + |h_{RD_1}|^2 l_{RD_1}\right) < G_1\left[I_{X_{D_1}} + I_{Y_{D_1}} + \sigma^2/P\right] \Bigg\}\Bigg].
\end{aligned} \tag{B.20}$$

Since $|h_{SR}|^2$ follows an exponential distribution with unit mean, we get

$$\begin{aligned}
\mathbb{P}\Big(\mathcal{A}_{R_1}^{C} \cap \mathcal{C}_{D_1}\Big) = \mathbb{E}_{I_X,I_Y}\Bigg[\mathbb{P}\Bigg\{ &\exp\left(\frac{G_1}{l_{SR}}\left[I_{X_R} + I_{Y_R} + \sigma^2/P\right]\right)\Bigg\} \\
&\times 1 - \Bigg\{\mathbb{P}\left(|h_{SD_1}|^2 l_{SD_1} + |h_{RD_1}|^2 l_{RD_1}\right) \geq G_1\left[I_{X_{D_1}} + I_{Y_{D_1}} + \sigma^2/P\right]\Bigg\}\Bigg].
\end{aligned} \tag{B.21}$$

We write the second probability in (B.21) as

$$\mathbb{P}(\delta \geq G_1[I_{X_{D_1}} + I_{Y_{D_1}} + \sigma^2/P]),$$

where $\delta = |h_{RD_1}|^2 l_{RD_1} + |h_{SD_1}|^2 l_{SD_1}$.

The complementary cumulative distribution function of the random variable δ, denoted $\bar{F}_\delta(.)$, is given by

$$\bar{F}_\delta(u) = \frac{l_{RD_1} e^{-u/l_{RD_1}} - l_{SD_1} e^{-u/l_{SD_1}}}{l_{RD_1} - l_{SD_1}}.$$

Then, we have

$$\mathbb{P}\big[|h_{SD_1}|^2 l_{SD_1} + |h_{RD_1}|^2 l_{RD_1} \geq G_1(I_{X_{D_1}} + I_{Y_{D_1}} + \sigma^2/P)\big] = \frac{l_{RD_1} \exp\Big[-\frac{G_1}{l_{RD_1}}(I_{X_{D_1}} + I_{Y_{D_1}} + \sigma^2/P)\Big] - l_{SD_1} \exp\Big(-\frac{G_1}{l_{SD_1}}[I_{X_{D_1}} + I_{Y_{D_1}} + \sigma^2/P)\Big]}{l_{RD_1} - l_{SD_1}}. \tag{B.22}$$

Plugging (B.22) into (B.21) yields

$$\begin{aligned}
\mathbb{P}\Big(\mathcal{A}_{R_1}^C \cap \mathcal{C}_{D_1}\Big) &= \mathbb{E}_{I_X,I_Y}\Bigg[\exp\left(\frac{G_1}{l_{SR}}[I_{X_R}+I_{Y_R}+\sigma^2/P]\right) \\
&\quad \times\Bigg\{1-\frac{l_{RD_1}\exp\Big(-\frac{G_1}{l_{RD_1}}(I_{X_{D_1}}+I_{Y_{D_1}}+\sigma^2/P)\Big)}{l_{RD_1}-l_{SD_1}} \\
&\quad -\frac{l_{SD_1}\exp\Big(-\frac{G_1}{l_{SD_1}}[I_{X_{D_1}}+I_{Y_{D_1}}+\sigma^2/P]\Big)}{l_{RD_1}-l_{SD_1}}\Bigg\}\Bigg] \\
&= \mathbb{E}_{I_X,I_Y}\Bigg[\exp\left(\frac{G_1}{l_{SR}}[I_{X_R}+I_{Y_R}+\sigma^2/P]\right)-\exp\left(\frac{G_1}{l_{SR}}[I_{X_R}+I_{Y_R}+\sigma^2/P]\right) \\
&\quad \times\frac{l_{RD_1}\exp\Big(-\frac{G_1}{l_{RD_1}}[I_{X_{D_1}}+I_{Y_{D_1}}+\sigma^2/P]\Big)}{l_{RD_1}-l_{SD_1}} \\
&\quad -\frac{l_{SD_1}\exp\Big(-\frac{G_1}{l_{SD_1}}[I_{X_{D_1}}+I_{Y_{D_1}}+\sigma^2/P]\Big)}{l_{RD_1}-l_{SD_1}})\Bigg].
\end{aligned}$$

Given that $\mathbb{E}[e^{sI}]=\mathcal{L}_I(s)$, we finally get

$$\begin{aligned}
\mathbb{P}\Big(\mathcal{A}_{R_1}^C \cap \mathcal{C}_{D_1}\Big) =& \mathcal{L}_{I_{X_R}}\left(\frac{G_1}{l_{SR}}\right)\mathcal{L}_{I_{Y_R}}\left(\frac{G_1}{l_{SR}}\right)\exp\left(-\frac{\sigma^2 G_1}{P l_{SR}}\right) \\
&-\mathcal{L}_{I_{X_R}}\left(\frac{G_1}{l_{SR}}\right)\mathcal{L}_{I_{Y_R}}\left(\frac{G_1}{l_{SR}}\right)\exp\left(-\frac{\sigma^2 G_1}{P l_{SR}}\right) \\
&\frac{l_{RD_1}\mathcal{L}_{I_{X_{D_1}}}\left(\frac{G_1}{l_{RD_1}}\right)\mathcal{L}_{I_{Y_{D_1}}}\left(\frac{G_1}{l_{RD_1}}\right)\exp\left(-\frac{\sigma^2 G_1}{P l_{RD_1}}\right)}{l_{RD_1}-l_{SD_1}} \\
&-\frac{l_{SD_1}\mathcal{L}_{I_{X_{D_1}}}\left(\frac{G_1}{l_{SD_1}}\right)\mathcal{L}_{I_{Y_{D_1}}}\left(\frac{G_1}{l_{SD_1}}\right)\exp\left(-\frac{\sigma^2 G_1}{P l_{SD_1}}\right)}{l_{RD_1}-l_{SD_1}}.
\end{aligned} \tag{B.23}$$

The probability $\mathbb{P}\Big(\mathcal{B}_{D_1} \cap \mathcal{A}_{D_1}\Big)$ can be expressed as

$$\begin{aligned}\mathbb{P}\Big(\mathcal{B}_{D_1} \cap \mathcal{A}_{D_1}\Big) &= 1 - \mathbb{P}\Big(\mathcal{B}^C_{D_1} \cup \mathcal{A}^C_{D_1}\Big) \\ &= 1 - \mathbb{P}\Big(\mathcal{B}^C_{D_1}\Big) - \mathbb{P}\Big(\mathcal{A}^C_{D_1}\Big) + \mathbb{P}\Big(\mathcal{B}^C_{D_1} \cap \mathcal{A}^C_{D_1}\Big). \end{aligned} \tag{B.24}$$

The probabilities in (B.24) can be calculated following the same steps above.

In the same way, we calculate $\mathbb{P}(O_{(2)})$ as

$$\begin{aligned}\mathbb{P}(O_{(2)}) &= \mathbb{P}\left[\left\{\bigcup_{i=1}^{2} \mathcal{B}_{D_{2-i}}(\Theta_i)\right\} \cap \left\{\bigcup_{i=1}^{2} \mathcal{A}_{R_i}(\Theta_i)\right\}\right] \\ &\quad + \mathbb{P}\left[\left\{\bigcap_{i=1}^{2} \mathcal{A}^C_{R_i}(\Theta_i)\right\} \cap \left\{\bigcup_{i=1}^{2} \mathcal{C}_{D_{2-i}}(\Theta_i)\right\}\right]. \end{aligned} \tag{B.25}$$

To calculate the first probability in (B.25), we proceed as follows

$$\begin{aligned}\mathbb{P}\left[\left\{\bigcup_{i=1}^{2} \mathcal{B}_{D_{2-i}}(\Theta_i)\right\} \cap \left\{\bigcup_{i=1}^{2} \mathcal{A}_{R_i}(\Theta_i)\right\}\right] &= 1 - \mathbb{P}\left[\left\{\bigcap_{i=1}^{2} \mathcal{B}^C_{D_{2-i}}(\Theta_i)\right\} \cup \left\{\bigcap_{i=1}^{2} \mathcal{A}^C_{R_i}(\Theta_i)\right\}\right] \\ &= 1 - \mathbb{P}\left[\bigcap_{i=1}^{2} \mathcal{B}^C_{D_{2-i}}(\Theta_i)\right] - \mathbb{P}\left[\bigcap_{i=1}^{2} \mathcal{A}^C_{R_i}(\Theta_i)\right] \\ &\quad + \mathbb{P}\left[\left\{\bigcap_{i=1}^{2} \mathcal{B}^C_{D_{2-i}}(\Theta_i)\right\} \cap \left\{\bigcap_{i=1}^{2} \mathcal{A}^C_{R_i}(\Theta_i)\right\}\right]. \end{aligned} \tag{B.26}$$

The first two probabilities in (B.26) can be calculated in a straightforward manner as above.

The last probability in (B.26), that we denote by $\mathcal{P}_1$, is expressed as

$$\begin{aligned}\mathcal{P}_1 =&\mathbb{E}_{I_X,I_Y}\Bigg[\mathbb{P}\Bigg\{\frac{P|h_{SD_2}|^2 l_{SD_2}a_1}{P|h_{SD_2}|^2 l_{SD_2}a_2 + I_{X_{D_2}} + I_{Y_{D_2}} + \sigma^2} \geq \Theta_1 \\ &\bigcap \frac{P|h_{SD_2}|^2 l_{SD_2}a_2}{\beta P|h_{SD_2}|^2 l_{SD_2}a_1 + I_{X_{D_2}} + I_{Y_{D_2}} + \sigma^2} \geq \Theta_2 \\ &\bigcap \frac{P|h_{SR}|^2 l_{SR}a_1}{P|h_{SR}|^2 l_{SR}a_2 + I_{X_R} + I_{Y_R} + \sigma^2} \geq \Theta_1 \\ &\bigcap \frac{P|h_{SR}|^2 l_{SR}a_2}{\beta P|h_{SR}|^2 l_{SR}a_1 + I_{X_R} + I_{Y_R} + \sigma^2} \geq \Theta_2\Bigg\}\Bigg].\end{aligned}$$

When $\Theta_1 < a_1/a_2$ and $\Theta_2 < a_2/\beta a_1$,we get

$$\begin{aligned}\mathcal{P}_1 =&\mathbb{E}_{I_X,I_Y}\Bigg[\mathbb{P}\Bigg\{|h_{SD_2}|^2 \geq \frac{G_1}{l_{SD_2}}[I_{X_{D_2}} + I_{Y_{D_2}} + \sigma^2/P] \\ &\bigcap |h_{SD_2}|^2 \geq \frac{G_2}{l_{SD_2}}[I_{X_{D_2}} + I_{Y_{D_2}} + \sigma^2/P] \\ &\bigcap |h_{SR}|^2 \geq \frac{G_1}{l_{SR}}[I_{X_R} + I_{Y_R} + \sigma^2/P] \\ &\bigcap |h_{SR}|^2 \geq \frac{G_2}{l_{SR}}[I_{X_R} + I_{Y_R} + \sigma^2/P]\Bigg\}\Bigg]. \\ =&\mathbb{E}_{I_X,I_Y}\Bigg[\mathbb{P}\Bigg\{|h_{SD_2}|^2 \geq \frac{\max(G_1,G_2)}{l_{SD_2}}[I_{X_{D_2}} + I_{Y_{D_2}} + \sigma^2/P] \\ &\bigcap |h_{SR}|^2 \geq \frac{\max(G_1,G_2)}{l_{SR}}[I_{X_R} + I_{Y_R} + \sigma^2/P]\Bigg\}\Bigg].\end{aligned} \tag{B.27}$$

Finally, we obtain

$$\begin{aligned}\mathbb{P}\left[\left\{\bigcap_{i=1}^{2}\mathcal{B}^C_{D_{2-i}}(\Theta_i)\right\}\cap\left\{\bigcap_{i=1}^{2}\mathcal{A}^C_{R_i}(\Theta_i)\right\}\right] =& \mathcal{L}_{I_{X_{D_2}}}\left(\frac{G_{\max}}{l_{SD_2}}\right)\mathcal{L}_{I_{Y_{D_2}}}\left(\frac{G_{\max}}{l_{SD_2}}\right)\exp\left(-\frac{\sigma^2 G_{\max}}{P l_{SD_2}}\right) \\ &\times \mathcal{L}_{I_{X_R}}\left(\frac{G_{\max}}{l_{SR}}\right)\mathcal{L}_{I_{Y_R}}\left(\frac{G_{\max}}{l_{SR}}\right)\exp\left(-\frac{\sigma^2 G_{\max}}{P l_{SR}}\right),\end{aligned}$$

where $G_{\max} = \max(G_1, G_2)$.

The second probability in (B.25) can be calculated following the same steps above.

Appendix C.

Appendix to chapter 3

C.1. Outage probability of ACN protocol

The probability $\mathbb{P}[\mathcal{O}_{\mathrm{ACN}}(D_1)]$ is expressed as

$$\mathbb{P}[\mathcal{O}_{\mathrm{ACN}}(D_1)] = 1 - \mathbb{P}[\mathcal{O}^C_{\mathrm{ACN}}(D_1)]. \tag{C.1}$$

The probability $\mathbb{P}[\mathcal{O}^C_{\mathrm{ACN}}(D_1)]$ is given by

$$\mathbb{P}[\mathcal{O}^C_{\mathrm{ACN}}(D_1)] = \mathbb{P}\left(\mathrm{DT}^C_{SD_1}\right) + \left\{\mathbb{P}\left(\mathrm{DT}_{SD_1}\right) \times \mathbb{P}\left(\mathrm{RT}^C_{S,D_2,D_1}\right)\right\}. \tag{C.2}$$

To calculate $\mathbb{P}\left(\mathrm{DT}^C_{SD_1}\right)$, we proceed as follows

$$\mathbb{P}\left(\mathrm{DT}^C_{SD_1}\right) = \mathbb{P}\left(\mathrm{SIR}_{SD_{1-1}} \geq \Theta_1^{(1)}\right). \tag{C.3}$$

Plugging (3.1) into (C.3), we get

$$\begin{aligned}
\mathbb{P}\left(\mathrm{DT}^C_{SD_1}\right) &= \mathbb{E}_{I_X,I_Y}\left[\mathbb{P}\left\{\frac{|h_{SD_1}|^2 l_{SD_1} a_1}{|h_{SD_1}|^2 l_{SD_1} a_2 + I_{X_{D_1}} + I_{Y_{D_1}}} \geq \Theta_1^{(1)}\right\}\right] \\
&= \mathbb{E}_{I_X,I_Y}\left[\mathbb{P}\left\{|h_{SD_1}|^2 l_{SD_1}(a_1 - \Theta_1^{(1)} a_2) \geq \Theta_1^{(1)}[I_{X_{D_1}} + I_{Y_{D_1}}]\right\}\right].
\end{aligned} \tag{C.4}$$

We can see from (C.4) that, when $\Theta_1^{(1)} \geq a_1/a_2$, the success probability $\mathbb{P}\left(\mathrm{DT}_{SD_1}^C\right) = 0$. Then, when $\Theta_1^{(1)} < a_1/a_2$, and after setting $\mathcal{G}_1^{(1)} = \Theta_1^{(1)}/(a_1 - \Theta_1^{(1)}a_2)$, we get

$$\mathbb{P}\left(\mathrm{DT}_{SD_1}^C\right) = \mathbb{E}_{I_X,I_Y}\left[\mathbb{P}\left\{|h_{SD_1}|^2 \geq \frac{\mathcal{G}_1^{(1)}}{l_{SD_1}}[I_{X_{D_1}} + I_{Y_{D_1}}]\right\}\right].$$

Since $|h_{SD_1}|^2$ follows an exponential distribution with unit mean, and using the independence of the PPP on the road X and Y, we obtain

$$\mathbb{P}\left(\mathrm{DT}_{SD_1}^C\right) = \mathbb{E}_{I_X}\left[\exp\left(-\frac{\mathcal{G}_1^{(1)}}{l_{SD_1}}I_{X_{D_1}}\right)\right]\mathbb{E}_{I_Y}\left[\exp\left(-\frac{\mathcal{G}_1^{(1)}}{l_{SD_1}}I_{Y_{D_1}}\right)\right].$$

Given that $\mathbb{E}[e^{sI}] = \mathcal{L}_I(s)$, we finally get

$$\mathbb{P}\left(\mathrm{DT}_{SD_1}^C\right) = \mathcal{L}_{I_{X_{D_1}}}\left(\frac{\mathcal{G}_1^{(1)}}{l_{SD_1}}\right)\mathcal{L}_{I_{Y_{D_1}}}\left(\frac{\mathcal{G}_1^{(1)}}{l_{SD_1}}\right). \tag{C.5}$$

Following the same steps, we obtain

$$\mathbb{P}\left(\mathrm{DT}_{SD_1}\right) = 1 - \mathcal{L}_{I_{X_{D_1}}}\left(\frac{\mathcal{G}_1^{(1)}}{l_{SD_1}}\right)\mathcal{L}_{I_{Y_{D_1}}}\left(\frac{\mathcal{G}_1^{(1)}}{l_{SD_1}}\right). \tag{C.6}$$

To calculate $\mathbb{P}\left(\mathrm{RT}_{S,D_2,D_1}^C\right)$, we proceed as follows

$$\mathbb{P}\left(\mathrm{RT}_{S,D_2,D_1}^C\right) = \mathbb{P}\left(\mathrm{SIR}_{SD_{2-1}} \geq \Theta_1^{(2)}\right) \times \mathbb{P}\left(\mathrm{SIR}_{D_2D_1}^{(\mathrm{OMA})} \geq \Theta_1^{(2)}\right). \tag{C.7}$$

The probability $\mathbb{P}\left(\mathrm{SIR}_{SD_{2-1}} \geq \Theta_1^{(2)}\right)$ can be acquired following the same steps above, and it is given by

$$\mathbb{P}\left(\mathrm{SIR}_{SD_{2-1}} \geq \Theta_1^{(2)}\right) = \mathcal{L}_{I_{X_{D_2}}}\left(\frac{\mathcal{G}_1^{(2)}}{l_{SD_2}}\right)\mathcal{L}_{I_{Y_{D_2}}}\left(\frac{\mathcal{G}_1^{(2)}}{l_{SD_2}}\right). \tag{C.8}$$

The probability $\mathbb{P}\left(\mathrm{SIR}_{D_2D_1}^{(\mathrm{OMA})} \geq \Theta_1^{(2)}\right)$ can be easily calculated, and it is given by

$$\mathbb{P}\left(\mathrm{SIR}_{D_2D_1}^{(\mathrm{OMA})} \geq \Theta_1^{(2)}\right) = \mathcal{L}_{I_{X_{D_1}}}\left(\frac{\Theta_1^{(2)}}{l_{D_2D_1}}\right)\mathcal{L}_{I_{Y_{D_1}}}\left(\frac{\Theta_1^{(2)}}{l_{D_2D_1}}\right). \tag{C.9}$$

In the same way, we express The probability $\mathbb{P}[\mathcal{O}_{\mathrm{ACN}}(D_2)]$ as a function of a success probability $\mathbb{P}[\mathcal{O}_{\mathrm{ACN}}^C(D_2)]$ as follows

$$\mathbb{P}[\mathcal{O}_{\mathrm{ACN}}(D_2)] = 1 - \mathbb{P}[\mathcal{O}_{\mathrm{ACN}}^C(D_2)]. \tag{C.10}$$

The probability $\mathbb{P}[\mathcal{O}_{\mathrm{ACN}}^C(D_2)]$ is given by

$$\mathbb{P}[\mathcal{O}_{\mathrm{ACN}}^C(D_2)] = \mathbb{P}\left(\mathrm{DT}_{SD_2}^C\right) + \left\{\mathbb{P}\left(\mathrm{DT}_{SD_2}\right) \times \mathbb{P}\left(\mathrm{RT}_{S,D_1,D_2}^C\right)\right\}. \tag{C.11}$$

To calculate $\mathbb{P}\left(\mathrm{DT}_{SD_2}^C\right)$, we proceed as follows

$$\begin{aligned}\mathbb{P}\left(\mathrm{DT}_{SD_2}^C\right) &= \mathbb{P}\left(\bigcap_{i=1}^{2} \mathrm{SIR}_{SD_{2-i}} \geq \Theta_i^{(1)}\right) \\ &= \mathbb{P}\left(\mathrm{SIR}_{SD_{2-1}} \geq \Theta_1^{(1)} \cap \mathrm{SIR}_{SD_{2-2}} \geq \Theta_2^{(1)}\right).\end{aligned} \tag{C.12}$$

Following the same steps as for $\mathbb{P}\left(\mathrm{DT}_{SD_1}^C\right)$, we get

$$\mathbb{P}\left(\mathrm{DT}_{SD_2}^C\right) = \mathbb{E}_{I_X,I_Y}\left[\mathbb{P}\left\{\frac{|h_{SD_2}|^2 l_{SD_2} a_1}{|h_{SD_2}|^2 l_{SD_2} a_2 + I_{X_{D_2}} + I_{Y_{D_2}}} \geq \Theta_1^{(1)}, \frac{|h_{SD_2}|^2 l_{SD_2} a_2}{I_{X_{D_2}} + I_{Y_{D_2}}}\right] \geq \Theta_2^{(1)}\right\}.$$

When $\Theta_1^{(1)} > a_1/a_2$, then $\mathbb{P}\left(\mathrm{DT}_{SD_2}^C\right) = 0$, otherwise we continue the derivation. We set $\mathcal{G}_2^{(1)} = \Theta_2^{(1)}/a_2$, then

$$\mathbb{P}\left(\mathrm{DT}_{SD_2}^C\right) = \mathbb{E}_{I_X,I_Y}\left[\mathbb{P}\left\{|h_{SD_2}|^2 \geq \frac{\mathcal{G}_1^{(1)}}{l_{SD_2}}[I_{X_{D_2}} + I_{Y_{D_2}}], |h_{SD_2}|^2 \geq \frac{\mathcal{G}_2^{(1)}}{l_{SD_2}}[I_{X_{D_2}} + I_{Y_{D_2}}]\right\}\right].$$

Finally, $\mathbb{P}\left(\mathrm{DT}^{C}_{SD_2}\right)$ equals

$$\mathbb{P}\left(\mathrm{DT}^{C}_{SD_2}\right) = \mathcal{L}_{I_{X_{D_2}}}\left(\frac{\mathcal{G}^{(1)}_{\max}}{l_{SD_2}}\right)\mathcal{L}_{I_{Y_{D_2}}}\left(\frac{\mathcal{G}^{(1)}_{\max}}{l_{SD_2}}\right), \tag{C.13}$$

where $\mathcal{G}^{(1)}_{\max} = \max(\mathcal{G}^{(1)}_1, \mathcal{G}^{(1)}_2)$.

To calculate $\mathbb{P}\left(\mathrm{RT}^{C}_{S,D_1,D_2}\right)$, we follow the same steps as in $\mathbb{P}\left(\mathrm{RT}^{C}_{S,D_2,D_1}\right)$.

C.2. NOMA outage probability of mmWave vehicular networks

To calculate $\mathbb{P}(O_{(1)})$, we express it as a function of a success probability $\mathbb{P}(O^{C}_{(1)})$, where $\mathbb{P}(O^{C}_{D_1})$ is expressed as

$$\mathbb{P}(O_{(1)}) = 1 - \mathbb{P}(O^{C}_{(1)}). \tag{C.14}$$

The probability $\mathbb{P}(O^{C}_{(1)})$ is expressed as

$$\mathbb{P}(O^{C}_{(1)}) = 1 - \mathbb{P}(O^{C}_{R_1} \cap O^{C}_{D_1}) = \mathbb{P}(O^{C}_{R_1})\mathbb{P}(O^{C}_{D_1}), \tag{C.15}$$

where

$$O^{C}_{R_1} \triangleq \bigcup_{\mathrm{Z}\in\{\mathrm{LOS},\mathrm{NLOS}\}} \{\mathrm{Z}_{SR} \cap (\mathrm{SIR}^{(\alpha_{\mathrm{Z}})}_{R_1} \geq \Theta_1)\} \tag{C.16}$$

$$O^{C}_{D_1} \triangleq \bigcup_{\mathrm{Z}\in\{\mathrm{LOS},\mathrm{NLOS}\}} \{\mathrm{Z}_{RD_1} \cap (\mathrm{SIR}^{(\alpha_{\mathrm{Z}})}_{D_1} \geq \Theta_1)\}. \tag{C.17}$$

We calculate The probability $\mathbb{P}(O_{R_1}^C)$ as

$$\begin{aligned}
\mathbb{P}(O_{R_1}^C) &= \sum_{\mathrm{Z}\in\{\mathrm{LOS},\mathrm{NLOS}\}} \mathbb{E}_{I_X,I_Y}\left[\mathbb{P}\left\{\ \mathrm{Z}_{SR}\cap(\mathrm{SIR}_{R_1}^{(\alpha_\mathrm{Z})}\geq\Theta_1)\right\}\right] \\
&= \sum_{\mathrm{Z}\in\{\mathrm{LOS},\mathrm{NLOS}\}} \mathbb{P}(\mathrm{Z}_{SR})\ \mathbb{E}_{I_X,I_Y}\left[\mathbb{P}\left\{\ \mathrm{SIR}_{R_1}^{(\alpha_\mathrm{Z})}\geq\Theta_1\right\}\right] \\
&= \sum_{\mathrm{Z}\in\{\mathrm{LOS},\mathrm{NLOS}\}} \mathbb{P}(\mathrm{Z}_{SR})\ \mathbb{E}_{I_X,I_Y}\left[\mathbb{P}\left\{\ \frac{|h_{SR}|^2 r_{SR}^{-\alpha_\mathrm{Z}}\Upsilon a_1}{|h_{SR}|^2 r_{SR}^{-\alpha_\mathrm{Z}}\Upsilon a_2 + I_{X_R} + I_{Y_R}}\geq\Theta_1\right\}\right] \\
&= \sum_{\mathrm{Z}\in\{\mathrm{LOS},\mathrm{NLOS}\}} \mathbb{P}(\mathrm{Z}_{SR})\ \mathbb{E}_{I_X,I_Y}\left[\mathbb{P}\left\{|h_{SR}|^2 r_{SR}^{-\alpha_\mathrm{Z}}\Upsilon(a_1-\Theta_1 a_2)\geq\Theta_1\left[I_{X_R}+I_{Y_R}\right]\right\}\right].
\end{aligned} \tag{C.18}$$

We can notice from (C.18) that, when $\Theta_1 \geq a_1/a_2$, the success probability $\mathbb{P}(O_{R_1}^C)$ is always zero, that is, $\mathbb{P}(O_{R_1}) = 1$. Then, when $\Theta_1 < a_1/a_2$, and after setting $\Psi_1 = \Theta_1/(a_1 - \Theta_1 a_2)$, then

$$\mathbb{P}(O_{R_1}^C) = \sum_{\mathrm{Z}\in\{\mathrm{LOS},\mathrm{NLOS}\}} \mathbb{P}(\mathrm{Z}_{SR})\ \mathbb{E}_{I_X,I_Y}\left[\mathbb{P}\left\{|h_{SR}|^2 \geq \frac{\Psi_1}{r_{SR}^{-\alpha_\mathrm{Z}}\Upsilon}\left[I_{X_R}+I_{Y_R}\right]\right\}\right].$$

Since $|h_{SR}|^2$ follows a gamma distribution, its complementary cumulative distribution function (CCDF) is given by

$$\bar{F}_{|h_{SR}|^2}(X) = \mathbb{P}(|h_{SR}|^2 > X) = \frac{\Gamma(m_\mathrm{Z}, \frac{m_\mathrm{Z}}{\mu}X)}{\Gamma(m_\mathrm{Z})}, \tag{C.19}$$

hence

$$\mathbb{P}(O_{R_1}^C) = \sum_{\mathrm{Z}\in\{\mathrm{LOS,NLOS}\}} \mathbb{P}(\mathrm{Z}_{SR})\ \mathbb{E}_{I_X,I_Y}\left[\frac{\Gamma\Big(m_{\mathrm{Z}}, \frac{m_{\mathrm{Z}}\,\Psi_1}{\mu\, r_{SR}^{-\alpha_{\mathrm{Z}}}\Upsilon}(I_{X_R}^{\mathrm{LOS}} + I_{Y_R}^{\mathrm{LOS}})\Big)}{\Gamma(m_{\mathrm{Z}})}\right]$$
$$\times\, \mathbb{E}_{I_X,I_Y}\left[\frac{\Gamma\Big(m_{\mathrm{Z}}, \frac{m_{\mathrm{Z}}\,\Psi_1}{\mu\, r_{SR}^{-\alpha_{\mathrm{Z}}}\Upsilon}(I_{X_R}^{\mathrm{NLOS}} + I_{Y_R}^{\mathrm{NLOS}})\Big)}{\Gamma(m_{\mathrm{Z}})}\right]$$
$$= \sum_{\mathrm{Z}\in\{\mathrm{LOS,NLOS}\}} \mathbb{P}(\mathrm{Z}_{SR}) \prod_{\mathrm{K}\in\{\mathrm{LOS,NLOS}\}} \mathbb{E}_{I_X,I_Y}\left[\frac{\Gamma\Big(m_{\mathrm{Z}}, \frac{m_{\mathrm{Z}}\,\Psi_1}{\mu\, r_{SR}^{-\alpha_{\mathrm{Z}}}\Upsilon}(I_{X_R}^{\mathrm{K}} + I_{Y_R}^{\mathrm{K}})\Big)}{\Gamma(m_{\mathrm{Z}})}\right]. \tag{C.20}$$

The exponential sum function when m_{Z} is an integer is defined as

$$e_{(m_{\mathrm{Z}})} = \sum_{k=0}^{m_{\mathrm{Z}}-1} \frac{(\frac{m_{\mathrm{Z}}}{\mu}X)^k}{k!} = e^X \frac{\Gamma(m_{\mathrm{Z}}, \frac{m_{\mathrm{Z}}}{\mu}X)}{\Gamma(m_{\mathrm{Z}})}, \tag{C.21}$$

then

$$\frac{\Gamma(m_{\mathrm{Z}}, \frac{m_{\mathrm{Z}}}{\mu}X)}{\Gamma(m_{\mathrm{Z}})} = e^{-\frac{m_{\mathrm{Z}}}{\mu}X} \sum_{k=0}^{m_{\mathrm{Z}}-1} \frac{1}{k!}\Big(\frac{m_{\mathrm{Z}}\,X}{\mu}\Big)^k. \tag{C.22}$$

We denote the expectation in equation (C.20) by $\mathcal{E}(I_X, I_Y)$, then $\mathcal{E}(I_X, I_Y)$ equals

$$\begin{aligned}\mathcal{E}(I_X, I_Y) &= \mathbb{E}_{I_X,I_Y}\left[\exp\Big(-\frac{m_{\mathrm{Z}}\,\Psi_1}{\mu\, r_{SR}^{-\alpha_{\mathrm{Z}}}\Upsilon}(I_{X_R}^{\mathrm{K}} + I_{Y_R}^{\mathrm{K}})\Big) \times \sum_{k=0}^{m_{\mathrm{Z}}-1} \frac{1}{k!}\Big(\frac{m_{\mathrm{Z}}\,\Psi_1}{\mu\, r_{SR}^{-\alpha_{\mathrm{Z}}}\Upsilon}(I_{X_R}^{\mathrm{K}} + I_{Y_R}^{\mathrm{K}})\Big)^k\right] \\ &= \sum_{k=0}^{m-1} \frac{1}{k!}\Big(\frac{m_{\mathrm{Z}}\,\Psi_1}{\mu\, r_{SR}^{-\alpha_{\mathrm{Z}}}\Upsilon}\Big)^k \mathbb{E}_{I_X,I_Y}\left[\exp\Big(-\frac{m_{\mathrm{Z}}\,\Psi_1}{\mu\, r_{SR}^{-\alpha_{\mathrm{Z}}}\Upsilon}(I_{X_R}^{\mathrm{K}} + I_{Y_R}^{\mathrm{K}})\Big)(I_{X_R}^{\mathrm{K}} + I_{Y_R}^{\mathrm{K}})^k\right].\end{aligned} \tag{C.23}$$

Applying the binomial theorem in (C.23), we get

$$\begin{aligned}\mathcal{E}(I_X, I_Y) &= \sum_{k=0}^{m_{\mathrm{Z}}-1} \frac{1}{k!} \Big(\frac{m_{\mathrm{Z}}\,\Psi_1}{\mu\, r_{SR}^{-\alpha_{\mathrm{Z}}}\Upsilon}\Big)^k \\ &\quad \times \mathbb{E}_{I_X,I_Y}\Bigg[\exp\Big(-\frac{m_{\mathrm{Z}}\,\Psi_1}{\mu\, r_{SR}^{-\alpha_{\mathrm{Z}}}\Upsilon}[I^{\mathrm{K}}_{X_R} + I^{\mathrm{K}}_{Y_R}]\Big)\sum_{n=0}^{k}\binom{k}{n}(I^{\mathrm{K}}_{X_R})^{k-n}\,(I^{\mathrm{K}}_{Y_R})^{n}\Bigg] \\ &= \sum_{k=0}^{m_{\mathrm{Z}}-1} \frac{1}{k!}\,\Omega^k \mathbb{E}_{I_X,I_Y}\Bigg[\exp\Big(-\Omega[I^{\mathrm{K}}_{X_R} + I^{\mathrm{K}}_{Y_R}]\Big)\sum_{n=0}^{k}\binom{k}{n}(I^{\mathrm{K}}_{X_R})^{k-n}\,(I^{\mathrm{K}}_{Y_R})^{n}\Bigg],\end{aligned} \tag{C.24}$$

where $\Omega = \dfrac{m_{\mathrm{Z}}\,\Psi_1}{\mu\, r_{SR}^{-\alpha_{\mathrm{Z}}}\Upsilon}$. To calculate the expectation in (C.24), we use the following notation

$$\mathbb{E}(I_{X_R}, I_{Y_R}) = \mathbb{E}_{I_X,I_Y}\Bigg[e^{-\Omega\, I^{\mathrm{K}}_{X_R}}\, e^{-\Omega\, I^{\mathrm{K}}_{Y_R}}\sum_{n=0}^{k}\binom{k}{n}(I^{\mathrm{K}}_{X_R})^{k-n}\,(I^{\mathrm{K}}_{Y_R})^{n}\Bigg].$$

Then,

$$\begin{aligned}\mathbb{E}(I_{X_R}, I_{Y_R}) &= \sum_{n=0}^{k}\binom{k}{n}\mathbb{E}_{I_X,I_Y}\Big[e^{-\Omega\, I^{\mathrm{K}}_{X_R}}\, e^{-\Omega\, I^{\mathrm{K}}_{Y_R}}(I^{\mathrm{K}}_{X_R})^{k-n}\,(I^{\mathrm{K}}_{Y_R})^{n}\Big] \\ &= \sum_{n=0}^{k}\binom{k}{n}\mathbb{E}_{I_X}\Big[e^{-\Omega\, I^{\mathrm{K}}_{X_R}}(I^{\mathrm{K}}_{X_R})^{k-n}\Big]\mathbb{E}_{I^{\mathrm{K}}_{Y_R}}\Big[e^{-\Omega\, I^{\mathrm{K}}_{Y_R}}\,(I^{\mathrm{K}}_{Y_R})^{n}\Big] \\ &\overset{(a)}{=} \sum_{n=0}^{k}\binom{k}{n}(-1)^{k-n}\frac{\mathrm{d}^{k-n}\mathcal{L}_{I^{\mathrm{K}}_{X_R}}(\Omega)}{\mathrm{d}^{k-n}\Omega}(-1)^{n}\frac{\mathrm{d}^{n}\mathcal{L}_{I^{\mathrm{K}}_{Y_R}}(\Omega)}{\mathrm{d}^{n}\Omega} \\ &= (-1)^k\sum_{n=0}^{k}\binom{k}{n}\frac{\mathrm{d}^{k-n}\mathcal{L}_{I^{\mathrm{K}}_{X_R}}(\Omega)}{\mathrm{d}^{k-n}\Omega}\frac{\mathrm{d}^{n}\mathcal{L}_{I^{\mathrm{K}}_{Y_R}}(\Omega)}{\mathrm{d}^{n}\Omega},\end{aligned} \tag{C.25}$$

where (a) stems form the following property

$$\begin{aligned}\mathbb{E}_I\Big[e^{-\Omega I}I^N\Big] &= (-1)^N\frac{\mathrm{d}^N\mathbb{E}_I\Big[e^{-\Omega\, I}I^N\Big]}{\mathrm{d}^N\Omega} \\ &= (-1)^N\frac{\mathrm{d}^N\mathcal{L}_I(\Omega)}{\mathrm{d}^N\Omega}.\end{aligned} \tag{C.26}$$

Finally, we obtain

$$\mathcal{E}(I_X, I_Y) = \sum_{k=0}^{m_{\mathrm{Z}}-1} \frac{1}{k!} \big(- \frac{m_{\mathrm{Z}}\, \Psi_1}{\mu\, r_{SR}^{-\alpha_{\mathrm{Z}}} \Upsilon} \big)^k \sum_{n=0}^{k} \binom{k}{n} \frac{\mathrm{d}^{k-n} \mathcal{L}_{I^{\mathrm{K}}_{X_R}} \big(\frac{m_{\mathrm{Z}}\, \Psi_1}{\mu\, r_{SR}^{-\alpha_{\mathrm{Z}}} \Upsilon} \big)}{\mathrm{d}^{k-n} \big(\frac{m_{\mathrm{Z}}\, \Psi_1}{\mu\, r_{SR}^{-\alpha_{\mathrm{Z}}} \Upsilon} \big)} \frac{\mathrm{d}^{n} \mathcal{L}_{I^{\mathrm{K}}_{Y_R}} \big(\frac{m_{\mathrm{Z}}\, \Psi_1}{\mu\, r_{SR}^{-\alpha_{\mathrm{Z}}} \Upsilon} \big)}{\mathrm{d}^{n} \big(\frac{m_{\mathrm{Z}}\, \Psi_1}{\mu\, r_{SR}^{-\alpha_{\mathrm{Z}}} \Upsilon} \big)}. \tag{C.27}$$

Then plugging (C.27) in (C.20) yields

$$\begin{aligned} \mathbb{P}(O^C_{R_1}) \;=\; & \sum_{\mathrm{Z}\in\{\mathrm{LOS},\mathrm{NLOS}\}} \mathbb{P}(\mathrm{Z}_{SR}) \prod_{\mathrm{K}\in\{\mathrm{LOS},\mathrm{NLOS}\}} \sum_{k=0}^{m_L-1} \frac{1}{k!} \big(- \frac{m_{\mathrm{Z}}\, \Psi_1}{\mu\, r_{SR}^{-\alpha_{\mathrm{Z}}} \Upsilon} \big)^k \\ & \times \sum_{n=0}^{k} \binom{k}{n} \frac{\mathrm{d}^{k-n} \mathcal{L}_{I^{\mathrm{K}}_{X_R}} \big(\frac{m_{\mathrm{Z}}\, \Psi_1}{\mu\, r_{SR}^{-\alpha_{\mathrm{Z}}} \Upsilon} \big)}{\mathrm{d}^{k-n} \big(\frac{m_{\mathrm{Z}}\, \Psi_1}{\mu\, r_{SR}^{-\alpha_{\mathrm{Z}}} \Upsilon} \big)} \frac{\mathrm{d}^{n} \mathcal{L}_{I^{\mathrm{K}}_{Y_R}} \big(\frac{m_{\mathrm{Z}}\, \Psi_1}{\mu\, r_{SR}^{-\alpha_{\mathrm{Z}}} \Upsilon} \big)}{\mathrm{d}^{n} \big(\frac{m_{\mathrm{Z}}\, \Psi_1}{\mu\, r_{SR}^{-\alpha_{\mathrm{Z}}} \Upsilon} \big)}. \end{aligned} \tag{C.28}$$

The expression of $\mathrm{d}^{k-n}\mathcal{L}_{I^{\mathrm{K}}_X}(s)/\mathrm{d}^{k-n}(s)$ and $\mathrm{d}^{n}\mathcal{L}_{I^{\mathrm{K}}_Y}(s)/\mathrm{d}^{n}(s)$ are given by (1.62) and (1.63). The probability $\mathbb{P}(O^C_{D_1})$ can be calculated following the same steps above.

In the same way we express $\mathbb{P}(O_{(2)})$ as a function of a success probability $\mathbb{P}(O^C_{(2)})$, where $\mathbb{P}(O^C_{(2)})$ is given by

$$\mathbb{P}(O_{(2)}) = 1 - \mathbb{P}(O^C_{(2)}). \tag{C.29}$$

The probability $\mathbb{P}(O^C_{(2)})$ is expressed as

$$\begin{aligned} \mathbb{P}(O^C_{(2)}) \;&=\; 1 - \mathbb{P}(O^C_{R_2} \cap O^C_{D_2}) \\ &=\; 1 - \mathbb{P}(O^C_{R_2}) \mathbb{P}(O^C_{D_2}), \end{aligned} \tag{C.30}$$

where

$$O^C_{R_2} \triangleq \bigcup_{\mathrm{Z}\in\{\mathrm{LOS},\mathrm{NLOS}\}} \bigcap_{i=1}^{2} \{\mathrm{Z}_{SR} \cap (\mathrm{SIR}^{(\alpha_{\mathrm{Z}})}_{R_i} \geq \Theta_i)\}, \tag{C.31}$$

and

$$O^C_{D_2} \triangleq \bigcup_{\mathrm{Z}\in\{\mathrm{LOS},\mathrm{NLOS}\}} \bigcap_{i=1}^{2} \{\mathrm{Z}_{RD_2} \cap (\mathrm{SIR}^{(\alpha_{\mathrm{Z}})}_{D_{2-i}} < \Theta_i)\}. \tag{C.32}$$

To calculate $\mathbb{P}(O_{R_2}^C)$ we proceed as follows

$$\begin{aligned}\mathbb{P}(O_{R_2}^C) &= \sum_{\mathrm{Z}\in\{\mathrm{LOS},\mathrm{NLOS}\}} \mathbb{E}_{I_X,I_Y}\left[\mathbb{P}\left\{\bigcap_{i=1}^{2}\{\mathrm{Z}_{SR}\cap(\mathrm{SIR}_{R_i}^{(\alpha_\mathrm{Z})}\geq\Theta_i)\right\}\right]\\ &= \sum_{\mathrm{Z}\in\{\mathrm{LOS},\mathrm{NLOS}\}} \mathbb{P}(\mathrm{Z}_{SR})\ \mathbb{E}_{I_X,I_Y}\left[\mathbb{P}\left\{\bigcap_{i=1}^{2}\mathrm{SIR}_{R_i}^{(\alpha_\mathrm{Z})}\geq\Theta_i\right\}\right]\\ &= \sum_{\mathrm{Z}\in\{\mathrm{LOS},\mathrm{NLOS}\}} \mathbb{P}(\mathrm{Z}_{SR})\ \mathbb{E}_{I_X,I_Y}\left[\mathbb{P}\left\{\mathrm{SIR}_{R_1}^{(\alpha_\mathrm{Z})}\geq\Theta_1\cap\mathrm{SIR}_{R_2}^{(\alpha_\mathrm{Z})}\geq\Theta_2\right\}\right].\end{aligned} \tag{C.33}$$

Following the same steps as for $\mathbb{P}(O_{R_1}^C)$, we get

$$\mathbb{P}(O_{R_2}^C)=\mathbb{E}_{I_X,I_Y}\left[\mathbb{P}\left\{\frac{|h_{SR}|^2 r_{SR}^{-\alpha_\mathrm{Z}}\Upsilon a_1}{|h_{SR}|^2 r_{SR}^{-\alpha_\mathrm{Z}}\Upsilon a_2+I_{X_R}+I_{Y_R}}\geq\Theta_1,\frac{|h_{SR}|^2 r_{SR}^{-\alpha_\mathrm{Z}}\Upsilon a_2}{I_{X_R}+I_{Y_R}}\geq\Theta_2\right\}\right].$$

When $\Theta_1 > a_1/a_2$, then $\mathbb{P}(O_{R_2})=1$, otherwise we continue the derivation We set $\Psi_2=\Theta_2/a_2$, then

$$\begin{aligned}\mathbb{P}(O_{R_2}^C) &= \mathbb{E}_{I_X,I_Y}\left[\mathbb{P}\left\{|h_{SR}|^2\geq\frac{\Psi_1}{r_{SR}^{-\alpha_\mathrm{Z}}\Upsilon}[I_{X_R}+I_{Y_R}],|h_{SR}|^2\geq\frac{\Psi_2}{r_{SR}^{-\alpha_\mathrm{Z}}\Upsilon}[I_{X_R}+I_{Y_R}]\right\}\right]\\ &= \mathbb{E}_{I_X,I_Y}\left[\mathbb{P}\left\{|h_{SR}|^2\geq\frac{\max(\Psi_1,\Psi_2)}{r_{SR}^{-\alpha_\mathrm{Z}}\Upsilon}[I_{X_R}+I_{Y_R}]\right\}\right].\end{aligned}$$

Following the same steps above, $\mathbb{P}(O_{R_2}^C)$ equals

$$\begin{aligned}\mathbb{P}(O_{R_2}^C) &= \sum_{\mathrm{Z}\in\{\mathrm{LOS},\mathrm{NLOS}\}}\mathbb{P}(\mathrm{Z}_{SR})\prod_{\mathrm{K}\in\{\mathrm{LOS},\mathrm{NLOS}\}}\sum_{k=0}^{m_L-1}\frac{1}{k!}\left(-\frac{m_\mathrm{Z}\,\Psi_{\max}}{\mu\, r_{SR}^{-\alpha_\mathrm{Z}}\Upsilon}\right)^k\\ &\quad\times\sum_{n=0}^{k}\binom{k}{n}\frac{\mathrm{d}^{k-n}\mathcal{L}_{I_{X_R}^\mathrm{K}}\left(\frac{m_\mathrm{Z}\,\Psi_{\max}}{\mu\, r_{SR}^{-\alpha_\mathrm{Z}}\Upsilon}\right)}{\mathrm{d}^{k-n}\left(\frac{m_\mathrm{Z}\,\Psi_{\max}}{\mu\, r_{SR}^{-\alpha_\mathrm{Z}}\Upsilon}\right)}\frac{\mathrm{d}^{n}\mathcal{L}_{I_{Y_R}^\mathrm{K}}\left(\frac{m_\mathrm{Z}\,\Psi_{\max}}{\mu\, r_{SR}^{-\alpha_\mathrm{Z}}\Upsilon}\right)}{\mathrm{d}^{n}\left(\frac{m_\mathrm{Z}\,\Psi_{\max}}{\mu\, r_{SR}^{-\alpha_\mathrm{Z}}\Upsilon}\right)},\end{aligned} \tag{C.34}$$

where $\Psi_{\max}=\max(\Psi_1,\Psi_2)$. The probability $\mathbb{P}(O_{D_2}^C)$ can be calculated following the same

steps above.

C.3. Laplace transform expressions considering two lanes

The expression of the Laplace transform of interference originated from the X_2 road at M is given by

$$\mathcal{L}_{I_{X_2 M}}(s) = \exp\left(- p\lambda_{X_2} \int_{-\infty}^{+\infty} \frac{1}{1 + \frac{(\|x - M\|^{\alpha})}{s}} dx \right), \tag{C.35}$$

where

$$\|x - M\| = \sqrt{m_{y_2}^2 + (x - m_{x_2})^2}, \tag{C.36}$$

and m_{x_2} and m_{y_2} are the coordinate of M at the X_2 and Y_2 road.

For $\alpha = 2$, (C.35) becomes

$$\mathcal{L}_{I_{X_2 M}}(s) = \exp\left(- p\lambda_{X_2} s \int_{-\infty}^{+\infty} \frac{1}{s + m_{y_2}^2 + (x - m_{x_2})^2} dx \right), \tag{C.37}$$

and the integral inside the exponential in (C.37) equals

$$\int_{-\infty}^{+\infty} \frac{1}{s + m_{y_2}^2 + (x - m_{x_2})^2} dx = \frac{\pi}{s + m_{y_2}^2}. \tag{C.38}$$

We express m_{x_2} and m_{y_2} as a function of m and θ_M as follows

$$m_{x_2} = m\cos(\theta_M) - d_{X_{Road}}, \tag{C.39}$$

and

$$m_{y_2} = m\sin(\theta_M) - d_{Y_{Road}}. \tag{C.40}$$

Substituting (C.40) in (C.38), then in (C.37) yields (3.64). Following the same steps we obtain (3.65).

C.4. NOMA outage probability using multiple relays

To calculate the outage probability at D_1, denoted $\mathbb{P}(O_{(1)})$, we proceed as follows

$$\begin{aligned}\mathbb{P}(O_{(1)}) &= \sum_{f=0}^{nb_{Relay}} \sum_{\mathcal{V}_f^{(1)}} \mathbb{P}\Big(O_{D_1} \cap \mathcal{V}_f^{(1)}\Big) \\ &= \sum_{f=0}^{nb_{Relay}} \sum_{\mathcal{V}_f^{(1)}} \mathbb{P}\Big(O_{D_1}/\mathcal{V}_f^{(1)}\Big)\mathbb{P}\Big(\mathcal{V}_f^{(1)}\Big). \end{aligned} \tag{C.41}$$

The probability $\mathbb{P}(\mathcal{V}_f^{(1)})$ equals

$$\begin{aligned}\mathbb{P}(\mathcal{V}_f^{(1)}) &= \prod_{i\in\mathcal{V}_f^{(1)}} \mathbb{P}(\mathrm{SIR}_{SR_{i\to 1}} \geq \Theta_1) \prod_{j\notin\mathcal{V}_f^{(1)}} \mathbb{P}(\mathrm{SIR}_{SR_{j\to 1}} < \Theta_1) \\ &= \prod_{i\in\mathcal{V}_f^{(1)}} \mathbb{E}_{I_X,I_Y}\left[\mathbb{P}\left\{ \frac{|h_{SR_i}|^2 l_{SR_i} a_1}{|h_{SR_i}|^2 l_{SR_i} a_2 + I_{X_{R_i}} + I_{Y_{R_i}}} \geq \Theta_1 \right\}\right] \\ &\quad \times \prod_{j\notin\mathcal{V}_f^{(1)}} \mathbb{E}_{I_X,I_Y}\left[\mathbb{P}\left\{ \frac{|h_{SR_j}|^2 l_{SR_j} a_1}{|h_{SR_j}|^2 l_{SR_j} a_2 + I_{X_{R_j}} + I_{Y_{R_j}}} < \Theta_1 \right\}\right]. \end{aligned} \tag{C.42}$$

Following the same steps as in Appendix B.2, we obtain

$$\mathbb{P}(\mathcal{V}_f^{(1)}) = \prod_{i\in\mathcal{V}_f^{(1)}} \mathcal{H}_{(R_i)}\Big(\frac{G_1}{l_{SR_i}}\Big) \prod_{j\notin\mathcal{V}_f^{(1)}} \Big(1 - \mathcal{H}_{(R_j)}\Big(\frac{G_1}{l_{SR_j}}\Big)\Big). \tag{C.43}$$

The probability $\mathbb{P}\Big(O_{D_1}/\mathcal{V}_f^{(1)}\Big)$ equals

$$\mathbb{P}\Big(O_{D_1}/\mathcal{V}_f^{(1)}\Big) = \prod_{i\in\mathcal{V}_f^{(1)}} \mathbb{P}(\mathrm{SIR}_{R_iD_{1\to1}} < \Theta_1)$$
$$= \prod_{i\in D_l} \Big(1 - \mathcal{H}_{(D_1)}(\frac{G_1}{l_{R_iD_1}})\Big). \tag{C.44}$$

Plugging (C.43) and (C.44) into (C.41) we get

$$\mathbb{P}(O_{(1)}) = \sum_{f=0}^{nb_{Relay}} \sum_{\mathcal{V}_f^{(1)}} \prod_{i\in\mathcal{V}_f^{(1)}} \mathcal{H}_{(R_i)}(\frac{G_1}{l_{SR_i}})\Big(1 - \mathcal{H}_{(D_1)}(\frac{G_1}{l_{R_iD_1}})\Big) \prod_{j\notin\mathcal{V}_f^{(1)}} \Big(1 - \mathcal{H}_{(R_j)}(\frac{G_1}{l_{SR_j}})\Big)$$
$$= \prod_{k=1}^{nb_{Relay}} \Big(1 - \mathcal{H}_{(R_k)}(\frac{G_1}{l_{SR_k}})\mathcal{H}_{(D_1)}(\frac{G_1}{l_{R_kD_1}})\Big). \tag{C.45}$$

To calculate the outage probability at D_2, denoted $\mathbb{P}(O_{(2)})$, we proceed as follows

$$\mathbb{P}(O_{(2)}) = \sum_{g=0}^{nb_{Relay}} \sum_{\mathcal{V}_g^{(2)}} \mathbb{P}\Big(O_{D_2} \cap \mathcal{V}_g^{(2)}\Big)$$
$$= \sum_{g=0}^{nb_{Relay}} \sum_{\mathcal{V}_g^{(2)}} \mathbb{P}\Big(O_{D_2}/\mathcal{V}_g^{(2)}\Big)\mathbb{P}\Big(\mathcal{V}_g^{(2)}\Big)$$
$$= \sum_{g=0}^{nb_{Relay}} \sum_{\mathcal{V}_g^{(2)}} \mathbb{P}\Big(O_{D_{2\to1}} \cup O_{D_{2\to2}}/\mathcal{V}_g^{(2)}\Big)\mathbb{P}\Big(\mathcal{V}_g^{(2)}\Big). \tag{C.46}$$

The probability $\mathbb{P}(\mathcal{V}_g^{(2)})$ equals

$$\begin{aligned}\mathbb{P}(\mathcal{V}_g^{(2)}) = & \prod_{i\in\mathcal{V}_g^{(2)}} \mathbb{P}(\mathrm{SIR}_{SR_{i\to 1}} \geq \Theta_1 \bigcap \mathrm{SIR}_{SR_{i\to 2}} \geq \Theta_2) \\ & \times \prod_{j\notin\mathcal{V}_g^{(2)}} \mathbb{P}(\mathrm{SIR}_{SR_{j\to 1}} < \Theta_1 \bigcup \mathrm{SIR}_{SR_{j\to 2}} < \Theta_2) \\ = & \prod_{i\in\mathcal{V}_g^{(2)}} \mathbb{E}_{I_X,I_Y}\left[\mathbb{P}\left\{ \frac{|h_{SR_i}|^2 l_{SR_i} a_1}{|h_{SR_i}|^2 l_{SR_i} a_2 + I_{X_{R_i}} + I_{Y_{R_i}}} \geq \Theta_1 \bigcap \frac{|h_{SR_i}|^2 l_{SR_i} a_2}{I_{X_{R_i}} + I_{Y_{R_i}}} \geq \Theta_2 \right\}\right] \\ & \times \prod_{j\notin\mathcal{V}_g^{(2)}} \mathbb{E}_{I_X,I_Y}\left[\mathbb{P}\left\{ \frac{|h_{SR_j}|^2 l_{SR_j} a_1}{|h_{SR_j}|^2 l_{SR_j} a_2 + I_{X_{R_j}} + I_{Y_{R_j}}} < \Theta_1 \bigcup \frac{|h_{SR_j}|^2 l_{SR_j} a_2}{I_{X_{R_j}} + I_{Y_{R_j}}} < \Theta_2 \right\}\right].\end{aligned} \tag{C.47}$$

Following the same steps as in Appendix B.2, we obtain

$$\mathbb{P}(\mathcal{V}_g^{(2)}) = \prod_{i\in\mathcal{V}_g^{(2)}} \mathcal{H}_{(R_i)}(\frac{G_{\max}}{l_{SR_i}}) \prod_{j\notin\mathcal{V}_g^{(2)}} \Big(1 - \mathcal{H}_{(R_j)}(\frac{G_{\max}}{l_{SR_j}})\Big). \tag{C.48}$$

The probability $\mathbb{P}\Big(O_{D_{2\to 1}} \cup O_{D_{2\to 2}}/\mathcal{V}_g^{(2)}\Big)$ equals

$$\begin{aligned}\mathbb{P}\Big(O_{D_{2\to 1}} \cup O_{D_{2\to 2}}/\mathcal{V}_g^{(2)}\Big) &= \prod_{i\in\mathcal{V}_g^{(2)}} \mathbb{P}(\mathrm{SIR}_{R_i D_{2\to 1}} < \Theta_1 \bigcup \mathrm{SIR}_{R_i D_{2\to 2}} < \Theta_2) \\ &= \prod_{i\in\mathcal{V}_g^{(2)}} \Big(1 - \mathcal{H}_{(D_2)}(\frac{G_{\max}}{l_{R_i D_2}})\Big).\end{aligned} \tag{C.49}$$

Plugging (C.48) and (C.49) into (C.46) we get

$$\mathbb{P}(O_{(2)}) = \sum_{g=0}^{nb_{Relay}} \sum_{\mathcal{V}_g^{(2)}} \prod_{i \in \mathcal{V}_g^{(2)}} \mathcal{H}_{(R_i)}(\frac{G_{\max}}{l_{SR_i}}) \Big(1 - \mathcal{H}_{(D_2)}(\frac{G_{\max}}{l_{R_i D_2}})\Big) \prod_{j \notin \mathcal{V}_g^{(2)}} \Big(1 - \mathcal{H}_{(R_j)}(\frac{G_{\max}}{l_{SR_j}})\Big)$$
$$= \prod_{l=1}^{nb_{Relay}} \Big(1 - \mathcal{H}_{(R_k)}(\frac{G_{\max}}{l_{SR_k}}) \mathcal{H}_{(D_2)}(\frac{G_{\max}}{l_{R_k D_2}})\Big). \tag{C.50}$$

Bibliography

[123a] 123RF. *Banque d'images - Tokyo, Japon vue de Shibuya Crossing, un des passages les plus fréquentés au monde.* URL: https://fr.123rf.com/photo_42247313_tokyo-japon-vue-de-shibuya-crossing-un-des-passages-les-plus-fr%5C%C3%5C%A9quent%5C%C3%5C%A9s-au-monde-.html (visited on) (cit. on p. 11).

[123b] 123RF. *Banque d'images - Tokyo, Japon vue de Shibuya Crossing, un des passages les plus fréquentés au monde.* URL: https://fr.123rf.com/photo_42247313_tokyo-japon-vue-de-shibuya-crossing-un-des-passages-les-plus-fr%5C%C3%5C%A9quent%5C%C3%5C%A9s-au-monde-.html (visited on) (cit. on p. 13).

[ABG11] J. G. Andrews, F. Baccelli, and R. K. Ganti. "A tractable approach to coverage and rate in cellular networks". In: *IEEE Transactions on communications* 59.11 (2011), pp. 3122–3134 (cit. on p. 7).

[AlH+18] A. Al-Hourani, R. J. Evans, S. Kandeepan, B. Moran, and H. Eltom. "Stochastic geometry methods for modeling automotive radar interference". In: *IEEE Transactions on Intelligent Transportation Systems* 19.2 (2018), pp. 333–344 (cit. on pp. 10, 30).

[Alt+14] A. Altieri, L. R. Vega, P. Piantanida, and C. G. Galarza. "On the outage probability of the full-duplex interference-limited relay channel". In: *arXiv preprint arXiv:1403.7317* (2014) (cit. on pp. 29, 39, 46).

[Apa+10] A. Apavatjrut, C. Goursaud, K. Jaffres-Runser, C. Comaniciu, and J.-M. Gorce. "Toward increasing packet diversity for relaying LT fountain codes in wireless sensor networks". In: *IEEE Communications Letters* 15.1 (2010), pp. 52–54 (cit. on p. 7).

[ASW16] M. Abdulla, E. Steinmetz, and H. Wymeersch. "Vehicle-to-vehicle communications with urban intersection path loss models". In: *Globecom Workshops (GC Wkshps), 2016 IEEE*. IEEE. 2016, pp. 1–6 (cit. on pp. 11, 30).

[AW17] M. Abdulla and H. Wymeersch. "Fine-grained reliability for V2V communications around suburban and urban intersections". In: *arXiv preprint arXiv:1706.10011* (2017) (cit. on p. 11).

[Bel+18] K. Belbase, Z. Zhang, H. Jiang, and C. Tellambura. "Coverage analysis of millimeter wave decode-and-forward networks with best relay selection". In: *IEEE Access* 6 (2018), pp. 22670–22683 (cit. on pp. 128, 144).

[BHE19a] B. E. Y. Belmekki, A. Hamza, and B. Escrig. "Outage Performance of NOMA at Road Intersections Using Stochastic Geometry". In: *2019 IEEE Wireless Communications and Networking Conference (WCNC) (IEEE WCNC 2019)*. IEEE. 2019, pp. 1–6 (cit. on pp. 130, 137).

[BHE19b] B. E. Y. Belmekki, A. Hamza, and B. Escrig. "Cooperative vehicular communications at intersections over nakagami-m fading channels". In: *Vehicular Communications* (July 2019), doi:10.1016/j.vehcom.2019.100165 (cit. on p. 23).

[BHE19c] B. E. Y. Belmekki, A. Hamza, and B. Escrig. "On the Outage Probability of Cooperative 5G NOMA at Intersections". In: *2019 IEEE 89th Vehicular Technology Conference (VTC2019-Spring)*. IEEE. 2019, pp. 1–6 (cit. on p. 75).

[BHE19d] B. E. Y. Belmekki, A. Hamza, and B. Escrig. "On the Performance of 5G Non-Orthogonal Multiple Access for Vehicular Communications at Road Intersections". In: *Vehicular Communications* (2019), doi:10.1016/j.vehcom.2019.100202 (cit. on p. 75).

[BHE19e] B. E. Y. Belmekki, A. Hamza, and B. Escrig. "On the Performance of Cooperative NOMA Using MRC at Road Intersections". In: *Under review in the journal of IEEE Transactions on Cognitive Communications and Networking* (2019) (cit. on p. 75).

[BHE19f] B. E. Y. Belmekki, A. Hamza, and B. Escrig. "Outage Analysis of Cooperative NOMA in Millimeter Wave Vehicular Network at Intersections". In: *arXiv preprint arXiv:1904.11022* (2019) (cit. on pp. 130, 137).

[BHE19g] B. E. Y. Belmekki, A. Hamza, and B. Escrig. "Outage analysis of cooperative noma using maximum ratio combining at intersections". In: *2019 International Conference on Wireless and Mobile Computing, Networking and Communications (WiMob)*. IEEE. 2019, pp. 1–6 (cit. on p. 75).

[BHE19h] B. E. Y. Belmekki, A. Hamza, and B. Escrig. "Outage Performance of NOMA at Road Intersections Using Stochastic Geometry". In: *2019 IEEE Wireless Communications and Networking Conference (WCNC) (IEEE WCNC 2019)*. IEEE. 2019, pp. 1–6 (cit. on p. 75).

[BHE19i] B. E. Y. Belmekki, A. Hamza, and B. Escrig. "Performance Analysis of Cooperative Communications at Road Intersections Using Stochastic Geometry Tools". In: *Under review in the journal Ad hoc Networks* (2019) (cit. on p. 23).

[BHE19j] B. E. Y. Belmekki, A. Hamza, and B. Escrig. "Performance Analysis of Cooperative NOMA at Intersections for Vehicular Communications in the Presence of Interference". In: *Ad hoc Networks* (2019), doi:10.1016/j.adhoc.2019.102036 (cit. on p. 75).

[BHE20a] B. E. Y. Belmekki, A. Hamza, and B. Escrig. “Interference Dynamic and Vehicles Mobility Analysis in Cooperative Vehicular Communications”. In: *2020 IEEE International Symposium on Personal, Indoor and Mobile Radio Communications (PIMRC)*. IEEE. 2020, pp. 1–6 (cit. on p. 23).

[BHE20b] B. E. Y. Belmekki, A. Hamza, and B. Escrig. “Multiple Relays Performance in NOMA Vehicular Networks”. In: *2020 IEEE International Symposium on Personal, Indoor and Mobile Radio Communications (PIMRC)*. IEEE. 2020, pp. 1–6 (cit. on p. 127).

[BHE20c] B. E. Y. Belmekki, A. Hamza, and B. Escrig. “On the Outage Probability of Vehicular Communications at Intersections Over Nakagami-m Fading Channels”. In: *Under review in IEEE 91th Vehicular Technology Conference (VTC2020-Spring)*. IEEE. 2020, pp. 1–6 (cit. on p. 23).

[BHE20d] B. E. Y. Belmekki, A. Hamza, and B. Escrig. “Outage Analysis of Cooperative NOMA for Millimeter Wave Vehicular Networks at Intersections”. In: *Under review in IEEE 91th Vehicular Technology Conference (VTC2020-Spring)*. IEEE. 2020, pp. 1–6 (cit. on p. 127).

[BHE20e] B. E. Y. Belmekki, A. Hamza, and B. Escrig. “Performance Evaluation of Adaptive Cooperative NOMA Protocol at Road Junctions”. In: *Under review in IEEE 91th Vehicular Technology Conference (VTC2020-Spring)*. IEEE. 2020, pp. 1–6 (cit. on p. 127).

[Bis+16] S. Biswas, S. Vuppala, J. Xue, and T. Ratnarajah. “On the performance of relay aided millimeter wave networks”. In: *IEEE Journal of Selected Topics in Signal Processing* 10.3 (2016), pp. 576–588 (cit. on p. 128).

[BMA12] B. Blaszczyszyn, P. Muhlethaler, and N. Achir. “Vehicular ad-hoc networks using slotted Aloha: point-to-point, emergency and broadcast communications”. In: *Wireless Days (WD), 2012 IFIP*. IEEE. 2012, pp. 1–6 (cit. on pp. 10, 30).

[BMT09] B. Blaszczyszyn, P. Muhlethaler, and Y. Toor. “Performance of MAC protocols in linear VANETs under different attenuation and fading conditions”. In: *Intelligent Transportation Systems, 2009. ITSC'09. 12th International IEEE Conference on*. IEEE. 2009, pp. 1–6 (cit. on pp. 10, 24, 30).

[BMT13] B. Błaszczyszyn, P. Mühlethaler, and Y. Toor. “Stochastic analysis of Aloha in vehicular ad hoc networks”. In: *Annals of telecommunications-Annales des télécommunications* 68.1-2 (2013), pp. 95–106 (cit. on pp. 10, 30).

[BTJ18] K. Belbase, C. Tellambura, and H. Jiang. “Two-way relay selection for millimeter wave networks”. In: *IEEE Communications Letters* 22.1 (2018), pp. 201–204 (cit. on p. 128).

[BVH14] T. Bai, R. Vaze, and R. W. Heath. “Analysis of blockage effects on urban cellular networks”. In: *IEEE Transactions on Wireless Communications* 13.9 (2014), pp. 5070–5083 (cit. on pp. 142, 150).

[Cai+11] Y. Cai, D. Le Ruyet, R. C. de Lamare, and D. Roviras. “Linear precoding based on switched relaying processing for multiuser MIMO relay systems”. In: *2011 IEEE 12th International Workshop on Signal Processing Advances in Wireless Communications*. IEEE. 2011, pp. 351–355 (cit. on p. 7).

[CB18] C.-S. Choi and F. Baccelli. “An analytical framework for coverage in cellular networks leveraging vehicles”. In: *IEEE Transactions on Communications* (2018) (cit. on p. 12).

[CD18] V. V. Chetlur and H. S. Dhillon. “Coverage analysis of a vehicular network modeled as cox process driven by poisson line process”. In: *IEEE Transactions on Wireless Communications* (2018) (cit. on p. 10).

[Che+07] L. Cheng, B. E. Henty, D. D. Stancil, F. Bai, and P. Mudalige. “Mobile vehicle-to-vehicle narrow-band channel measurement and characterization of the 5.9

GHz dedicated short range communication (DSRC) frequency band". In: *IEEE Journal on Selected Areas in Communications* 25.8 (2007), pp. 1501–1516 (cit. on pp. 30, 37, 82).

[CLR10] Y. Cai, D. Le Ruyet, and D. Roviras. "Joint interference suppression and power allocation techniques for multiuser multiantenna relay broadcast systems". In: *2010 7th International Symposium on Wireless Communication Systems*. IEEE. 2010, pp. 265–269 (cit. on p. 7).

[Cri+15] A. Crismani, S. Toumpis, U. Schilcher, G. Brandner, and C. Bettstetter. "Cooperative relaying under spatially and temporally correlated interference". In: *IEEE Transactions on Vehicular Technology* 64.10 (2015), pp. 4655–4669 (cit. on p. 24).

[CT06] T. M. Cover and J. A. Thomas. "Elements of information theory 2nd edition (wiley series in telecommunications and signal processing)". In: (2006) (cit. on p. 6).

[Dai+15] L. Dai, B. Wang, Y. Yuan, S. Han, I. Chih-Lin, and Z. Wang. "Non-orthogonal multiple access for 5G: solutions, challenges, opportunities, and future research trends". In: *IEEE Communications Magazine* 53.9 (2015), pp. 74–81 (cit. on p. 76).

[DDP16a] Z. Ding, H. Dai, and H. V. Poor. "Relay selection for cooperative NOMA". In: *IEEE Wireless Communications Letters* 5.4 (2016), pp. 416–419 (cit. on pp. 76, 80, 143).

[DDP16b] Z. Ding, L. Dai, and H. V. Poor. "MIMO-NOMA design for small packet transmission in the Internet of Things". In: *IEEE access* 4 (2016), pp. 1393–1405 (cit. on pp. 80, 143).

[DGC13] M. Di Renzo, A. Guidotti, and G. E. Corazza. "Average rate of downlink heterogeneous cellular networks over generalized fading channels: A stochastic geometry approach". In: *IEEE Transactions on Communications* 61.7 (2013), pp. 3050–3071 (cit. on p. 7).

[DGG18] D. Duchemin, J.-M. Gorce, and C. Goursaud. "Code Domain Non Orthogonal Multiple Access versus ALOHA: a simulation based study". In: *2018 25th International Conference on Telecommunications (ICT)*. IEEE. 2018, pp. 445–450 (cit. on p. 76).

[DGG19] D. Duchemin, J.-M. Gorce, and C. Goursaud. "Low complexity Detector for massive uplink random access with NOMA in IoT LPWA networks". In: 2019 (cit. on p. 76).

[DGS10] M. Di Renzo, F. Graziosi, and F. Santucci. "A comprehensive framework for performance analysis of cooperative multi-hop wireless systems over log-normal fading channels". In: *IEEE Transactions on Communications* 58.2 (2010), pp. 531–544 (cit. on p. 8).

[DH17] N. Deng and M. Haenggi. "The meta distribution of the SINR in mm-wave D2D networks". In: *GLOBECOM 2017-2017 IEEE Global Communications Conference*. IEEE. 2017, pp. 1–6 (cit. on p. 145).

[Di +18] M. Di Renzo, A. Zappone, T. T. Lam, and M. Debbah. "System-level modeling and optimization of the energy efficiency in cellular networks—A stochastic geometry framework". In: *IEEE Transactions on Wireless Communications* 17.4 (2018), pp. 2539–2556 (cit. on p. 6).

[Di 15] M. Di Renzo. "Stochastic geometry modeling and performance evaluation of mmwave cellular communications". In: *2015 IEEE International Conference on Communications (ICC)*. IEEE. 2015, pp. 5992–5997 (cit. on p. 128).

[DIG12] M. Di Renzo, M. Iezzi, and F. Graziosi. "On diversity order and coding gain of multisource multirelay cooperative wireless networks with binary network coding". In: *IEEE Transactions on Vehicular Technology* 62.3 (2012), pp. 1138–1157 (cit. on p. 8).

[Din+14] Z. Ding, Z. Yang, P. Fan, and H. V. Poor. "On the performance of non-orthogonal multiple access in 5G systems with randomly deployed users". In: *IEEE Signal Processing Letters* 21.12 (2014), pp. 1501–1505 (cit. on pp. 76, 80).

[Din+17a] Z. Ding, X. Lei, G. K. Karagiannidis, R. Schober, J. Yuan, and V. K. Bhargava. "A survey on non-orthogonal multiple access for 5G networks: Research challenges and future trends". In: *IEEE Journal on Selected Areas in Communications* 35.10 (2017), pp. 2181–2195 (cit. on p. 76).

[Din+17b] Z. Ding, Y. Liu, J. Choi, Q. Sun, M. Elkashlan, I. Chih-Lin, and H. V. Poor. "Application of non-orthogonal multiple access in LTE and 5G networks". In: *IEEE Communications Magazine* 55.2 (2017), pp. 185–191 (cit. on p. 76).

[DL14a] M. Di Renzo and W. Lu. "End-to-end error probability and diversity analysis of AF-based dual-hop cooperative relaying in a Poisson field of interferers at the destination". In: *IEEE Transactions on Wireless Communications* 14.1 (2014), pp. 15–32 (cit. on p. 8).

[DL14b] M. Di Renzo and W. Lu. "The equivalent-in-distribution (EiD)-based approach: On the analysis of cellular networks using stochastic geometry". In: *IEEE Communications Letters* 18.5 (2014), pp. 761–764 (cit. on p. 7).

[DL15] M. Di Renzo and W. Lu. "Stochastic geometry modeling and performance evaluation of MIMO cellular networks using the equivalent-in-distribution (EiD)-based approach". In: *IEEE Transactions on Communications* 63.3 (2015), pp. 977–996 (cit. on pp. 6, 128).

[DLG16] M. Di Renzo, W. Lu, and P. Guan. "The intensity matching approach: A tractable stochastic geometry approximation to system-level analysis of cellular networks". In: *IEEE Transactions on Wireless Communications* 15.9 (2016), pp. 5963–5983 (cit. on p. 7).

[DPP15] Z. Ding, M. Peng, and H. V. Poor. "Cooperative non-orthogonal multiple access in 5G systems". In: *IEEE Communications Letters* 19.8 (2015), pp. 1462–1465 (cit. on pp. 80, 128, 138).

[Dzi+10] A. Dziri, D. Le Ruyet, D. Roviras, and M. Terre. "Symbol Error Probability Analysis of the Decode and Forward Relaying over the composite fading multipath/shadowing channels". In: *The 10th IEEE International Symposium on Signal Processing and Information Technology*. IEEE. 2010, pp. 171–176 (cit. on p. 7).

[Dzi+11] A. Dziri, D. Le Ruyet, D. Roviras, and M. Terre. "Closed form of performance analysis of decode and forward relaying over the Generalized-K channels". In: *2011 IEEE International Symposium on Signal Processing and Information Technology (ISSPIT)*. IEEE. 2011, pp. 399–403 (cit. on p. 7).

[Ega+17] M. Egan, L. Clavier, M. De Freitas, L. Dorville, J.-M. Gorce, and A. Savard. "Wireless Communication in Dynamic Interference". In: *GLOBECOM 2017-2017 IEEE Global Communications Conference*. IEEE. 2017, pp. 1–6 (cit. on p. 6).

[Esc+08] B. Escrig, B. Paillassa, D. Roviras, and W. Panichpattanakul. "A framework for cooperative communications at the system level". In: *2008 5th IEEE International Conference on Mobile Ad Hoc and Sensor Systems*. IEEE. 2008, pp. 653–658 (cit. on p. 7).

[Esc10] B. Escrig. "On-demand cooperation MAC protocols with optimal diversity-multiplexing tradeoff". In: *2010 IEEE Wireless Communication and Networking Conference*. IEEE. 2010, pp. 1–6 (cit. on p. 8).

[Esc11] B. Escrig. "DMT optimal cooperative protocols with destination-based selection of the best relay". In: *IEEE Transactions on Wireless Communications* 10.7 (2011), pp. 2218–2227 (cit. on p. 8).

[FEA16] M. J. Farooq, H. ElSawy, and M.-S. Alouini. "A stochastic geometry model for multi-hop highway vehicular communication". In: *IEEE Transactions on Wireless Communications* 15.3 (2016), pp. 2276–2291 (cit. on pp. 10, 24, 30, 62).

[FGG12] P. Ferrand, C. Goursaud, and J.-M. Gorce. "Energy-delay tradeoffs in a linear sequence of relay channels". In: *2012 IEEE Wireless Communications and Networking Conference (WCNC)*. IEEE. 2012, pp. 1140–1145 (cit. on p. 7).

[GH09] R. K. Ganti and M. Haenggi. "Spatial and temporal correlation of the interference in ALOHA ad hoc networks". In: *IEEE Communications Letters* 13.9 (2009) (cit. on pp. 24, 56).

[Gol05] A. Goldsmith. *Wireless communications*. Cambridge university press, 2005 (cit. on pp. 1, 5).

[Gor+09] J.-M. Gorce, C. Goursaud, G. Villemaud, R. d'Errico, and L. Ouvry. "Opportunistic relaying protocols for human monitoring in BAN". In: *2009 IEEE 20th International Symposium on Personal, Indoor and Mobile Radio Communications*. IEEE. 2009, pp. 732–736 (cit. on p. 7).

[Hae09] M. Haenggi. "Outage, local throughput, and capacity of random wireless networks". In: *IEEE Transactions on Wireless Communications* 8.8 (2009) (cit. on pp. 24, 57).

[Hae12a] M. Haenggi. "Diversity loss due to interference correlation". In: *IEEE Communications Letters* 16.10 (2012), pp. 1600–1603 (cit. on pp. 24, 65).

[Hae12b] M. Haenggi. *Stochastic geometry for wireless networks*. Cambridge University Press, 2012 (cit. on pp. 7, 24, 183).

[HAG13] C. Hasan, E. Altman, and J.-M. Gorce. "Partner selection for decode-and-forward cooperative relaying: A matching theoretic approach". In: *2013 IEEE 24th Annual International Symposium on Personal, Indoor, and Mobile Radio Communications (PIMRC)*. IEEE. 2013, pp. 2275–2280 (cit. on p. 7).

[Ham+16a] S. Hamda, M. Pischella, D. Roviras, and R. Bouallegue. "Cooperative uplink OFDMA-MIMO resource allocation with multiplexing relays". In: *2016 IEEE Wireless Communications and Networking Conference Workshops (WCNCW)*. IEEE. 2016, pp. 24–30 (cit. on p. 7).

[Ham+16b] S. Hamda, M. Pischella, D. Roviras, and R. Bouallegue. "Uplink resource allocation in cooperative OFDMA with multiplexing mobile relays". In: *EURASIP Journal on Wireless Communications and Networking* 2016.1 (2016), p. 215 (cit. on p. 7).

[Has+03] M. O. Hasna, M.-S. Alouini, A. Bastami, and E. S. Ebbini. "Performance analysis of cellular mobile systems with successive co-channel interference cancellation". In: *IEEE Transactions on Wireless Communications* 2.1 (2003), pp. 29–40 (cit. on pp. 84, 112, 131, 146).

[HG+09] M. Haenggi, R. K. Ganti, et al. "Interference in large wireless networks". In: *Foundations and Trends® in Networking* 3.2 (2009), pp. 127–248 (cit. on pp. 7, 24).

[HGS17] Y. Hu, M. C. Gursoy, and A. Schmeink. "Efficient transmission schemes for low-latency networks: NOMA vs. relaying". In: *2017 IEEE 28th Annual Inter-*

national Symposium on Personal, Indoor, and Mobile Radio Communications (PIMRC). IEEE. 2017, pp. 1–6 (cit. on p. 128).

[HYH13] J. Hu, L.-L. Yang, and L. Hanzo. "Maximum average service rate and optimal queue scheduling of delay-constrained hybrid cognitive radio in Nakagami fading channels". In: *IEEE Transactions on Vehicular Technology* 62.5 (2013), pp. 2220–2229 (cit. on p. 36).

[Isl+17] S. R. Islam, N. Avazov, O. A. Dobre, and K.-S. Kwak. "Power-domain non-orthogonal multiple access (NOMA) in 5G systems: Potentials and challenges". In: *IEEE Communications Surveys & Tutorials* 19.2 (2017), pp. 721–742 (cit. on p. 76).

[IUA13] S. S. Ikki, P. Ubaidulla, and S. Aıssa. "Regenerative cooperative diversity networks with co-channel interference: Performance analysis and optimal energy allocation". In: *IEEE Transactions on Vehicular Technology* 62.2 (2013), pp. 896–902 (cit. on pp. 10, 24).

[Jeo+13] Y. Jeong, J. W. Chong, H. Shin, and M. Z. Win. "Intervehicle communication: Cox-fox modeling". In: *IEEE Journal on Selected Areas in Communications* 31.9 (2013), pp. 418–433 (cit. on p. 10).

[JH] J. P. Jeyaraj and M. Haenggi. "A Transdimensional Poisson Model for Vehicular Networks". In: () (cit. on p. 12).

[JH17] J. P. Jeyaraj and M. Haenggi. "Reliability Analysis of V2V Communications on Orthogonal Street Systems". In: *GLOBECOM 2017-2017 IEEE Global Communications Conference*. IEEE. 2017, pp. 1–6 (cit. on pp. 11, 30).

[JH18] J. P. Jeyaraj and M. Haenggi. "Nearest-Vehicle Communication in Regular Street Systems". In: *2018 IEEE 88th Vehicular Technology Conference (VTC-Fall)*. IEEE. 2018, pp. 1–5 (cit. on pp. 12, 28, 30).

[Jia+16] C. Jiang, H. Zhang, Z. Han, Y. Ren, V. C. Leung, and L. Hanzo. "Information-sharing outage-probability analysis of vehicular networks". In: *IEEE Transactions on Vehicular Technology* 65.12 (2016), pp. 9479–9492 (cit. on pp. 10, 30, 31).

[KCG19] H. Kallam, L. S. Cardoso, and J. M. Gorce. "Topological Interference Management: Trade-off Between DoF and SIR for Cellular Systems". In: *2019 26th International Conference on Telecommunications (ICT)*. IEEE. 2019, pp. 96–101 (cit. on p. 6).

[KS17] T. Kimura and H. Saito. "Theoretical interference analysis of inter-vehicular communication at intersection with power control". In: *Computer Communications* (2017) (cit. on pp. 10, 12, 30).

[LD17] W. Lu and M. Di Renzo. "mmWave cellular networks: Stochastic geometry modeling, analysis, and experimental validation". In: *mmWave Massive MIMO*. Elsevier, 2017, pp. 313–341 (cit. on p. 128).

[LDS16] P. Liu, M. Di Renzo, and A. Springer. "Line-of-sight spatial modulation for indoor mmWave communication at 60 GHz". In: *IEEE Transactions on Wireless Communications* 15.11 (2016), pp. 7373–7389 (cit. on p. 128).

[LDS17] P. Liu, M. Di Renzo, and A. Springer. "Variable-N_{u} generalized spatial modulation for indoor LOS mmWave communication: Performance optimization and novel switching structure". In: *IEEE Transactions on Communications* 65.6 (2017), pp. 2625–2640 (cit. on p. 128).

[LTW04] J. N. Laneman, D. N. Tse, and G. W. Wornell. "Cooperative diversity in wireless networks: Efficient protocols and outage behavior". In: *IEEE Transactions on Information theory* 50.12 (2004), pp. 3062–3080 (cit. on pp. 7, 46, 68).

[Med+09] Y. Medjahdi, M. Terre, D. Le Ruyet, D. Roviras, J. Nossek, and L. Baltar. "Inter-cell interference analysis for OFDM/FBMC systems". In: *2009 IEEE 10th Workshop on Signal Processing Advances in Wireless Communications*. IEEE. 2009, pp. 598–602 (cit. on p. 6).

[Med+11] Y. Medjahdi, M. Terre, D. Le Ruyet, D. Roviras, and A. Dziri. "Performance analysis in the downlink of asynchronous OFDM/FBMC based multi-cellular networks". In: *IEEE transactions on wireless communications* 10.8 (2011), pp. 2630–2639 (cit. on p. 6).

[Mes+16] A. Mesodiakaki, F. Adelantado, L. Alonso, M. Di Renzo, and C. Verikoukis. "Energy-and spectrum-efficient user association in millimeter-wave backhaul small-cell networks". In: *IEEE transactions on vehicular technology* 66.2 (2016), pp. 1810–1821 (cit. on p. 128).

[Nav18] T. Navman. *Are truck-only highways the solution to increased fleet safe*. 2018. URL: https://www.teletracnavman.com/resources/blog/are-truck-only-highways-the-solution-to-increased-fleet-safety (visited on) (cit. on p. 11).

[Ngu+13] T. V. Nguyen, F. Baccelli, K. Zhu, S. Subramanian, and X. Wu. "A performance analysis of CSMA based broadcast protocol in VANETs". In: *2013 Proceedings IEEE INFOCOM*. IEEE. 2013, pp. 2805–2813 (cit. on p. 28).

[Org15] W. H. Organization. *Global status report on road safety 2015*. World Health Organization, 2015 (cit. on p. 12).

[Pai+11] B. Paillassa, B. Escrig, R. Dhaou, M.-L. Boucheret, and C. Bes. "Improving satellite services with cooperative communications". In: *International Journal of Satellite Communications and Networking* 29.6 (2011), pp. 479–500 (cit. on p. 8).

[Per+16] N. S. Perović, P. Liu, M. Di Renzo, and A. Springer. "Receive spatial modulation for LOS mmWave communications based on TX beamforming". In: *IEEE Communications Letters* 21.4 (2016), pp. 921–924 (cit. on p. 128).

[Qui+18] V. Quintero, S. M. Perlaza, J.-M. Gorce, and H. V. Poor. "Approximate Nash region of the Gaussian interference channel with noisy output feedback". In: *2018 IEEE Information Theory Workshop (ITW)*. IEEE. 2018, pp. 1–5 (cit. on p. 6).

[Rap02] T. S. Rappaport. "Wireless Communications–Principles and Practice, (The Book End)". In: *Microwave Journal* 45.12 (2002), pp. 128–129 (cit. on p. 65).

[Res14] H. Research. *What Exactly Is The "Internet of Things?* Harbor Research, March, 2014 (cit. on pp. 1, 5).

[RP16] A. Rakhshan and H. Pishro-Nik. "Packet success probability derivation in a vehicular ad hoc network for a highway scenario". In: *2016 Annual Conference on Information Science and Systems (CISS)*. IEEE. 2016, pp. 210–215 (cit. on pp. 30, 160).

[Sch+13] U. Schilcher, S. Toumpis, A. Crismani, G. Brandner, and C. Bettstetter. "How does interference dynamics influence packet delivery in cooperative relaying?" In: *Proceedings of the 16th ACM international conference on Modeling, analysis & simulation of wireless and mobile systems*. ACM. 2013, pp. 347–354 (cit. on p. 24).

[SEB13] S. Sreng, B. Escrig, and M.-L. Boucheret. "Exact outage probability of a hybrid satellite terrestrial cooperative system with best relay selection". In: *2013 IEEE International Conference on Communications (ICC)*. IEEE. 2013, pp. 4520–4524 (cit. on p. 8).

[Sia+19] M. N. Sial, Y. Deng, J. Ahmed, A. Nallanathan, and M. Dohler. "Stochastic Geometry Modeling of Cellular V2X Communication over Shared Channels". In: *IEEE Transactions on Vehicular Technology* (2019) (cit. on p. 12).

[Sin+15] S. Singh, M. N. Kulkarni, A. Ghosh, and J. G. Andrews. "Tractable model for rate in self-backhauled millimeter wave cellular networks". In: *IEEE Journal on Selected Areas in Communications* 33.10 (2015), pp. 2196–2211 (cit. on p. 143).

[Ste+15a] E. Steinmetz, M. Wildemeersch, T. Q. Quek, and H. Wymeersch. "A stochastic geometry model for vehicular communication near intersections". In: *Globecom Workshops (GC Wkshps), 2015 IEEE*. IEEE. 2015, pp. 1–6 (cit. on pp. 11, 30, 40).

[Ste+15b] E. Steinmetz, M. Wildemeersch, T. Q. Quek, and H. Wymeersch. "Packet reception probabilities in vehicular communications close to intersections". In: *arXiv preprint arXiv:1509.00399* (2015) (cit. on p. 11).

[Sto] Stomp. *This horrific traffic jam in Brazil is every driver's worst nightmare.* URL: https://stomp.straitstimes.com/singapore/this-horrific-traffic-jam-in-brazil-is-every-drivers-worst-nightmare (visited on) (cit. on p. 13).

[Sub+12] S. Subramanian, M. Werner, S. Liu, J. Jose, R. Lupoaie, and X. Wu. "Congestion control for vehicular safety: synchronous and asynchronous MAC algorithms". In: *Proceedings of the ninth ACM international workshop on Vehicular inter-networking, systems, and applications*. ACM. 2012, pp. 63–72 (cit. on p. 28).

[Tas+17] A. Tassi, M. Egan, R. J. Piechocki, and A. Nix. "Modeling and Design of Millimeter-Wave Networks for Highway Vehicular Communication". In: *IEEE*

Transactions on Vehicular Technology 66.12 (2017), pp. 10676–10691 (cit. on pp. 10, 30).

[TJJ13] R. Tanbourgi, H. Jäkel, and F. K. Jondral. "Cooperative relaying in a Poisson field of interferers: A diversity order analysis". In: *Information Theory Proceedings (ISIT), 2013 IEEE International Symposium on*. IEEE. 2013, pp. 3100–3104 (cit. on pp. 8, 46).

[TK15] S. Timotheou and I. Krikidis. "Fairness for non-orthogonal multiple access in 5G systems". In: *IEEE Signal Processing Letters* 22.10 (2015), pp. 1647–1651 (cit. on p. 76).

[Ton+16] Z. Tong, H. Lu, M. Haenggi, and C. Poellabauer. "A stochastic geometry approach to the modeling of DSRC for vehicular safety communication". In: *IEEE Transactions on Intelligent Transportation Systems* 17.5 (2016), pp. 1448–1458 (cit. on p. 30).

[US 17] U.S. Dept. of Transportation, National Highway Traffic Safety Administration. *Traffic Safety Facts 2015*. Jan. 2017 (cit. on p. 12).

[Wan+15] L. Wang, M. Elkashlan, R. W. Heath, M. Di Renzo, and K.-K. Wong. "Millimeter wave power transfer and information transmission". In: *2015 IEEE Global Communications Conference (GLOBECOM)*. IEEE. 2015, pp. 1–6 (cit. on p. 128).

[Wu+17] S. Wu, R. Atat, N. Mastronarde, and L. Liu. "Coverage analysis of D2D relay-assisted millimeter-wave cellular networks". In: *2017 IEEE Wireless Communications and Networking Conference (WCNC)*. IEEE. 2017, pp. 1–6 (cit. on p. 128).

[ZH17] Z. Zhang and R. Q. Hu. "Uplink Non-Orthogonal Multiple Access with Fractional Power Control". In: *Wireless Communications and Networking Conference (WCNC), 2017 IEEE*. IEEE. 2017, pp. 1–6 (cit. on p. 76).

[Zha+16] Z. Zhang, H. Sun, R. Q. Hu, and Y. Qian. "Stochastic geometry based performance study on 5G non-orthogonal multiple access scheme". In: *Global Communications Conference (GLOBECOM), 2016 IEEE*. IEEE. 2016, pp. 1–6 (cit. on p. 76).

[Zho+17] X. Zhou, J. Guo, S. Durrani, and M. Di Renzo. "Power beacon-assisted millimeter wave ad hoc networks". In: *IEEE Transactions on Communications* 66.2 (2017), pp. 830–844 (cit. on p. 128).

[ZSH17] Z. Zhang, H. Sun, and R. Q. Hu. "Downlink and uplink non-orthogonal multiple access in a dense wireless network". In: *IEEE Journal on Selected Areas in Communications* 35.12 (2017), pp. 2771–2784 (cit. on p. 76).